Scholars' Mine

Doctoral Dissertations

Student Theses and Dissertations

Summer 2021

Computational studies of carbon nanocluster solidification

Chathuri Chandani Silva

Follow this and additional works at: https://scholarsmine.mst.edu/doctoral_dissertations

Part of the Physics Commons

Department: Physics

Recommended Citation

Silva, Chathuri Chandani, "Computational studies of carbon nanocluster solidification" (2021). *Doctoral Dissertations*. 3018.
https://scholarsmine.mst.edu/doctoral_dissertations/3018

This thesis is brought to you by Scholars' Mine, a service of the Missouri S&T Library and Learning Resources. This work is protected by U. S. Copyright Law. Unauthorized use including reproduction for redistribution requires the permission of the copyright holder. For more information, please contact scholarsmine@mst.edu.

COMPUTATIONAL STUDIES OF CARBON NANOCLUSTER SOLIDIFICATION

by

CHATHURI CHANDANI SILVA

A DISSERTATION

Presented to the Graduate Faculty of the

MISSOURI UNIVERSITY OF SCIENCE AND TECHNOLOGY

and

UNIVERSITY OF MISSOURI – ST. LOUIS

In Partial Fulfillment of the Requirements for the Degree

DOCTOR OF PHILOSOPHY

in

PHYSICS

2021

Approved by:

Philip B. Fraundorf, Advisor
Julia E. Medvedeva, Co-Advisor
Eric H. Majzoub
Yew San Hor
Stephen M. Holmes

© 2021

Chathuri Chandani Silva

All Rights Reserved

ABSTRACT

A subset of micron-size meteoritic carbon particles formed in red giant atmospheres show a core-rim structure, likely condensed from a vapor phase into super-cooled carbon droplets that nucleated graphene sheets (~40Å) on randomly oriented 5-atom loops during solidification, followed by coating with a graphite rim. Similar particles form during slow cooling of carbon vapor in the lab.

Here we investigate the nucleation and growth of carbon rings and graphene sheets using density functional theory (DFT). Our objectives: (1). explore different computational techniques in DFT-VASP for various carbon structures and compare the results with literature, (2). investigate the nucleation and growth of carbon rings and graphene sheets at the experimental 1.8 g/cc density estimate, by supercell relaxation of randomized liquid-like carbon atom clusters, and (3). Compare carbon cluster energies for combinations of DFT-VASP and long-range carbon bond order potential (LCBOP) relaxations.

Observations show: (a) that 29 atom diamond clusters relax into the C28 fullerene with a central carbon atom, (b) new evidence for the instability of an Fm3m carbon phase with the diamond unit cell, and (c) that pent-loop formation is energetically favored over hex-loop formation in a relaxed melt. Literature work on the effectiveness of pent-loops as nucleation seed for graphene structures, plus the fact that each pent-loop can give rise to 5 differently oriented sheets, helps explain electron-microscope data on graphene-sheet number densities and provides guidance for nucleation/growth models being developed.

ACKNOWLEDGMENTS

First of all, I wish to extend my deepest gratitude to Prof. Philip Fraundorf for his continuous guidance and endless support throughout my Ph.D. study. His guidance, motivation, and extensive knowledge contributed to my successful completion of graduate studies and growth as a researcher. Also, I would like to give special thanks to Prof. Eric H. Majzoub, who is assisting me throughout my research project, especially regarding the computational details. Without his guidance and patience, this achievement would not be possible. My sincere appreciation goes out to my current and former committee members: Dr. Stephen Holmes, Dr. Yew San Hor, Dr. Julia Medvedeva and Dr. Alexey Yamilov for their efforts on the committee and for providing me with valuable feedback. Thank you as well to the Department of Physics and Astronomy-UMSL for financially supporting me through my Ph.D. program. It has been an honor to work with the faculty and staff over the years and I greatly appreciate all of their help and support. I am also grateful to Missouri University of Science and Technology for providing the facilities for me to use the FORGE cluster and to my group members for helping me develop ideas that were very useful for my research.

Additionally, I would like to express my love and gratitude for my parents, my brother, and my friends who have supported me in everything, encouraged me, and inspired me to reach for my dreams. Finally, I would also like to express my love and appreciation to my husband, Isuru for creating an environment that helped me stay positive and happy throughout my university experience.

TABLE OF CONTENTS

Page

ABSTRACT iii

ACKNOWLEDGMENTS iv

LIST OF ILLUSTRATIONS ix

LIST OF TABLES xiv

SECTION

1. INTRODUCTION 1
    1.1. ELEMENTAL CARBON 2
        1.1.1. Graphite, Diamond, and Fullerene 3
        1.1.2. Carbyne 5
        1.1.3. Fcc-carbon and Icosahedral Arrangement 5
        1.1.4. Carbon Phase Diagram 6
        1.1.5. Carbon Particle Size vs. Carbon Phase Diagram 8
        1.1.6. Commercial and Industrial Value of Carbon 9
    1.2. EXTRATERRESTRIAL MATERIALS 10
        1.2.1. Presolar Grains 10
        1.2.2. Density Estimation of Unlayered Graphene 15
    1.3. OUTLINE OF THE DISSERTATION 16
2. DENSITY FUNCTIONAL THEORY (DFT) 18
    2.1. BACKGROUND OF DFT 18
        2.1.1. The Many-body Schrödinger Equation 18

2.1.2. Static Nuclei Approximation (Born-Oppenheimer Approximations)....19

2.1.3. Hohenberg-Kohn Approximations..19

2.1.4. Exchange-correlation Approximation.....................................21

2.1.5. Periodic Boundary Conditions, Bloch's Theorem and Plane Wave Basis Set...22

2.1.6. Projector Augmented-Wave Method (PAW Method)......................24

2.2. VIENNA AB INITIO SIMULATION PACKAGE (VASP)......................26

2.2.1. POSCAR Input File..27

2.2.2. INCAR Input File..27

2.2.3. K-point Input File...29

2.2.4. POTCAR Input File..29

2.2.5. OUTCAR Output File...30

2.2.6. CONTCAR Output File...30

2.3. VASP SIMULATION METHODS...30

2.3.1. The Static Structure Method (N1-Method)...............................30

2.3.2. The Relaxation Method..31

3. AB INITIO STUDIES OF NANO CARBON STRUCTURES.........................32

3.1. THE IMPORTANCE OF VASP EXPLORATIONS...............................32

3.2. VASP COMPUTATIONS IN CARBON 5-ATOM CHAIN.......................32

3.3. ENERGY COMPARISON FOR CARBON 5-ATOM AND 6-ATOM CHAINS...37

3.4. DIAMOND - 8 ATOMS CUBIC SUPERCELL RELAXATION...............40

3.5. FCC CARBON - 4 ATOMS SUPERCELL RELAXATION......................42

3.6. STATIC STRUCTURE CALCULATION OF 13-ATOM ICOSAHEDRAL CAGE (ICO-13) AS A FUNCTION OF EDGE-LENGTH.......................44

3.7. CENTRAL ATOM BINDING ENERGY AS A FUNCTION OF INTERATOM SPACING FOR ICO-13 AND GRAPHENE-13 46

3.7.1. Central Atom Binding Energy Calculation for ico-13 47

3.7.2. Central Atom Binding Energy Calculation for Graphene-13 48

3.8. ENERGY VERSUS VOLUME CALCULATION FOR NON-CUBIC CELLS 50

3.8.1. 2-atom Diamond Primitive Cell 50

3.8.2. 4-atom Graphite Hexagonal Cell 52

3.9. RELAXATION OF TETRAHEDRAL NANO DIAMOND CLUSTER 53

3.10. SUMMARY OF FINDINGS 57

4. THE NUCLEATION OF UNLAYERED GRAPHENE IN LIQUID CARBON USING VASP-DIRECT SUPERCELL RELAXATION METHOD AT T=0K AND LOW PRESSURE 59

4.1. ROAD MAP TO UNLAYERED GRAPHENE 59

4.2. COMPUTATIONAL METHODS 60

4.3. VASP-DIRECT RELAXATION RESULTS 61

4.3.1. Carbon 13-atom Sets in a Supercell Volume 144.04 Å^3 62

4.3.2. Carbon 20-atom Sets in a Supercell Volume 221.55 Å^3 64

4.3.3. Carbon 30-atom Sets in a Supercell Volume 332.41 Å^3 66

4.3.4. Carbon 40-atom Sets in a Supercell Volume 443.21 Å^3 68

4.3.5. Carbon 60-atom Sets in a Supercell Volume 664.81 Å^3 70

4.3.6. Carbon 100-atom Sets in a Supercell Volume 1108.02 Å^3 72

4.4. DISCUSSION OF VASP- DIRECT RELAXATIONS 74

4.4.1. Interatom Distance Separation 75

4.4.2. Coordination Number Statistics 75

4.4.3. Loop Count Statistics.....77

4.5. SUMMARY.....81

5. THE COMPARISON STUDY OF VASP- DIRECT RELAXATION AND VASP RE- RELAXATION METHODS.....82

5.1. A COMPARATIVE STUDY OF TWO COMPUTATIONAL PROCEDURES.....82

5.2. COMPUTATIONAL METHODS.....82

5.3. VASP RE-RELAXATION RESULTS.....83

5.3.1. Carbon 13-atom Re-relaxed Sets.....83

5.3.2. Carbon 20-atom Re-relaxed Sets.....86

5.3.3. Carbon 100-atom Re-relaxed Sets.....88

5.4. DISCUSSION OF VASP RE-RELAXATIONS.....91

5.4.1. Interatom Distance Separation.....91

5.4.2. Coordination Number Statistics.....92

5.4.3. Loop Count Statistics.....94

5.4.4. Total Energy Comparison.....95

5.5. OVERVIEW.....99

6. CONCLUSIONS.....101

APPENDICES

A. DFT STUDY OF “UNLAYERED - GRAPHENE SOLID” FORMATION, IN LIQUID CARBON DROPLETS AT LOW PRESSURES.....104

B. ATOM POSITIONS AND VASP SCRIPT FILES FOR VASP-DIRECT RELAXATIONS.....120

REFERENCES.....176

VITA.....182

LIST OF ILLUSTRATIONS

Page

Figure 1.1. Allotropes of carbon..2

Figure 1.2. Molecular structure of graphene...3

Figure 1.3. A zigzag fullerene..5

Figure 1.4. Arrangements of nearest neighbors in carbon...................................6

Figure 1.5. Phase diagram of carbon 7

Figure 1.6. Log-log phase diagram of carbon..8

Figure 1.7. Murchison-Meteorite in National Museum of Natural History..................10

Figure 1.8. Evolution of presolar grain...11

Figure 1.9. TEM image of KFC1A:7E of presolar onions taken by EM430ST TEM in William L. Clay Center for Nanoscience at University of Missouri St. Louis...13

Figure 1.10. Pre-solar carbon core/rim particles..13

Figure 1.11. Road map of red giant stars to unlayered graphene in the lab................14

Figure 1.12. An example configuration of faceted pentacones...............................15

Figure 1.13. Density vs. inter-atom spacing for elemental carbon phases..................16

Figure 2.1. Self-consistency loop in DFT...22

Figure 2.2. Periodic cell..23

Figure 2.3. POSCAR file example...27

Figure 2.4. K-point file example..29

Figure 3.1. 5-carbon atom chain with redirection angles......................................32

Figure 3.2. Minimum energy bond spacings (a), and energy (b) in relation to redirection angle……………………………………….………………34

Figure 3.3. 5-atom chain closure comparison between VASP and Tersoff models……..35

Figure 3.4. VASP total energy vs. redirection angle for 5-atom chain in different bond spacings……………………………………………………………………..36

Figure 3.5. An overview of the average Tersoff energies for 6 (red) and 5 (blue) carbon chains based on redirection angles……………………………..……38

Figure 3.6. Energies with respect to redirected angles………………………………..…39

Figure 3.7. Total energy vs. unit cell volume for 8-atom diamond-fcc cell……………..41

Figure 3.8. Energy per atom vs. side length for fcc - 4 atoms…………………………...43

Figure 3.9. The icosahedral cage model for liquid phase atoms of carbon……………...44

Figure 3.10. The total binding energy for a 13-atom icosahedral cage as a function of edge spacing…………………………………………………………………...45

Figure 3.11. Central atom binding energy vs. fixed atom nearest-neighbor spacing for ico-13…………………………………………………………………………..47

Figure 3.12. Planar graphene-13 structure………………………………………………48

Figure 3.13. Central atom binding energy vs. fixed atom nearest-neighbor spacing for graphene-13……………………………………………………………………49

Figure 3.14. Unit-cells for diamond………………………….…………………………51

Figure 3.15. Energy vs. volume for 2-atom diamond primitive cell……………………..51

Figure 3.16. VASP hexagonal cell………………………………………………………52

Figure 3.17. Energy vs. volume for 4 atom- graphite hexagonal cell……………………53

Figure 3.18. Initial configuration of diamond -29 cluster………………………………..53

Figure 3.19. Relaxed configuration of diamond -29 cluster……………………………..54

Figure 3.20. The coordination number and the types of atoms in diamond -29 relaxed cluster…………………………………………………………………………54

Figure 3.21. Relaxed structure and coordination for case (i)……………………..…………56

Figure 3.22. Relaxed structure and coordination for case (ii)……..……………………….56

Figure 4.1. A network of atom-pair separations smaller than 1.6Å…………………...…61

Figure 4.2. Composite interatom spacing histogram of 13-atom sets……………………62

Figure 4.3. Loop connection diagram (e.g.,13-atoms VASP-direct relaxed list 1)……...63

Figure 4.4. Composite coordination number plot with the total counts on each bar for 13-atom sets……………………………………………………………………63

Figure 4.5. Composite interatom spacing histogram of 20-atom sets……………………65

Figure 4.6. Loop connection diagram (e.g.,20-atoms VASP-direct relaxed list 1)……...65

Figure 4.7. Composite coordination number plot with the total counts on each bar for 20-atom sets……………………………………………………………………65

Figure 4.8. Composite interatom spacing histogram of 30-atom sets……………………67

Figure 4.9. Loop connection diagram (e.g.,30-atoms VASP-direct relaxed list 1)……...67

Figure 4.10. Composite coordination number plot with the total counts on each bar for 30-atom sets……………………………………………………………67

Figure 4.11. Composite interatom spacing histogram of 40-atom sets……………………69

Figure 4.12. Loop connection diagram (e.g., 40-atoms VASP-direct relaxed list 1)……69

Figure 4.13. Composite coordination number plot with the total counts on each bar for 40-atom sets……………………………………………………………………69

Figure 4.14. Composite interatom spacing histogram of 60-atom sets…………………..71

Figure 4.15. Loop connection visualization (e.g.,60-atoms VASP-direct relaxed list 1)..71

Figure 4.16. Composite coordination number plot with the total counts on each bar for 60-atom sets…………………………………………………………………..71

Figure 4.17. Composite interatom spacing histogram of 100-atom sets…………………73

Figure 4.18. Loop connection visualization (e.g., 100-atoms VASP-direct relaxed list 1)………………………………………………………………………………...73

Figure 4.19. Composite coordination number plot with the total counts on each bar for 100-atom sets…………………………………………………………………73

Figure 4.20. Composite interatom spacing histograms for all relaxation sets...............75

Figure 4.21. Coordination numbers per atom as a percentage (%) vs. coordination number..76

Figure 4.22. Percentage of loops per atom versus loop type.................................78

Figure 4.23. The ratio of 5-loops to 6-loops vs. the number of atoms in the simulation cell...79

Figure 5.1. Composite interatom spacing histogram of 13-atom sets (VASP re-relaxed)..83

Figure 5.2. The loop connection plot (e.g., 13-atoms VASP re-relaxed list 1)..............84

Figure 5.3. Composite coordination number plot with the total counts on each bar for 13-atom sets (VASP re-relaxed)..85

Figure 5.4. Composite interatom spacing histogram of 20-atom sets (VASP re-relaxed)...86

Figure 5.5. The loop connection plot (e.g., 20-atoms VASP re-relaxed list 1)..............86

Figure 5.6. Composite coordination number plot with the total counts on each bar for 20-atom sets (VASP re-relaxed)..87

Figure 5.7. Composite interatom spacing histogram of 100-atom sets (VASP re-relaxed)...89

Figure 5.8. The loop connection plot (e.g., 100-atoms VASP re-relaxed list 1)............89

Figure 5.9. Composite coordination number plot with the total counts on each bar for 100-atom sets (VASP re-relaxed)..90

Figure 5.10. Composite interatom spacing histograms for re-relaxation sets...............92

Figure 5.11. Number of coordination number (per atom) as a percentage (%) vs. coordination number for both VASP- direct & VASP re-relaxed sets........93

Figure 5.12. Number of loops per atom as a percentage vs. loop type for both VASP-direct & VASP re-relaxed sets..95

Figure 5.13. Energy (per atom) for LAMMPS pre-relaxed, VASP-direct relaxed, VASP re-relaxed vs. 13-atom set number (Set #1, Set #2, ...Set #20).........96

Figure 5.14. Energy (per atom) for LAMMPS pre-relaxed, VASP-direct relaxed, VASP re-relaxed vs. 20-atom set number (Set #1, Set #2, ...Set #20).........96

Figure 5.15. Energy (per atom) for LAMMPS pre-relaxed, VASP-direct relaxed, VASP re-relaxed vs. 100-atom set number (Set #1, Set #2, ...Set #20)......97

Figure 5.16. VASP- direct (green) and re-relaxed (red) binding energies per atom with simply weighted uncertainties for 13-atom sets..............................98

Figure 5.17. VASP- direct (green) and re-relaxed (red) binding energies per atom with simply weighted uncertainties for 20-atom sets.............................98

Figure 5.18. VASP- direct (green) and re-relaxed (red) binding energies per atom with simply weighted uncertainties for 100-atom sets..........................99

LIST OF TABLES

Page

Table 3.1. Closure cost (eV) for different bond spacings in 5 atom chain closure ……...37

Table 4.1. List by list loop count for 13-atoms, VASP-direct relaxed sets……………...64

Table 4.2. List by list loop count for 20-atoms, VASP-direct relaxed sets……………...66

Table 4.3. List by list loop count for 30-atoms, VASP-direct relaxed sets……………...68

Table 4.4. List by list loop count for 40-atoms, VASP-direct relaxed sets……………...70

Table 4.5. List by list loop count for 60-atoms, VASP-direct relaxed sets……………...72

Table 4.6. List by list loop count for 100-atoms, VASP-direct relaxed sets…………….74

Table 4.7. Total coordination numbers for all VASP- direct relaxed sets……………….76

Table 4.8. Total loop counts for all VASP- direct relaxed sets………………………….77

Table 4.9. Fraction-crystalline observations…………………………………………….80

Table 5.1. List by list loop count for 13-atoms, VASP re-relaxed sets…………………..84

Table 5.2. Energy comparison of VASP-direct relaxed vs. VASP re-relaxed (13-atoms)……………………………………………………………………..85

Table 5.3. List by list loop count for 20-atoms, VASP re-relaxed sets…………………87

Table 5.4. Energy comparison of VASP-direct relaxed vs. VASP re-relaxed (20-atoms)……………………………………………………………………88

Table 5.5. List by list loop count for 100-atoms, VASP re-relaxed sets………………..90

Table 5.6. Energy comparison of VASP-direct relaxed vs. VASP re-relaxed (100-atoms)…………………………………………………………………..91

Table 5.7. Coordination numbers for VASP re-relaxed and VASP- direct relaxed sets...93

Table 5.8. Total loop counts for VASP re-relaxed and VASP- direct relaxed sets……...94

1. INTRODUCTION

Elemental carbon at low (ambient) pressure sublimates to vapor near 4000K temperature, so that liquid carbon is seldom considered to play a role in nature even though quenched carbon droplets have been reported in laboratory laser ablation studies [1,2]. However, a subset of pre-solar micron-sized graphite spheres, extracted from meteorites and containing isotopic signatures of formation in the atmosphere of red giant stars, have spherical cores that show diffraction rings from atom-thick graphene possibly formed by solidification of liquid carbon at low pressure [3]. High-resolution transmission electron microscope (HRTEM) imaging suggests [4] that some of the randomly-oriented (and unlayered) graphene sheets take the form of faceted pentacones, as though they were nucleated on pentagonal loops during solidification. Laboratory synthesis, as well as model studies, suggest that these particles are formed in container-less settings by the slow cooling of carbon vapor [5]. It remains a challenge to study the properties of liquid carbon in a lab due to the difficulty of experimentation under extreme conditions like high temperature and high pressure. Hence, research interest has increased in computational methods, such as density functional theory (DFT).

This research work crosses three major fields of study in Physics: carbon material science, astrophysics, and computational atomistic simulations. These fields are introduced briefly in this section. Section 1.1 will discuss the general background of carbon material, its properties, why carbon studies are important and carbon-based applications in industry and science.

Section 1.2 introduces extraterrestrial material (and presolar material) and explains the relation between this research study and carbon material. The outline of this dissertation will be discussed in Section 1.3.

1.1. ELEMENTAL CARBON

Carbon, the sixth element of the periodic table that is named after the Latin word “carbo” which means coal. It is one of the building blocks of every living organism and lifeless things. Figure 1.1 represents the seven allotropes of carbon. The most familiar states of elemental carbon are graphite, fullerene, graphene, and diamond.

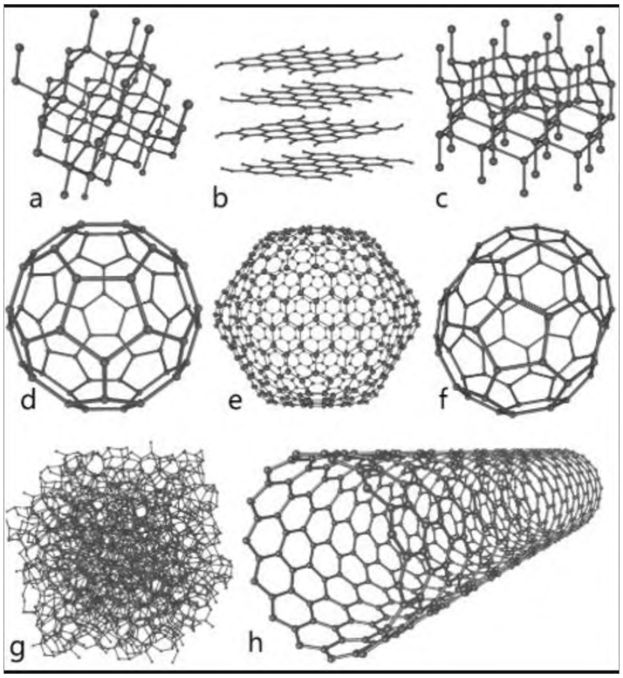

Figure 1.1. Allotropes of carbon; (a). diamond, (b). graphite, (c). Lonsdaleite, (d). C60 (Buckminsterfullerene), (e). C540 (Fullerene), (f). C70 (Fullerene), (g). Amorphous carbon and (h). single-walled carbon nanotube. Source: GNU Free Documentation License by Michael Ströck on Wikimedia commons.

Based on the structure, these four categories can be introduced as, each atom bonded to three others and forming hexagonal sheets categorized as graphite which contains sp^2 hybridization. Under high pressure, each atom is bonded to four other atoms which shows the hybridization as sp^3 and built the hardest material on earth categorized as diamond. A spherical molecule with sp^2 coordination formed by 60 or 70 carbon atoms indicated as fullerene. The youngest allotropes of carbon found in 2004 named as graphene, is the one atom thick layer having sp^2 coordination which is extracted from graphite.

1.1.1. Graphite, Diamond, and Fullerene.

Graphene is a 2-dimensional material consist of a hexagonal array of sp^2 hybridized carbon. A stack of graphene layers on top of each other made the most common allotrope of carbon called graphite which is the most stable form of solid carbon under standard conditions shown in Figure 1.2.

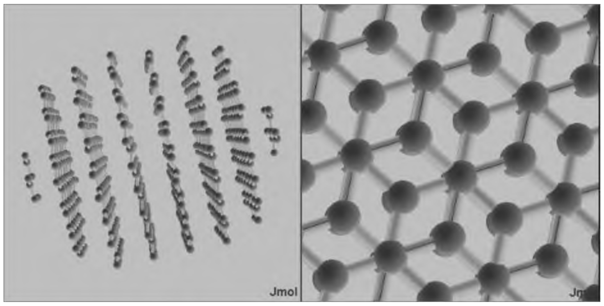

Figure 1.2. Molecular structure of graphene; left: The layering, right: The view of layers faced up, Source: UMSL wiki

In the molecular structure, three carbon atoms form strong covalent bonds to its nearest three neighbor atoms leaving the fourth electron to form a weak van der Waals attraction in order to keep these layers together with an interplanar space of 3.35 Å.

The melting point of graphite is the same as diamond is around 4000K at low or atmospheric pressure, at which point it sublimates rather than melting. Besides graphite, the other forms of allotropes are diamond and fullerene. The atomic arrangement in these three materials is different that makes them have different properties even though they are all made of carbon atoms.

In diamond, the atoms bonded covalently to four other carbon atoms which show sp^3 coordination. Diamond is the hardest known material on earth formed under extreme conditions like high temperature and pressure normally forms at a depth of hundreds of kilometers below inside Earth's mantle. The crystallization of diamond is in the cubic crystal system while another form of diamond that is packed in a hexagonal lattice is called lonsdaleite, or hexagonal diamond. Lonsdaleite was first discovered in Canyon Diablo meteorite in 1967 which was formed because of meteoric graphite hit the earth. Graphite transforms into diamond but remains in a hexagonal symmetry due to the energy and pressure upon the impact when uniaxial pressure is applied to liquid carbon during the solidification [6]. Both diamond and lonsdaleite are composed of sp^3 coordinated carbon bonds with the difference of stacking pattern of carbon layers where diamond stacks in the sequence of ABCABC... and lonsdaleite in the order of ABAB... stacking sequence. Recent studies have predicted that lonsdaleite exhibits many excellent mechanical properties better than diamond that can be used in areas of high-pressure research and applications [7].

Another form of carbon allotrope which is highly symmetrical is called fullerene. Fullerene is sp^2-hybridized molecule, and each carbon atom is bonded to three others. The structure is shown in Figure 1.3. There different sizes of fullerenes based on the number of carbon atoms involved such as C_{60} buckyball, C_{70}, C_{76} and C_{84}.

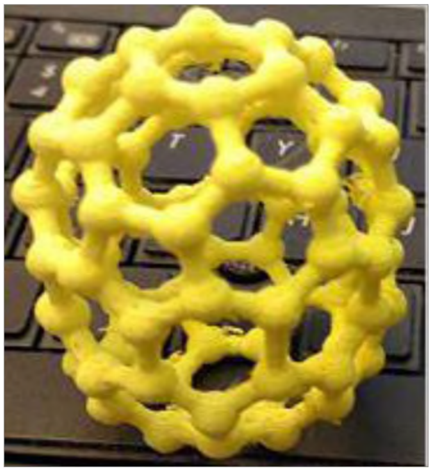

Figure 1.3. A zigzag fullerene; Source: UMSL wiki.

The structure of fullerene depends on the number of pentagonal and hexagonal rings involved. The general rule for making a fullerene includes 12 pentagons exactly without touching or placed nearby. The number of hexagons varies depending on the number of carbon atoms in a basis of an icosahedral symmetry.

1.1.2. Carbyne. A chemical structure that repeats a chain of carbon atoms. It is a long chain of sp- hybridized carbon atoms joined together by alternating single and triple bonds or by consecutive double bonds as a one-dimensional structure. Carbynes were detected naturally in interstellar dust and meteorites [8] and also, studies have reported a long chain up to 44 carbon atoms synthesized experimentally in the lab [9].

1.1.3. Fcc-carbon and Icosahedral Arrangement. The possible arrangements of carbon atoms in the melt and amorphous carbon are shown in Figure 1.4.

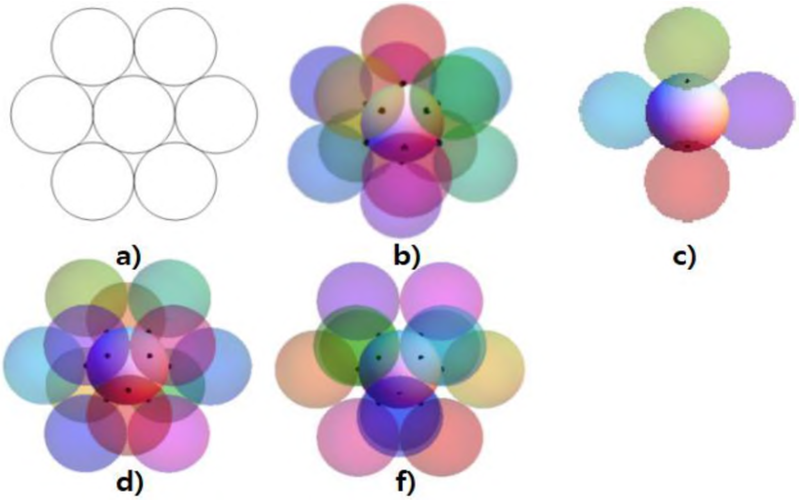

Figure 1.4. Arrangements of nearest neighbors in carbon; a). planar, b). icosahedral, c). tetrahedral, d). cubic close-packed, e). hexagonal close-packed. Source: UMSL wiki.

Figure 1.4.a) represents 6 nearest neighbors in a plane, b) is the icosahedral with 12 nearest neighbors, mostly presence in some metallic liquids and in quasicrystals, c) 4 nearest neighbors that are common in diamond and many semiconductors, d). is the cubic close-packed having 12 nearest neighbor arrangements with all spheres touch, and finally e). is the hexagonal close-packed arrangement with 12 nearest neighbors. Also, compared to icosahedral cage, a new carbon form with fcc crystal lattice called fcc-carbon, where the coordination number is 12 and metal-like interatom distances is 2.52 Å. In this structure the density reported is about 1.7 g/cc lower compared to graphite and diamond [10]. This arrangement is a common feature for amorphous carbon and melt carbon. But in melt, the arrangements are more favorable to the icosahedral structure than the face centered cubic [11,12].

1.1.4. Carbon Phase Diagram. The phase diagram of carbon can be seen below in Figure 1.5.

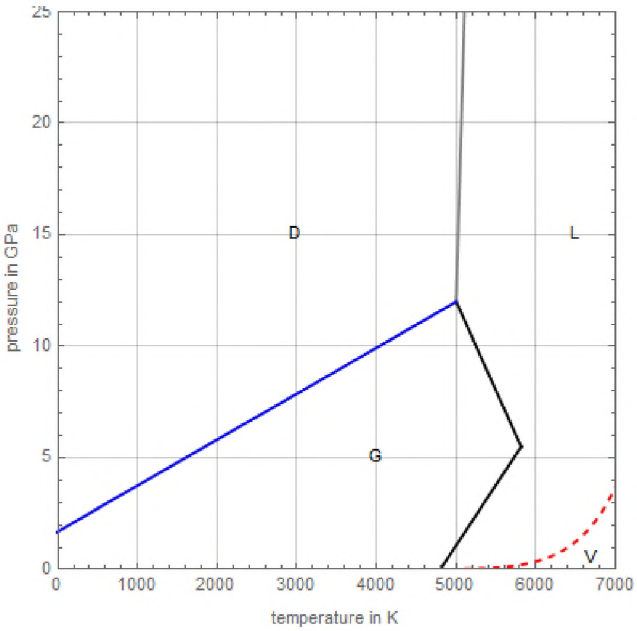

Figure 1.5. Phase diagram of carbon; Source: UMSL wiki.

The most common solid states form of carbon is graphite and diamond. The liquid phase of carbon only exists under extreme conditions like high temperature (higher than 4500K) and high pressure (tens of MPa). The gaseous or vapor phase is favorable in the region of high temperature and low pressures. As a known fact, when carbon heats up it directly converts the solid state to the vapor phase. But, when carbon vapor cools down, the vapor phase converts into the metastable liquid and then to the solid phase. Under high temperature and low-pressure regions, carbon can produce a metastable form of liquid, but evaporates fast because of the short lifetime. The metastable form of solid (graphite-diamond) indicates in the regions of high and low pressure. In addition, the coexistence point of all three phases, solid, liquid and gas appear at around 4600 K and 10.8 MPa and the sublimation temperature appears at 3915 K at lower pressure.

In a super cooled liquid, the crystallization temperature is below 30% of the melting temperature, 4600 K is 3220 K as seen in the vapor phase diverts to solid-liquid phase line at low pressure [13].

1.1.5. Carbon Particle Size vs. Carbon Phase Diagram. Carbon clusters are stable that are smaller sized in the liquid phase below the triple point at very low pressures in containerless settings. Moreover, carbon vapor can be nucleated as the liquid and supercooled after the size of a particle above 2 nm in these settings. Another way to look at it is the possibility of synthesizing nano-diamonds at low pressure. This suggests that the diamond synthesis is not only under high temperature and high-pressure settings, but also in a low-pressure region with nanometer-sized particles. Figure 1.6 below represents the particle size effect on the carbon phase diagram which is the log-log version of the phase diagram of graphite-diamond [14].

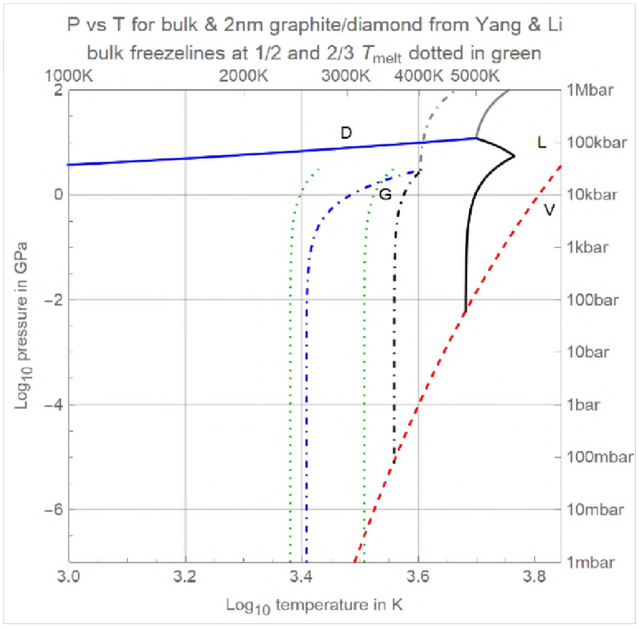

Figure 1.6. Log-log phase diagram of carbon; Source: UMSL wiki.

The figure represents the terms D: diamond, G: graphite, L: liquid carbon, V: carbon vapor, blue line: transition of D-G, black line: transition of G-L, grey line: transition of D-L. Also, the particle size effect on the phase diagram in bulk (solid line) and 2 nm size carbon (dot-dashed line) including the vapor phase curve (red-dashed line). Here, carbon vapor condenses as a stable liquid before the melting temperature in the cooling process at low pressure settings. This suggests that the nano sized particles diamond might be more stable than graphite in low pressure and low temperature settings that opens the possibility of synthesizing nano-diamond and diamond-like carbon at low pressure. In a previous study it was shown that the laser ablation in liquid is used to synthesize the nano-diamonds from graphite under water confinement and proposed that the nano-diamonds nucleate from supercooled liquid carbon [15]. These nano-diamonds can be used for commercial applications and also found in a variety of extraterrestrial materials [16].

1.1.6. Commercial and Industrial Value of Carbon. Carbon became the most popular commercial element in the industry due to its remarkable properties that can be tuned to use in a vast variety of industrial applications. Advanced carbon materials like graphene and carbon nanotubes became an essential element in the production of a wide range of technological and industrial applications. According to Adroit Market Research, in a few years the market for advanced carbon materials will expect the Compound Annual Growth Rate of 9.1% to hit $12.66 Billion by 2025 [17]. And from the scientific viewpoint, carbon plays a big role in a wide range of research studies since it is one of the building blocks of organic lives as well as in inorganics. Not only that, but also studies of carbon provide the key to understanding the cosmic evolution of the universe.

1.2. EXTRATERRESTRIAL MATERIALS

Extraterrestrial martial is an object that occurred naturally that can be found on earth but originated outside the earth or carried from outer space. These materials are subcategorized for study on earth as cosmic dust, presolar grains, moon rocks, and meteorites. Cosmic dust and meteorites are the collectibles found on earth, moon rocks samples are carried from outer space and presolar grains are dust particles extracted from meteorites or interplanetary objects. Figure 1.7 below is an example of a meteorite found in 1969 in Australia named ‘Murchison’. According to a study in 2020, silicon carbide extracted from this meteorite was reported as the oldest material on earth that is 7 billion years old [18].

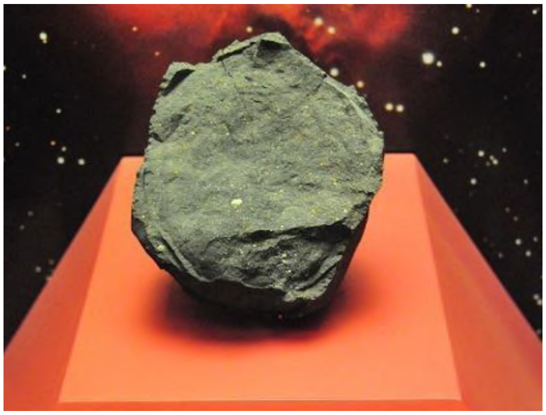

Figure 1.7. Murchison-Meteorite in National Museum of Natural History; Source: Art Bromage - originally posted to Flickr as ‘Murchison Meteorite’.

1.2.1. Presolar Grains. In the categories of extraterrestrial materials, presolar grains are the most primitive minerals in the solar system. These grains have formed in outflows in red giant stars or in supernovae that contain the information about the formation of the solar system. The evolution of presolar grains can be seen in the Figure 1.8.

In the formation of the solar system, the dust coming out from many red giant stars and supernovae formed a molecule cloud that formed the solar nebula. During this nuclear reaction, the pre-solar particles survived and escaped and remained in meteorites and interplanetary objects. In other words, presolar particles are minerals that have emerged or survived from these strong radiant fluxes and extreme environments over the years, and many studies are now being conducted in the laboratory [19,20].

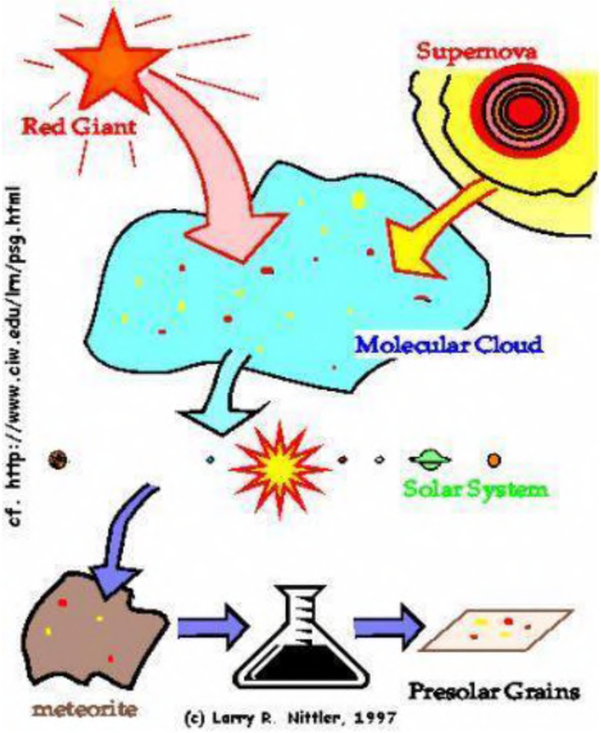
Red Giant
Supernova
Molecular Cloud
Solar System
meteorite
Presolar Grains
(c) Larry R. Nittler, 1997
cf. http://www.ciw.edu/lrn/psg.html

Figure 1.8. Evolution of presolar grain; Source: Figure from Larry R. Nittler (1997).

Presolar grains include various types of elements with different isotopic ratios. Some of the minerals that can be found inside these presolar grains are nano-diamonds, graphite-based compounds, titanium carbide, silicon carbide, silicon nitride. Our solar system is made up of multiple star sources.

This suggests that the changes in these minerals indicate evidence of the production of pre-solar particles in different parent stars and produce information about the mixing of stars. Therefore, among all types of extraterrestrial matter, the presolar particle is a very important test object for characterizing the physical and chemical properties of the atmosphere of its parent star [21,22].

Over the years, the exploration of carbon-based compounds in presolar particles has become a hot field. Those studies have shown that carbon atoms have been formed in red giant stars during the first five billion years of the Galaxy's lifetime. These presolar grains include graphite-only particles formed around carbide seeds, micrometer-sized silicon carbide crystals, and nano diamonds. [19, 23-26]. The carbon-based presolar particles separated from the Murchison meteorite contain different density fractions, for example,

KFA1 (2.05 g/cm^3 – 2.10 g/cm^3)
KFB1 (2.10 g/cm^3 – 2.15 g/cm^3)
KFC1 (2.15 g/cm^3 – 2.20 g/cm^3)

The high-density fractions have well-ordered onion like graphite rims which contain “slow neutron process” isotopes, indicating formation in AGB stars after dredge-up of carbon formed within the star’s interior and low-density fraction contains disordered graphite that signified the origin of supernovae [27]. These micron-sized particles were extracted by University of Chicago’s Murchison-KFC1, and “sliced up” at Washington University St. Louis were used for this study. Those samples were examined by diffraction and electron phase contrast (lattice) imaging using the 300kV Transmission Electron Microscope (TEM) at University of Missouri St. Louis as shown in Figure 1.9.

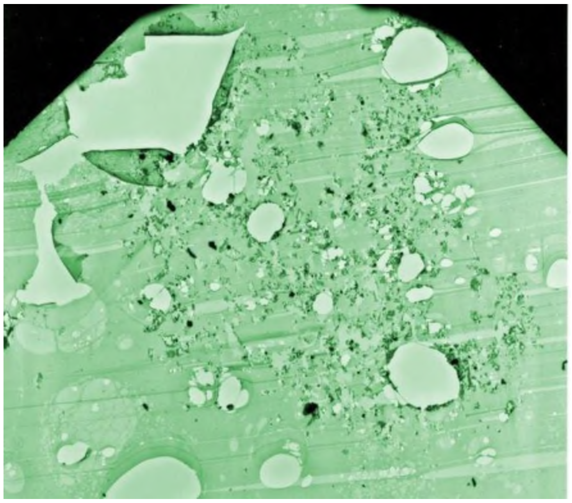

Figure 1.9. TEM image of KFC1A:7E of presolar onions taken by EM430ST TEM in William L. Clay Center for Nanoscience at University of Missouri St. Louis; Source: P. Fraundorf, UMSL wiki.

These micron-size particles in the high density (KFC1) fraction with frozen liquid cores & graphite onion rims shown in the Figure 1.10.

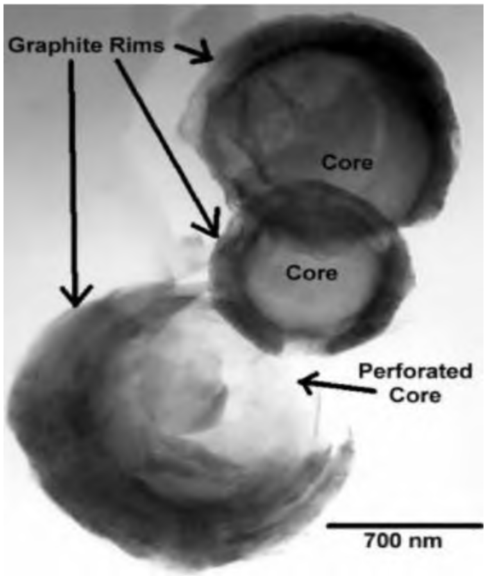
Graphite Rims
Core
Core
Perforated Core
700 nm

Figure 1.10. Pre-solar carbon core/rim particles; Source: UMSL wiki-Refrence:3

These structures have demonstrated evidence for randomly oriented onion-like graphitic rim particles formed by the condensation of super-cooled carbon droplets from the vapor phase. The electron powder diffraction patterns of a selected area of these particles showed that the cores contain unlayered graphene sheets, with 40 Å coherence widths. The lattice imaging confirmed and suggested that these sheets are a part of faceted pentacones [3-5].

The Figure 1.11 below is the composite illustration of the research work done in UMSL about presolar onions.

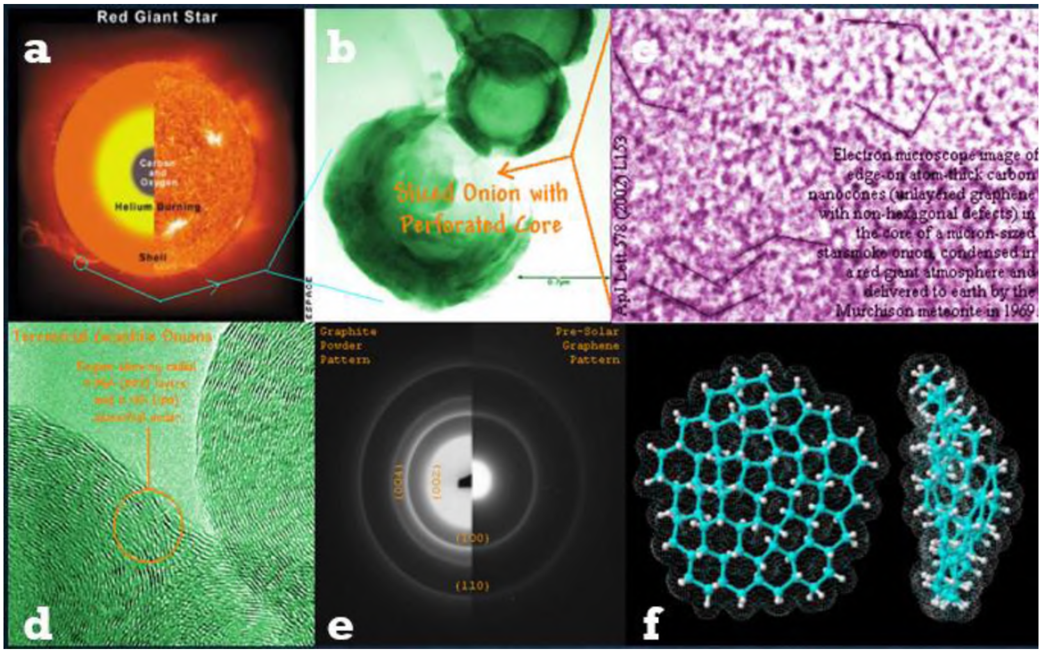
Red Giant Star
a
Carbon and Oxygen
Helium Burning
Shell
b
Sliced Onion with Perforated Core
0.7µm
ESPACE
c
ApJ Lett 578 (2002) L153
Electron microscope image of edge-on atom-thick carbon nanocones (unlayered graphene with non-hexagonal defects) in the core of a micron-sized starsmoke onion, condensed in a red giant atmosphere and delivered to earth by the Murchison meteorite in 1969.
Terrestrial Graphite Onions
d
Graphite Powder Pattern
Pre-Solar Graphene Pattern
(004)
(002)
(100)
(110)
e
f

Figure 1.11. Road map of red giant stars to unlayered graphene in the lab; Source: UMSL wiki-Reference:3-5.

Figure 1.11b. shows the sliced core-rim presolar graphite onion extracted from Murchison meteorite and 1.11c. is the high-resolution TEM image of intersecting line segments of edge-on graphene sheets. These line segments are around 2-5 nm long. The intersection angle between 39' - 65' degrees. As seen in Figure 1.11e, the electron diffraction pattern shows only hk0 spacings and also a very strange absence of graphite layering lines (absence of 002 layering). It also indicates a comparison between graphite and unlayered graphene patterns. The graphite layering within the wall of graphite onions shown in Figure 1.11d. and Figure 1.11f. represents the effect on the flatness of the graphene sheet in the presence of pentacones.

Figure 1.12 provides an example configuration of faceted pentacones from the side created by Jmol software. Previous laboratory studies reported these types of core-rim and core-only particles synthesized in an "evaporating carbon oven" with much smaller graphene-sheet coherence widths around 1 nm [3-5].

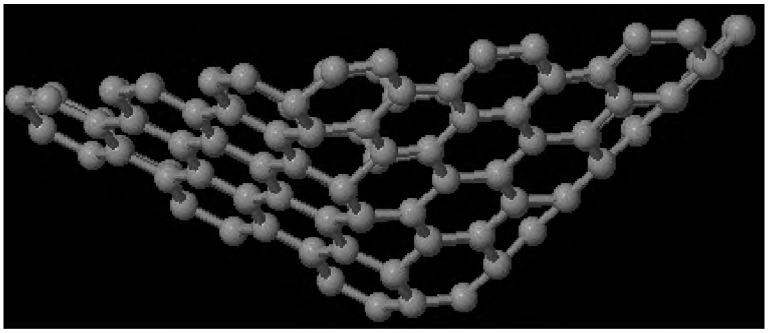

Figure 1.12. An example configuration of faceted pentacones; Source: P. Fraundorf - UMSL wiki.

1.2.2. Density Estimation of Unlayered Graphene. Figure 1.13 below shows the relationship between the mass density of the elemental carbon phases versus nearest neighbor distance. The density range for liquid carbon lies between 1.2 g/cc - 1.8 g/cc as shown in figure.

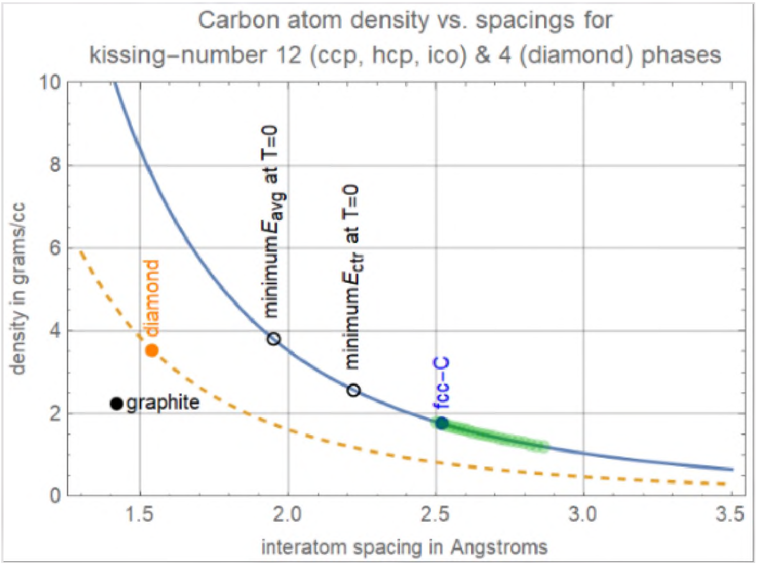

Figure 1.13. Density vs. inter-atom spacing for elemental carbon phases; (i). orange dashed: tetrahedral diamond fcc arrangement, (ii). dark blue: coordination 12 cubic close pack of fcc-carbon and icosahedral symmetry of clusters in liquid carbon, (iii). liquid carbon. Source: P. Fruandorf, UMSL wiki

Experimental studies report the density estimation is around 1.8 g/cc end for unlayered graphene found in the core of presolar core-rim graphite onion [2, 12, 28].

1.3. OUTLINE OF THE DISSERTATION

The research work introduces a study of nucleation of carbon material in different stages using density functional theory. The DFT calculations are performed using a simulation tool called Vienna ab initio simulation package (VASP). Section 2 summarizes the theoretical background of density functional theory that categorizes into three sections such as 2.1. Introduction, 2.2. Vienna ab initio simulation package and 2.3. VASP simulation methods. The discussion of 2.1, 2.2 make a detailed theoretical background of DFT and VASP while Section 2.3 is the methods of calculations.

Section 3 is known as the exploration of VASP computations. This is often more like representing the various calculations we performed using different methods of VASP. There will be separate sections for nine calculations and discuss its results and therefore the accuracy of using such methods in VASP.

The main two sections in this research work are Section 4 and Section 5. Section 4 discusses the study about the nucleation of carbon loops and graphene sheets from a carbon liquid, at low pressure employing a method named as “VASP-direct relaxation”. VASP-direct relaxation method is a calculation technique that relaxes the position of liquid-like carbon atoms in a fixed cubical volume with periodic boundary conditions (supercell). More details are going to be discussed about this calculation method in Section 3. Also, it will be the place to debate the results and therefore the consistency with the previous research reports like inter-atom distances characteristic of covalent interactions, ring size variation, coordination number statistics etc.

Section 5 presents a comparison study of two computational techniques, VASP-direct relaxation vs. ‘VASP re-relaxation’ method. Here, ‘VASP re-relaxation’ is named because VASP relaxes a structure that is already relaxed by another semi empirical computational model. Since it is more sort of a re-relaxation of the system, it is named as VASP re-relaxation technique. Same as in Section 4, during this section it will be discussed about the differences of the results. Specially based on the energy values obtained to test which method can be used to get a better local minimum of energy. Finally, the last section is designated to talk about the conclusions and possible further work based on this dissertation’s research.

2. DENSITY FUNCTIONAL THEORY (DFT)

2. 1. BACKGROUND OF DFT

This section introduces the computational simulation methods used in this research work, and it talks about the importance of such computational modeling for exploring systems that requires extreme experimental conditions. In particular the experimental investigations of the liquid phase of carbon at low pressures are difficult because of its metastability even at temperatures in the 3000K range. Hence, most research studies follow theoretical methods or computational simulations, rather than experimental methods.

Quantum mechanical wave functions provide our best descriptions to date of atomistic behavior. Density Functional Theory (DFT) uses electron wavefunctions to find an approximation of system energy using the many-body Schrodinger equation. This has proven useful for understanding the properties of a large molecular systems.

2.1.1. The Many-body Schrödinger Equation. In solid state physics and quantum chemistry, one of the approaches to study about a given system is solving the time independent, non-relativistic Schrödinger equation. The wavefunction (ψ)contains all the information about the system and solving the Schrödinger equation is possible for a simple 2-D square potential, or even for the Hydrogen atom. But it is hard to solve the Schrödinger equation for many-body systems that include N electrons and M nuclei where i, j represents the electrons and A, B run over the nuclei of the system. The Hamiltonian (H) for many-body systems can be written as,

$$\mathrm{H} = \mathrm{T}\,(\text{kinetic enery}) + \mathrm{V}(\text{coulombic potential}) \tag{2.1}$$

$$H = -\frac{1}{2m_e}\sum_{i=1}^{N}\nabla_i^2 - \frac{1}{2m_n}\sum_{A=1}^{M}\nabla_A^2 - \sum_{i=1}^{N}\sum_{A=1}^{M}\frac{Z_A e^2}{|r_i - r_A|} + \frac{1}{2}\sum_{i=1}^{N}\sum_{j=1, j\neq i}^{N}\frac{e^2}{|r_i - r_j|} + \sum_{A=1}^{M}\sum_{B=1, B\neq A}^{M}\frac{Z_A Z_B e^2}{|r_A - r_B|} \quad (2.2)$$

The first two terms are the kinetic energy of electrons and nuclei. Third term is the electrostatic attraction energy among the electrons and the nuclei, fourth term is the electron- electron potential energy and the last term is the repulsion between nuclei-nuclei.

For a many-body system with '*N*' electrons and '*M*' nuclei, it will be a very hard task of solving the Schrödinger equation. So, some approximations need to be involved in solving the many body Schrödinger equation which is described as DFT.

2.1.2. Static Nuclei Approximation (Born-Oppenheimer Approximations). In Equation 2.2, the mass of nucleus can be considered as much greater than electrons. Based on this fact, the nuclei move much slower compared to the electrons and the kinetic energy is nearly zero. Therefore, the potential energy of nuclei-nuclei is just a constant and this separation of electronic and nuclear motion is known as the Born-Oppenheimer approximation [29]. The new (*H'*) can be rewritten as,

$$H' = -\frac{1}{2m_e}\sum_{i=1}^{N}\nabla_i^2 - \sum_{i=1}^{N}\sum_{A=1}^{M}\frac{Z_A e^2}{|r_i - r_A|} + \frac{1}{2}\sum_{i=1}^{N}\sum_{j=1, j\neq i}^{N}\frac{e^2}{|r_i - r_j|} = T_e + V_{en} + V_{ee} \quad (2.3)$$

2.1.3. Hohenberg-Kohn Approximations. The Hohenberg-Kohn approximations stated that the ground state energy of a system is a unique functional of the electron density that can be obtained variationally [30, 31]. Also, using the electron density instead of solving the many-body wave function directly results fast calculations. Thus, the many-body Schrödinger equation can be simplified in to a one-electron Schrödinger equation.

The answer to the Schrödinger equation with $H_{elec}$is the electronic wave function Ψ_{elec} and therefore the electronic energy E_{elec}.

$$H_{elec}\,\Psi_{elec} = E_{elec}\Psi_{elec} \tag{2.4}$$

$$E_{total} = E_{elec} + E_{nuc} \quad \text{where } E_{nuc} = \sum_{A=1}^{M}\sum_{B>A}^{M}\frac{Z_A Z_B}{r_{AB}} \tag{2.5}$$

The electron density of a system can be written as shown in Equation 2.6 and this manner it eliminates 3N variables and simplifies into three spatial variables (x, y, z).

$$n(r) = \psi^*(r_{1,}r_{2,}r_{3,} \ldots\ldots r_{N,})\,\psi\,(r_{1,}r_{2,}r_{3,} \ldots\ldots r_{N,}) \tag{2.6}$$

As a result, a single electron can be viewed as a point charge with respect to all the other electrons. Essentially, the many electrons are converted to several single electron systems [32]. Therefore, the wavefunction in a single electron is then shortened to,

$$\Psi(r_{1,}r_{2,}r_{3,} \ldots\ldots r_{N,}) = \psi_1(r_1) * \psi_2(r_2) * \psi_3(r_3) \ldots\ldots..\psi_N(r_N) \tag{2.7}$$

Now, the electron density defined as in Equation 2.8 and the total energy as in Equations 2.9 and 2.10,

$$n(r) = 2\sum_i^N \psi_i^*(r)\,\psi_i(r) \tag{2.8}$$

$$E = E\{n(r)\} \tag{2.9}$$

$$E_g\{n_g(r)\} \leq E\{n(r)\} \tag{2.10}$$

The density $(n_g(r))$ minimalizes the energy functional, and its minimum value is the ground state energy (E_g). Two energy functional are contained in this equation: (i) a known energy function (E_{known}) and (ii) an unknown energy function (E_{exc}).

$$E(\psi_i) = E_{known}(\psi_i) + E_{exc}(\psi_i) \tag{2.11}$$

The energy in terms of density looks like,

$$E(n) = E_{known}(n) + E_{exc}(n) \tag{2.12}$$

$$E\{n\} = T_e + E_{ext}(n) + E_{ee}(n) + E_{exc}(n) \tag{2.13}$$

$$T_e = \text{Kohn–Sham kinetic energy} = \sum_{i=1}^{N} \int \psi_i^*(r) \left[-\frac{\hbar^2}{2m_e} \nabla^2\right] \psi_i(r)\ d^3r \tag{2.14}$$

$$E_{ext}(n) = \int V_{ext}(r) n(r)\ d^3r \tag{2.15}$$

$V_{ext}(r)$ is the fixed external potential acting on the interacting system.

$$E_{ee}(n) = \text{Coulomb energy} = \frac{e^2}{2} \int d^3r \int d^3r' \frac{n(r)n(r')}{|r-r'|}$$

We can obtain Kohn–Sham equations by varying the total energy expression in terms of orbitals ψ_i and written as follows (in atomic units) [31].

$$[-\frac{1}{2}\nabla^2 + V_{ext}(r) + V_{ee}(r) + V_{exc}(r)\,]\,\psi_i(r) = E_i\ \psi_i(r) \tag{2.16}$$

$$H = -\frac{1}{2}\nabla^2 + v_{eff}(r) \tag{2.17}$$

This effective potential $v_{eff}(r)$, incorporates both external potentials and electrons interactions that are represented by,

$$v_{eff}(r) = V_{ext}(r) + e^2 \int \frac{n(r)'}{|r-r'|}\ dr' + V_{exc}(r) \tag{2.18}$$

$V_{exc}(r) = \frac{\delta E_{exc}(n)}{\delta n(r)}$ is referred to as the exchange-correlation potential, which is the only unknown term in the Kohn-Sham equation described below and can be approximates using different approximating functions.

2.1.4. Exchange-correlation Approximation. The E_{exc} is known as the exchange-correlation energy, which is equivalent to all many-particle interactions. Using the Local Density Approximation (LDA) it is possible to approximate the E_{exc}. As LDA assumes a homogenous electron gas locally, thus E_{exc} is solely dependent on the density at the coordinates at which the function is evaluated [31,33].

$$LDA:\ E_{exc}(n) = \int d^3r\, n(r)\ \epsilon_{exc}\,(n(r)) \qquad (2.19)$$

$\epsilon_{exc}\ (n(r))$ is the exchange-correlation energy of a homogenous electron gas of density (n). Another form of approximation is known as the Generalized Gradient Approximation (GGA). Consequently, this gradient corrections are more efficient in systems whose electron density is low, for example ionic crystals and covalent crystals.

$$GGA:\ E_{exc}(n) = \int d^3r\, n(r)\ \epsilon_{exc}\,[n(r), \nabla n(r)] \qquad (2.20)$$

The Figure 2.1 below shows the self-consistency loop that DFT uses in solving the Kohn-Sham equations in a problem.

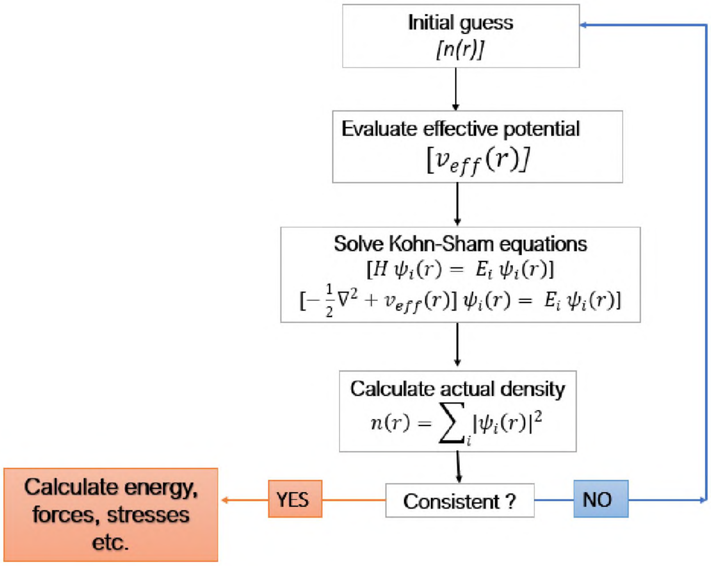
Initial guess
[n(r)]
Evaluate effective potential
$[v_{eff}(r)]$
Solve Kohn-Sham equations
$[H\,\psi_i(r) = E_i\,\psi_i(r)]$
$[-\frac{1}{2}\nabla^2 + v_{eff}(r)]\,\psi_i(r) = E_i\,\psi_i(r)]$
Calculate actual density
$n(r) = \sum_i |\psi_i(r)|^2$
Consistent ?
YES
NO
Calculate energy, forces, stresses etc.

Figure 2.1. Self-consistency loop in DFT.

2.1.5. Periodic Boundary Conditions, Bloch's Theorem and Plane Wave Basis Set.

Supercell is a method of analyzing crystal structures with periodic boundary conditions, used in DFT. As surface atoms dominate bulk atoms in small clusters, the size of a large atomic cluster must be estimated.

Combining limited repeating primitive cells with periodic boundary conditions can achieve this. In this way, the simulation cell is used to model the system's periodicity by creating an artificial periodicity. When a crystal is at 0K, ions arrange in a periodic pattern. The external potential also acts in a periodic fashion on electrons. Therefore, the periodic potential [$U(r)$] as shown in the Figure 2.2 and can be calculated using Bloch's theorem.

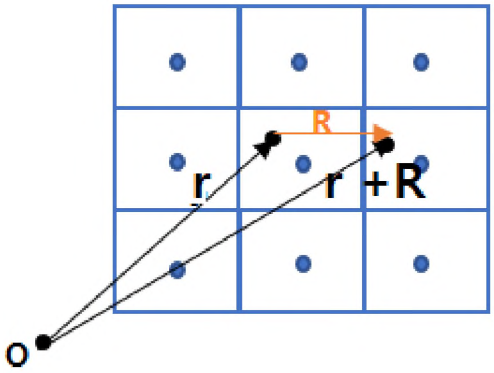

Figure 2.2. Periodic cell.

$$U(r) = U(r + R) \tag{2.21}$$

The wave function of the infinite periodic solid can be expressed in terms of reciprocal space vectors (k),

$$\psi(r + R) = exp(\,ikR)\,\psi(r) \tag{2.22}$$

It can be expressed as periodic function as follows,

$$u(r) = u(R + r) \tag{2.23}$$

$$\psi(r) = exp(\,ikr)\,u(r) \tag{2.24}$$

The Fourier expansion of this would result in a finite number of plane wave sets. Therefore, the term u(r) becomes,

$$u(r) = \textstyle\sum_G u_G\, exp(iGr) \tag{2.25}$$

The terms represent u_G as Fourier coefficients and 'G' as the reciprocal lattice vectors of the crystal. This summarizes the Equation 2.24 as,

$$\psi(r) = \sum_G u_G \, exp \, i(G + k)r \tag{2.26}$$

Now, it is possible to resolve the electronic wave function with k-point sampling since it contains reciprocal vectors instead of an infinite number of electrons within the first Brillouin zone. In reciprocal space, sampling k points corresponds to evaluating integrals for all the possible k (the phase). An electronic wave function is represented by each k point. Assuming a continuum plane wave basis set, the basis set calculation in real space will be infinite. Thus, it can be expressed as a discrete plan wave basis set and add up the sum of all k-points in the first Brillouin zone. $\frac{\hbar^2}{2m_e} \, |k + G|^2$ is the discrete kinetic energy associated with Fourier coefficients (u_G). In a plane wave energy cutoff, the basis will be set to a finite value, but this can sometimes lead to errors in the total energy. A higher energy cutoff is needed to solve this issue or, to put it another way, increasing the number of k points will result in a more accurate calculation.

2.1.6. Projector Augmented-Wave Method (PAW Method). To reduce the numerical effort, DFT-based computations use pseudopotentials to keep the core electron frozen. Because the electron wave functions oscillate at an incredibly rapid rate since the kinetic energy of electrons near the nucleus (core) is so great. Therefore, this complicates the Schrödinger equation and using plane wave basis set for expanding the wave functions would not be the best technique for getting accurate results using a large number of Fourier components. Accordingly, in the pseudopotential approach, the core electron is treated as frozen and replaced by a smoother potential that can be represented using plane waves instead of the strong nuclear potential.

It is the valence electrons that have a greater impact on a physical system than the core electrons. Using this method, we can approximate this without compromising accuracy. In this way, reducing Fourier components leads to a faster calculation.

PAW method was developed by Blöchl in 1994 and transforms the true (real) wave function (ψ) into imaginary wave functions (φ) near a nucleus to solve oscillation wave function problem. It combines all imaginary wave function components into a basis set to determine the properties that correspond to these imaginary wave functions [34]. The transformation can be written as follows,

$$|\psi> = \mathcal{T}\,|\varphi> \tag{2.27}$$

$$\mathcal{T} = 1 + \sum S_R \tag{2.28}$$

S_R refers to the local transformation operator in atomic region R. For isolated atoms, S_R can be defined in terms of solutions (ϕ_i) to the Schrödinger equation. And it is possible to transform this partial wave functions (ϕ_i) into an imaginary wave function (φ). Therefore, around each atom, the real wave function,

$$|\psi> = \textstyle\sum_i c_i\,|\phi_i> \;\; ; \; i \in R \tag{2.29}$$

During the calculations, the core electron is taken into account separately since they are frozen. These partial wave functions contain only valence states which are orthogonal to core wave functions, and which serve as a basis set near the nucleus. In the new framework, partial wave functions can be derived by linearizing pseudo partial wave functions $\widetilde{\phi}_i$.

$$|\phi_i> = (1 + S_R)\,|\widetilde{\phi}_i> \tag{2.30}$$

$$|\phi_i> - |\widetilde{\phi}_i> = S_R\,|\widetilde{\phi}_i> \tag{2.31}$$

Based on the mathematical steps presented in references [34, 35], we can formulate the transformation operator as in equation 2.32 where $< \rho_i|$ is called the projection functions.

$$\mathcal{T} = 1 + \sum_i(|\phi_i > - |\widetilde{\phi_\iota} >) < \rho_i| \tag{2.32}$$

Pseudo partial wave functions $(\widetilde{\phi_\iota})$ can be expanded locally from any imaginary wave function. As a result, the real wave function can be written as in equation 2.33 when $< \rho_i|\widetilde{\phi_\iota} > = \delta_{i,j}$ and $c_{i=} < \rho_i|\varphi >$

$$|\psi > = |\varphi > + \sum_i(|\phi_i > - |\widetilde{\phi_\iota} >) < \rho_i|\varphi > \tag{2.33}$$

With this information, we can calculate electron density, expectation values, and total energy function $(E[\psi_n])$. Additionally, we can solve for the electronic ground state by minimizing the total energy functional [34,35].

Our computations based on the PAW-GGA pseudopotentials provided by DFT based VASP model [34]. Pseudopotentials derived from PAW-GGA are considered to be much more accurate than ultra-soft pseudopotentials [36,37]. Because radial cutoffs used in this case are smaller, so the energy cutoffs and basis sets are bigger. Furthermore, PAW creates wave functions that are exact for all nodes in the core area.

2.2. VIENNA AB INITIO SIMULATION PACKAGE (VASP)

The VASP model is an example of a computational quantum mechanical model developed by a group of scientists at the University of Vienna to solve the quantum problem for materials by utilizing DFT [38]. In the following chapters, we will present calculations that were performed using the VASP model. The objective of this section is to explore the VASP calculation methods that we used in order to conduct the simulation.

During VASP simulations, the input and output files contain information about how the computations are performed. The VASP input parameters describe how simulations are performed using the algorithms and these tags are populated in the files used in VASP. The four main input files required by VASP while performing a calculation are listed below.

2.2.1. POSCAR Input File. All atomic positions and lattice parameters as well as the scaling factor are included here. Three lattice parameters define the volume of the unit cell, while direct or cartesian coordinates can be used to specify atomic positions. Furthermore, the universal scaling factor specifies the scaling of three lattice vectors and atomic coordinates. Figure 2.3 illustrates what a POSCAR file will look like if its atomic coordinates are displayed in cartesian coordinates.

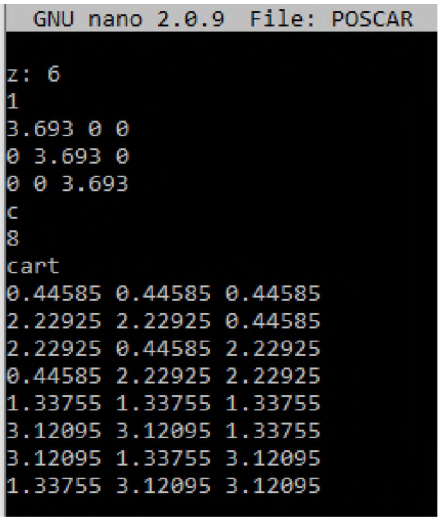

```
z: 6
1
3.693 0 0
0 3.693 0
0 0 3.693
c
8
cart
0.44585 0.44585 0.44585
2.22925 2.22925 0.44585
2.22925 0.44585 2.22925
0.44585 2.22925 2.22925
1.33755 1.33755 1.33755
3.12095 3.12095 1.33755
3.12095 1.33755 3.12095
1.33755 3.12095 3.12095
```

Figure 2.3. POSCAR file example.

2.2.2. INCAR Input File. File that contains the main inputs of the VASP simulation. There are a number of tags (parameters) in this file that determine what type of simulation should be performed and how it should be performed.

Default values are set for most of these tags in VASP, and these are well suited for most computations. Tags such as IBRION, ISIF, ISMEAR etc. determine what and how computational steps should be executed.

In the IBRION tag, the relaxation algorithm specifies how the ions should move. In this computation, we used the IBRION = 2 tag, which refers to the conjugate gradient algorithm. The algorithm relaxes the ions into a ground state that requires line minimization. By varying the ions positions and cell shape in the direction of steepest descent, the energy and forces are calculated from the initial structure marked in POSCAR as the first step. A minimum total energy is then predicted in the second step due to the change in the total energy and the forces. The third step recalculates the forces and energy and is a corrector step. Once the line minimization is sufficiently accurate, move on to the next step. A correction step will be carried out if it does not improve.

An ISIF tag specifies which properties in an ionic system can be changed at initialization. Additionally, it determines whether or not the stress tensor is computed. In this study, most of the simulations were performed by using constant volume or setting up the ISIF tag to ISIF-2 or ISIF-4 according to the calculation requirements. This tag also specifies degrees of freedom that are changeable, such as position, volume, and shape of cells. It is possible to change the ionic position of ISIF-2 tags, but cell shape and volume remain constant. It is possible for both position and cell shape to change in ISIF-4, but cell volume remains unchanged. Consequently, the default value of ISIF used in VASP is 2, which only allows ions to move to relax without changing the shape or volume of the cell. An ISMEAR tag has been used to set partial occupancy values for wave functions. The smearing used was ISMEAR=-1, which is Fermi smearing.

The use of partial occupancies in band structure energy calculations reduces the number of k points required.

2.2.3. K-point Input File. The k-point grid and its details, including the number of k-points, the coordinates, and the method of generating the mesh are described in this file as shown in Figure 2.4. The Brillion zone is sampled by these k points. In order to achieve good convergence, choosing an appropriate k-point mesh is very important. The mesh used in most of our computations was generated automatically by VASP called the Monkhorst-Pack. Through this method, the Brillouin points are evenly distributed across the mesh. Meshes that are denser ensure that models are more accurate [39].

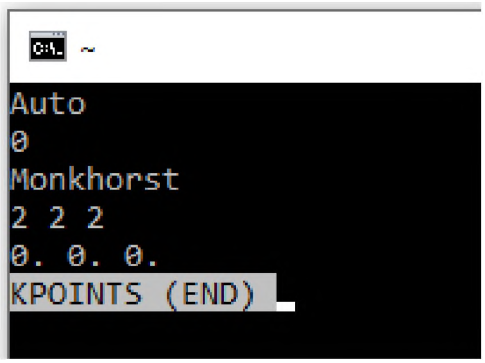

```
Auto
0
Monkhorst
2 2 2
0. 0. 0.
KPOINTS (END)
```

Figure 2.4. K-point file example.

2.2.4. POTCAR Input File. Pseudopotentials for all the atoms specified in the POTCAR file. This file contains the relevant information required for a calculation, including atomic mass, energy cutoff, number of valence electrons, and how to generate a pseudopotential. As the POSCAR file contains the different atomic types, the pseudopotentials must also be in the same order as the atomic types in the file.

Below is a list of few VASP's main output files. In this project, the data from most of these files will be gathered for analysis.

2.2.5. OUTCAR Output File. The main and one of the longest VASP output files. In addition to giving a description of the force acting on the atoms, the output shows the energy tensor, as well as the parameters entered.

2.2.6. CONTCAR Output File. The file contains the results of the run including the updated geometry data such as the positions of the ions and the lattice parameters. There is no difference in the format of CONTCAR and POSCAR files. Once a run is completed, both the CONCAT and POCAR files are updated. In this file, the position of the last ionic step was stored.

2.3. VASP SIMULATION METHDOS

For this project, there have been two main types of VASP simulations called "Static structure method" and "Relaxation method".

2.3.1. The Static Structure Method (N1-Method). Using this method, the total energy of a system can be calculated without changing the positions of its atoms. Hence, after the calculation is performed, all atom locations will remain the same. The purpose of this is basically to estimate an approximate amount of energy of a system before it begins to relax. VASP calculates the forces between every atom in the crystal and constructs the force constant matrix in this calculation. Using this force constant matrix, one can calculate the normal modes of any wavevector. According to Section 2.2.2, a constant cell volume and shape is maintained in this method by including ISIF-2 tags in the INCAR input file. The other settings are the same as described in Section 2.2.2.

2.3.2. The Relaxation Method. In the relaxation method, atomic systems' energy is lowered by finding their optimal positions using conjugate gradient algorithm. Atoms are moved around in the volume given and find the position that minimizes the system's energy. As a method of finding local minima using DFT-VASP, this one gives the most accurate energy calculations. Our computations have been based on different ISIF tags settings as discussed in Section 2.2.2 depending on the atomic system and the calculation requirement (e.g., cubic cell with periodic boundary conditions (supercells) or isolated cluster (finitary system). As well, K-points differ based on the calculations required. Also, the number of k points varies with size of a cartesian cubic cell.

3. AB INITIO STUDIES OF NANO CARBON STRUCTURES

3.1. THE IMPORTANCE OF VASP EXPLORATIONS

The general methods discussed in Section 2 are used in this section to explore carbon-based systems more generally, and also to test the accuracy of such methods in VASP. In this as well as subsequent chapters, our calculations will be discussed in technical detail (input parameters, type of boundary conditions etc.). The focus in Section 3 is discussing the exploration calculations performed in the beginning of this project. In addition to learning about the method itself, we will also report on unexpected insights gained about the stability a C-28 fullerene with a central carbon atom, and about the stability of a previously-proposed non-diamond face-centered-cubic carbon phase.

3.2. VASP COMPUTATIONS IN CARBON 5-ATOM CHAIN

Figure 3.1 shows a carbon chain composed of five carbon atoms arranged to create a "redirection angle" of approximately 50-75 degrees.

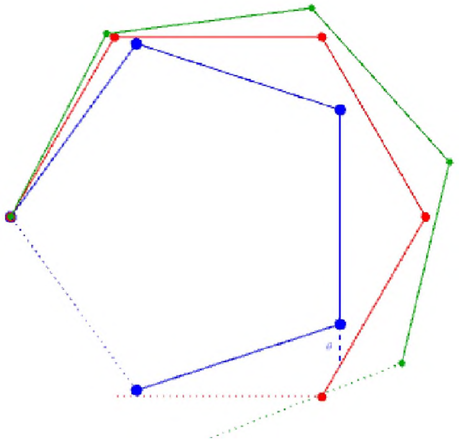

Figure 3.1. 5-carbon atom chain with redirection angles.

The bond lengths are fixed at 1.45Å or set to their minimum energy value. The insertion of a sixth carbon atom from the liquid is possible when the redirection angle at each carbon atom is about 60 degrees. At 72 degrees, however, there is a nice local energy minimum occurring when the pentagon becomes closed, when the chain gets past the barrier created by ongoing folding. The green line represents the low energy position, increasing to a red "6-fold" 60-degree position with a redirection angle of 55.25 degrees. At a redirection angle of 72 degrees, the blue closed-pentagon position appears. Based on the fraction of chains that reach the 5-atom closure, pentagonal graphene sheets might be distinguishable from hexagonal sheets. Each of these will then grow into pentacones and flat sheets, respectively.

The first exploration calculation compared these facts using DFT-VASP to a semi-empirical model called Tersoff [40-42]. The plot at Figure 3.2 below shows minimum energy spacings and energy as a function of redirection angles for 5 atom carbon chains, using Tersoff's model. In the simulation, a dashed line indicates when the distance between its standard "abrupt interaction cutoff" of 1.95 Å is moved to 2.3 Å. The Tersoff barrier to pentagon closure is lower than that of hexagon, given that pentagon settlement has a higher chance of survival than hexagon settlement. The 5-atom chains must exceed the height of the energy barrier that exists between open chains (55 degrees) and closed chains (72 degrees) in order to become a complete loop. By bending a 5-atom chain from its preferred bend, Tersoff shows an energy barrier of 1.29 eV for creating a pentagon from a hexagon that lacks one atom (Figure 3.2.b). Energy and spacing are both increased by passing through the pentagonal closure. Because the fixed redirection angle causes the atom 5 to be too close to the atom 1 due to the Pauli exclusion principle.

There is a minimum energy atom spacing of 1.47 Å, 1.453 Å, 1.49 Å reports at various angles of 55.25, 60, and 72 degrees (Figure 3.2.a). Based on this information, it appears the closed pentagon bonds should be around 1.5Å.

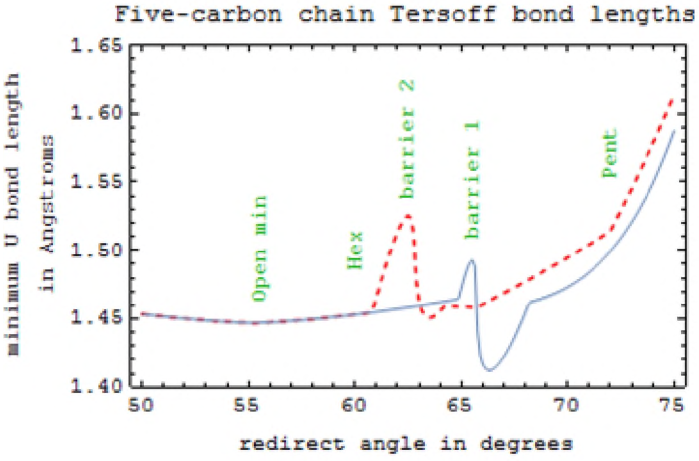

(a).

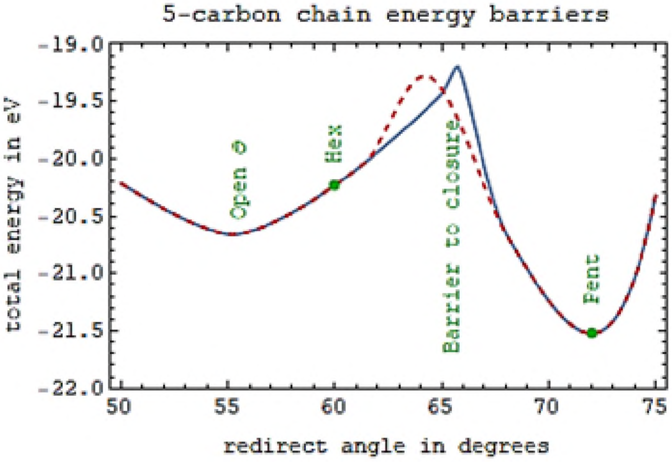

(b).

Figure 3.2. Minimum energy bond spacings (a), and energy (b) in relation to redirection angle; Source: P. Fraundorf, UMSL-Wiki.

A VASP simulation has been performed using the static structure method as in Section 2.3.1 with the ISIF tag 2. Figure 3.3 compares the two models of 5-atom closure.

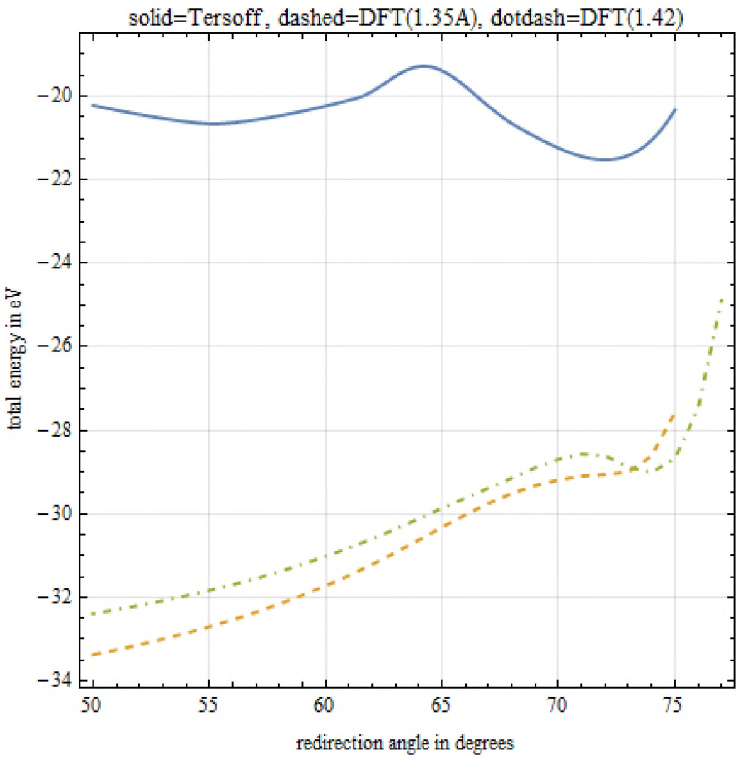

Figure 3.3. 5-atom chain closure comparison between VASP and Tersoff models.

VASP curves for the 5-atom chain closure appear to shift towards larger angles, rather than 72 degrees at the minimum. Additionally, the minimum creates a barrier. According to Tersoff, the closed pentagon bond length should be something closer to 1.5 Å, so the following calculation did the same thing, but with an even larger spacings.

VASP testing results are presented in Figure 3.4 as a comparison of energy levels versus redirection angle when different bond spacings are used. DFT-VASP calculations for extended bond spacings are shown in Figure 3.4 starting from 1.35Å to 2 Å with redirection angle from 60 to 80 degrees. Both these figures illustrate that the energy minimum shifted towards lager angles from 72 degrees as the bond spacing increases.

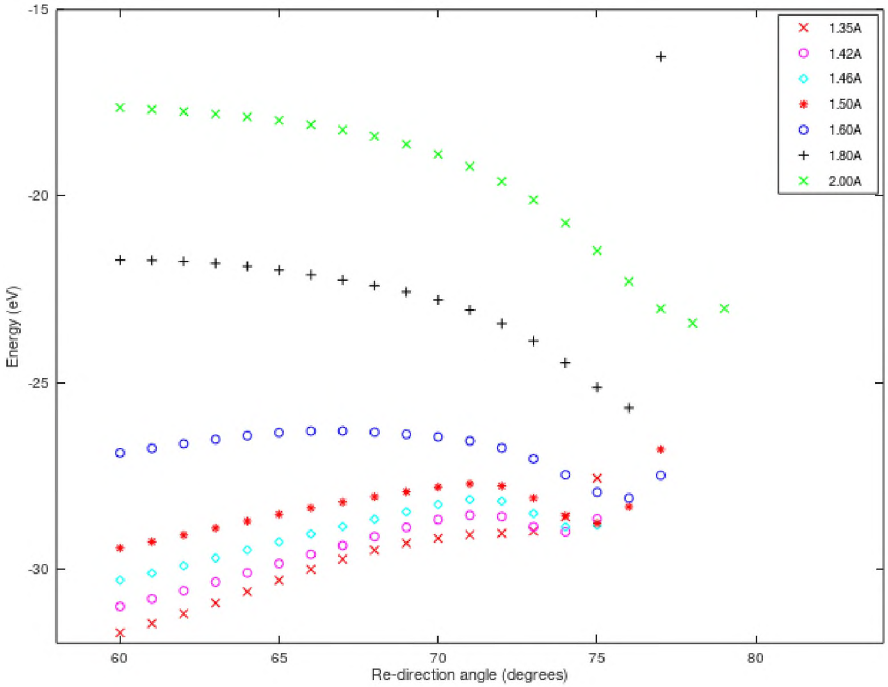

Figure 3.4. VASP total energy vs. redirection angle for 5-atom chain in different bond spacings.

The closing cost or "closure energy" may be lower for longer bonds. The presence of "liquid atoms" suggests that greater bonds are formed when there are more nearest neighbors. The following Table 3.1 shows the energy difference between 5-atom chain nucleation at different bond spacings. Energy difference (dE) to the pentagon nucleation is equal to Energy (at 60') – E (at minimum). Therefore, we want to find what bond length gives us the lowest dE. These numbers show us the barrier to 5-atom ring-closure getting smaller for bond lengths from 1.34 Å up to 1.60 Å. Comparing these results, we can see when the spacing increases, the redirection angle recorded for minimum energy is shifted from 72' to 75'. The dE to the pentagon nucleation was increased when the spacing is increased. The bond length for the minimum dE was at 1.34 Å according to this data table.

Table 3.1. Closure cost (eV) for different bond spacings in 5 atom chain closure

Bond spacing (Å)	Minimum angle (degrees)	$(Energy_{@\,60\,degrees} - Energy_{@\,minimum})$ (eV)
1.34	73	-2.72161
1.36	73	- 2.61017
1.38	73	-2.44922
1.40	74	-2.29299
1.42	74	-2.00232
1.44	74	-1.71364
1.46	74	-1.42856
1.50	75	-0.66495

If the angle of redirection becomes 60 degrees, a carbon atom from the liquid or say the 6th carbon atom can be inserted into the 5-atom chain structure and create a hexagonal structure. The spacing which gave the smaller dE which was 1.34 Å, should have a minimum that makes a pentagon structure at around 72' (in this case 73'). However, it is too early to make solid assumptions at this point. Therefore, we performed the next step of the calculation as shown in the following Section 3.3.

3.3. ENERGY COMPARISON FOR CARBON 5-ATOM AND 6-ATOM CHAINS

This calculation was performed to find out how much energy it would take to close a chain of 5 carbon atoms that had formed in the melt. The two possibilities for these 5-atom chains when they are moving towards the closure are: (a) inserting another carbon atom from a liquid or (b) enlarging the pentagon by passing the energy barrier. The Tersoff energy comparison study shown in the Figure 3.5 below.

It is the energy comparison of creating a 5-atom loop by closing the 5-atom chain vs. creating a 6-atom loop by adding an addition atom to the 5-atom chain. As in the cooling history of individual core-rim particles in red giant stars, one of the goals is to understand the ratio between graphene sheets that form on pentagons versus hexagons.

In this case, the insertion of the sixth carbon atom from the liquid results in the formation of a hexagon at an angle of 60 degrees. For a pentagon to be created at 72 degrees, there is a 1.29 eV energy barrier to overcome.

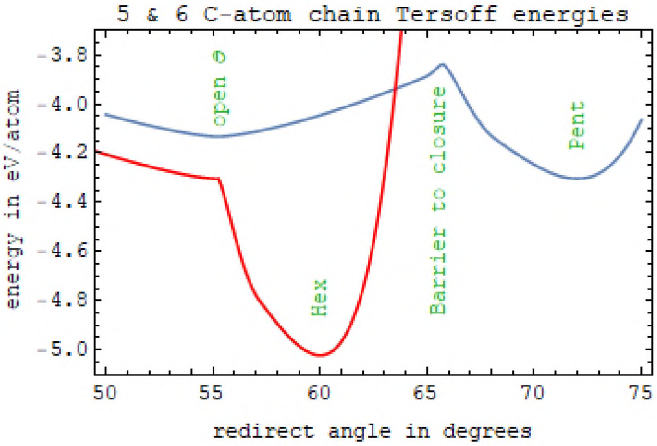

Figure 3.5. An overview of the average Tersoff energies for 6 (red) and 5 (blue) carbon chains based on redirection angles; Source: P. Fraundorf, UMSL Wiki

A similar calculation was made by VASP at 0K temperature to see how it compares to specific energy calculations. In this study, the static structure method was used in isolated cluster settings, as described in Section 2.3.1 where the cell shape and volume cannot change during the calculation. As can be seen in the Figure 3.6 below, the results were compared to the Tersoff model. Before beginning the calculation, VASP performed relaxations to determine the nearest neighbor spacing for both closed 5 and 6-atoms.

Using that, the Tersoff model positions at 1.45 Å are rescaled by multiplying all their values by the factor "nearest neighbor spacing /(1.45)". Therefore, the closed pentagon and hexagon energies in VASP will be calibrated to their true minima.

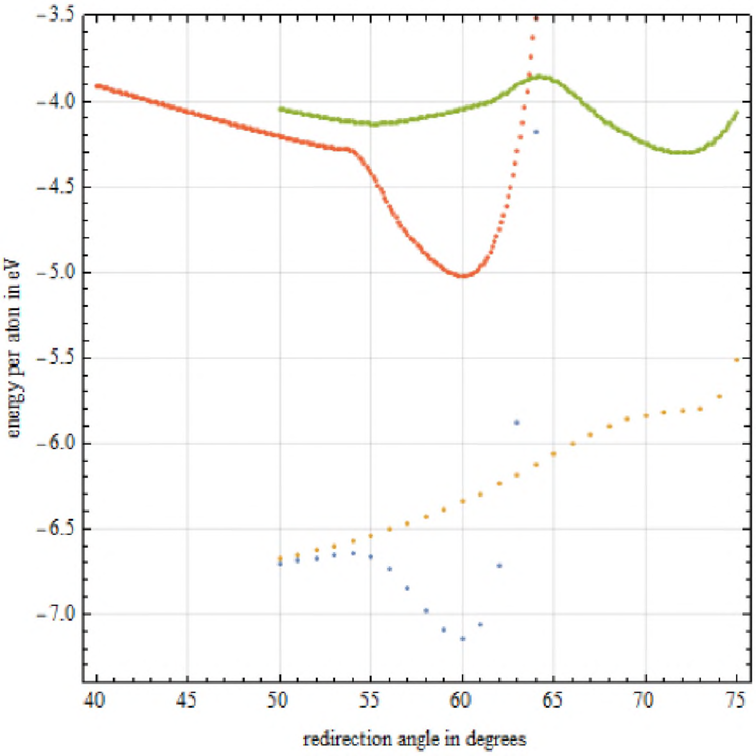

Figure 3.6. Energies with respect to redirected angles; Orange: DFT-VASP 5-atoms, blue: DFT-VASP 6-atoms, green: Tersoff 5-atoms, red: Tersoff 6-atoms
Source: P. Fraundorf, UMSL-Wiki

During relaxation, the rings remain in one plane (fixed z) with the TTF flag set in the POSCAR file. The atom positions for closed pentagon used at 72 degrees and for closed 6-atoms with 60 degrees of redirection angle. According to the VASP output, for a closed pentagon the minimum nearest neighbor is 1.3475 Å, while for a hexagon it is 1.3075 Å. Once all the positions are rescaled, the results are shown in Figure 3.6 in plot form. Carbon atom bonding energies reported are comparable to graphene, which is 7.4 eV.

The energies of the 5-atom chain were around 7.1 eV/atom. These energies are not exactly what Tersoff's model demonstrates, but they clearly indicate the physical structure that was reported by VASP.

3.4. DIAMOND - 8 ATOMS CUBIC SUPERCELL RELAXATION

The purpose of this study is to perform space-filling, periodic-boundary-condition superlattice relaxation at a fixed volume (supercell relaxation), instead of an isolated cluster calculation described in Sections 3.2 and 3.3. Solving these kinds of calculations involves modeling the nucleation of loops in liquids. We relied on them to get an experience with the quantities we will be working with, as well as confirm their correspondence with literature. Throughout this section and the next one, carbon atom arrangements are shown, including an 8-atom diamond carbon cell and a 4-atom fcc-carbon cell. Hence, these methods can be applied to study atom collections of liquids with 12 nearest neighbors ("kissing number 12").

A diamond - fcc cell with a lattice constant of 3.5668 Å was used to perform the first supercell relaxation. In this arrangement, diamond has four nearest neighbors atoms (kissing number - 4), as illustrated in Figure 1.4c in Section 1. For this calculation, VASP used the conjugate gradient relaxation method described in Section 2.3.2 with an ISIF 4 tag. After relaxation, the total energy obtained for this structure was -57.244 eV, corresponding to the energy per atom being -7.156 eV. It is almost the same as the experimental binding energy for cubic diamonds, which is -7.2 eV. The lattice constant for diamond cubic according to experimental literature is 3.567 Å [43].

So, in order to compare our measurements with these numbers, Figure 3.7 illustrates the relationship between energy and volume.

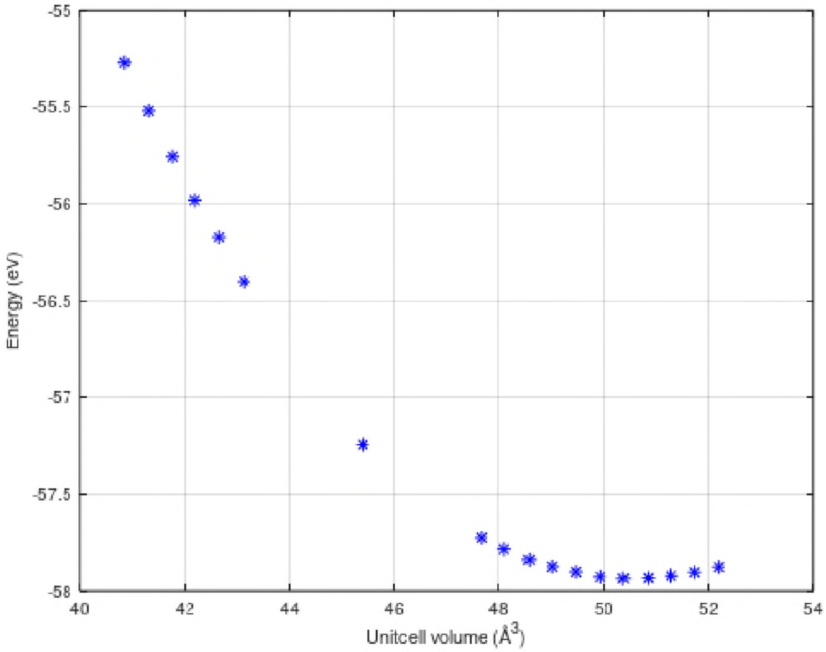

Figure 3.7. Total energy vs. unit cell volume for 8-atom diamond-fcc cell.

The initial volume (Vo) was set as (3.5668 Å) ^3 = 45.38 Å^3 then different volumes were picked with equal plus and minus deviations from Vo. According to ISIF-4 relaxation calculations, the lowest energy was recorded at volume 50.37 Å^3, or 1.11 of Vo, with 3.693 Å as the lattice parameter.

The VASP manual recommends volume changes of 5%-10%, but VASP's minimum value was reported as 1.11 of Vo in our calculation. Thus, the VASP relaxation E vs V curve found the lowest minimum energy at the diamond cubic lattice constant of 3.693 Å in comparison to 3.567 Å. The error between the observed and expected experimental value is 3.54%.

Considering VASP's supercell relaxation approach and experimental data, these results of lattice constant and energy support the conclusion that the first supercell relaxation approach closely matches the experimental results.

3.5. FCC CARBON - 4 ATOMS SUPERCELL RELAXATION

Figure 1.4d in Section 1 shows a symmetry for a noncubic structure that consists of 4 atoms in a face-centered cubic cell. This arrangement only contains a one corner atom and three other atoms on the faces. There is only one corner atom and three other atoms on the faces in this arrangement. Only four atoms fill the unit cell, with each atom having a kissing number of 12. Earlier experiments have reported that the equilibrium lattice constant for fcc crystal structure ranges from 3.539 Å - 3.563 Å [12]. This structure has a metallic-like inter-atom distance of 2.52 Å and a nearest neighbors number of 12. In this phase, the density is about 1.6 g/cc, which is lower than graphite's 2.3 g/cc and diamond's 3.2 g/cc. Accordingly, low density fcc structures allow two times as many atoms to be filled into a single unit cell [44]. The equilibrium lattice parameter for fcc-carbon has also previously been predicted from prior literature using first-principles calculations to be around 3.08 Å [45]. Nevertheless, this is smaller than the experiment reported value of 3.563 Å.

Diamond, by its diffraction pattern, should have only a subset of fcc-carbon spots. Although diffraction patterns with glide-related disallowances often appear in double diffraction. This led to the question of whether the unit cell size proposed before [12] represents the lowest energy configuration. Hence, it could be argued that experimental evidence is suspect in the case of a fcc 4-atom carbon cube.

In other words, the proposed structure as it is nowhere near as stable as diamond's 8-atom cell. Thus, the following calculation is used to test the validity of this claim. To analyse fcc carbon equilibrium scaling, we will produce an energy-volume plot. To calculate the energy of the system, we work with a starting unit cell with a width of 3.582 Å on all four sides and use static structure method described in Section 2.3.1. Following energy vs. unit cell size plot is searching for a local energy minimum as a function of the 4-atom cubic unit cell size for a (non-diamond) fcc structure. The graph in Figure 3.8 shows the determination of a local minimum energy for a (non-diamond) fcc structure based on the unit cell size of four atoms.

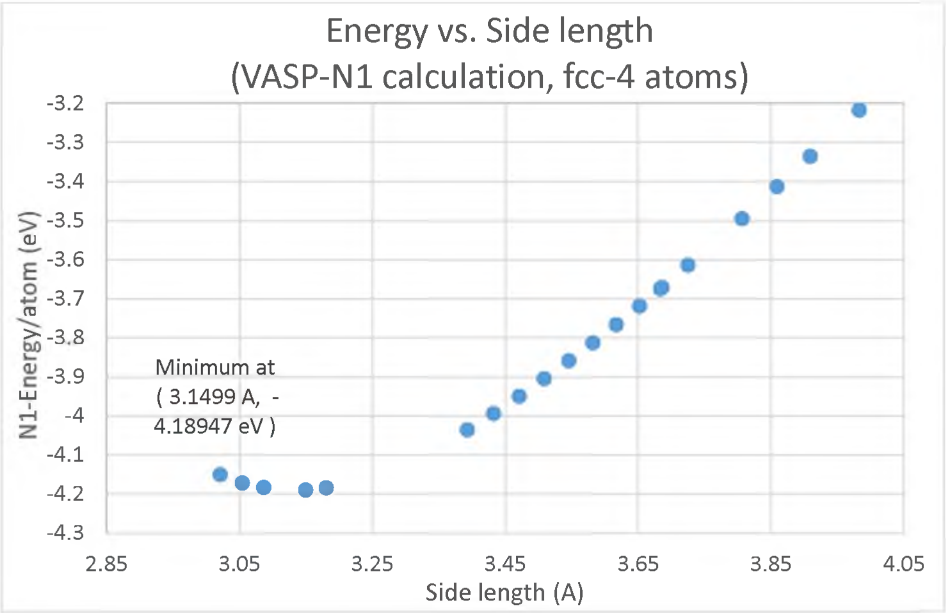

Figure 3.8. Energy per atom vs. side length for fcc - 4 atoms.

The side of the initial cell is 3.582 Å, and the initial volume (V_0) is 45.9597 Å^3. Then the energy was determined in different volumes by expanding the lattice parameters from 3.0212 Å to 4.019 Å.

The minimum energy was reported at 3.15 Å where its value was -4.1895 eV. The VASP results produce contradictory results to those found in literature that indicate an energy minimum at the density reported. Instead, the VASP static structure calculation found a local energy minimum within a density that was higher than what was observed experimentally [12]. As the next step is to ensure that the structure stability (or format of the fcc carbon) remains the same at this energy minimum. This might be able to be checked with a relaxation of the system. In this case, by examining the results of relaxation, it would be possible to determine whether fcc carbon structure is metastable or not at that density.

3.6. STATIC STRUCTURE CALCULATION OF 13-ATOM ICOSAHEDRAL CAGE (ICO-13) AS A FUNCTION OF EDGE-LENGTH

Section 1, Figure 1.4b indicates the most preferable arrangement of liquid carbon atoms is a kissing number-12 with icosahedral arrangement [46]. As shown in Figure 3.9, a liquid carbon atom model can be seen. It was suggested by the Tersoff model to create this icosahedral cage.

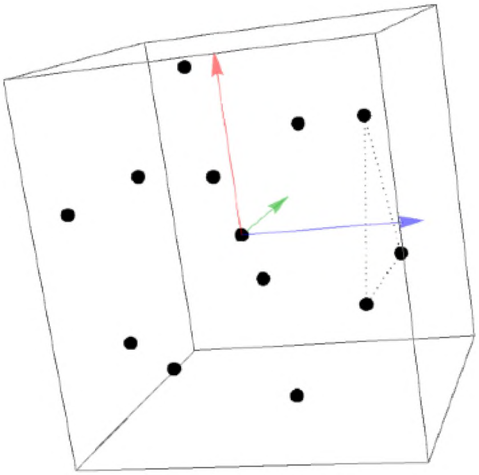

Figure 3.9. The icosahedral cage model for liquid phase atoms of carbon;
Source: P. Fraundorf, UMSL-Wiki

It has been proposed that the nearest neighbour bond distance at minimum energy is about 2Å and the density of 2.2 g/cc is quite high compared to liquid densities of 1.2 to 1.8 g/cc. To study the shape of total-energy as a function of edge-length, a VASP calculation has been performed on this icosahedral cage in this section. It was the purpose of the static structure calculation of ico-13 to investigate the binding energy of carbon atoms in the liquid. This comparison may provide information on how liquid carbon's density varies with temperature. Particularly if the potential has a long asymmetric tail on the long side of the energy minimum, more thermal energy will cause it to spend more time at a greater distance. This could also be useful to investigate the barriers to carbon atom removal during the nucleation of a supercooled liquid phase.

Similarly, to the settings described earlier in Section 2.3.1, the VASP input settings were the same in the calculation. A comparison between the Tersoff and VASP models is shown in Figure 3.10.

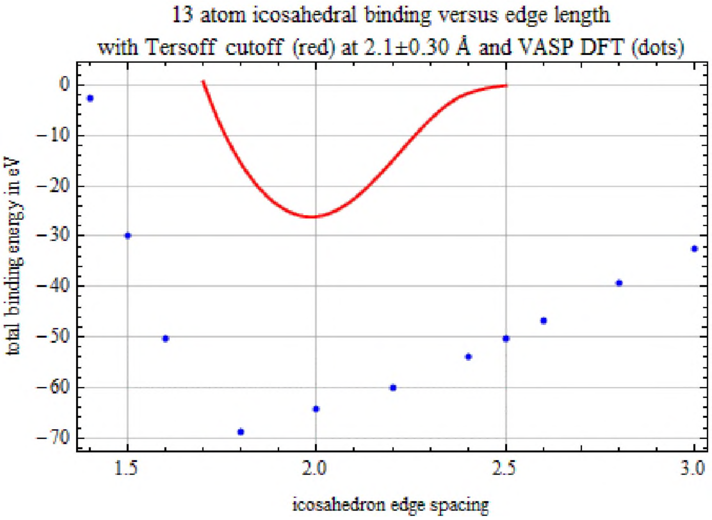

Figure 3.10. The total binding energy for a 13-atom icosahedral cage as a function of edge spacing; Source: P. Fraundorf, UMSL-Wiki

The red solid line represents the Tersoff model's results, while the blue dotted line represents the VASP model's results. Based on the plot, we see a very asymmetric potential well with a minimal energy found at spacings ranging between 1.8-2 Å for both models. There is a discrepancy between the two energy values because the VASP indicates a higher total binding energy than the Tersoff calculation. The VASP calculations at T=0 K indicate that the lowest energy appears to be at about 1.8 Å spacing with an energy of 68.77/13 = -5.29 eV/atom. On the other hand, Tersoff's results are at -27 eV / 13 = -2.077 eV energy with a spacing of 2.0 Å. Despite their differences, both models follow the same pattern in the potential well. Also, it looks like both models indicate that the minimum has moved to larger bond spacings with the increase of number of nearest neighbors. Due to high temperature effects, it is possible to increase the spacings between atoms by 20%, so that these models fall into the density range of liquid carbon (1.2 -1.8 g/cc) [12].

3.7. CENTRAL ATOM BINDING ENERGY AS A FUNCTION OF INTERATOM SPACING FOR ICO-13 AND GRAPHENE-13

This section presents binding energies of central atoms as a function of fixed interatom spacing for ico-13 and graphene-13. In this context, we are mainly interested in determining the bond lengths and binding energies of carbon atoms in a graphene-like setting, for comparison to literature data. The central atom binding energy (E_c) is equal to the difference between the combined and the sum of the separate components' energies. The first step was to calculate the total energy of a 13-atom cluster. Taking out the central atom at (0,0,0) then calculated the energy of the remaining 12-atom cluster. As a third step, determine the energy of the central atom itself at (0,0,0). The final step is to determine the (E_c) with the following equation:

$$\boldsymbol{E_c = E_{13\_atom\ cluster} - \{E_{one\ atom\ at\ (0,0,0)} + E_{12\_atom\ cluster}\}} \tag{3.1}$$

3.7.1. Central Atom Binding Energy Calculation for ico-13. Figure 3.11 shows the average total energy (E_{avg}) and central atom binding energy (E_c) for ico-13 with respect to nearest-neighbor spacing. VASP static structure method has been applied to ico-13's initial structure shown in Figure 3.9.

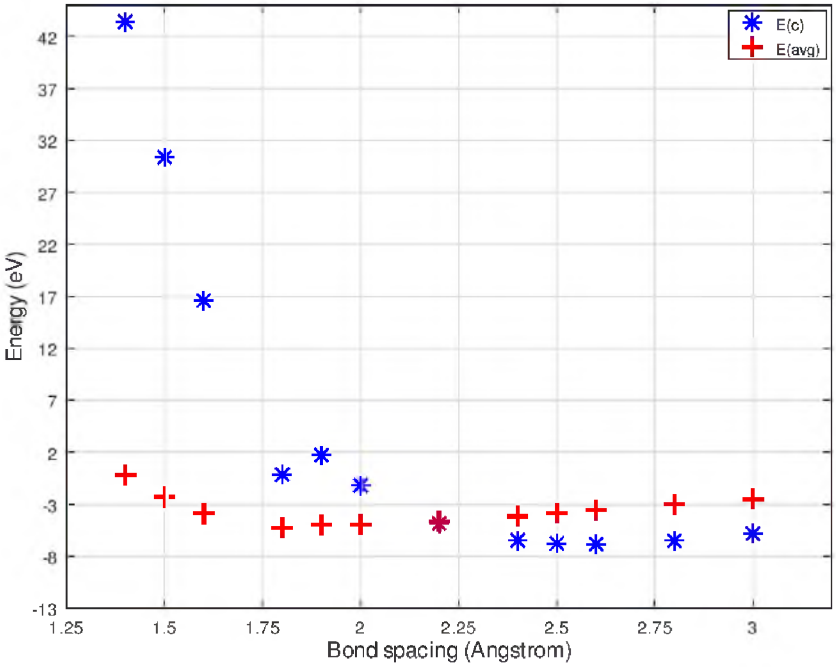

Figure 3.11. Central atom binding energy vs. fixed atom nearest-neighbor spacing for ico-13.

The central-atom binding energies per atom are closer to 7eV and the nearest neighbor spacing moves into a range over 2.5Å (minimum E_c = - 6.8398 eV at 2.6 Å). According to these results, the cluster prefers a bond spacing over 2.5 Å. In other words, the spacing is moved to a range that corresponds to the experimental data of liquid carbon's density.

3.7.2. Central Atom Binding Energy Calculation for Graphene-13. The planar graphene-13 with a 1.42Å bond spacing with 3 nearest neighbors is shown in Figure 3.12. The atoms in this model are arranged in the z=0 plane, moving from the center outward, 1, 3, 6, then 3 atoms. Similarly, to the ico-13, this calculation shows the energies of graphene-13 for various bond lengths. To conduct a comparison against the standard of 7.4 eV obtained from the literature, it would be useful to determine the binding energy of the center atom in the minimum energy atom positions setting.

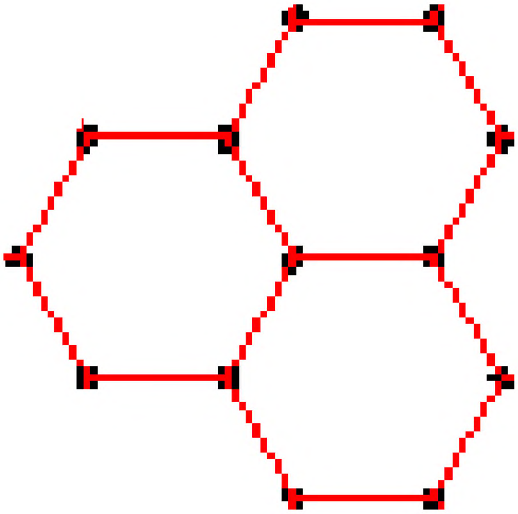

Figure 3.12. Planar graphene-13 structure; Source: UMSL-Wiki

In the Figure 3.13 below is the VASP static structure calculation performed to graphene-13 arrangement to find (E_{avg}) and (E_c) with respect to nearest-neighbor spacings. This plot shows the preferred spacing to be just over 1.4 Å, which is consistent with literature values for graphite and graphene. But the atomic binding energy for the central atoms (minimum E_c = -12.718 eV at 1.45 Å) is different from what we expect at 7.4 eV, as calculated by the static structure calculation method.

We found that both cases reported energy numbers differed from static structure calculations, allowing us to study VASP relaxations which is another approach for our analysis.

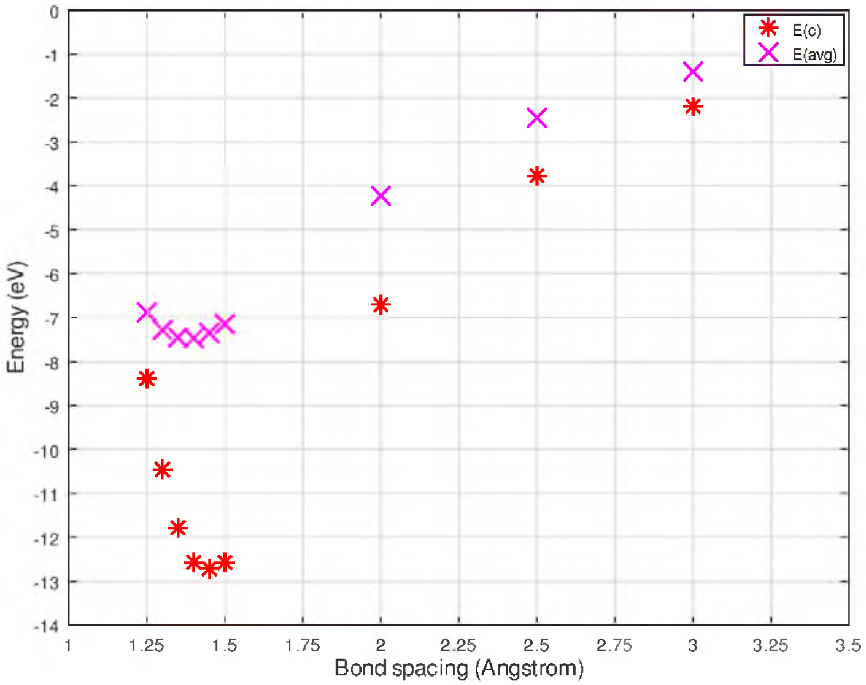

Figure 3.13. Central atom binding energy vs. fixed atom nearest-neighbor spacing for graphene-13.

In order to check whether the binding energy for one bond space (1.42Å) can be closer to, we perform a recalculation using the relaxation method in isolated cluster settings (Section 2.3.2). The energy numbers were obtained after relaxing as follows.

$E_{13\_\text{atom cluster}}$ = - 99. 28733124 eV

$E_{12\_\text{atom cluster}}$ = -99.29715442 eV

$E_{\text{central atom}}$ = -0.19928165 eV

$E_c = E_{13\_\text{atom cluster}} - \{E_{\text{one atom}} + E_{12_{\text{atom}}\text{cluster}}\}$ = -7.79 eV

According to relaxation results, the central atom binding energy is 7.79 eV, which is close to 7.4 eV. This is not a significant difference when compared to the static structure calculation numbers. The energy value here is in agreement with what we would expect from graphene's binding energy. Because, due to the ion-relaxation being able to move the atoms, it will find the optimal position to be as low in energy as possible.

3.8. ENERGY VERSUS VOLUME CALCULATION FOR NON-CUBIC CELLS

In this research, we are not primarily focusing on setting up non-cubic cell configurations. However, the attempt to calculate outside of a cubic cell may be useful to examine our VASP methods through literature comparison. This section discusses two types of cells, such as 2-atom diamond primitive cells and 4-atom graphite hexagonal cells, which are used to determine how energy changes with volume. Due to the fact that a diamond's primitive cells and non-primitive cells results should be the same, the VASP results can be used to investigate literature values as well as to test our method.

3.8.1. 2-atom Diamond Primitive Cell. Figure 3.14 illustrates the two-unit cells for diamond (i) face-centered and (ii) primitive unit-cell. In the primitive unit cell (green), only two atoms are present. The volume of the cell is 11.344 Å^3 with the lattice vectors {2.18421,0,1.26106} Å, {0.72807,2.05929,1.26106} Å, and {0,0,2.52211} Å. Coordinates for the atoms along the long body diagonal are {0, 0, 0} and {1/4, 1/4, 1/4}. The energy vs. volume curve for 2-atom diamond primitive cell performed by using the VASP static structure calculation method. The minimum energy is reported at Figure 3.15 as -18.116797 eV at 11.34 Å^3 volume. According to the experimental 8-atom diamond cubic cell, the volume of 45.3847Å^3 is equal to 3.567 Å side length.

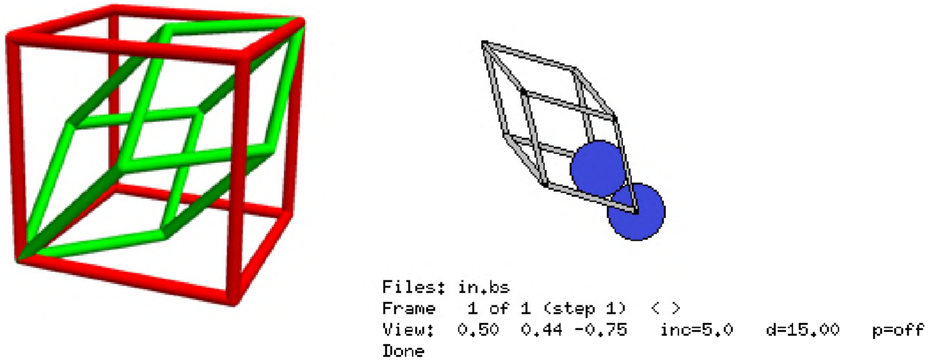

```
Files: in.bs
Frame   1 of 1 (step 1)  < >
View:  0.50  0.44 -0.75   inc=5.0   d=15.00   p=off
Done
```

a.) b.)

Figure 3.14. Unit-cells for diamond; face-centered (red) and face-primitive (green) at left; Source: P. Fraundorf, UMSL-Wiki. VASP visualization of the primitive settings at right.

Dividing that by 4, we would expect the 2-atom diamond primitive volume to be 11.3462 Å^3. Thus, this experimental volume agrees with our numbers, suggesting we are taking the appropriate approach in calculating non-cubic 2-atom diamond primitive cell.

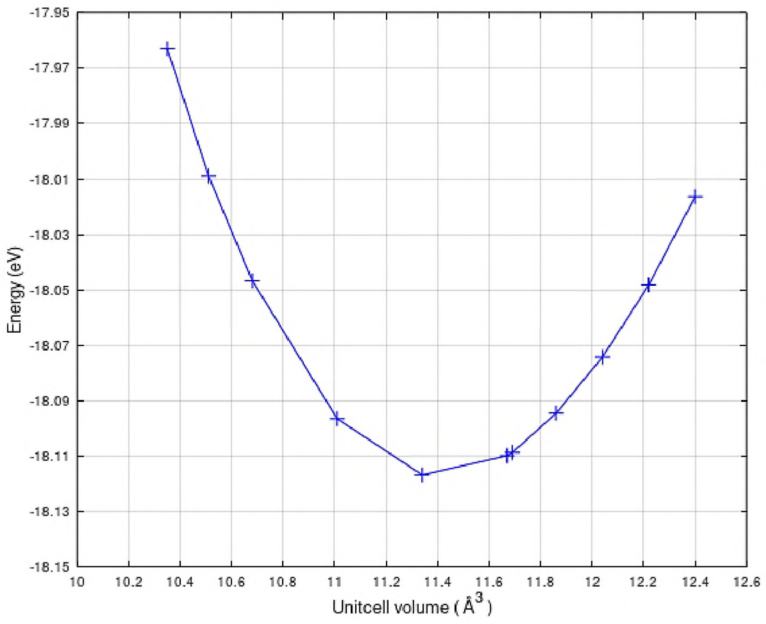

Figure 3.15. Energy vs. volume for 2-atom diamond primitive cell.

3.8.2. 4-atom Graphite Hexagonal Cell. In VASP simulations, to create a hexagonal cell, vectors should be created on each side of the box instead of working down the length of each side of the box as shown in Figure 3.16.

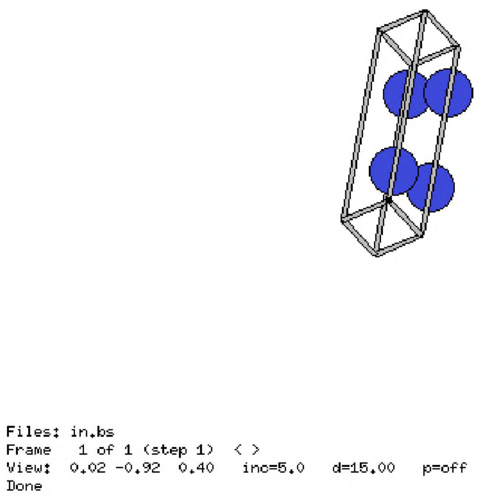

```
Files: in.bs
Frame   1 of 1 (step 1)  < >
View:  0.02 -0.92  0.40   inc=5.0   d=15.00   p=off
Done
```

Figure 3.16. VASP hexagonal cell.

Using this technique, lattice vectors are able to encode angles and lengths. Three particular vectors are used, {2.456,0,0}Å, {-1.228,2.13696,0}Å, and {0,0,6.696}Å. The calculation has performed by using VASP static structure method and energy versus volume curve can be seen in the Figure 3.17 below. The minimum energy -37.8987 eV is reported at the volume of 34.62 Å^3. In comparison to the experimental binding energy of graphite (7.4 eV/atom), VASP's result does not agree with the experimental value. There is a possibility that this disagreement is due to the layered structure of graphite. Due to the sensitive nature of the van der Waals layering, modeling these types of structures to achieve accurate results may be a difficult task for VASP.

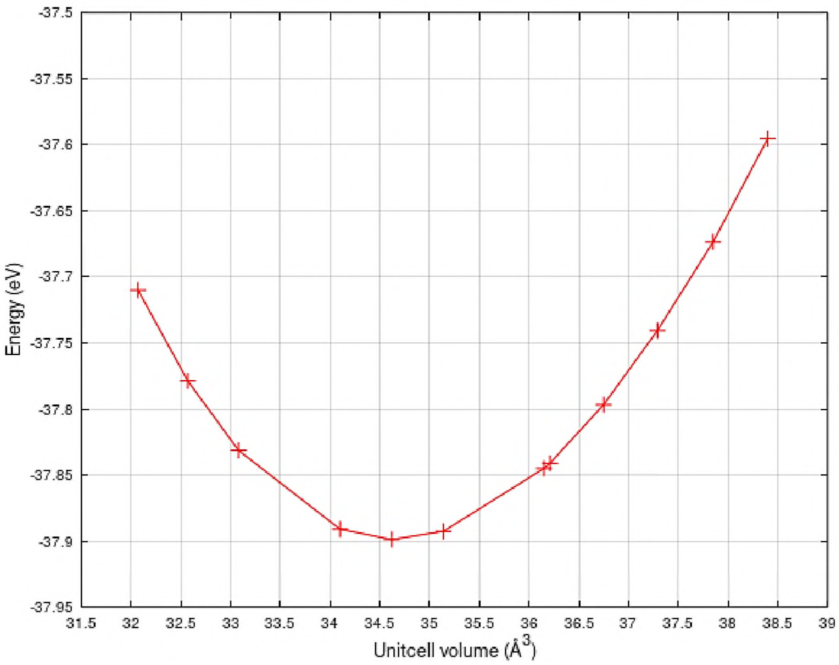

Figure 3.17. Energy vs. volume for 4 atom- graphite hexagonal cell.

3.9. RELAXATION OF TETRAHEDRAL NANO DIAMOND CLUSTER

This section examines the relaxation of a 29-atom tetrahedrally-symmetric diamond cluster as represented in Figure 3.18, with a single carbon atom at the center (nano-diamond).

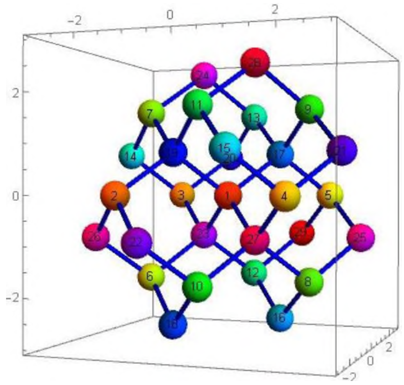

Figure 3.18. Initial configuration of diamond -29 cluster

A cluster like this does not have open ends, and the carbon atom at the center probably feels more or less like it is in bulk diamond. This calculation was performed using the relaxation method described in Section 2.3.2. A larger volume (1000Å^3) was used to prevent periodic boundary conditions for atoms. The relaxation used ISIF-2 tag where the cell volume and cell shape were not allowed to change during the relaxation. Results from the relaxation are shown below in Figure 3.19 and Figure 3.20.

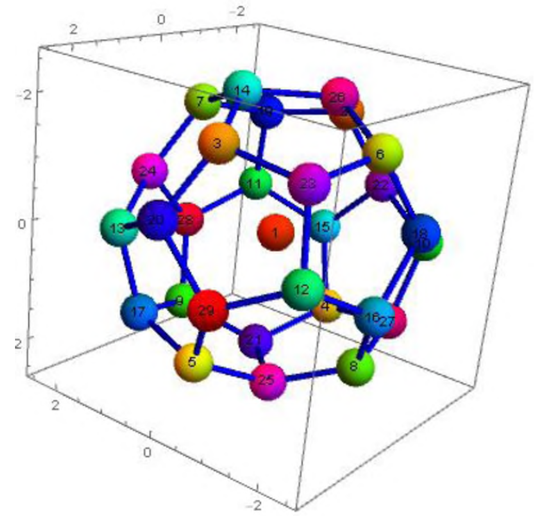

Figure 3.19. Relaxed configuration of diamond -29 cluster.

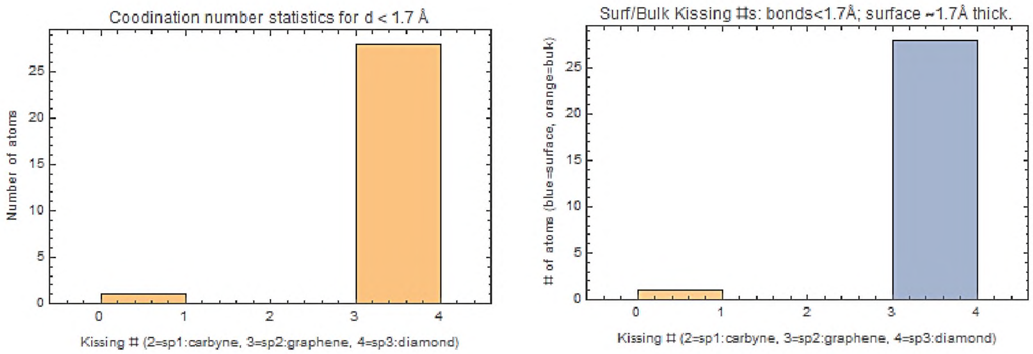

Figure 3.20. The coordination number and the types of atoms in diamond -29 relaxed cluster.

According to Figure 3.20 (plot at right), most atoms are surface atoms (blue) rather than bulk atoms (orange). Additionally, there are 28 atoms with four-fold coordination (sp^3) on Figure 3.20 (left), while one atom is not coordinated. With a carbon atom in the center, diamond-29 appears to have the shape of the smallest and tetrahedral C-28 fullerene [47]. There are 12-pentagons and 4-hexagons, and none of the hexagons touch each other but are separated by pentagons. Our results seem consistent with those earlier reports, since any closed convex combination of hexagons and pentagons must have 12-pentagons and no more or no less [47-51].

Moreover, we measure the distance between the plane of each hexagon and the center carbon atom in order to determine whether it is similar to the distance between layers in graphite. After checking the hexagonal loop connections, we calculate the distance between (0, 0, 0) and each hexagon plane. The distances that were reported between each hexagonal plane and the center alone atom was 2.38 Å and 2.46 Å. The bonding distance tells us how close randomly selected bonds are to each other. Therefore, we check the bonding distances between randomly selected bonds.

e.g., The bonding distance between the 18th and 16th atom is 1.5 Å, between 12th and 16th atom is 1.4 Å and between 29th and 20th atom is 1.5Å.

In turn, this means that the distances are either shorter or longer than the bonding length of graphene, 1.42 Å and rather short compared to the sp^3-bond; 1.54 Å in bulk diamonds [52]. The distance between plane of hexagon and center atom is quite short compared to the graphite layer separation of 3.35 Å. The binding energy per atom in the relaxed structure in Figure 3.19 is -8.04 eV.

In order to check the stability of this structure we conducted another two extra relaxations to calculate the binding energies of (i) asymmetric C-28 (by removing a surface atom) and (ii) C-28 (by removing the center carbon atom).

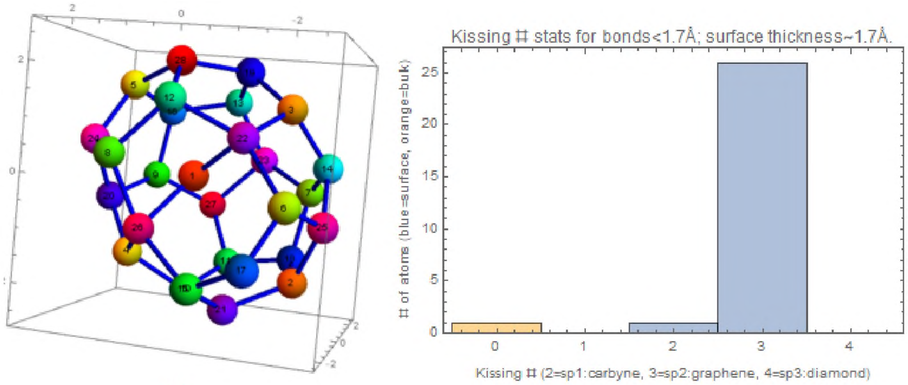

(a).

(b).

Figure 3.21. Relaxed structure and coordination for case (i): asymmetric C-28

As with the C-29 structure above, the relaxed structure of case (i) also has 12 pentagons and 4 hexagons as shown in Figure 3.21.

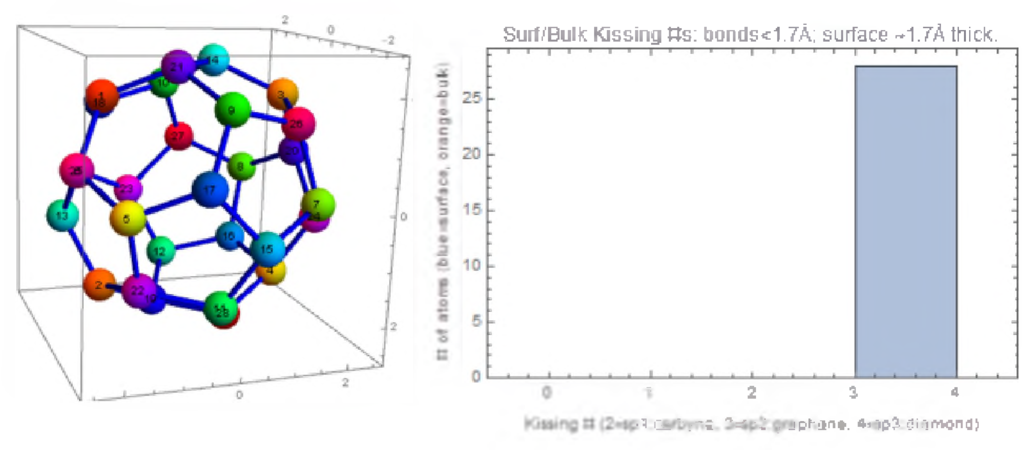

(a).

(b).

Figure 3.22. Relaxed structure and coordination for case (ii):C-28

One difference here is that the central atom (labeled as 1 atom) is connected to a hexagon. Additionally, it does not have a concave surface where the hexagons are not flat. The other difference is that there are two hexagons joined to each other and that all the others are surrounded by pentagons. The total energy is -224.8133 eV / 28 = 8.03 eV per atom. Based on the relaxation of C-28 (case ii: without the center atom of diamond-29) as indicates in Figure 3.22, the binding energy is -233.653/28= -8.34 eV per atom. It is lower than the C-29 and asymmetric C-28. The tetrahedral C-28 structure, without the carbon atom in the center, is therefore much more stable than the asymmetric C-28 structure. In addition, it produces a fullerene that has 12 pentagons and 4 hexagons with all the atoms being surface like with sp2 coordination.

Overall, these observations support the accuracy of the VASP-relaxation method. According to the relaxation results obtained from the VASP method (supercell or isolated cluster), most of the data supports the earlier literature observations.

3.10. SUMMARY OF FINDINGS

Throughout Section 3, we report on exploration studies to test the VASP simulation methods, and which will be most appropriate for our liquid carbon solidification. We mainly use two simulation methods: the static structure method (Section 2.3.1), and a relaxation method (Section 2.3.2). Based on the findings in Section 3, the relaxation method was most consistent with results in the literature. In particular, in Section 3.4 on diamond-8 atom supercell relaxation, Section 3.7.2 on central atom binding energy for graphene-13, and Section 3.9 on relaxation of tetrahedral diamond-29, the results were consistent with earlier literature findings.

Aside from the tests of calculation method, we also examined different conditions, specifically a bulk structures in a cubical box with (supercell) and an isolated cluster (finite system). The isolated cluster approach opens the door to study e.g., of surface reconstructions and perhaps even evaporation, but raises questions about how to define surface, volume, and density. The supercell configuration (e.g., Section 3.4: diamond-8 atom supercell relaxation) is of course more relevant to the problem of nucleation of graphene sheets inside a micron sized droplets of carbon liquid. Hence, this is the method we will focus on in the next section.

4. THE NUCLEATION OF UNLAYERED GRAPHENE IN LIQUID CARBON USING VASP-DIRECT SUPERCELL RELAXATION METHOD AT T=0K AND LOW PRESSURE

4.1. ROAD MAP TO UNLAYERED GRAPHENE

As discussed in Section 1, the liquid form of carbon is only stable at high temperatures and (except possibly in the case of nanoscale clusters) at high temperature. In planetary interiors as well as in diamond-anvil cells here on earth, for example, solid-state forms may transform into liquid phases when exposed to high pressures and temperatures. However some micron-size graphite spheres found in meteorites exhibit isotopic signatures of formation at low pressure in the atmosphere of red giant stars. The core has spherical surfaces that show atom-thick rings of graphene likely formed by solidifying liquid carbon at low pressure [3]. Furthermore, HRTEM imaging reveals [4] that certain randomly oriented (and unlayered) graphene sheets exhibit faceted pentagonal shapes, suggesting that they form from pentagonal loops during solidification. Laboratory synthesis and model studies indicate that these particles can be formed by the slow cooling of carbon vapor in container-less settings [5]. Over the past few decades, graphene study has gained considerable attention in both material science and astrophysics. This section models the nucleation of carbon loops as nuclei for graphene sheets is a solidifying carbon liquid, by allowing the positions of liquid-like carbon atoms to be relaxed, in a fixed cubical volume (supercell).

4.2. COMPUTATIONAL METHODS

VASP-direct supercell relaxations are performed using randomized starting positions of liquid-like carbon atom clusters. As a result of the solidified droplets (later coated with graphite) having similar densities, we used 1.8 g/cc density of carbon in our relaxation calculation [53,54]. The relaxations were performed in a supercell using the Projector-Augmented-Wave (PAW) method [34] and generalized gradient approximation (GGA) for exchange correlation functional [55] at an energy cutoff of 400 eV. As discussed in Section 2.2.2, the ISIF 2 tag was used in VASP relaxations in order to keep the volume and the cell shape as a constant. In ISIF 2 tag configuration, only the ions could change their position since we need to keep the periodic boundary conditions in a constant density 1.8g/cc of carbon in a cubical volume. The following sections provide a detailed analysis of the results.

The simulations are based on a low pressure, 0K temperature, and randomly distributed positions of liquid-like carbon atom clusters. Initially, interatom spacings are greater than 1.9 Å in random collections of atoms. In this case, we are applying the supercell relaxation method described in Section 2.3.2. Section 4.3 includes a listing of all the results broken down by the number of carbon atoms in the cluster, into six subgroups, such as: 13-atom sets (4.3.1), 20-atom sets (4.3.2), 30-atom sets (4.3.3), 40-atom sets (4.3.4), 60-atom sets (4.3.5), and 100-atom sets (4.3.6). Section 4.4 presents an in-depth analysis of the results using various statistical procedures.

4.3. VASP-DIRECT RELAXATION RESULTS

There are several outputs from the analysis program, including connections between atom pairs as indicates in Figure 4.1, loop counts, statistics on coordination numbers, and an interatom distance histogram.

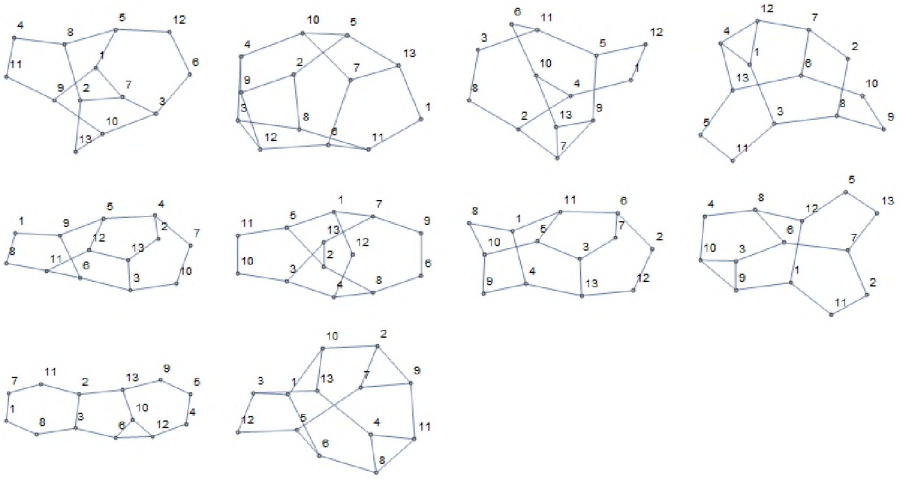
4
8
5
12
11
1
6
9
2
7
3
10
13
10
5
4
13
2
7
9
1
3
8
12
6
11
6
11
3
12
5
10
1
4
8
13
9
2
7
12
7
4
1
2
6
13
10
8
3
9
5
11
5
4
1
9
2
7
12
13
8
11
6
10
3
1
7
11
5
13
9
12
2
10
3
6
4
8
11
6
8
1
5
7
2
10
3
4
12
9
13
5
13
4
8
12
6
7
10
3
9
1
2
11
9
11
13
7
2
5
10
1
8
3
6
12
4
10
2
9
3
1
13
7
12
5
4
11
6
8

Figure 4.1. A network of atom-pair separations smaller than 1.6 Å

In the process of counting loops, we used standard graph theory methods, fitting n-loop coordinates (n = 3 to 7) onto a plane to find the standard deviation. Then, it checks for the flatness of the loop using the result. However, sometimes the program counts fake loops based on the lower rms error for loops than the fit - plane rms error. As a result, the program counts more loops than it actually has (spanning loops). Furthermore, the number of fault loops among hexagons is called a "super loop." Programs tend to count a triangle and pentagon together as a hexagon, especially if they are present together. So, the final loop count table eliminated all these fault hexagonal counts as well as spanning loop counts based on the standard algorithms [56]. The analysis program has reported the results for each of the calculations outlined below.

4.3.1 Carbon 13-atom Sets in a Supercell Volume 144.04 Å^3. The section focuses on the direct relaxation of 20 sets, each containing 13 atoms, over a supercell volume of 144.04 Å^3. The side length of the supercell is 5.242 Å. The analysis presented in this section includes composite interatom spacing plots (Figure 4.2), loop connection diagram (Figure 4.3), and composite coordination number plot (Figure 4.4). The composite plots use different colors for different list identities in the interatom histograms and coordination number histograms. For example, list 1 of 13-atom sets indicated by 'sky blue', list 2 of 13-atom sets indicated by 'powder blue' etc. As can be seen in the coordinate number plot, each bar is labelled with the total number associated with that coordinate number. For example, in this list there are 100 atoms that have 2-fold (sp) coordination.

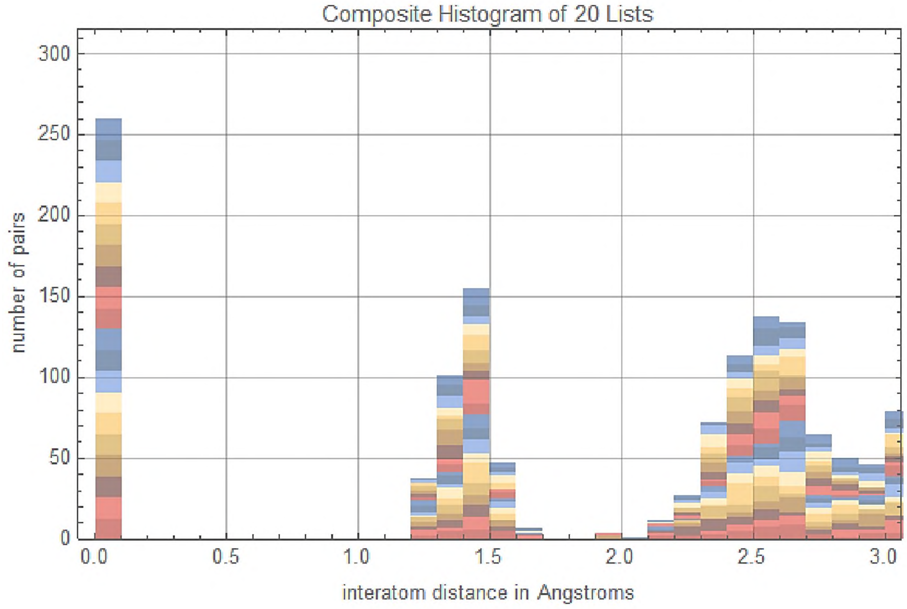

Figure 4.2. Composite interatom spacing histogram of 13-atom sets.

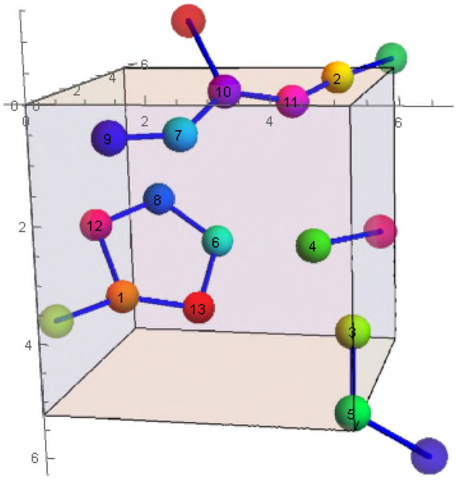

Figure 4.3. Loop connection diagram (e.g., 13-atoms VASP-direct relaxed list 1)

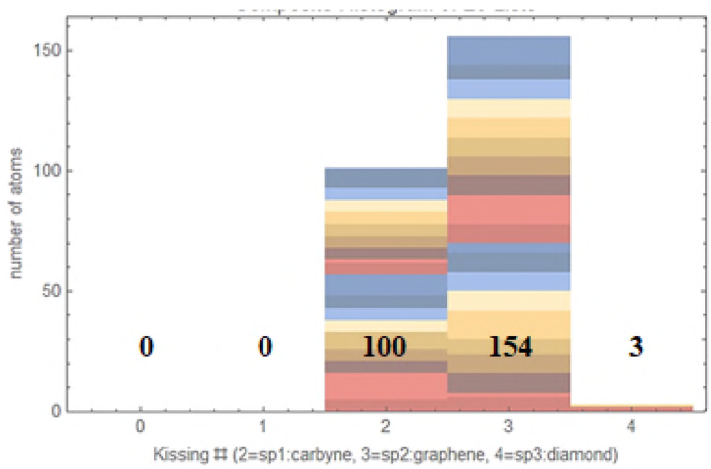

Figure 4.4. Composite coordination number plot with the total counts on each bar for 13-atom sets

Table 4.1 below contains the total loop-count table. In the end of the loop-count table, we calculated the percentage (n%) of each loop in comparison to the experimental data on the number of graphene sheets per atom. Here, n% = [the total number of n-loops (n= 3 to 7) /total atoms in 20 trials] %.

Table 4.1. List by list loop count for 13-atoms, VASP-direct relaxed sets

List	triangle	square	pentagon	hexagon	heptagon
1	1	1	1		
2					
3			2		
4		2			
5				1	1
6	2		1	1	1
7	1				
8			2		
9	1	1			
10					1
11			1		
12		2		1	
13	1				
14	1			1	1
15				1	
16			2		
17			2		
18	1		1		1
19	1				
20	2			1	1
Total	**11**	**6**	**12**	**6**	**6**
***n% loops/atom**	**4.23%**	**2.31 %**	**4. 62 %**	**2.31 %**	**2.31 %**

4.3.2. Carbon 20-atom Sets in a Supercell Volume 221.55 Å^3. The VASP- direct relaxation of 20 sets form 20-atoms in a supercell volume (6.051 Å)^3 = 221.55 Å^3.

The summarized results of the composite interatom spacing histograms (Figure 4.5), the visualization of loop connections (Figure 4.6), the composite coordination number plot (Figure 4.7) and the total loop count table (Table 4.2) can be seen below.

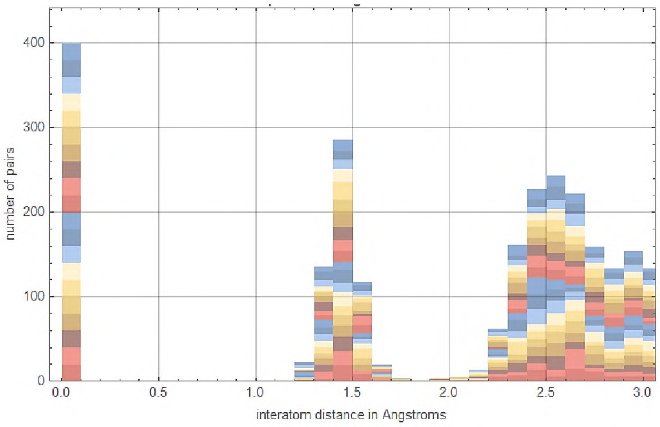

Figure 4.5. Composite interatom spacing histogram of 20-atom sets.

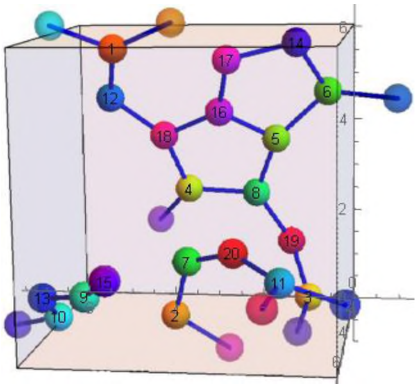
1
14
17
12
6
16
18
5
4
8
19
20
7
15
11
13
9
3
10
2
6
4
2
0
4
6

Figure 4.6. Loop connection diagram (e.g., 20-atoms VASP-direct relaxed list 1)

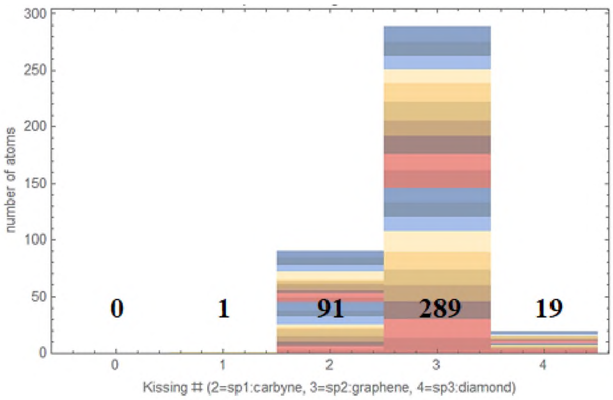

Figure 4.7. Composite coordination number plot with the total counts on each bar for 20-atom sets

Table 4.2. List by list loop count for 20-atoms, VASP-direct relaxed sets

List	**triangle**	**square**	**pentagon**	**hexagon**	**heptagon**
1	2	1	2	1	3
2	3	1			
3	1		2	1	
4	1	1	1		1
5		1	1		1
6	1	1	3		3
7	3				2
8			1	2	
9			3	1	
10			2	1	
11	2			2	1
12	2		2		
13	2	1	1		1
14			1	2	1
15	1	1	2	1	3
16	1	1	1	1	1
17	1			1	1
18	1	2	1		
19	1		1		
20	1		2	1	
Total	**23**	**10**	**26**	**14**	**18**
loops/atom	**5.75 %**	**2.50 %**	**6.50 %**	**3.50 %**	**4.5 %**

4.3.3. Carbon 30-atom Sets in a Supercell Volume 332.41 Å^3. This section deals with the direct relaxation of 20 trials in a supercell consisting of 30 atoms where the side length of the supercell is 6.92718 Å. These analyses include the composite interatom spacing histogram (Figure 4.8), visualization of loop connections (Figure 4.9), composite coordination number plot (Figure 4.10) and the loop count table (Table 4.3).

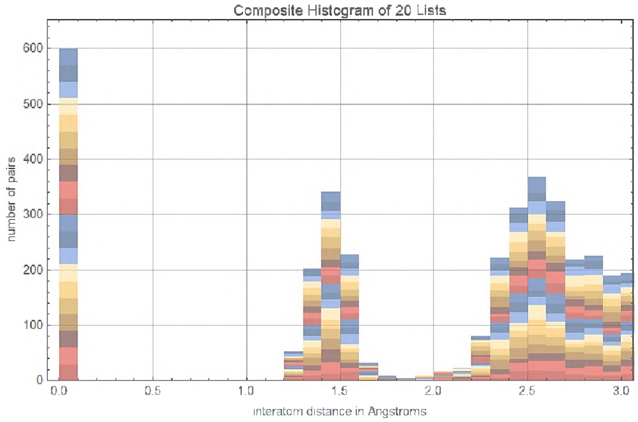

Figure 4.8. Composite interatom spacing histogram of 30-atom sets.

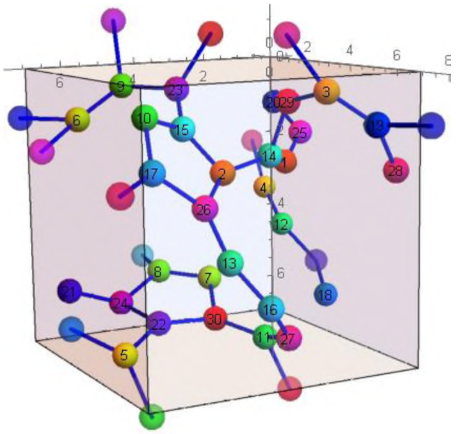
9
23
6
10
15
20
29
3
25
19
28
14
1
17
2
4
26
12
13
8
7
18
21
24
22
30
16
11
27
5
2
4
6
8
0
6

Figure 4.9. Loop connection diagram (e.g., 30-atoms VASP-direct relaxed list 1)

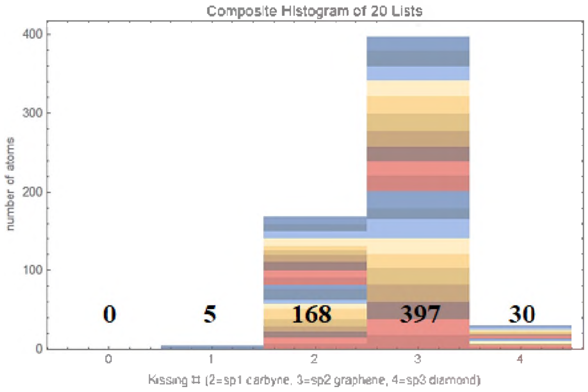

Figure 4.10. Composite coordination number plot with the total counts on each bar for 30-atom sets.

Table 4.3. List by list loop count for 30-atoms, VASP-direct relaxed sets

List	**triangle**	**square**	**pentagon**	**hexagon**	**heptagon**
1	2	1	1	1	
2	2	2		1	2
3	2	1		1	1
4	2	1	1	1	2
5		2			1
6				3	
7	2	1	1	1	2
8	1	2	1	1	2
9				1	
10	2	1	3		
11	1		3		1
12	4			1	2
13	1	1			1
14		3	3		
15	1	1	4	1	2
16	1		4		1
17	1	1	1		
18	2		1	2	2
19	1	1	1	1	1
20			3		
Total	**25**	**18**	**27**	**15**	**20**
loops/atom	**4.17 %**	**3 %**	**4.5 %**	**2.5 %**	**3.33 %**

4.3.4. Carbon 40-atom Sets in a Supercell Volume 443.21 Å^3. Detailed analysis of VASP- direct relaxation of 20 trials in a supercell volume of 40-atoms can be found below. The results of the study include the composite interatom spacing plot (Figure 4.11), loop network visualization (Figure 4.12), coordinate number plot (Figure 4.13) as well as the loop count table (Table 4.4).

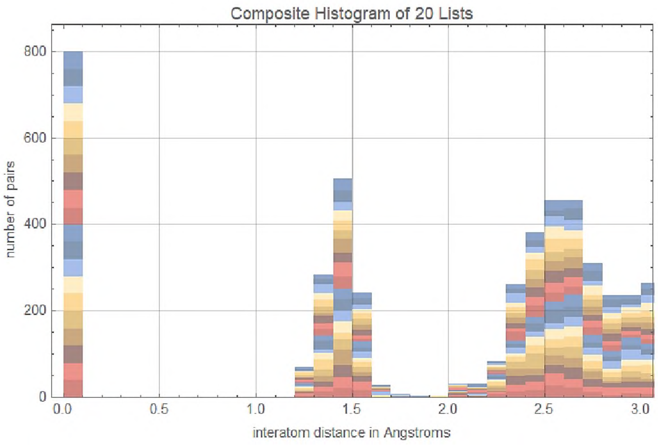

Figure 4.11. Composite interatom spacing histogram of 40-atom sets.

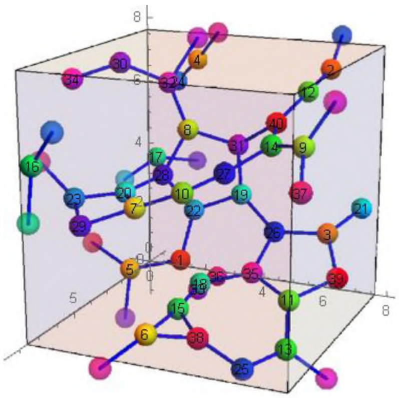
8
6
4
2
0
5
4
6
8
34
30
32
24
4
2
12
40
8
31
14
9
17
28
27
16
20
10
19
23
7
22
37
21
29
26
3
5
1
36
35
39
18
11
15
6
38
13
25

Figure 4.12. Loop connection diagram (e.g., 40-atoms VASP-direct relaxed list 1)

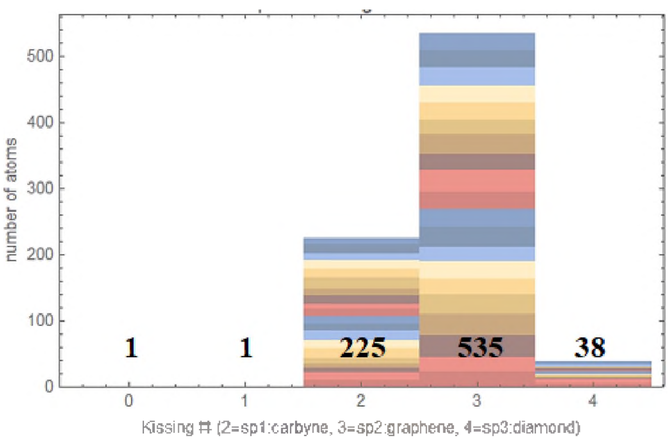

Figure 4.13. Composite coordination number plot with the total counts on each bar for 40-atom sets.

Table 4.4. List by list loop count for 40-atoms, VASP-direct relaxed sets

List	triangle	square	pentagon	hexagon	heptagon
1	2	3	4	1	4
2	3	3	2		4
3	1	2	1	2	1
4	5	1	4	1	3
5	2	1	3	3	4
6	3		1		2
7	3			2	1
8	3	1	2	1	
9	2	2		2	2
10	2	2		1	1
11	1	1	1	4	1
12	2	2	1	2	2
13	4		1		1
14	1	1	3	1	2
15	1	1	1	1	
16		2		1	1
17	1	1			1
18	2	2	2		1
19	4	1			1
20	5	1	1		1
Total	**47**	**27**	**27**	**22**	**33**
Loops/atom	**5.87 %**	**3 .38 %**	**3.38 %**	**2.75 %**	**4.13 %**

4.3.5. Carbon 60-atom Sets in a Supercell Volume 664.81 Å^3. Following are the results reported for VASP- direct relaxation of 20 groups of 60 atoms in a supercell volume (8.72769Å)^3= 664.81Å^3. Among the results are the composite interatom spacing histograms (Figure 4.14), loop visualization (Figure 4.15), plot of composite coordination numbers (Figure 4.16) and the count of all loops (Table 4.5).

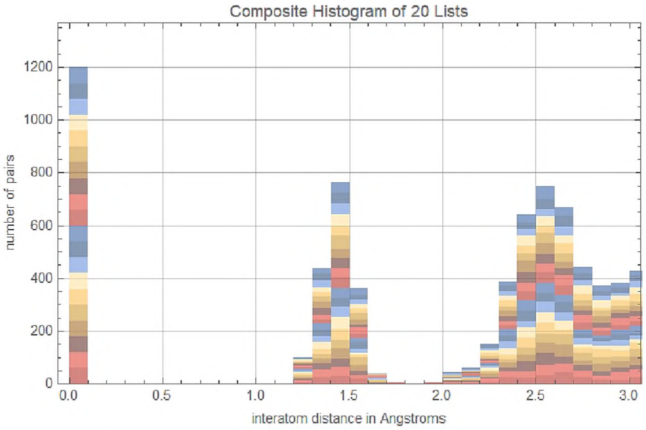

Figure 4.14. Composite interatom spacing histogram of 60-atom sets

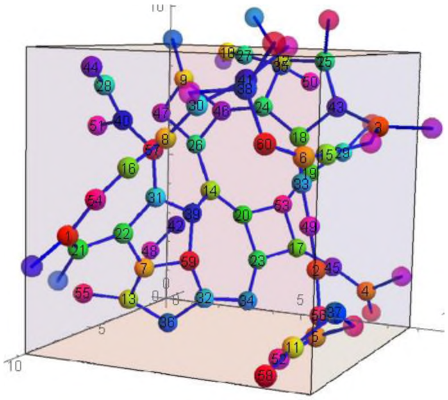

Figure 4.15. Loop connection visualization (e.g., 60-atoms VASP-direct relaxed list 1)

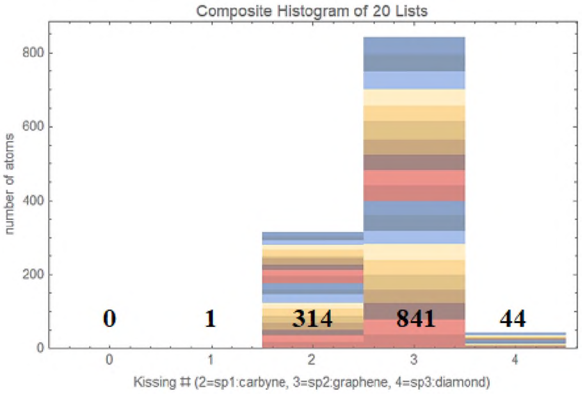

Figure 4.16. Composite coordination number plot with the total counts on each bar for 60-atom sets

Table 4.5. List by list loop count for 60-atoms, VASP-direct relaxed sets

List	triangle	square	pentagon	hexagon	heptagon
1	4	1	2		1
2		3	5	1	3
3	1	2	3	3	3
4	2	1	5	1	1
5	1	3	1		1
6	2	1	1	3	3
7	3	2	3	2	3
8	2		1	2	1
9	4	1	4	3	5
10	1	2	2	2	2
11	1	1	1	3	1
12	3	1	2	1	1
13	3	3	2	2	7
14	2	1	1	5	2
15	1	7	4	1	9
16	1	2	4	1	3
17	3	1	1	4	2
18	4	4	3		2
19	4	1	3	2	3
20	3	2	2	3	3
Total	**45**	**39**	**50**	**39**	**56**
loops/atom	**3.75%**	**3.25%**	**4.17%**	**3.25%**	**4.67%**

4.3.6. Carbon 100-atom Sets in a Supercell Volume 1108.02 Å^3. The analysis presented in this section is for the largest atom set tested in VASP-direct relaxation. The simulation is carried out in a supercell with length of side 10.34783 Å containing 100 atoms. Similar to the previous sections, Figure 4.17 shows a composite interatom spacing histogram, Figure 4.18 is the visualization of loop connections, Figure 4.19 shows the coordination numbers, and finally, Table 4.6 provides the loop counts.

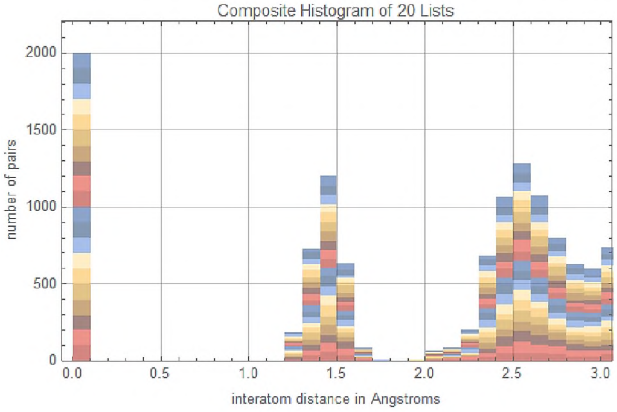

Figure 4.17. Composite interatom spacing histogram of 100-atom sets.

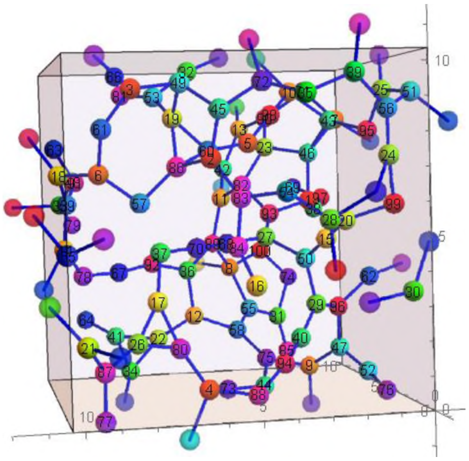

Figure 4.18. Loop connection visualization (e.g., 100-atoms VASP-direct relaxed list 1)

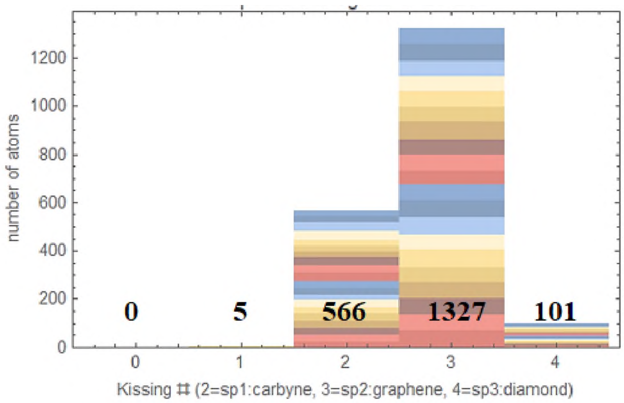

Figure 4.19. Composite coordination number plot with the total counts on each bar for 100-atom sets

Table 4.6. List by list loop count for 100-atoms, VASP-direct relaxed sets

List	**triangle**	**square**	**pentagon**	**hexagon**	**heptagon**
1	3	5	4	6	1
2	7	3	4	1	4
3	6		5	3	6
4	6	3	4		3
5	2	3	7	3	5
6	4	8	4	2	3
7	6	3	4		3
8	4	2	9	4	9
9	8		2	4	3
10	6	1	2	4	4
11	3	2	6	4	2
12	4	2	4	1	4
13	4	2	5	1	2
14	7	2	4	2	7
15	8	4	3		6
16	5	3	5	4	6
17	3	1	5	2	3
18	4	2	3	2	3
19	4	4	6	2	7
20	6		6	3	8
Total	**100**	**50**	**92**	**48**	**89**
loops/atom	**5 %**	**2.5 %**	**4.6 %**	**2.4 %**	**4.45 %**

4.4. DISCUSSION OF VASP- DIRECT RELAXATIONS

In this section we discuss the direct relaxation results shown in the section above. Based on the results, discussion topics are categorized into three groups, including interatom spacings (4.4.1.), coordination number statistics (4.4.2.), and loop count statistics (4.4.3.). In that context, each section will discuss the results of each atom set and compare them with those in the previous literature.

Specifically, an explanation of the analysis techniques as well as some insights into the experimental evidence in nature (and in the lab) will be discussed.

4.4.1. Interatom Distance Separation. As shown in the Figure 4.20, all of the composite interatom distance histograms exhibited an interatom distance abundance gap between 1.7Å - 2Å.

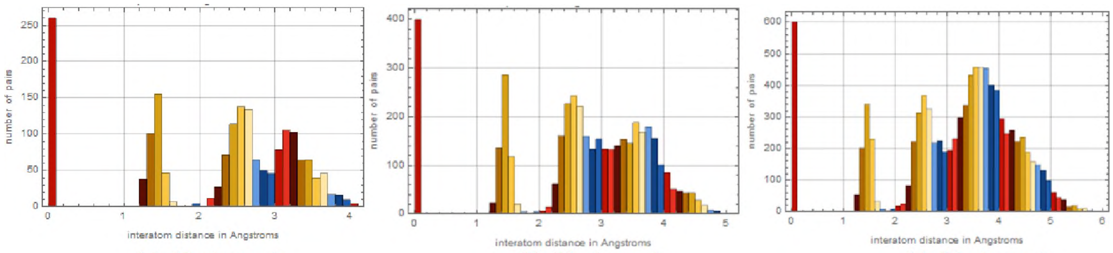

(a). 13-atom sets **(b). 20-atom sets** **(c). 30-atom sets**

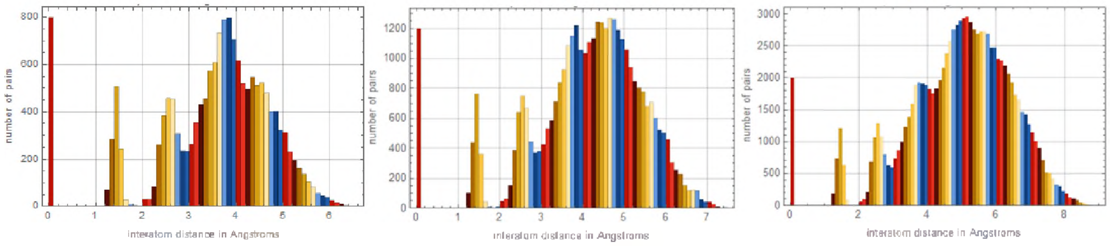

(d). 40-atom sets **(e). 60-atom sets** **(f). 100-atom sets**

Figure 4.20. Composite interatom spacing histograms for all relaxation sets

In general, separations smaller than 1.7Å - 2Å are considered to be covalent due to the inter-atom distance abundance gap. Since atom-pair separations less than 1.7Å are usually referred to as "covalent bonds" (common in the literature), we use the same practice. “Non-covalent” bonding will be defined as the larger side of the spacing gap (greater than 2Å).

4.4.2. Coordination Number Statistics. Following Table 4.7 is showing the total coordination numbers, as well as the coordination number percentages shown in Figure 4.21 for all VASP-direct relaxations.

Table 4.7. Total coordination numbers for all VASP- direct relaxed sets.

Coordination number	**0**	**1=sp^0**	**2=sp**	**3=sp^2**	**4=sp^3**
13 atom sets	0	0	100	154	3
20 atom sets	0	1	91	289	19
30 atom sets	0	5	168	397	30
40 atom sets	1	1	225	535	38
60 atom sets	0	1	314	841	44
100 atom sets	0	5	566	1327	101

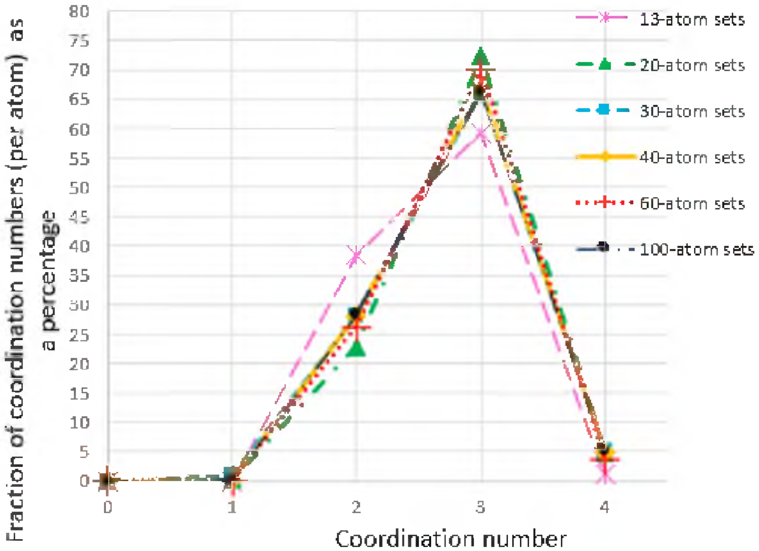

Figure 4.21. Coordination numbers per atom as a percentage (%) vs. coordination.

The majority of carbon atoms appeared to have an atomic covalent-coordination of 2-fold (sp) or 3-fold (sp2) in the atom lists that we relaxed to minimum energy. In previous studies, it was observed that at low densities (1.5 g/cc), 55% of the carbon liquid formed was a two-fold, a mix of 2-fold and 3-fold was formed at intermediate densities.

As an example, the densities around 2.2 g/cc-3.6 g/cc, considered as intermediate density and at higher densities (3.6 g/cc or higher) 4-fold. These reports are consistent with our findings here, in that most atoms are covalently bonded in 2-fold and 3-fold, and 4-fold coordination is less than 5% at this density [57-61].

4.4.3. Loop Count Statistics. Table 4.8 lists the total loop counts for loops of 3 to 7 atoms, and Figure 4.22 plots the loop counts per atom.

Table 4.8. Total loop counts for all VASP- direct relaxed sets.

Loop type	**3-loop**	**4-loop**	**5-loop**	**6-loop**	**7-loop**
13-atom sets	11	6	12	6	6
20-atom sets	23	10	26	14	18
30-atom sets	25	18	27	15	20
40-atom sets	47	27	27	22	33
60-atom sets	45	39	50	39	56
100-atom sets	100	50	92	48	89

According to the literature [61], 3-loop formation occurs as often as 5-loop formation in these direct-relaxation experiments. However, graphene sheets do not grow in a 3-loop or 4-loop structure physically as seen by experiment [50,62,63]. Likewise, we also found higher order loops (7 or more loops), in line with the literature [61]. These 7-loops cause graphene sheets to bend like saddles, and also alter the diameter of carbon nanotubes through their combination with 5-loops.

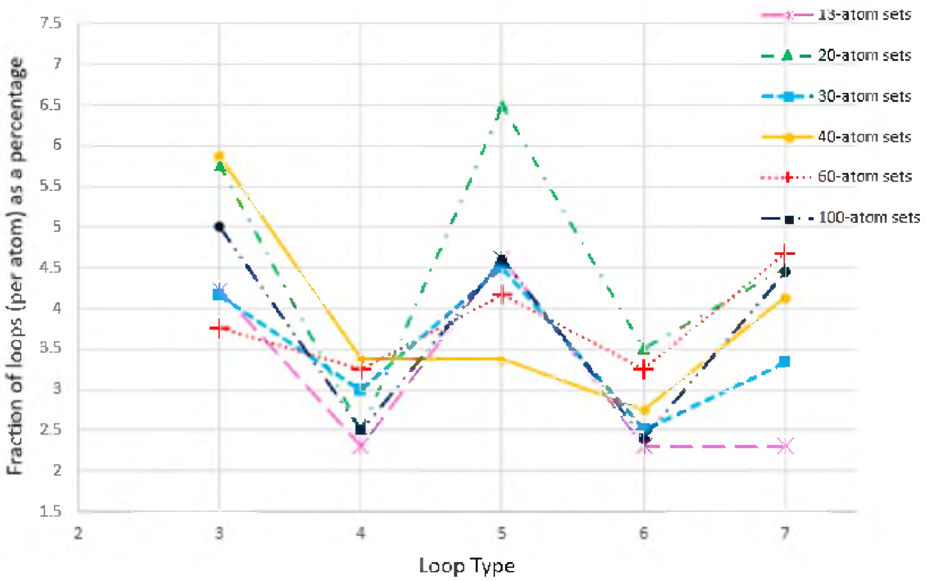

Figure 4.22. Percentage of loops per atom versus loop type

In summary, based on the table and the figure above, 5-loops are generally more abundant than 6-atom loops at this density. The next step was to compare the dependency of the total number of atoms in a simulation cell to nucleation of 5-loop/6-loop ratios. A constant model, as well as two *ad hoc* models, are compared with the results shown in Figure 4.23 below to determine whether our high 5/6 atom ratio is an artifact of the small atom numbers in our sets. The solid green line on the figure denotes a constant model, dashed line signifies the 2-parameter model, and dotted line denotes the 3-parameter model. As demonstrated in the data, statistical uncertainty is reduced when a large number of atoms are present in the cell. The constant model assumes that the 5-loop/6-loop ratio is independent of number of atoms in the cell. The 2-parameter model indicates that loop ratio is a linear function '(a+br)' as a function of the ratio (r) between the number of ways to produce 5-loops and 6-loops using the input n atoms.

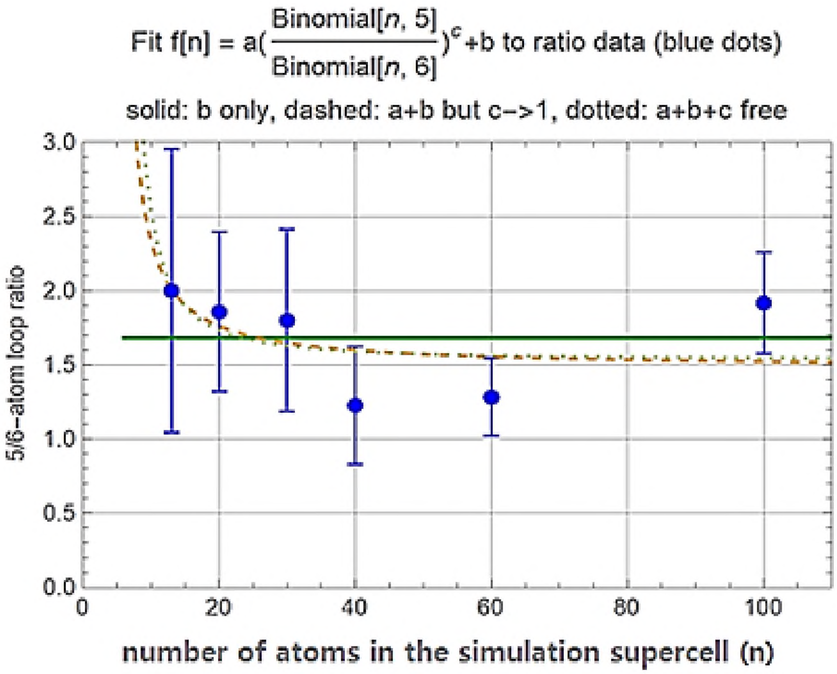

Figure 4.23. The ratio of 5-loops to 6-loops vs. the number of atoms in the simulation cell.

In addition, the 3-parameter model relies on the relationship between the ratios where all the parameters (a, b, c) are variables. According to the model selection criteria, Akaike/Bayesian (AIC/BIC) Information Criteria are 7.77/7.35 (constant model), compared to 8.93/8.31 (2-parameter) and 11.4/10.6 (3-parameter) suggest there is no significant decrease in 5/6 ratio with increasing number of atoms. Therefore, based on Bayesian model selection analysis, the constant model is the best option for predicting the data with the least amount of surprise.

A comparison was then made between the number of 5-loops and 6-loops per carbon atom in simulations with the number in experimental powder diffraction measurements. The following Table 4.9 shows the loops simulated with VASP calculations, as well as the number of graphene sheets per carbon atom observed in graphite-rimmed carbon spheres condensed within the atmosphere of red giant stars and in laboratory environments.

Table 4.9. Fraction-crystalline observations.

Seed type	Loops in a VASP- local minimum	Sheets seeded per loop	Lab condensed abundance of grown seeds	% Growing to 60 atoms in the lab	Presolar abundance of grown seeds	% Growing to 600 atoms presolar
6-loops	$2.6\times10^{21}/cm^3$	1	$1.8\times10^{20}/cm^3$	6.9%	$6.0\times10^{19}/cm^3$	2.3%
5-loops	$5.0\times10^{21}/cm^3$	5	$3.6\times10^{19}/cm^3$	0.72%	$1.2\times10^{19}/cm^3$	0.24%

According to the table, 40% graphene sheets by mass in presolar samples are typically 600 atoms in size with 40Å coherence width. And 12% graphene sheets in lab-grown samples are normally 60 atoms in size which having 12.6Å coherence width. The remaining carbon atoms were disordered [62]. In an environment with a carbon density of 1.8 g/cc, containing 9×10^{22} carbon atoms/cc assumes that 6×10^{19} sheets/cc in the presolar, and 1.8×10^{20} sheets/cc in the lab grown specimens. So, considering the nucleation of either of these sheets was on a single 6-loop, this many 6-loops per cc would have survived growth to 600 atom size.

Likewise, it would require only one fifth as many 5-loops to seed the same number of flat sheets. Hence, a useful nucleation and growth model for unlayered graphene in a cooling carbon melt will predict that only one third as many sheets will survive at 600 atoms than at 60 atoms in a few milliseconds of growth in a laboratory. VASP simulations generated more loops per carbon atom, compared to the number of sheets per carbon atom on both presolar and lab-grown cores [5].

So, in the future, it will be necessary to use molecular dynamics-growth models to see if the 5-loops are successful in competing with the 6-loops during nucleation of larger structures.

4.5. SUMMARY

Both presolar and lab grown specimens contain interesting spheres made of unlayered graphene in a solid matrix, potentially opening the door to studying liquid carbon under low pressure. The carbon loops in DFT-VASP supercell relaxations range from 3 to 7or more atoms in size. In agreement with previous studies, 5-loops are more abundant than 6-loops. If 5-loops as well as 6-loops efficiently nucleate the growth of graphene sheets from the liquid, with each 5-loop able to nucleate 5 instead on only one such sheet, it is easily possible that nucleation on pent-loops with dominate the population. Although our group continues to explore this growth stage with atomistic simulations, it is already well-known that pent-first nucleation seeds the growth of carbon nanotubes on catalyst surfaces [64,65]. Therefore, graphene sheets nucleating on pentagonal loops may be used to explain HRTEM images of edge-on sheet intersections in pre-solar samples [3].

There is still need for further study, in order to show if pentagonal rings are capable of nucleating faceted pentagons at inferred densities.

Models to explore the threshold temperature for supercooled droplet solidification are needed, and as well as to explore laboratory methods to increase graphene sheet size and fraction crystalline to levels found in presolar specimens. The potential of such “unlayered graphene composite” as a diffusion barrier, with otherwise unprecedented properties, also remains to be explored.

5. THE COMPARISON STUDY OF VASP- DIRECT RELAXATION AND VASP RE- RELAXATION METHODS

5.1. A COMPARATIVE STUDY OF TWO COMPUTATIONAL PROCEDURES

Since carbon atom clusters are first pre-relaxed using a different computer model, and then used for VASP relaxation, Section 5 has the title "Re-relaxation of VASPs." We report here a comparison between relaxed energy results obtained from VASP re-relaxation and VASP-direct relaxation in order to discern which technique results in the lower energy local minimum. Re-relaxations were performed on three different sets of atoms, (13-atom sets, 20-atom sets, and 100-atom sets). All of these sets were previously relaxed with the long-range carbon bond order potential (LCBOP) model [66]. The Large-scale Atomic/Molecular Massively Parallel Simulator (LAMMPS) from Sandia National Lab was used to implement the LCBOP model. The LCBOP pre-relaxed structures were provided by Phil Chrostoski, a member of our research team. Our analysis here includes comparing re-relaxations to direct relaxation results by including the data, such as loop counts and coordination counts, in addition to energy values.

5.2. COMPUTATIONAL METHODS

For comparison, VASP calculated each system's total energy. Before re-relaxing, the initial total energy of the pre-relaxed LCBOP system was calculated by using VASP's static structure method. In the following step, the pre-relaxed system relaxes using the VASP relaxation method and calculates the energy. These calculations used the same relaxation method as those in Section 4 where Section 2.3.2 is described.

The total energy of the two relaxations was then compared to determine whether VASP re-relaxations lead to a lower-energy local minimum than direct relaxations do.

5.3. VASP RE-RELAXATION RESULTS

As in Section 4, we used the loop counting analysis program and the total energy was extracted from the VASP-OUTCAR file. This section is divided into three groups, depending on the number of atoms in a supercell, such as 13-atom sets (5.3.1.), 20-atom sets (5.3.2.) and 100-atom sets (5.3.3.).

5.3.1. Carbon 13-atom Re-relaxed Sets. Presented are the results from the VASP re-relaxation analysis of 20 trials from 13 atoms in a supercell volume (5.242 Å)^3 = 144.04 Å^3. These include the composite interatom spacing histogram (Figure 5.1), the loop connection plot (Figure 5.2), graph of the composite coordination number (Figure 5.3), loop count table (Table 5.1) and the table of energy comparisons (Table 5.2).

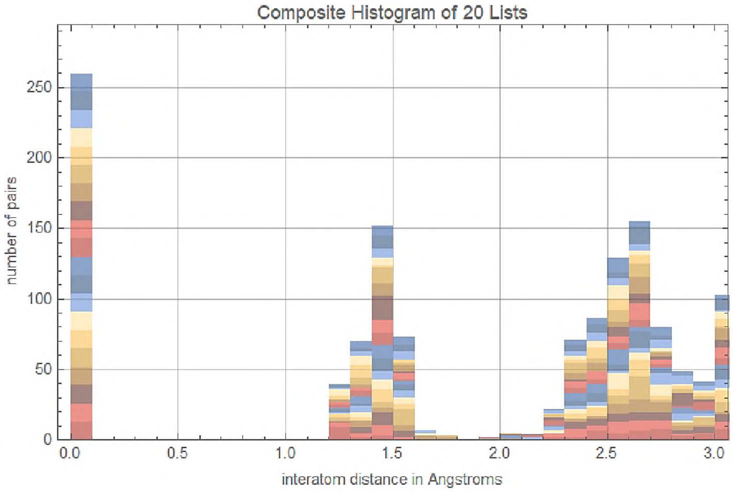

Figure 5.1. Composite interatom spacing histogram of 13-atom sets (VASP re-relaxed).

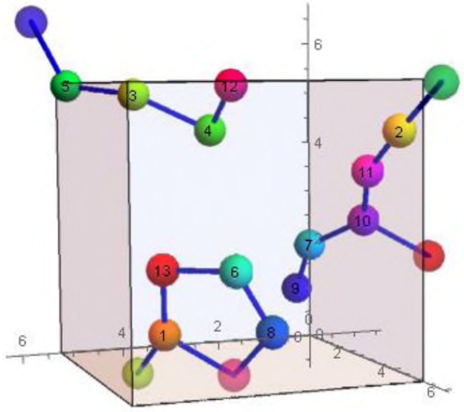

Figure 5.2. The loop connection plot (e.g., 13-atoms VASP re-relaxed list 1)

Table 5.1. List by list loop count for 13-atoms, VASP re-relaxed sets

List	**triangles**	**squares**	**pentagons**	**hexagons**	**heptagons**
1		1	1		2
2			2		
3	2	1		2	2
4			2		
5		1	1		
6	1				
7	1				
8	1		1	1	
9			2		
10	2			1	1
11					
12					
13	1				
14	1				
15	1			1	
16			2		
17		1			
18		1			
19			2		
20		1		1	
Total re-relaxed	**10**	**6**	**13**	**6**	**5**
n% loops / atom	**3.85 %**	**2.31 %**	**5 %**	**2.31 %**	**1.92 %**

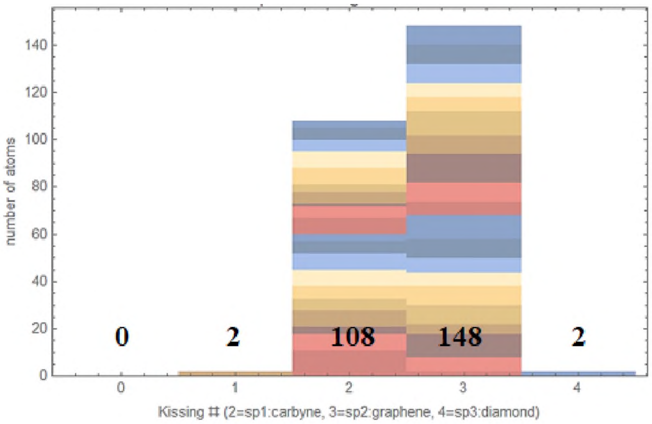

Figure 5.3. Composite coordination number plot with the total counts on each bar for 13-atom sets (VASP re-relaxed)

Table 5.2. Energy comparison of VASP-direct relaxed vs. VASP re-relaxed (13-atoms)

Trails	LAMMPS pre-relaxed Initial energy (eV)	VASP re-relaxed energy LAMMPS → VASP (eV)	VASP- direct relaxed energy (eV)
1	-93.6611	-101.5053	-103.9029
2	-89.1532	-109.4058	-103.8078
3	-91.4838	-105.9339	-107.6535
4	-94.7711	-109.4058	-105.8574
5	-87.7914	-103.3795	-106.1489
6	-93.8125	-104.1722	-109.2994
7	-86.8005	-106.3441	-104.6245
8	-94.3613	-104.8202	-109.4058
9	-84.9519	-109.4058	-107.3425
10	-91.6077	-105.5139	-104.5697
11	-88.2974	-103.8545	-109.5769
12	-92.6148	-103.6277	-106.3101
13	-90.5986	-106.9078	-105.1026
14	-98.1327	-104.1383	-106.7977
15	-97.7801	-105.3479	-107.4991
16	-95.3699	-109.4058	-109.4058
17	-96.4401	-106.2991	-104.4882
18	-86.7462	-105.8169	-105.3128
19	-91.3064	-109.4058	-107.3775
20	-94.2901	-106.4451	- 105.9987

5.3.2. Carbon 20-atom Re-relaxed Sets. The analysis includes here a total of 20 trials for VASP re-relaxation from 20 atoms. The sides of the supercell were 6.051Å , giving it a volume of 221.55 Å^3. A composite interatom spacing histogram (Figure 5.4), visualization of loop connections (Figure 5.5), composite coordination number plot (Figure 5.6), the loop count table (Table 5.3), and the energies for 20-atoms sets (Table 5.4) are presented in the following.

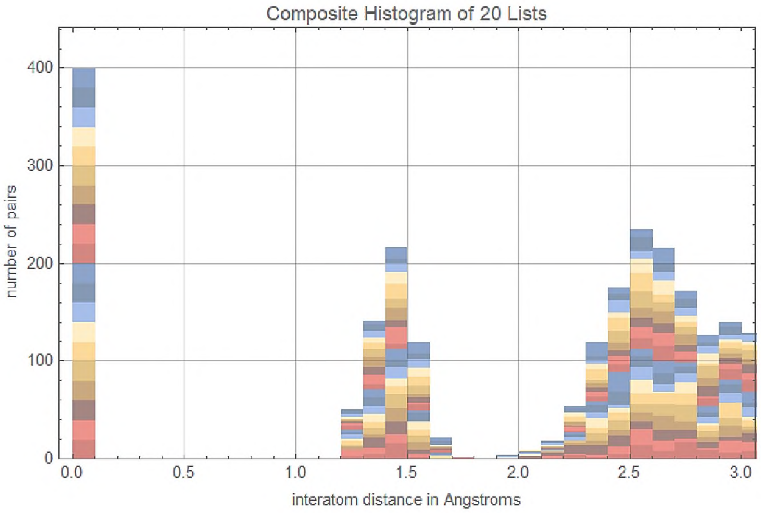

Figure 5.4. Composite interatom spacing histogram of 20-atom sets (VASP re-relaxed).

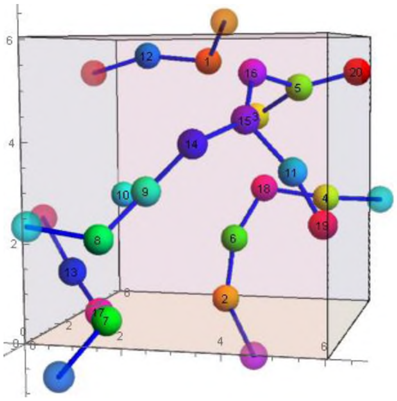

Figure 5.5. The loop connection plot (e.g., 20-atoms VASP re-relaxed list 1)

Table 5.3. List by list loop count for 20-atoms, VASP re-relaxed sets

List	triangle	square	pentagon	hexagon	heptagon
1					
2	2		1		
3	1				
4	2	1			
5				2	
6	2		3	1	2
7		2	2		1
8	1	2			
9			1		
10			2	2	
11	1				1
12		1			
13		1	3	2	2
14		1	1		
15	2		1		
16	1				
17		2	2		
18			1		
19			1	1	
20				1	
Total	**12**	**10**	**18**	**9**	**6**
loops / atom	**3 %**	**2.5 %**	**4.5 %**	**2.25 %**	**1.5 %**

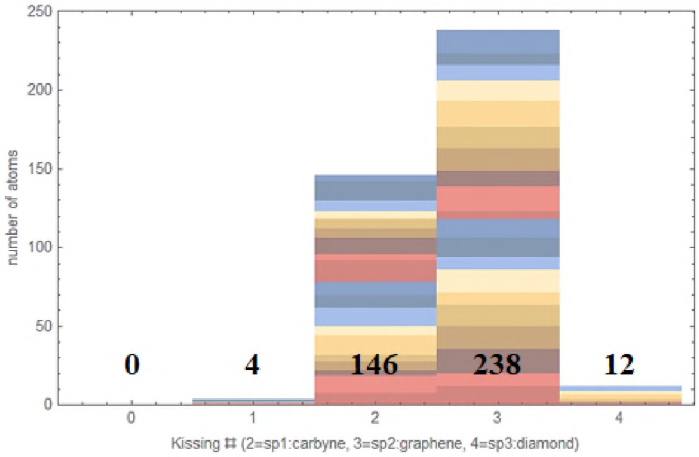

Figure 5.6. Composite coordination number plot with the total counts on each bar for 20-atom sets (VASP re-relaxed).

Table 5.4. Energy comparison of VASP-direct relaxed vs. VASP re-relaxed (20-atoms)

Trails	LAMMPS pre-relaxed Initial energy (eV)	VASP re- relaxed energy LAMMPS → VASP (eV)	VASP direct relaxed energy (eV)
1	-144.7528	-160.4146	-163.2388
2	-143.9232	-166.5305	-160.7472
3	-151.3274	-160.6729	-168.3421
4	-147.6775	-164.6130	-165.4665
5	-143.2295	-165.7889	-164.1482
6	-146.0269	-165.3875	-164.3582
7	-139.1281	-164.1444	-161.1948
8	-145.5359	-163.5139	-166.2602
9	-144.3705	-165.2104	-169.4235
10	-144.0683	-165.9182	-167.4111
11	-139.3018	-161.5219	-162.5669
12	-145.8612	-164.0189	-163.3889
13	-136.6806	-169.5419	-165.8487
14	-146.9183	-165.1566	-165.9665
15	-144.8463	-163.5630	-166.9811
16	-147.5952	-162.6154	-164.6873
17	-137.4143	-167.8528	-164.3924
18	-140.5394	-162.3245	-164.9625
19	-145.8825	-166.3014	-162.9828
20	-154.6672	-164.7132	-165.3790

5.3.3. Carbon 100-atom Re-relaxed Sets. The VASP re-relaxation of 19 trials from 100-atoms showed the following results for composite interatom spacing (Figure 5.7), loop connectivity (Figure 5.8), composite coordination diagram (Figure 5.9), the loop count table (Table 5.5), and energy data (Table 5.6). These re-relaxations took place in a supercell volume 1108.02 Å^3.

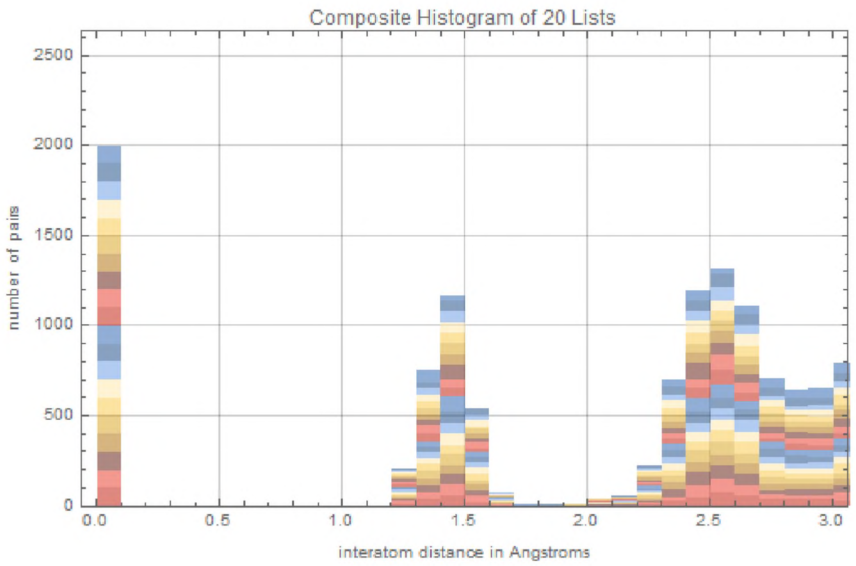

Figure 5.7. Composite interatom spacing histogram of 100-atom sets (VASP re-relaxed).

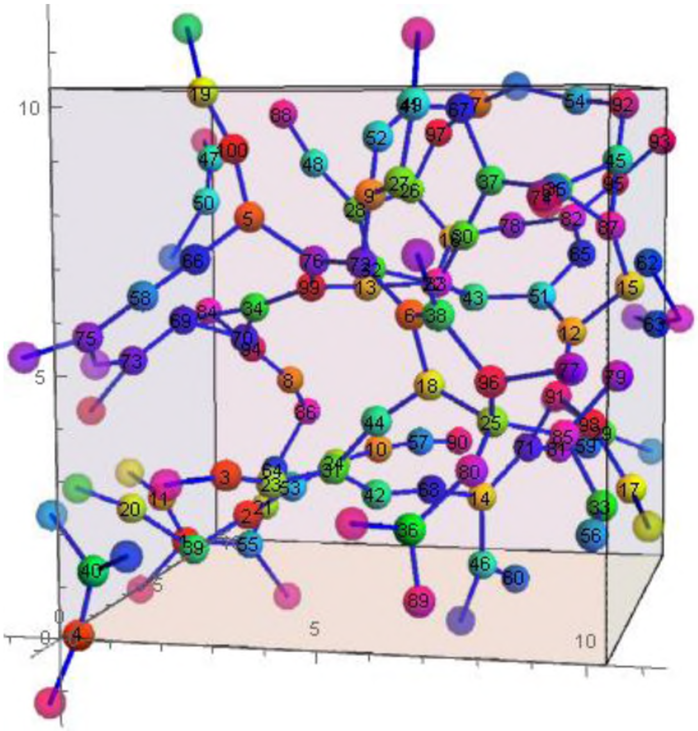

Figure 5.8. The loop connection plot (e.g., 100-atoms VASP re-relaxed list 1)

Table 5.5. List by list loop count for 100-atoms, VASP re-relaxed sets.

List	triangle	square	pentagon	hexagon	heptagon
1	4	2	1	3	2
2	7	2	5	3	4
3	1	2	5	5	7
4	3	1	2	1	3
5	3	1	7	4	3
6	2	4	2	2	3
7	2	4	2	2	3
8	4	2	2	4	1
9	1	3	2	4	4
10	2	2	8	6	7
11	4	4	2	4	3
12	2	0	3	2	2
13	2	1	3	6	2
14	3	1	3	4	5
15	4	3	5	1	3
16	0	0	2	3	2
17	2	1	7	3	2
18	1	3	5	4	5
19	4	1	6	5	6
Total	**51**	**37**	**72**	**66**	**67**
loops / atom	**2.68 %**	**1.95 %**	**3.79 %**	**3.47 %**	**3.52 %**

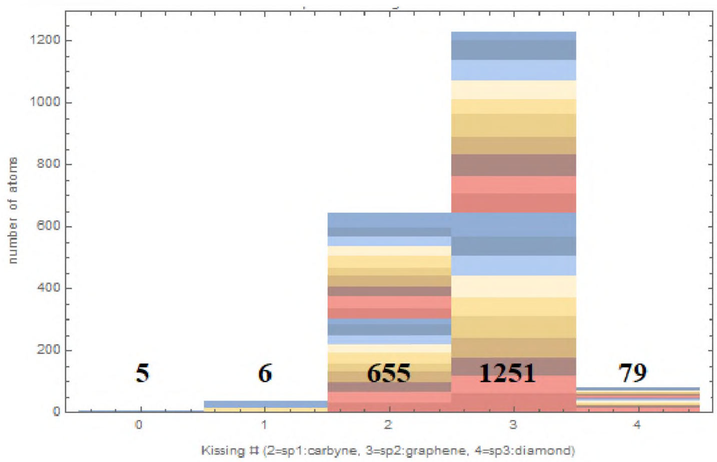

Figure 5.9. Composite coordination number plot with the total counts on each bar for 100-atom sets (VASP re-relaxed).

Table 5.6. Energy comparison of VASP-direct relaxed vs. VASP re-relaxed (100-atoms)

Trails	LAMMPS pre-relaxed Initial energy (eV)	VASP re- relaxed energy LAMMPS → VASP (eV)	VASP direct relaxed energy (eV)
1	-740.6029	-820.5447	-824.4770
2	-749.1038	-820.1918	-813.5874
3	-764.8616	-823.3504	-825.5207
4	-750.2965	-822.1755	-820.0162
5	-759.1236	-832.2240	-831.6217
6	-745.7328	-819.5515	-821.0530
7	-742.9662	-825.7393	-818.4257
8	-768.1894	-821.5820	-825.1736
9	-744.9479	-819.5636	-818.8767
10	-747.6546	-839.8158	-817.7307
11	-758.1827	-823.6753	-818.5592
12	-752.5724	-827.7559	-828.1053
13	-758.6287	-829.4675	-821.9725
14	-745.1567	-826.3055	-820.9590
15	-754.8708	-826.8532	-825.6808
16	-747.7704	-827.1596	-826.9667
17	-745.7626	-827.4776	-820.7340
18	-757.7420	-829.6871	-823.0678
19	-742.5754	-822.6027	-822.7582
20	-719.1127	-827.0135	-826.1018

5.4. DISCUSSION OF VASP RE-RELAXATIONS

The discussion is organized for three subtopics same as Section 4. The goal of this section is mainly comparing the methods of VASP-direct and VASP re-relaxation to see which method can obtain a better local minimum of energy. Moreover, the loop counts, coordination etc. will be discussed in detail in the following sections.

5.4.1. Interatom Distance Separation. As illustrated in Figure 5.10 below, all composite interatom distance histograms show a clear gap between 1.7Å - 2Å.

According to the composite interatom distance plots below the results are consistent with earlier VASP-direct relaxation results.

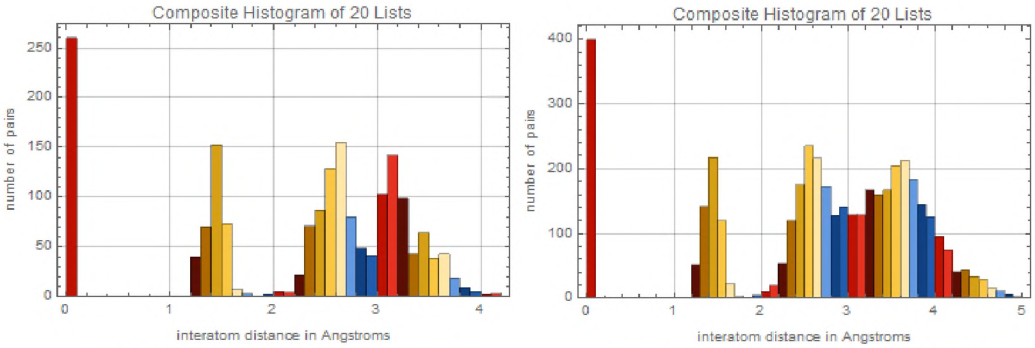

(a). 13-atom sets (re-relaxed) **(b). 20-atom sets (re-relaxed)**

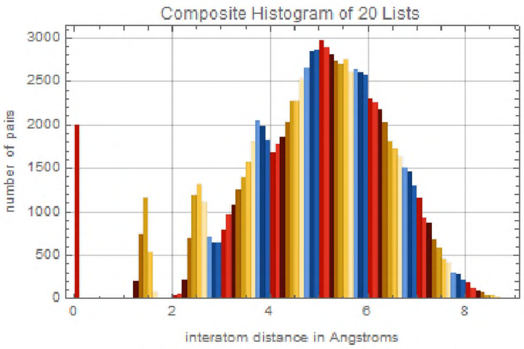

(c). 100-atom sets (re-relaxed)

Figure 5.10. Composite interatom spacing histograms for re-relaxation sets

Thus, the re-relaxation interatom histogram also supports the fact that covalent bonds have an atom-pair separation less than 1.7Å, while non-covalent bonds have a separation greater than 2 Å.

5.4.2. Coordination Number Statistics. Based on Table 5.7, most of the atoms had covalent coordination numbers that were 2-fold or 3-fold after T=0K re-relaxation. The coordination number statistics of the direct and relaxed results of VASP are shown in Figure 5.11.

Table 5.7. Coordination numbers for VASP re-relaxed and VASP- direct relaxed sets.

Coordination number	**0**	**1=sp^0**	**2=sp**	**3=sp^2**	**4=sp^3**
13-atom sets (re-relaxed)	0	2	108	148	2
20-atom sets (re-relaxed)	0	4	146	238	12
100-atom sets (re-relaxed)	5	6	655	1251	79
13-atom sets (direct relaxed)	0	0	100	154	3
20-atom sets (direct relaxed)	0	1	91	289	19
100-atom sets (direct relaxed)	0	5	566	1327	101

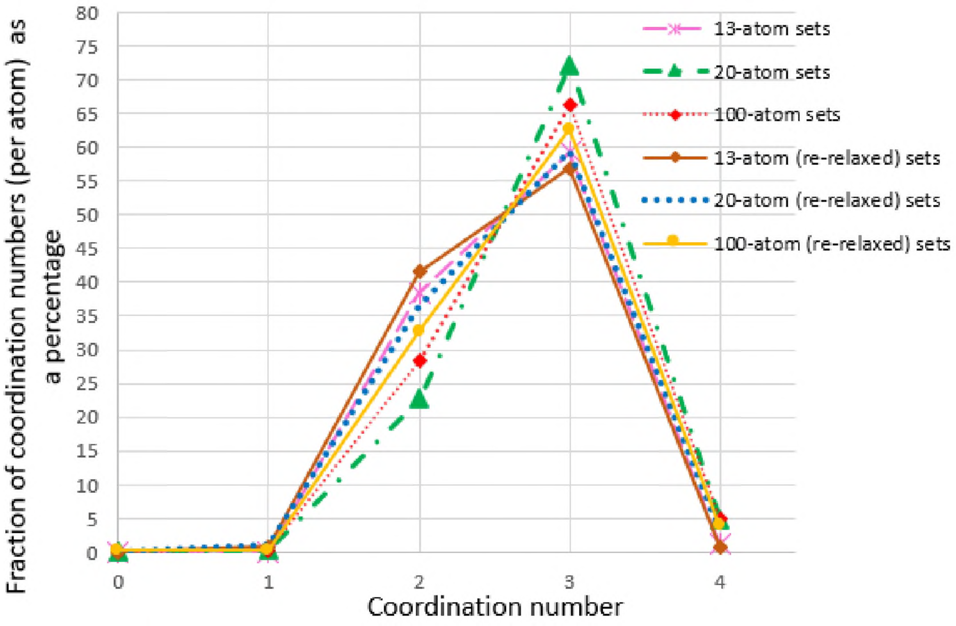

Figure 5.11. Number of coordination number (per atom) as a percentage (%) vs. coordination number for both VASP- direct & VASP re-relaxed sets.

Coordinate number results from both VASP-direct and VASP re-relaxed follow the same trend, which is a mixture of 2-fold and 3-fold that is also consistent with the literature.

It has been demonstrated that VASP-direct relaxations have a higher percentage of the 3-fold in the 20-atom sets. On the other hand, in 2-fold coordination, the percentage for the 2-fold is higher in VASP re-relaxations, which is reverse to the trend reported in 3-fold coordination. There is no evidence that direct or re-relaxing 13-atom sets differ in significant ways. Re-relaxation sets with 100 atoms report zero-coordination or liquid-like carbon atoms. However, there is no zero-coordination observed in 100-atom direct relaxations. In 100-atom VASP-direct relaxations, 2-fold and 1-fold coordination are higher, and in 100-atom VASP re-relaxation sets, 3-fold and 4-fold coordination are higher. In general, VASP re-relaxations had the same coordination pattern as VASP-direct relaxations, such as a mixture of 2-food and 3-fold coordination.

5.4.3. Loop Count Statistics. The Table 5.8 below is the loop counts and Figure 5.12 the loop count comparison study for VASP- direct and re-relaxations.

Table 5.8. Total loop counts for VASP re-relaxed and VASP- direct relaxed sets.

Loop type	3-loop	4-loop	5-loop	6-loop	7-loop
13-atom sets (direct-relaxed)	11	6	12	6	6
20-atom sets (direct-relaxed)	23	10	26	14	18
100-atom sets (direct relaxed)	100	50	92	48	89
13-atom sets (re-relaxed)	10	6	13	6	5
20-atom sets (re-relaxed)	12	10	18	9	6
100-atom sets (re-relaxed)	51	37	72	66	67

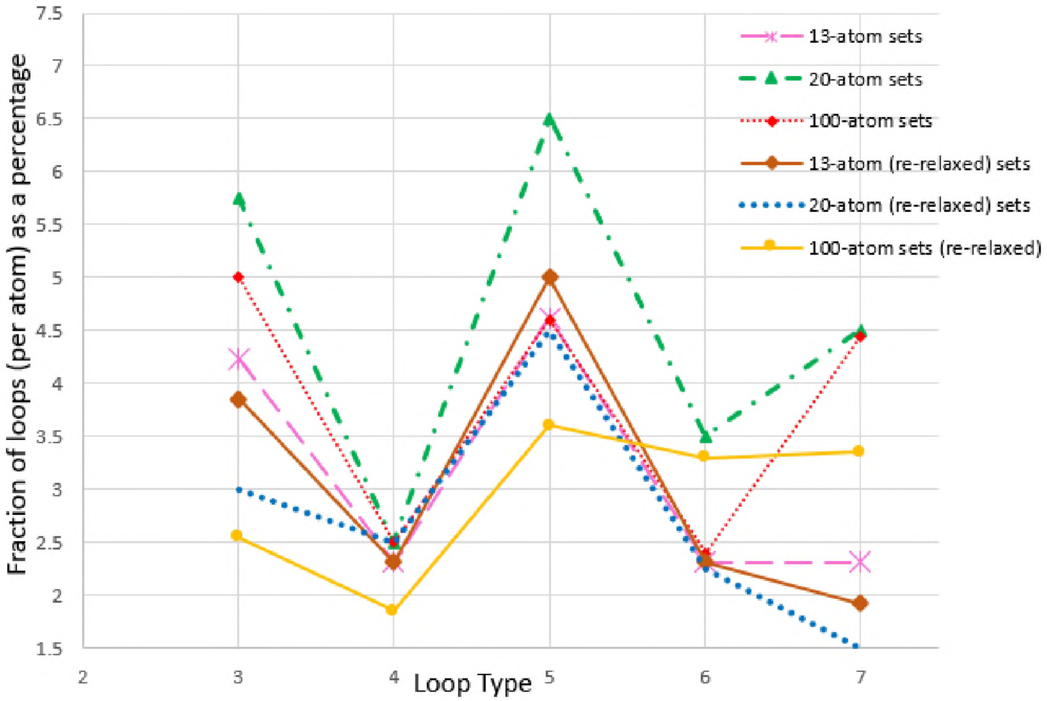

Figure 5.12. Number of loops per atom as a percentage vs. loop type for both VASP-direct & VASP re-relaxed sets.

In re-relaxed systems, the number of 3-loops and 4-loops is less than for direct relaxation. Because the LAMMPS pre-relaxation sets (before the VASP re-relaxation) only reported a smaller loop count, this should be expected. Due to this, even after VASP re-relaxation, loop counts are lower than direct relaxation. In summary, 5-loop loops still provide a greater loop count than 6-loop loops, explaining the trend seen among direct relaxations of VASP.

5.4.4. Total Energy Comparison. In Figure 5.13, we compare energy levels of LAMMPS pre-relaxations, VASP-direct relaxations, and the VASP re-relaxation of 13-atom sets, Figure 5.14 for 20-atom sets and Figure 5.15 for 100-atom sets.

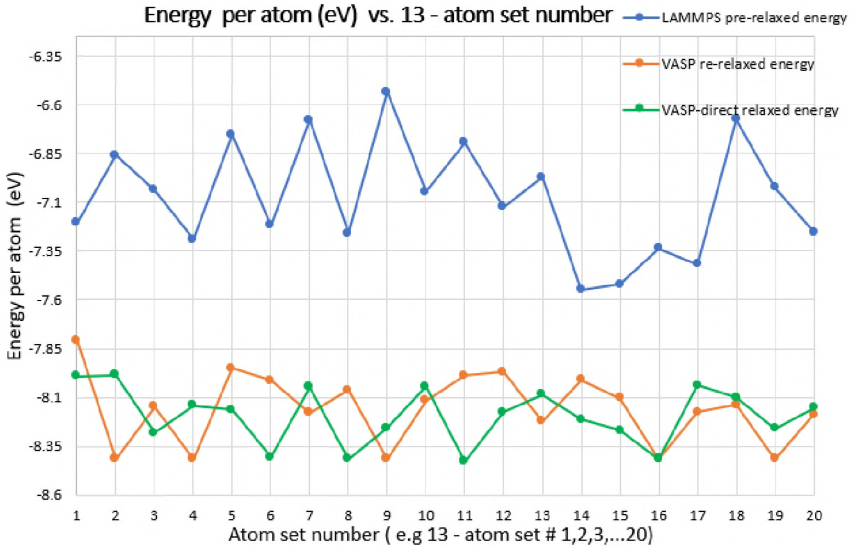

Figure 5.13. Energy (per atom) for LAMMPS pre-relaxed, VASP-direct relaxed, VASP re-relaxed vs. 13-atom set number (Set #1, Set #2, ...Set #20).

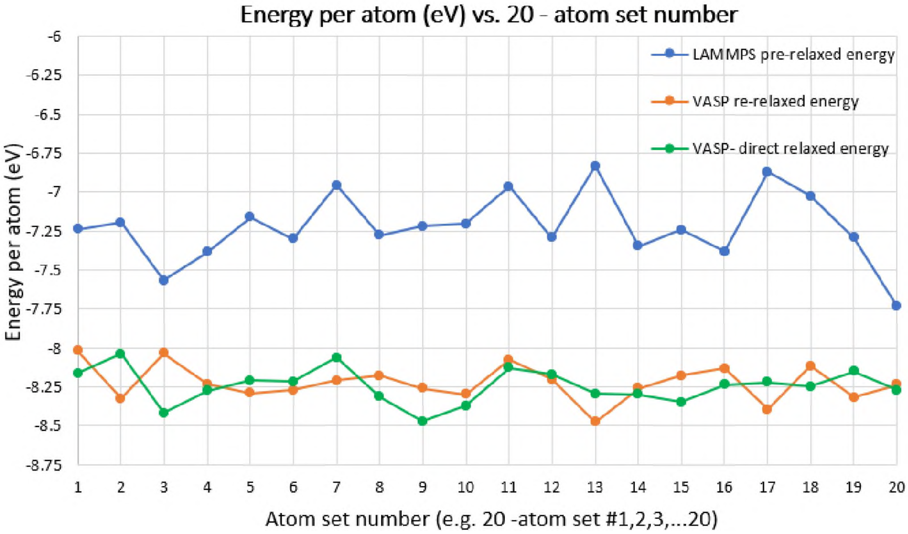

Figure 5.14. Energy (per atom) for LAMMPS pre-relaxed, VASP-direct relaxed, VASP re-relaxed vs. 20-atom set number (Set #1, Set #2, ...Set #20).

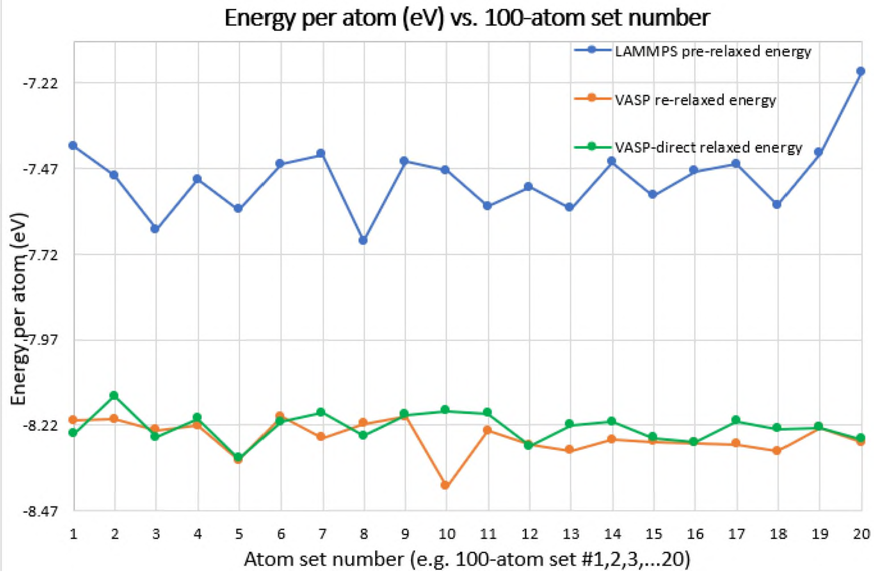

Figure 5.15. Energy (per atom) for LAMMPS pre-relaxed, VASP-direct relaxed, VASP re-relaxed vs. 100-atom set number (Set #1, Set #2, ...Set #20).

As shown on the plots, the LAMMPS pre-relaxed energies per atom are in the range 7eV -7.5 eV, while VASP relaxations range from 8-8.5 eV. Both direct and re-relaxed VASP structures have a lower energy minimum than LAMMPS pre-relaxed structures. Following plots, Figure 5.16 is assigned for 13-atom sets, Figure 5.17 is for 20-atom sets and Figure 5.18 is for 100-atom sets. These plots are providing a statistical analysis of binding energies of both VASP -direct and VASP re-relaxations calculations. VASP -direct relaxation is represented by the green solid line, whereas the red dashed line displays the re-relaxation with VASP following a pre-relaxation with LCBOP from LAMMPS. Bands across the horizontal axis are simply weighted mean binding energies (per atom) for 13-atoms, 20-atoms, and 100-atoms sets.

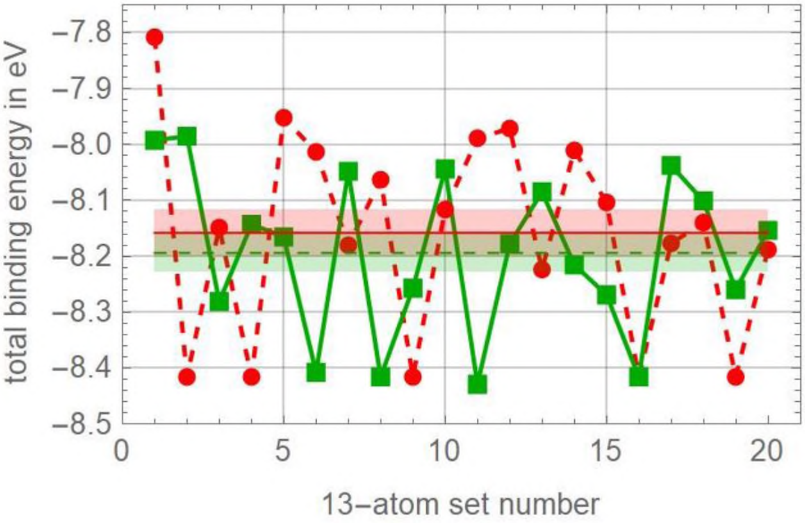

Figure 5.16. VASP- direct (green) and re-relaxed (red) binding energies per atom with simply weighted uncertainties for 13-atom sets.

In 13-atom sets the local minimum varies between -8.4 eV to -8.5 eV in both type of relaxation structures. But in the 20-atom sets, the energies scattered all over the plot giving the clue that the energy minimums are stacked in different local minimums.

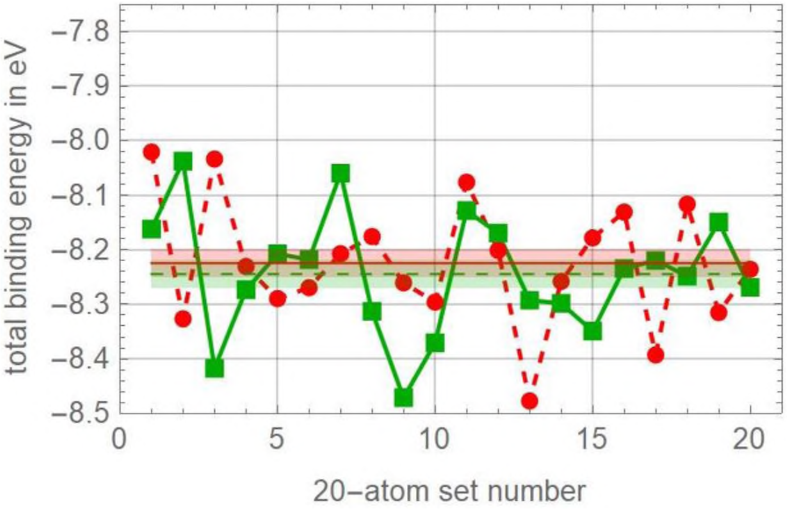

Figure 5.17. VASP- direct (green) and re-relaxed (red) binding energies per atom with simply weighted uncertainties for 20-atom sets.

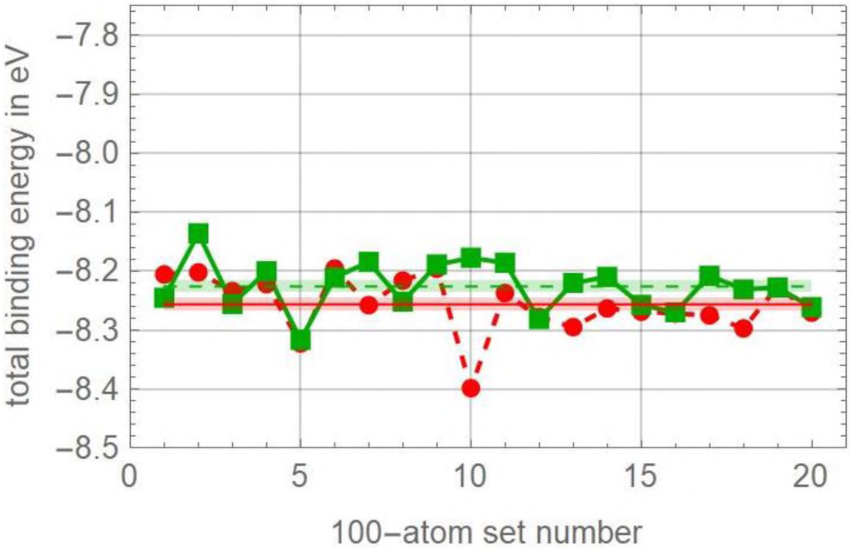

Figure 5.18. VASP- direct (green) and re-relaxed (red) binding energies per atom with simply weighted uncertainties for 100-atom sets.

The 100-atom sets exhibit more tightly bound in re-relaxation structures, with an average bind energy of 0.37% higher, where the argument relies heavily on one outlying point. However, the study needs to use better statistics to draw more reliable conclusions about average energies, such as calculating energy values using more atoms to lessen the spread in those values.

5.5. OVERVIEW

The VASP-relaxation results are consistent with VASP-direct relaxation structures in the following ways: (i). The gap between the 1.7Å - 2Å interatom distance histograms allows the identification of covalent bonds (less than 1.7Å) and noncovalent bonds (greater than 2Å), (ii). 5-loops occur more often than 6-loops, and (iii). contain a mixture of sp (2-fold) and sp^2 (3-fold) coordination. This study was primarily focused on finding an improved method to calculate local minima during relaxation calculations.

However, taking these energy results into consideration, this relaxations results clearly depend on the starting structure rather than the relaxation method. Because, as seen in the results, there was an adequate sampling for 13-atoms, less for 20-atom sets and larger clusters (e.g. 100 atom sets) clearly benefit from pre-relaxed structures using molecular dynamics to achieve a better local minimum. In terms of the next calculation, we can suggest using a simulated annealing semi-empirical potential relaxation structures first as this has proven useful elsewhere [67].

6. CONCLUSIONS

In this dissertation, mainly two types of simulations methods in DFT-VASP have been tested (e.g., conjugate gradient relaxation and static structure calculation). The isolated cluster relaxation of nano-diamond (Carbon 28 +1 single atom at the origin) suggests that the relaxed structure turns into the tetrahedral (and smallest) carbon-28 “touching-pentagon” fullerene, with a carbon atom at the center. The structure contains 4 hexagons plus the 12 pentagons required for fullerene closure with all hexagons surrounded by pentagons (as complement to the way all pentagons are surrounded by hexagons in the C-60 “buckyball” fullerene). Such stable nano-diamond structure at low pressure/temperature might be another interesting topic to explore in future, as discussed in earlier literature [14].

In the supercell relaxations, most of the calculation results reported (e.g., on 8-atom diamond, graphene-13) such as the dimensions of the crystal structure, binding energies etc. are consistent with the previous experimental work. Some of our work contradicts the literature, as in the case of (non-diamond) face-centered-cubic carbon’s reported stability.

Specifically, in the search for a local energy minimum as a function volume for the fcc- 4 atom (non-diamond) structure, we find no energy minimum near the proposed density from VASP static structure calculation. Our results indicate that energy will bottom out around 1.4 g/cc instead of the proposed 1.8 g/cc. Also, results of both fcc-32 or fcc-4 atom cells do not show an energy minimum at the reported volume. This is consistent with the fcc-carbon phase “discoverer’s” failure to show awareness in their discussion of diffraction data confirming this phase that double diffraction routinely allows spots disallowed by the diamond glide to show up in electron diffraction patterns e.g., of diamond fcc silicon. These observations, and the fact that the cubic cell of the proposed structure is essentially the same as that of diamond, suggest that this phase may not exist at all.

My calculations concerning the nucleation of unlayered graphene at T=0K are grouped into two main sections: VASP-direct relaxations and VASP re-relaxations. The atom lists resulting from the relaxation of initially random collections with inter-atom spacings greater that 1.9Å and the results used to study and compare the loops counts, inter atom distances, coordination numbers and total binding energies. The composite histograms in 1.8 g/cc specimens all exhibited an inter-atom distance abundance gap between 1.7Å-2Å, helping to justify the usual identification of bonds smaller than this as covalent and higher than 2Å as non-covalent in both VASP-direct and VASP re-relaxations. Coordination numbers for such atoms are also 4 or less, consistent with this interpretation. Using inter-atom distances in this way to identify covalent bonds, most carbon atoms were coordination 2-fold or 3-fold in all atom-lists that relaxed to minimum energy. The 4-fold coordination abundance is under 5%, for all different sizes of atoms sets in both relaxed and re-relaxed structures.

Concerning covalent loop formation, I examined primitive non-spanning loops with 3 to 7 carbon atoms. Since 3-loop and 4-loop are not experimentally reported in graphene sheet structures, they are unlikely nuclei for graphene sheet growth. Although 7-atom loops are seen experimentally e.g., as saddle structures in nanotube diameter transitions, their presence is not indicated experimentally (from edge-on sheet angle) in the presolar cores nor in standalone fullerene structures (which are generally convex). Hence our focus on promising sheet nuclei is on pent-loops and hex-loops.

My observations suggest that pent-loops are not only abundant but are often more abundant than hex-loops. The number of loops seen in our simulations, per carbon atom, is also greater than the number of sheets per carbon atom inferred from diffraction observations on both presolar and lab-grown cores. This work therefore provides seeds for use in nucleation and growth models for comparison to laboratory observations on slow cooled carbon particles from both presolar and laboratory sources downstream.

Future work might involve application of our atomistic results to the development of nucleation and "two-dimensional" growth models capable of extrapolating to much longer times (milliseconds and up) likely needed for significant growth of unlayered graphene sheets in a slowly cooled melt. For instance, molecular dynamics might help us determine parameters in analytical or numerical cluster size distribution models. Further work remains to see if such ab initio studies can confirm that abundant pentagonal rings at this density, during slow cooling of the liquid, can nucleate the growth of faceted pentacones. The properties of unlayered graphene sheets in a frozen liquid matrix, e.g., as a diffusion barrier, should be interesting to explore further both experimentally and computationally. The energy comparison study of two methods of relaxations, indicate that re-relaxed structures of LCBOP collections is effective at achieving a better local minimum. The literature reports of success with VASP re-relaxation structures of semi-empirical potential molecular dynamics (or simulate annealing) relaxations remain to be explored in future computations that might offer paths to a better lower energy minimum.

APPENDIX A.

DFT STUDY OF “UNLAYERED - GRAPHENE SOLID” FORMATION, IN LIQUID CARBON DROPLETS AT LOW PRESSURES

Chathuri Silva[1], Philip Chrostoski[1], P. Fraundorf [1,2]

[1] University of Missouri at St. Louis, Saint Louis, MO, United States,

[2] Washington University, Saint Louis, MO, United States

Received: 14 December 2020 / Accepted: 1 February 2021 / Published online: 18 February 2021 © The Author(s) 2021

ABSTRACT

This atomistic modeling study is companion to new experimental work on carbon vapor slow-cooled in: (a) the laboratory and (b) the atmosphere of ancient carbon-synthesizing stars. It specifically follows up on TEM clues about the nucleation of unlayered graphene sheets in a solidifying carbon liquid, to show that 5-atom loops may help explain evidence for faceted pentacones in a slow-cooled melt. This is also first in a series of modeling studies that may open the door to laboratory studies of: (i) condensation in cool-giant star atmospheres and (ii) liquid carbon at low pressures.

Keywords Computation/computing · Simulation · Extreme environment · Graphene · Liquid · Nucleation & growth

1. INTRODUCTION

Circumstellar dust in the laboratory [1-4] is providing insight into materials physics and nuclear physics [5,6], as well as the astrophysical processes by which such dust is made. Elemental carbon below 100 atmospheres on heating above 3900K sublimates to vapor, so liquid carbon is seldom considered to play a role at low pressures even though quenched carbon droplets have been reported in laboratory laser ablation studies [7,8]. The high-density (KFC1) subset of presolar micron-sized carbon spheres extracted from Murchison meteorite, with isotopic signatures of nucleosynthesis in late stage red giant stars suggesting that they likely condensed in or just outside the hydrogen-rich photosphere at between 10^{-3} and 10^{-5} atmospheres pressure, have spherical cores that show diffraction rings from randomly-oriented atom-thick graphene sheets. Their "graphene-core"/graphite-rim structure likely formed around super-cooled carbon droplets (diameter in the 300-700 nm range) that nucleated graphene sheets on randomly oriented pentagonal loops (5-loops) [9]. Laboratory synthesis of carbon particles in a turbo-pumped vacuum evaporating carbon oven also creates such core-rim (& core-only) particles, but graphene-sheet coherence widths are much smaller (around 1 nm). The lab-grown cores have diameters in the 100-400 nm range [10,11]. Selected area electron powder diffraction patterns of these cores show only (hk0) spacings with the high frequency tails expected for atom thick sheets, and the strange absence of any graphite (002) "layering" lines [10], suggest that they contain unlayered graphene sheets with 4 nm coherence width [10]. This is reinforced in high resolution transmission electron microscope (HRTEM) images [9] (cf. Fig.A.1) by the presence of intersecting line-segments pairs 2-5 nm in length with "redirection angles" between 39 and 65 degrees, but no evidence of adjacent "parallel layer" sheets. These intersections suggest that some of the randomly oriented graphene sheets take the form of faceted pentacones, as though they were nucleated on pentagonal loops during solidification [9,10].

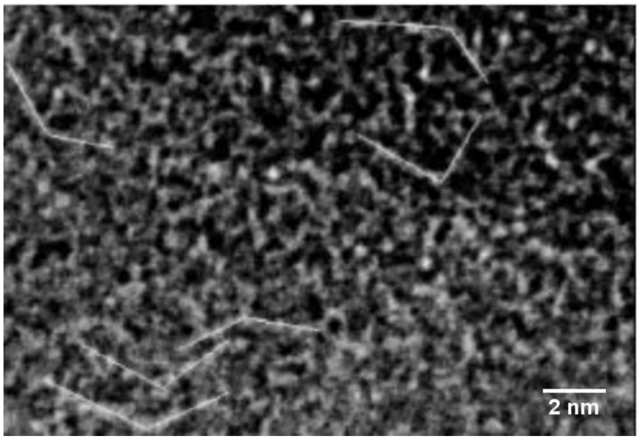

Figure A.1. HRTEM negative of disordered carbon “speckle” and edge-on graphene sheets, in a microtomed (sliced) presolar core, with likely intersecting graphene sheets marked. Adapted with permission from reference [9].

Additional recent results include the observations that: (i). analysis of electron diffraction patterns from the submicron cores of such particles [12] indicates a diffuse-scattering carbon matrix of which, in the presolar case about 40% is unlayered graphene sheets with a mass weighted average size of about 600 atoms, but so far in lab-grown cores is only about 12% graphene with a mass weighted average size of say 60 atoms, and (ii). atomistic and thermodynamic models of nucleation and growth suggest that laboratory specimens solidified in the 3000K range over millisecond times, while the presolar cores solidified at lower temperatures (closer to 2500K) over longer (e.g. 10 second) times [13]. These times are still consistent with the near-atomic sharpness of observed the core/rim interfaces, and much shorter than the time for ejection by radiation pressure from a stellar atmosphere.

We show here that density functional theory (DFT) studies with "Vienna ab-initio simulation package" (VASP) suggest that 5-loops compete favourably with 6-loops (hexagons) as nucleation seeds for the graphene sheets consistent with previous studies.

These studies, still in their infancy, are opening the door to low pressure studies of liquid carbon, and to laboratory studies of carbon condensation in asymptotic giant branch star atmospheres.

2. COMPUTATIONAL METHODS

Atom-position relaxations reported here use carbon in a 1.8 g/cc supercell because experimental observations on sliced presolar cores (with graphite rims) appear to have densities on that order [14,15]. The relaxations were performed in a supercell using the Projector-Augmented-Wave (PAW) method [16] and generalized gradient approximation (GGA) for exchange correlation functional [17]. We assume low pressure and relax randomized positions of liquid-like 13,20,30,40,60, and 100-carbon atom clusters in a supercell. This supercell relaxation was using the ISIF 2 tag in VASP in order to keep the periodic boundary conditions in a constant density 1.8g/cc of carbon in a constant volume and did 20 relaxations for each size of atom sets to obtain the results. The analysed atom lists follow VASP relaxation of initially random collections with inter-atom spacings greater that 1.9Å. The volume and the shape of the cell remained as a constant before and after the relaxations and contain six subgroups of results according to the number of atoms in each set (and the supercell volume), are 13-atom sets (144. 04$Å^3$), 20-atom sets (221.55$Å^3$), 30-atom sets (332.41 $Å^3$), 40-atom sets (443.21$Å^3$), 60-atom sets (664.81$Å^3$), 100-atom sets (1108.02$Å^3$).

Another calculation we conducted was 're-relaxing' the atom sets which are previously relaxed using the Long-range Carbon Bond Order Potential (LCBOP) model

[18]. To employ the LCBOP model, we used the Large-scale Atomic/Molecular Massively Parallel Simulator (LAMMPS) molecular dynamics program from Sandia National Labs. In this calculation we compare the loops counts, total energies, coordination numbers etc. to see if lower-energy local minima might be obtained thereby. LCBOP and other potentials are also being used to model later stage nucleation and growth of graphene sheets from the liquid melt, but these topics are not the primary goal of this paper. However, detailed re-relaxation results can be found in the supplementary material: Section 2.

3. RESULTS

Figure A.2 illustrates one way to visualize interatom covalent connections (here associated with the distinct class of interatom distances smaller than 1.7Å) using a 13-atom set for clarity. Bonds that cross supercell boundaries are shown only once, and the atoms outside the central volume are un-numbered.

Figure A.3 provides a complete analysis report from 100-atom sets that includes the total loop count table (Figure A.3a), the composite interatom spacing histogram (Figure A.3b) and the composite coordination number plot (Figure A.3c). Figure A.3a lists the number of loops found for each type (n = 3 (triangles) to 7 (heptagons)). Although graph theory can easily identify all n-atom loops e.g. with bond length shorter than say 1.7Å, a subset of these are “spanning loops” i.e. which return not to the starting atom but to a periodic instance of that starting atom. Topological loops also include “super loops”, for instance the hexagon associated with a pentagon and triangle sharing a common side. Primitive loops are the ones which cannot break further into smaller loops. In our loop analyses, we count only non-spanning primitive loops using standard algorithms [19]. Figure A.3b is the histogram of distances between each atom and Figure A.3c lists the total number of atoms that contain specific coordination. Figure A.3b and Figure A.3c track list identities by using different colors for each. In Figure A.3c, in each bar, the total number of atoms is marked for each coordination. For example, 566 atoms have 2-fold (sp) coordination in this list.

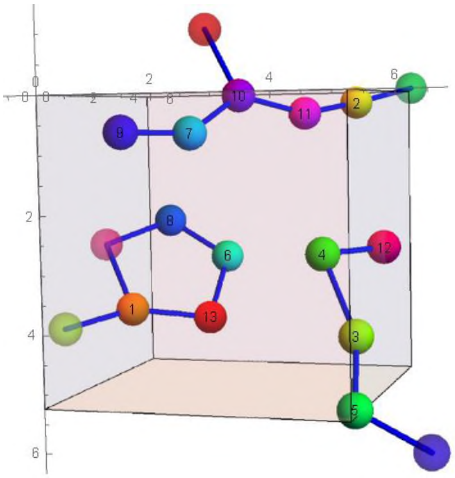

Figure A.2. Covalent bond visualization where 1.7Å as the covalent bond-length cut-off (13-atom set).

atoms/loop	#loops
3	100
4	50
5	92
6	48
7	89

a.)

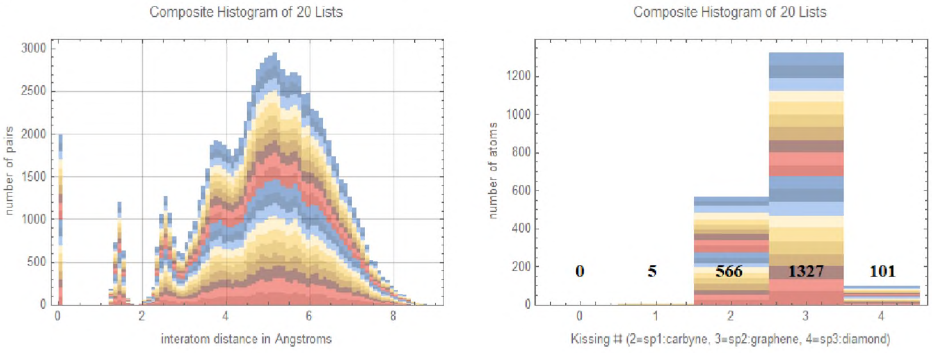

b.)

c.)

Figure A.3. Complete analysis report for 100 atom sets; (a). total loop count (b). composite interatom spacing histogram (c). composite coordination number plot.

Interatom distance histograms (available in supplementary material section 1) exhibited an inter-atom distance abundance gap between 1.7Å– 2Å, so that (in agreement with the literature) we categorize pair interactions for spacings less than 1.7Å as "covalent", but those higher than 2Å are listed as "non-covalent" interactions.

Table A.1 below lists coordination numbers, and Figure A.4 is coordination number percentages, for all relaxation reports.

Table A.1. Total coordination numbers for all relaxations.

Coordination number	0	1=sp^0	2=sp^1	3=sp^2	4=sp^3
13 atom sets	0	0	100	154	3
20 atom sets	0	1	91	289	19
30 atom sets	0	5	168	397	30
40 atom sets	1	1	225	535	38
60 atom sets	0	1	314	841	44
100 atom sets	0	5	566	1327	101

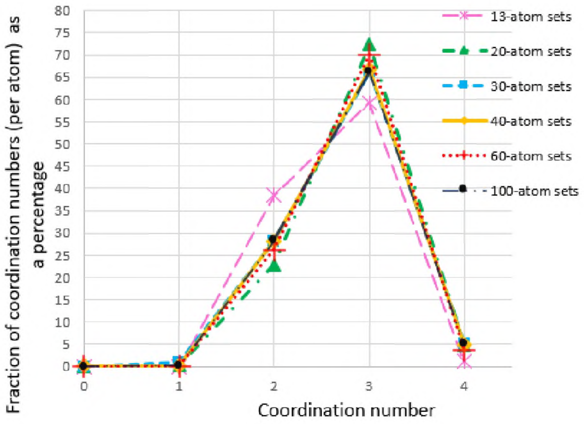

Figure A.4. Fraction of coordination numbers per atom as a percentage (%) vs. coordination number.

Table A.2 lists loop counts, and Figure A.5 loops per atom, for loops with 3 to 7 atoms.

Table A.2**.** Total loop counts for all relaxations.

Loop Type	3 - loop	4 - loop	5 - loop	6 - loop	7 - loop
13 atom sets	11	6	12	6	6
20 atom sets	23	10	26	14	18
30 atom sets	25	18	27	15	20
40 atom sets	47	27	27	22	33
60 atom sets	45	39	50	39	56
100 atom sets	100	50	92	48	89

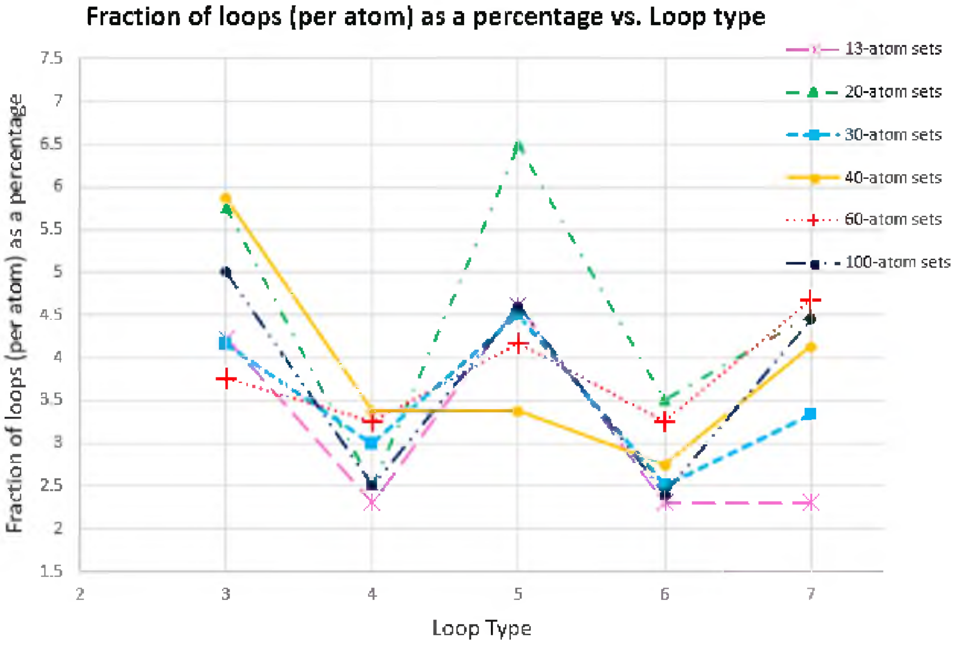

Figure A.5. Fraction of loops (per atom) as a percentage (%) vs. loop type.

DFT relaxation predict abundant 3-loops, consistent with earlier cited reports [18]. Three and four atom loops are not experimentally abundant in graphene sheet structures [9,19,20]. At this density, 5-loops (common experimentally e.g. in fullerenes) are generally more abundant than 6-atom loops. Loops with 7 or more atoms are also abundant in simulations [18], and 7-loops (combined with a 5-loop) are even used to change the diameter of carbon nanotubes. However, the saddle-like bend that a 7-loop introduces in a graphene sheet, unlike the conical-bend of a 5-loop, are not consistent with our observation of edge-on sheet intersection angles in the presolar cores.

4. DISCUSSION

The inter-atom distance abundance gap between 1.7Å and 2Å, helps to justify the practice (common in the literature) of identifying atom-pair separations less than 1.7Å as "covalent bonds". Inter-atom distances higher than 2Å are by default then associated with non-covalent (with coordination numbers up to 12) expected in a quenched liquid.

Most list atoms after "0K" relaxation had covalent-coordination 2 or 3. This agree with previous studies as our density is considered 'intermediate" and expected to show a mixture of 2 and 3-fold with 4-fold coordination under 5% [20, 23-26].

We also compare absolute number of 5-loops and 6-loops *per carbon atom*, with experimental data on the number of graphene sheets per carbon atom present in the cores of graphite-rimmed carbon spheres condensed in the atmosphere of red giant stars, and in core-only carbon spheres condense in our laboratory.

The latter data come from powder diffraction measurements of graphene sheet coherence widths (sizes) and the fraction of carbon atoms "crystallized" into graphene sheets [12]. If such loops seeded the nucleation and growth of those graphene sheets, the comparison provides us with estimates of the survival fraction of such loops during the subsequent crystallization process in both environments. That, powder diffraction data suggests that presolar specimens are 40% (by mass) graphene sheets typically 600 atoms in size (i.e. from a 40 Å coherence width), while lab grown specimens are 12% graphene sheets typically 60 atoms in size (i.e. from a 12.6 Å coherence width), with the remainder of the carbon atoms disordered. Given 9×10^{22} carbon atom/cc in carbon of 1.8 g/cc density, this suggests 6×10^{19} sheets/cc in the presolar specimens, and 1.8×10^{20} smaller sheets/cc in the lab grown specimens.

If each of these sheets was nucleated on a single 6-loop, then we require this many 6-loops per cc to have survived growth to 600 atom size. Since 5-loops each nucleate as many as 5 such sheets, only one fifth as many "fully grown" 5-loops would be needed to seed the same number for flat sheets. The implications of these model results, considering the final sheet size and fraction-crystalline observations reported here [12], are summarized in the Table A.3 below.

Table A.3. Fraction-crystalline observations

Seed type	Loops in a VASP *ab initio* local minimum	Sheets seeded. per loop	Lab condensed abundance of grown seeds	% growing to 60 atoms in the lab	Presolar abundance of grown seeds	% growing to 600 atoms presolar
6-loops	$2.6\times10^{21}/cm^3$	1	$1.8\times10^{20}/cm^3$	6.9%	$6.0\times10^{19}/cm^3$	2.3%
5-loops	$5.0\times10^{21}/cm^3$	5	$3.6\times10^{19}/cm^3$	0.72%	$1.2\times10^{19}/cm^3$	0.24%

This suggests that only about a 10^{th} as many "successful" 5-loops seeds is needed (in both types of specimen) to overtake the contribution from "successful" 6-loop seeds. It also suggests that a useful nucleation and growth model for unlayered graphene in a cooling carbon melt should predict that only a third as many sheets will survive in the slower growth to 600 atoms, than in the few millisecond growths to 60 atoms in our laboratory.

In context of such a model, we might be able to learn something about: (i) the cooling rate of carbon droplets condensed around red giant stars, and well as (ii) the conditions needed to synthesize comparable material (with its promising diffusion-barrier properties) in the laboratory. Figure A.6 shows 5-loop/6-loop ratio against the total number of atoms ‘n’ in the simulation cell.

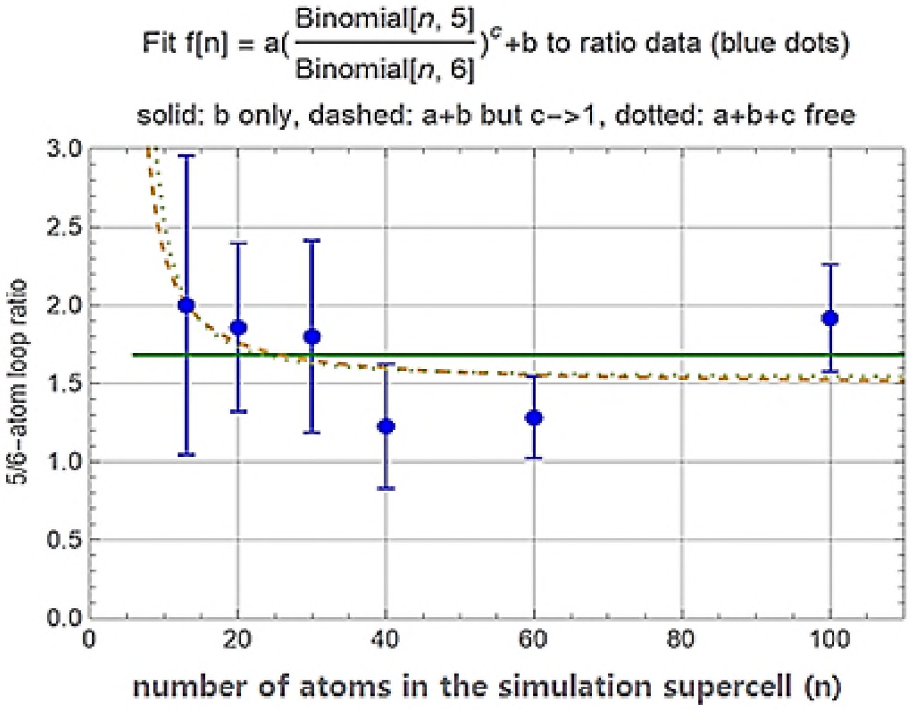

Figure A.6.5-loop/6-loop ratios vs. n, solid green: constant model, dashed: two-parameter model, dotted: three-parameter model.

It compares the data with a constant model, plus two *ad hoc*- models in which 5/6 ratio decreases with n, to see if our high 5/6 ratio is an artifact of the small number of atoms in our sets. The two-parameter model signifies that the loop ratio is a linear function of the ratio between the number of ways to create 5-loop & 6-loop in a set of n atoms, while the 3-parameter model assumes a quadratic dependence instead. Statistical uncertainties are smaller for larger n-sets, and model selection measures 'Akaike/Bayesian (AIC/BIC). Information Criteria of 7.77/7.35 (constant model), compared to 8.93/8.31 (2-parameter), and 11.4/10.6 (3-parameter) in weighted fits argue against a significant decrease in 5/6 ratio with increasing number of atoms in the set.

5. CONCLUSION

Presolar and lab-grown specimens contain interesting spheres made of unlayered graphene in a solid matrix, which may open the door to low pressure studies of liquid carbon. DFT-VASP supercell relaxation of random carbon atom clusters in the observed density range agree with existing literature and suggest that 5/6-loop abundance ratios around one are not an artefact of the number of atoms in the simulation. The number of loops seen in our simulations, per carbon atom, is also greater than the number of sheets per carbon atom inferred from diffraction observations on both presolar and lab-grown cores [10,12]. Therefore, the nucleation of graphene sheets on pentagonal loops might help explain the intersecting line segments seen in HRTEM images of presolar cores [9].

Separate molecular dynamics and nucleation growth modelling is still needed to see if indeed the 5-loops compete effectively with 6-loops in nucleating the larger observed structures. Separately, studies of the diffusion barrier properties of randomly-oriented sheets in a disordered matrix, oven design to provide greater control of cooling rate, and supercooling thresholds for container less carbon liquid, may help with materials science and astrophysical applications.

ACKNOWLEDGEMENT

The VASP calculations, and manuscript writing, were done by CS, the LCBOP calculations were provided by PC, the data on presolar and lab grown specimens as well as some Mathematica programs were provided by PF. A special thanks to Dr.Eric Majzoub who helped provide the access and supervised the VASP code, MST-Rolla for the access to the Forge cluster and UMSL department of Physics and Astronomy for a place to work.

CONFLICT OF INTEREST

On behalf of all authors, the corresponding author declares that there is no conflict of interest.

REFERENCES

[1] P. Fraundorf, D. E. Brownlee, R. M. Walker, Laboratory studies of interplanetary dust in *Comets*, (ed. L. Wilkening, U. Arizona Press, Tucson, 1982), pp. 383-409.

[2] J. P. Bradley, D. E. Brownlee, P. Fraundorf, *Science* **226**, 1432-1434 (1984).

[3] T. Bernatowicz, G. Fraundorf, T. Ming, E. Anders, B. Wopenka, E. Zinner, P. Fraundorf, *Nature* **330**, 728-730 (1987).

[4] Ernst Zinner, *Annual Review of Earth and Planetary Sciences* **26**:147-188 (1998).

[5] T. Bernatowicz, R. M. Walker, *Physics Today* **50**, 26 (1997).

[6] Larry R. Nittler, F. Ciesla, *Annu. Rev. Astron. Astrophys. **54**:53-93* (2016).

[7] D. Kasuya, M. Yudasaka, K. Takahashi, F. Kokai and S. Iijima, *J. Phys. Chem. B* **106**, 4947-4951 (2002).

[8] W. A De Heer, P. Poncharal, C. Berger, J.Gezo, Z. Song, J. Bettini and D. Ugarte, *Science* **307**:5711, 907-910 (2005).

[9] P. Fraundorf and M. Wackenhut, *Ap. J. Lett.* **578**(2): L153-156, (2002).

[10] P. Fraundorf, T. Hundley and M. Lipp, HAL-02238804. (2019).

[11] T. J. Hundley, P. Fraundorf, *49th Lunar and Planetary Science Conference 2018 (LPI Contrib. No. 2083),* 2154-2155, (2018).

[12] P. Fraundorf, M. Lipp, T. Hundley, C. Silva, and P. Chrostoski, *Microscopy and Microanalysis* **26**: S2 pp. 2838-2840, (2020).

[13] P. Fraundorf, S. Chathuri, P. Chrostoski and M. Lipp, *COSPAR 2021 Sydney*, International Council of Scientific Unions Committee on Space Research, (2021), (in prep).

[14] T. Bernatowicz, R. Cowsik, P. C. Gibbons, K. Lodders, B. F. Jr., S. Amari, and R. S. Lewis, Astrophysical Journal 472, 760, (1996).

[15] P. Fraundorf, K. Pisane, E. Mandell and R.Collins, *Microscopy and Microanalysis* **16** Supplement 2, 1534-1535, (2010).

[16] P. E. Blöchl, *Phys. Rev.* B 50, 17953, (1994).

[17] J.P. Perdew, K. Burke, and M. Ernzerhof, *Phys. Rev. Lett.* 77, 3865, (1996).

[18] J. H. Los and A. Fasolino, *Phys. Rev.* B.68.024107 (2003).

[19] D. S. Franzblau, *Phys. Rev.* 44, (1991).

[20] V. L. Deringer and G. Csányi, *Phys. Rev. B* 95, 094203, (2017).

[21] C. Toh, H. Zhang, J. Lin, A. S. Mayorov, Y.Wang and C. M. Orofeo et al., *Nature* **577**, 199-203, (2020).

[22] M.S. Dresselhaus, G. Dresselhaus and P.C. Eklund, *Science of Fullerenes and Carbon Nanotubes*, (Academic Press, San Diego, CA, 1996).

[23] C. Cannella and N. Goldman, *J.Phys.Chem* 119, 29-31, (2015).

[24] J. R. Morris, C. Z. Wang, and K. M. Ho, *Phys. Rev. B* **52**, (1995).

[25] Christine J. Wu, James N. Glosli, Giulia Galli, and Francis H. Ree, *Phys.Rev.Lett* **89**,135701,(2002).

[26] N. A. Marks, N. C. Cooper, and D. R. McKenzie, *Phys. Rev. B* **65**, 075411, (2002).

APPENDIX B.

ATOM POSITIONS AND VASP SCRIPT FILES FOR VASP-DIRECT RELAXATIONS

Based on randomly generated atom positions by Mathematica as listed below, the direct relaxations were carried out. In a step following, the positions of those atoms were subjected to VASP-direct relaxation by using the input parameters listed in the VASP script. A list is then provided of the relaxed positions. The data are classified based on the number of atoms in the supercell and the example shows only one of 20 calculations for each atom sets.

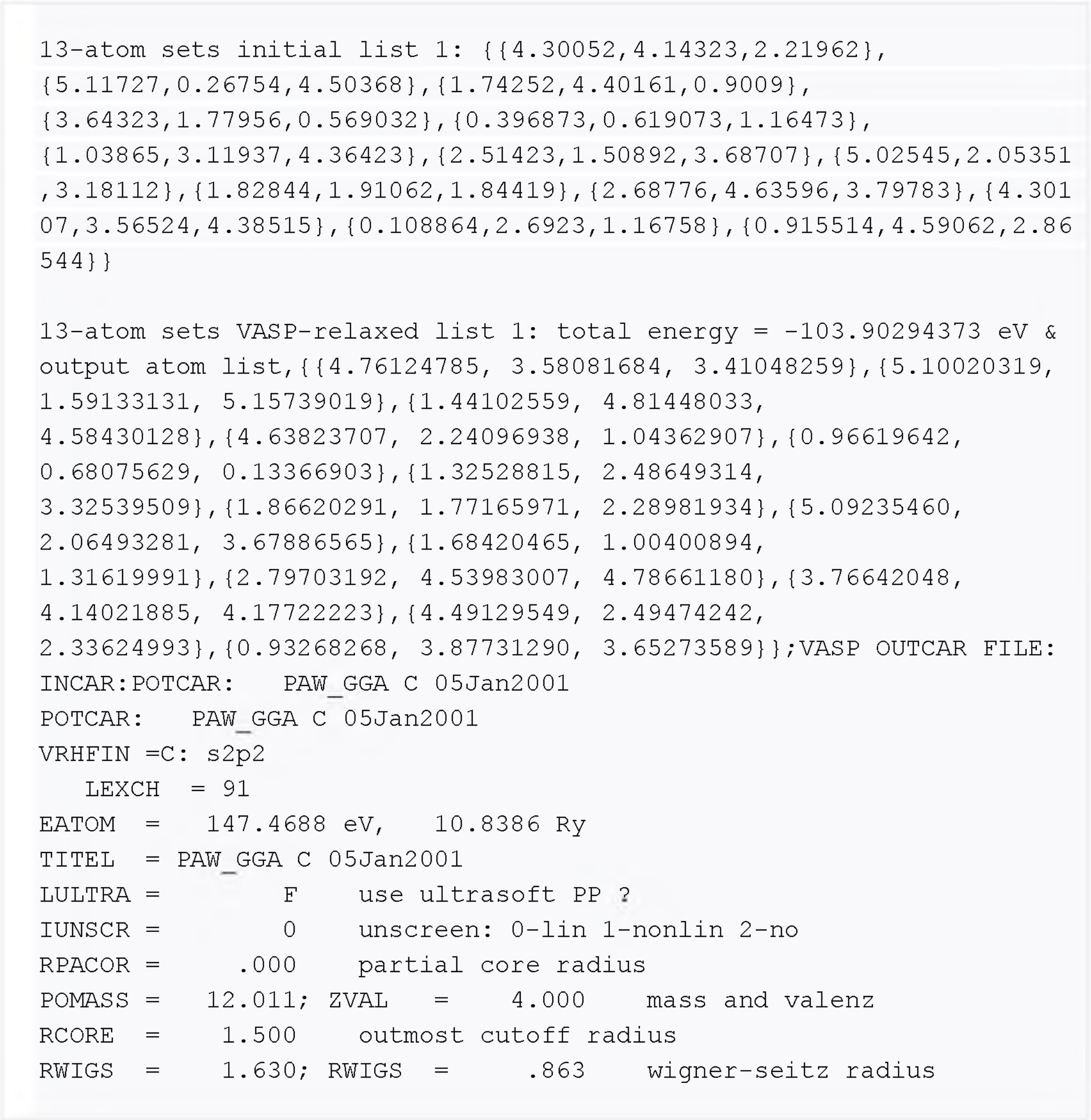

```
13-atom sets initial list 1: {{4.30052,4.14323,2.21962},
{5.11727,0.26754,4.50368},{1.74252,4.40161,0.9009},
{3.64323,1.77956,0.569032},{0.396873,0.619073,1.16473},
{1.03865,3.11937,4.36423},{2.51423,1.50892,3.68707},{5.02545,2.05351
,3.18112},{1.82844,1.91062,1.84419},{2.68776,4.63596,3.79783},{4.301
07,3.56524,4.38515},{0.108864,2.6923,1.16758},{0.915514,4.59062,2.86
544}}

13-atom sets VASP-relaxed list 1: total energy = -103.90294373 eV &
output atom list,{{4.76124785, 3.58081684, 3.41048259},{5.10020319,
1.59133131, 5.15739019},{1.44102559, 4.81448033,
4.58430128},{4.63823707, 2.24096938, 1.04362907},{0.96619642,
0.68075629, 0.13366903},{1.32528815, 2.48649314,
3.32539509},{1.86620291, 1.77165971, 2.28981934},{5.09235460,
2.06493281, 3.67886565},{1.68420465, 1.00400894,
1.31619991},{2.79703192, 4.53983007, 4.78661180},{3.76642048,
4.14021885, 4.17722223},{4.49129549, 2.49474242,
2.33624993},{0.93268268, 3.87731290, 3.65273589}};VASP OUTCAR FILE:
INCAR:POTCAR:    PAW_GGA C 05Jan2001
POTCAR:    PAW_GGA C 05Jan2001
VRHFIN =C: s2p2
   LEXCH  = 91
EATOM  =   147.4688 eV,   10.8386 Ry
TITEL  = PAW_GGA C 05Jan2001
LULTRA =        F    use ultrasoft PP ?
IUNSCR =        0    unscreen: 0-lin 1-nonlin 2-no
RPACOR =     .000    partial core radius
POMASS =   12.011; ZVAL   =    4.000    mass and valenz
RCORE  =    1.500    outmost cutoff radius
RWIGS  =    1.630; RWIGS  =     .863    wigner-seitz radius
```

Figure B.1. 13-atom set atom positions before and after with VASP script file

```
ENMAX  =  400.000; ENMIN  =  300.000 eVICORE  =        2    local
potential
LCOR   =        T    correct aug charges
   LPAW   =        T    paw PP
   EAUG   =  644.873
   DEXC   =     .000
   RMAX   =    2.266    core radius for proj-oper
   RAUG   =    1.300    factor for augmentation sphere
   RDEP   =    1.501    radius for radial grids
   RDEPT  =    1.300    core radius for aug-charge
   QCUT   =   -5.516; QGAM   =   11.033    optimization parameters
   Description
     l     E      TYP  RCUT    TYP  RCUT
     0    .000     23  1.200
     0    .000     23  1.200
     1    .000     23  1.500
     1   2.500     23  1.500
     2    .000      7  1.500
  local pseudopotential read in
  atomic valenz-charges read in
  non local Contribution for L=           0  read in
    real space projection operators read in
  non local Contribution for L=           0  read in
    real space projection operators read in
  non local Contribution for L=           1  read in
    real space projection operators read in
  non local Contribution for L=           1  read in
    real space projection operators read in
    PAW grid and wavefunctions read in
  number of l-projection  operators is LMAX  =           4
   number of lm-projection operators is LMMAX =           8

 PAW_GGA C 05Jan2001                   :
 energy of atom  1       EATOM= -147.4688
 kinetic energy error for atom=    0.0057 (will be added to EATOM!!)
POSCAR: z: 6
  positions in direct lattice
  velocities in cartesian coordinates
 exchange correlation table for  LEXCH =        7
   RHO(1)=    0.500       N(1)  =     2000
   RHO(2)=  100.500       N(2)  =     4000 ion  position
nearest neighbor table
```

Figure B.1. 13-atom set atom positions before and after with VASP script file (cont.)

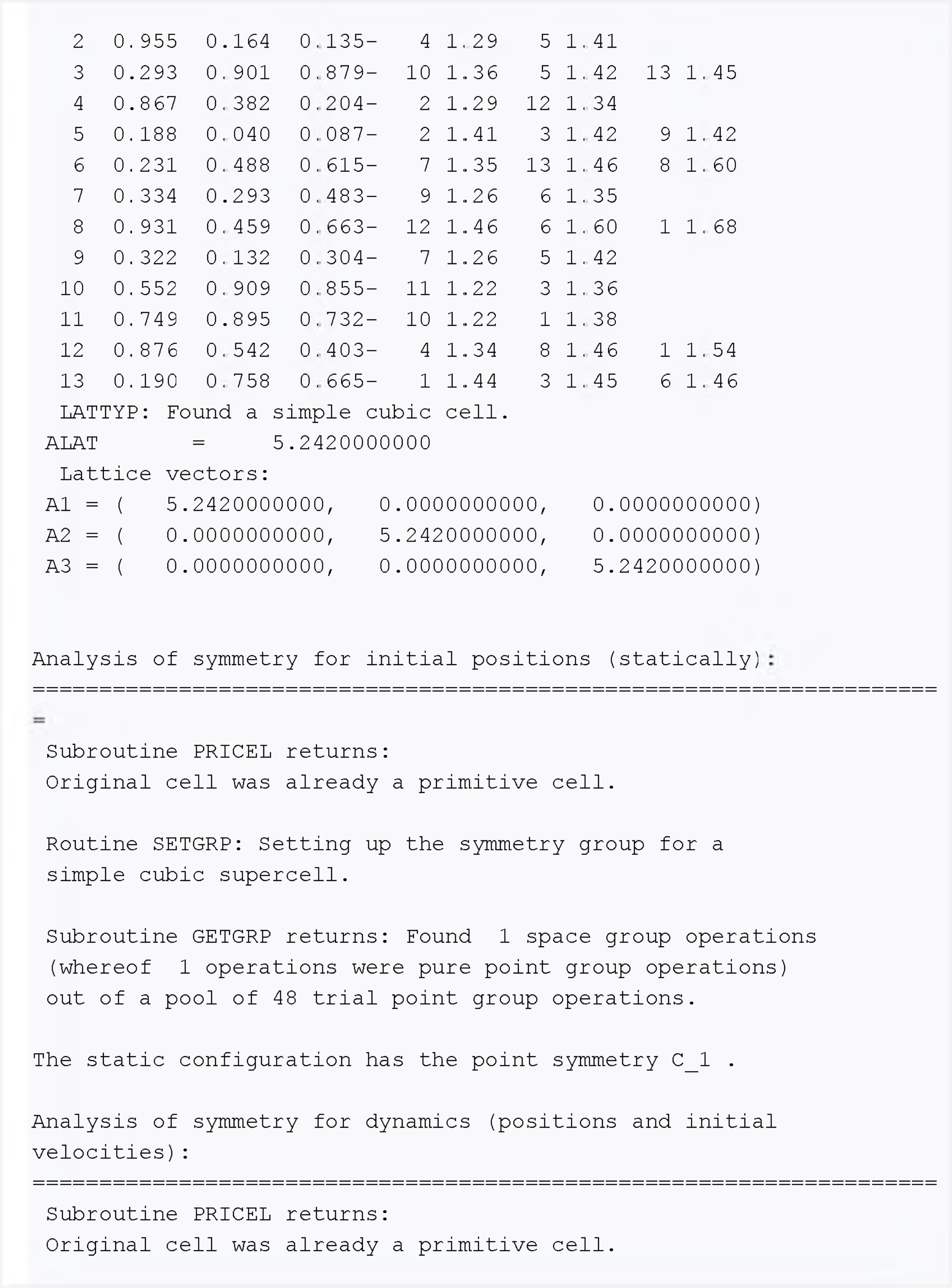

```
   2  0.955  0.164  0.135-   4 1.29   5 1.41
   3  0.293  0.901  0.879-  10 1.36   5 1.42  13 1.45
   4  0.867  0.382  0.204-   2 1.29  12 1.34
   5  0.188  0.040  0.087-   2 1.41   3 1.42   9 1.42
   6  0.231  0.488  0.615-   7 1.35  13 1.46   8 1.60
   7  0.334  0.293  0.483-   9 1.26   6 1.35
   8  0.931  0.459  0.663-  12 1.46   6 1.60   1 1.68
   9  0.322  0.132  0.304-   7 1.26   5 1.42
  10  0.552  0.909  0.855-  11 1.22   3 1.36
  11  0.749  0.895  0.732-  10 1.22   1 1.38
  12  0.876  0.542  0.403-   4 1.34   8 1.46   1 1.54
  13  0.190  0.758  0.665-   1 1.44   3 1.45   6 1.46
  LATTYP: Found a simple cubic cell.
 ALAT       =     5.2420000000
  Lattice vectors:
 A1 = (   5.2420000000,   0.0000000000,   0.0000000000)
 A2 = (   0.0000000000,   5.2420000000,   0.0000000000)
 A3 = (   0.0000000000,   0.0000000000,   5.2420000000)


Analysis of symmetry for initial positions (statically):
====================================================================
=
 Subroutine PRICEL returns:
 Original cell was already a primitive cell.

 Routine SETGRP: Setting up the symmetry group for a
 simple cubic supercell.

 Subroutine GETGRP returns: Found  1 space group operations
 (whereof  1 operations were pure point group operations)
 out of a pool of 48 trial point group operations.

The static configuration has the point symmetry C_1 .

Analysis of symmetry for dynamics (positions and initial
velocities):
====================================================================
 Subroutine PRICEL returns:
 Original cell was already a primitive cell.
```

Figure B.1. 13-atom set atom positions before and after with VASP script file (cont.)

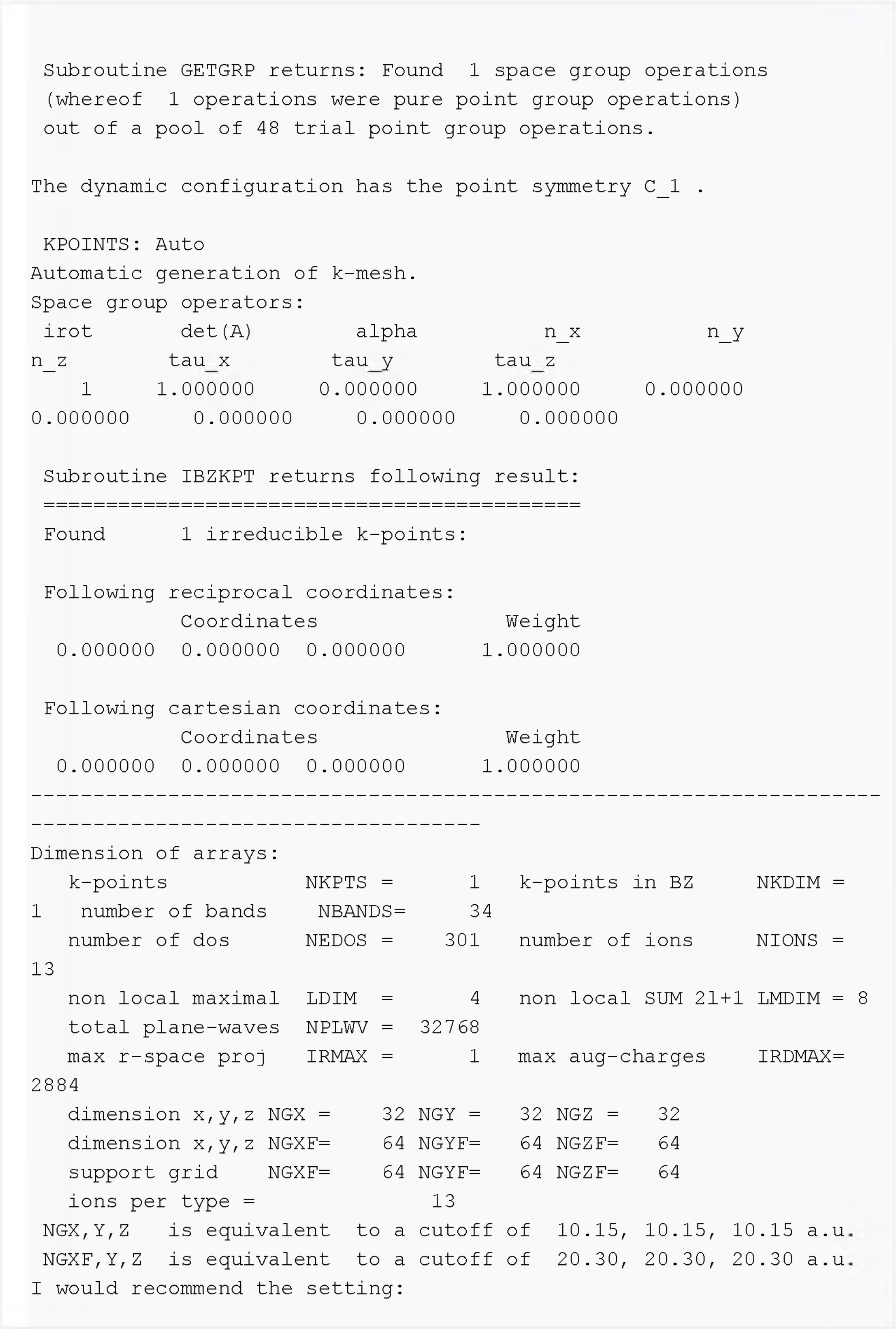

```
 Subroutine GETGRP returns: Found  1 space group operations
 (whereof  1 operations were pure point group operations)
 out of a pool of 48 trial point group operations.

The dynamic configuration has the point symmetry C_1 .

 KPOINTS: Auto
Automatic generation of k-mesh.
Space group operators:
 irot       det(A)        alpha          n_x          n_y
n_z        tau_x        tau_y        tau_z
    1     1.000000     0.000000     1.000000     0.000000
0.000000     0.000000     0.000000     0.000000

 Subroutine IBZKPT returns following result:
 ===========================================
 Found      1 irreducible k-points:

 Following reciprocal coordinates:
            Coordinates               Weight
  0.000000  0.000000  0.000000      1.000000

 Following cartesian coordinates:
            Coordinates               Weight
  0.000000  0.000000  0.000000      1.000000
--------------------------------------------------------------------
------------------------------------
Dimension of arrays:
   k-points           NKPTS =      1   k-points in BZ     NKDIM =
1   number of bands    NBANDS=     34
   number of dos      NEDOS =    301   number of ions     NIONS =
13
   non local maximal  LDIM  =      4   non local SUM 2l+1 LMDIM = 8
   total plane-waves  NPLWV =  32768
   max r-space proj   IRMAX =      1   max aug-charges    IRDMAX=
2884
   dimension x,y,z NGX =    32 NGY =    32 NGZ =   32
   dimension x,y,z NGXF=    64 NGYF=    64 NGZF=   64
   support grid    NGXF=    64 NGYF=    64 NGZF=   64
   ions per type =               13
 NGX,Y,Z   is equivalent  to a cutoff of  10.15, 10.15, 10.15 a.u.
 NGXF,Y,Z  is equivalent  to a cutoff of  20.30, 20.30, 20.30 a.u.
I would recommend the setting:
```

Figure B.1. 13-atom set atom positions before and after with VASP script file (cont.)

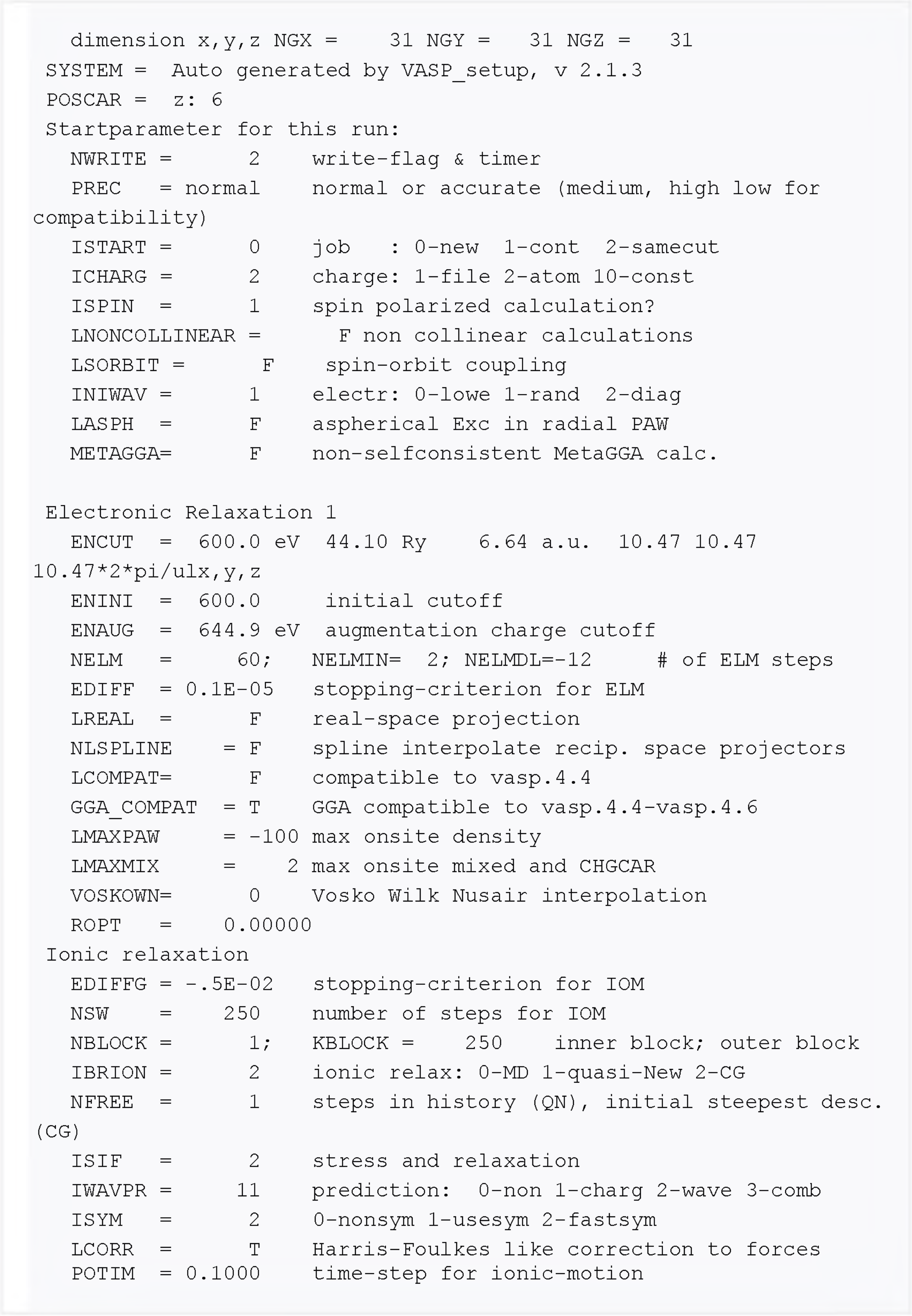

```
  dimension x,y,z NGX =    31 NGY =   31 NGZ =   31
 SYSTEM =  Auto generated by VASP_setup, v 2.1.3
 POSCAR =  z: 6
 Startparameter for this run:
   NWRITE =      2    write-flag & timer
   PREC   = normal    normal or accurate (medium, high low for
compatibility)
   ISTART =      0    job   : 0-new  1-cont  2-samecut
   ICHARG =      2    charge: 1-file 2-atom 10-const
   ISPIN  =      1    spin polarized calculation?
   LNONCOLLINEAR =      F non collinear calculations
   LSORBIT =      F    spin-orbit coupling
   INIWAV =      1    electr: 0-lowe 1-rand  2-diag
   LASPH  =      F    aspherical Exc in radial PAW
   METAGGA=      F    non-selfconsistent MetaGGA calc.

 Electronic Relaxation 1
   ENCUT  =  600.0 eV  44.10 Ry    6.64 a.u.  10.47 10.47
10.47*2*pi/ulx,y,z
   ENINI  =  600.0     initial cutoff
   ENAUG  =  644.9 eV  augmentation charge cutoff
   NELM   =     60;   NELMIN=  2; NELMDL=-12     # of ELM steps
   EDIFF  = 0.1E-05   stopping-criterion for ELM
   LREAL  =      F    real-space projection
   NLSPLINE    = F    spline interpolate recip. space projectors
   LCOMPAT=      F    compatible to vasp.4.4
   GGA_COMPAT  = T    GGA compatible to vasp.4.4-vasp.4.6
   LMAXPAW     = -100 max onsite density
   LMAXMIX     =    2 max onsite mixed and CHGCAR
   VOSKOWN=      0    Vosko Wilk Nusair interpolation
   ROPT   =    0.00000
 Ionic relaxation
   EDIFFG = -.5E-02   stopping-criterion for IOM
   NSW    =    250    number of steps for IOM
   NBLOCK =      1;   KBLOCK =    250    inner block; outer block
   IBRION =      2    ionic relax: 0-MD 1-quasi-New 2-CG
   NFREE  =      1    steps in history (QN), initial steepest desc.
(CG)
   ISIF   =      2    stress and relaxation
   IWAVPR =     11    prediction:  0-non 1-charg 2-wave 3-comb
   ISYM   =      2    0-nonsym 1-usesym 2-fastsym
   LCORR  =      T    Harris-Foulkes like correction to forces
   POTIM  = 0.1000    time-step for ionic-motion
```

Figure B.1. 13-atom set atom positions before and after with VASP script file (cont.)

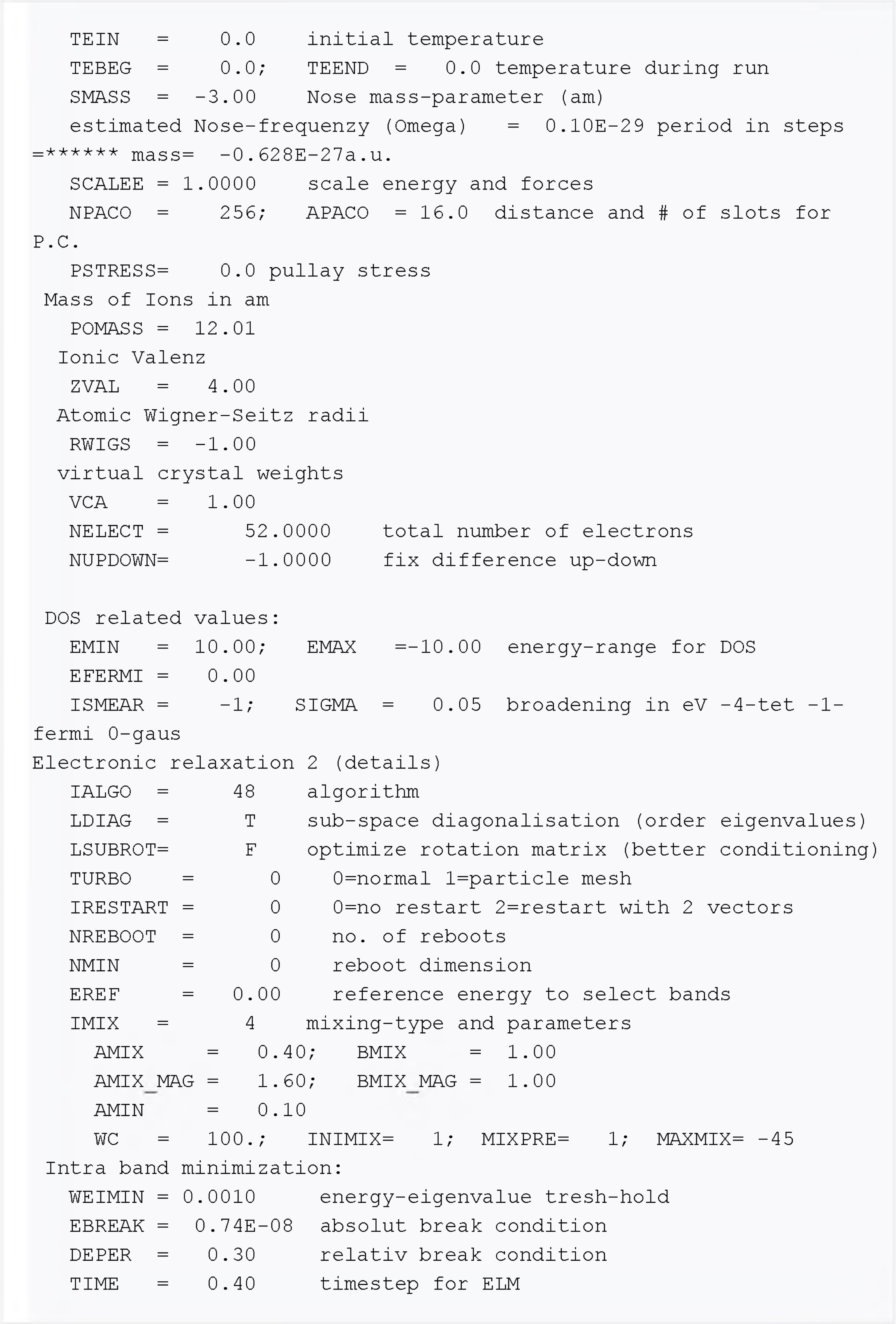

```
   TEIN   =    0.0    initial temperature
   TEBEG  =    0.0;   TEEND  =   0.0 temperature during run
   SMASS  =  -3.00    Nose mass-parameter (am)
   estimated Nose-frequenzy (Omega)   =  0.10E-29 period in steps
=****** mass=  -0.628E-27a.u.
   SCALEE = 1.0000    scale energy and forces
   NPACO  =    256;   APACO  = 16.0  distance and # of slots for
P.C.
   PSTRESS=    0.0 pullay stress
 Mass of Ions in am
   POMASS =  12.01
  Ionic Valenz
   ZVAL   =   4.00
  Atomic Wigner-Seitz radii
   RWIGS  =  -1.00
  virtual crystal weights
   VCA    =   1.00
   NELECT =      52.0000    total number of electrons
   NUPDOWN=      -1.0000    fix difference up-down

 DOS related values:
   EMIN   =  10.00;   EMAX   =-10.00  energy-range for DOS
   EFERMI =   0.00
   ISMEAR =    -1;   SIGMA  =   0.05  broadening in eV -4-tet -1-
fermi 0-gaus
Electronic relaxation 2 (details)
   IALGO  =     48    algorithm
   LDIAG  =      T    sub-space diagonalisation (order eigenvalues)
   LSUBROT=      F    optimize rotation matrix (better conditioning)
   TURBO    =      0    0=normal 1=particle mesh
   IRESTART =      0    0=no restart 2=restart with 2 vectors
   NREBOOT  =      0    no. of reboots
   NMIN     =      0    reboot dimension
   EREF     =   0.00    reference energy to select bands
   IMIX   =      4    mixing-type and parameters
     AMIX     =   0.40;   BMIX     =  1.00
     AMIX_MAG =   1.60;   BMIX_MAG =  1.00
     AMIN     =   0.10
     WC   =   100.;   INIMIX=   1;  MIXPRE=   1;  MAXMIX= -45
 Intra band minimization:
   WEIMIN = 0.0010     energy-eigenvalue tresh-hold
   EBREAK =  0.74E-08  absolut break condition
   DEPER  =   0.30     relativ break condition
   TIME   =   0.40     timestep for ELM
```

Figure B.1. 13-atom set atom positions before and after with VASP script file (cont.)

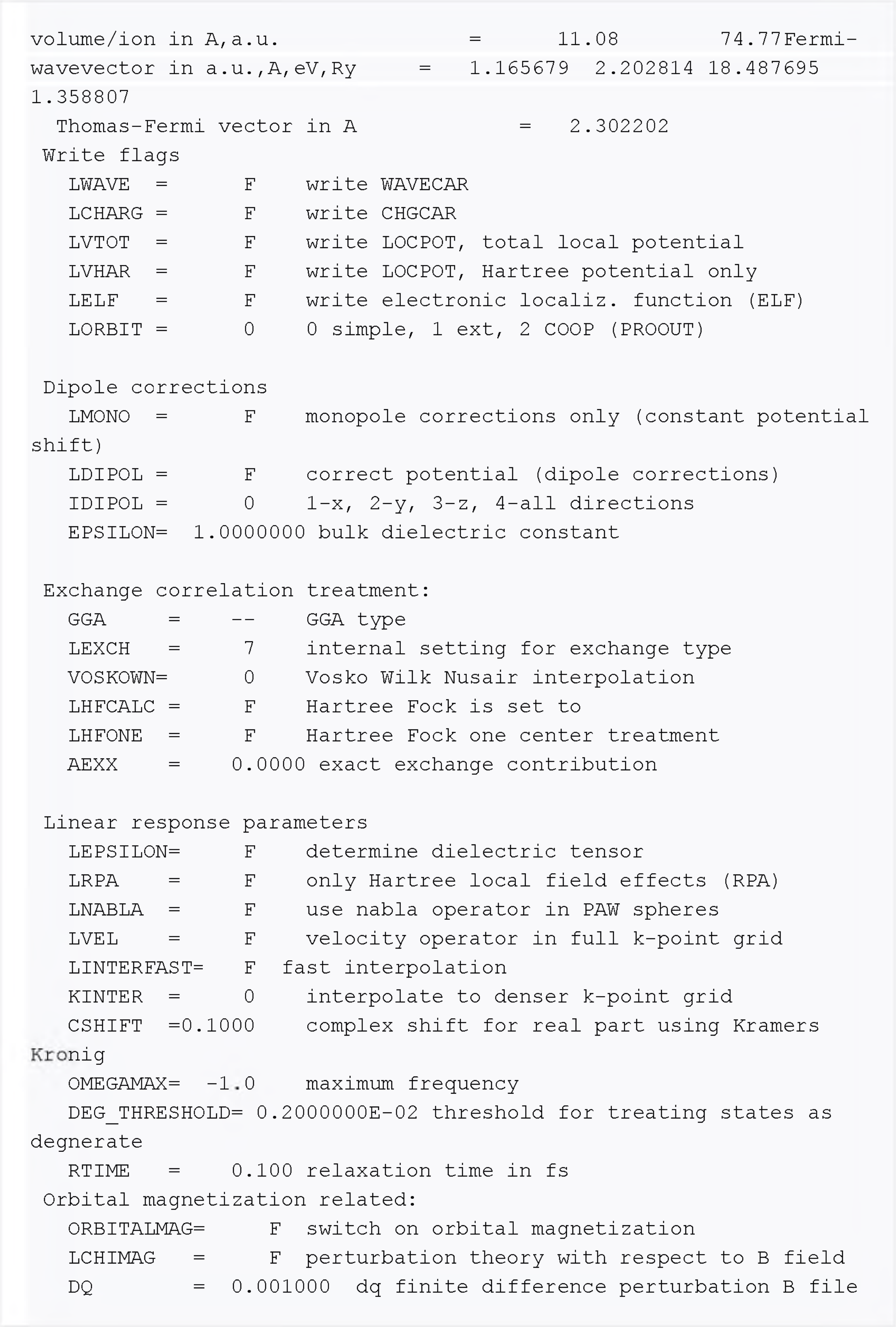

```
volume/ion in A,a.u.               =      11.08        74.77Fermi-
wavevector in a.u.,A,eV,Ry     =   1.165679  2.202814 18.487695
1.358807
  Thomas-Fermi vector in A             =   2.302202
 Write flags
   LWAVE  =      F    write WAVECAR
   LCHARG =      F    write CHGCAR
   LVTOT  =      F    write LOCPOT, total local potential
   LVHAR  =      F    write LOCPOT, Hartree potential only
   LELF   =      F    write electronic localiz. function (ELF)
   LORBIT =      0    0 simple, 1 ext, 2 COOP (PROOUT)

 Dipole corrections
   LMONO  =      F    monopole corrections only (constant potential
shift)
   LDIPOL =      F    correct potential (dipole corrections)
   IDIPOL =      0    1-x, 2-y, 3-z, 4-all directions
   EPSILON=  1.0000000 bulk dielectric constant

 Exchange correlation treatment:
   GGA     =    --    GGA type
   LEXCH   =     7    internal setting for exchange type
   VOSKOWN=      0    Vosko Wilk Nusair interpolation
   LHFCALC =     F    Hartree Fock is set to
   LHFONE  =     F    Hartree Fock one center treatment
   AEXX    =    0.0000 exact exchange contribution

 Linear response parameters
   LEPSILON=     F    determine dielectric tensor
   LRPA    =     F    only Hartree local field effects (RPA)
   LNABLA  =     F    use nabla operator in PAW spheres
   LVEL    =     F    velocity operator in full k-point grid
   LINTERFAST=   F  fast interpolation
   KINTER  =     0    interpolate to denser k-point grid
   CSHIFT  =0.1000    complex shift for real part using Kramers
Kronig
   OMEGAMAX=  -1.0    maximum frequency
   DEG_THRESHOLD= 0.2000000E-02 threshold for treating states as
degnerate
   RTIME   =    0.100 relaxation time in fs
 Orbital magnetization related:
   ORBITALMAG=     F  switch on orbital magnetization
   LCHIMAG   =     F  perturbation theory with respect to B field
   DQ        =  0.001000  dq finite difference perturbation B file
```

Figure B.1. 13-atom set atom positions before and after with VASP script file (cont.)

```
20-atom sets initial list 1:{{4.70894, 0.45358, 2.59878},
{1.25503, 0.795991, 3.99525},{0.613509,3.95759, 5.65658},
{3.36992, 1.0763, 5.54247},{5.9553, 2.50912, 1.3303},
{0.414664, 0.473751, 5.86733},{4.58637, 4.20777,2.51209},
{6.02323, 3.19577, 3.75961},{5.62087, 5.11147,4.39213},
{4.98608, 2.27953, 5.29235},{2.39883, 4.81326,2.61492},
{3.36845, 1.92227, 1.81569},{2.89041, 4.34887,5.10221},
{4.66011, 5.32474, 0.0934039},{0.537148, 4.83371,1.77385},
{1.55271, 0.659662, 1.90586},{2.91447, 2.59893,4.05912},{1.71865,
2.20664, 5.92054},{3.0675, 3.85395,0.985239}, {1.60569, 2.66824,
2.41366}}.
20-atom sets VASP-relaxed list 1: total energy = -163.23884452 eV &
output atom list,
{5.21992768, 5.76360078, 3.43900465},{0.40203472, 0.38417634,
3.34395925},
{1.36283019, 3.49141265, 5.18986589}, {4.42032429, 1.52195593,
5.17601460}, {1.67271745, 2.27823397, 3.25271548}, {0.58728354,
1.59670878, 4.11303913},
{4.84276445, 5.19514644, 2.22991502}, {6.02836825, 3.68907353,
5.16231132},
{5.32695275, 4.95118589, 5.73100970}, {5.52640044, 2.31802720,
4.82626618}, {1.10828241, 5.03081102, 1.43121796}, {2.10199258,
2.78716441, 2.03770731},
{2.59166964, 3.54629746, 5.95736528}, {4.77580104, 5.94351806,
4.89151217}, {5.68800678, 4.99730398, 1.14352814}, {1.34823181,
0.13827956, 2.28231517}, {3.14345317, 2.22457676, 5.44488821},
{1.88614690, 2.18489745, 4.67241271},
{2.15024454, 3.92959503, 1.20708041}, {2.06444837, 1.37017877,
2.15025430},

VASP OUTCAR FILE:
INCAR:
POTCAR:   PAW_GGA C 05Jan2001
 POTCAR:   PAW_GGA C 05Jan2001
   VRHFIN =C: s2p2
   LEXCH  = 91
   EATOM  =   147.4688 eV,   10.8386 Ry
   TITEL  = PAW_GGA C 05Jan2001
   LULTRA =        F    use ultrasoft PP ?
   IUNSCR =        0    unscreen: 0-lin 1-nonlin 2-no
   RPACOR =     .000    partial core radius
   POMASS =   12.011; ZVAL   =    4.000    mass and valenz
   RCORE  =    1.500    outmost cutoff radius  RWIGS  =    1.630;
RWIGS  =     .863    wigner-seitz radius (auA)
```

Figure B.2. 20-atom set atom positions before and after with VASP script file.

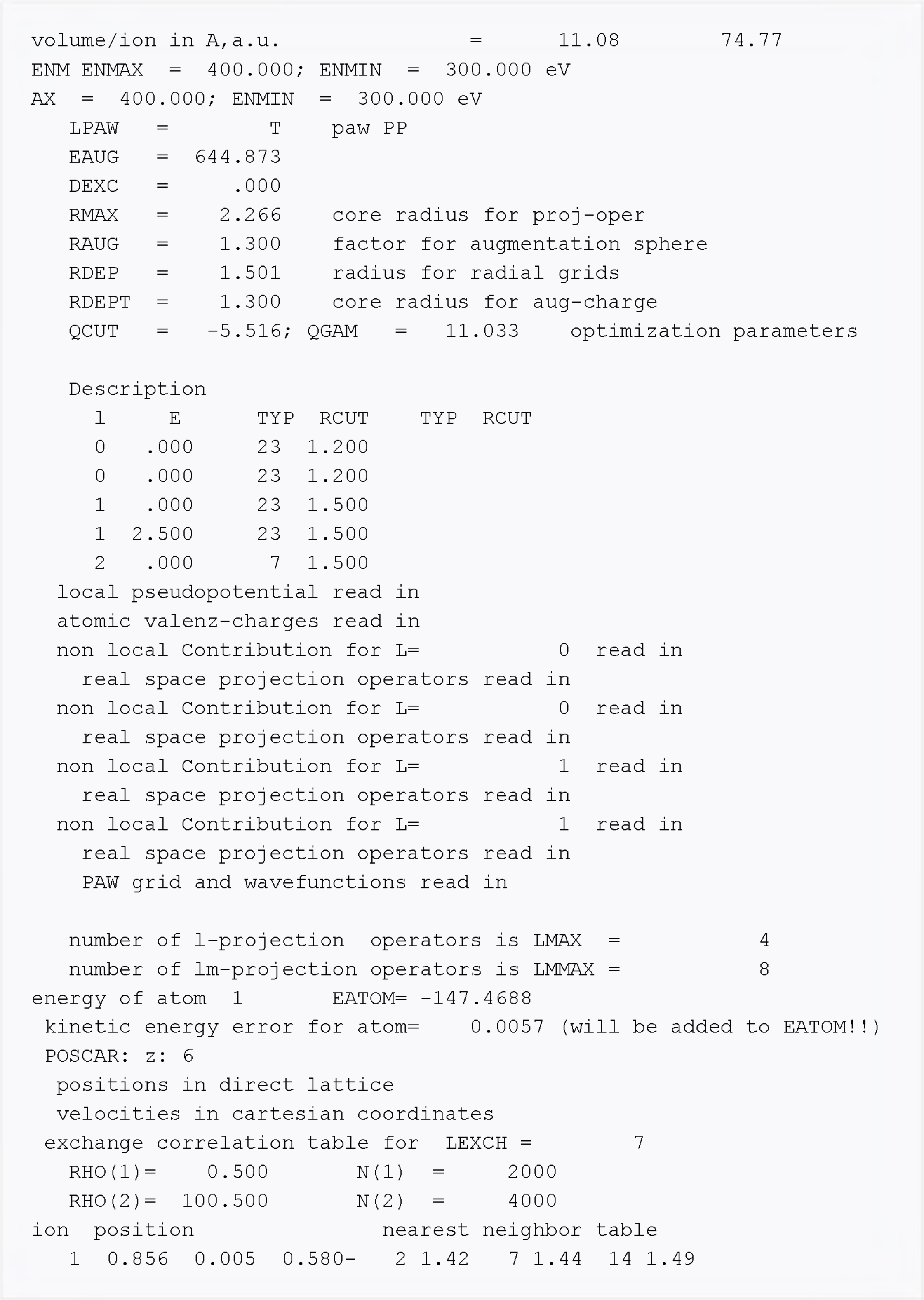

```
volume/ion in A,a.u.               =      11.08        74.77
ENM ENMAX  =  400.000; ENMIN  =  300.000 eV
AX  =  400.000; ENMIN  =  300.000 eV
   LPAW   =        T    paw PP
   EAUG   =  644.873
   DEXC   =     .000
   RMAX   =    2.266    core radius for proj-oper
   RAUG   =    1.300    factor for augmentation sphere
   RDEP   =    1.501    radius for radial grids
   RDEPT  =    1.300    core radius for aug-charge
   QCUT   =   -5.516; QGAM   =   11.033    optimization parameters

   Description
     l     E      TYP  RCUT    TYP  RCUT
     0   .000     23  1.200
     0   .000     23  1.200
     1   .000     23  1.500
     1  2.500     23  1.500
     2   .000      7  1.500
  local pseudopotential read in
  atomic valenz-charges read in
  non local Contribution for L=           0  read in
    real space projection operators read in
  non local Contribution for L=           0  read in
    real space projection operators read in
  non local Contribution for L=           1  read in
    real space projection operators read in
  non local Contribution for L=           1  read in
    real space projection operators read in
    PAW grid and wavefunctions read in

   number of l-projection  operators is LMAX  =           4
   number of lm-projection operators is LMMAX =           8
energy of atom  1       EATOM= -147.4688
 kinetic energy error for atom=    0.0057 (will be added to EATOM!!)
 POSCAR: z: 6
  positions in direct lattice
  velocities in cartesian coordinates
 exchange correlation table for  LEXCH =        7
   RHO(1)=    0.500       N(1)  =     2000
   RHO(2)=  100.500       N(2)  =     4000
ion  position               nearest neighbor table
   1  0.856  0.005  0.580-   2 1.42   7 1.44  14 1.49
```

Figure B.2. 20-atom set atom positions before and after with VASP script file (cont.)

```
   2  0.074  0.076  0.571-   1 1.42   6 1.43  16 1.44
   3  0.171  0.602  0.777-   8 1.40  13 1.46  18 1.54  17 2.03
   4  0.732  0.253  0.884-  17 1.35  10 1.42  14 1.48
   5  0.411  0.312  0.478-  12 1.33  20 1.49  18 1.50
   6  0.118  0.229  0.733-   2 1.43  10 1.43  18 1.46
   7  0.732  0.964  0.379-  15 1.43   1 1.44  20 1.52
   8  0.952  0.594  0.872-   3 1.40  10 1.43   9 1.50
   9  0.837  0.819  0.972-  14 1.37   8 1.50  15 1.53
  10  0.927  0.360  0.857-   4 1.42   8 1.43   6 1.43
  11  0.153  0.845  0.254-  16 1.43  15 1.47  19 1.48
  12  0.439  0.466  0.314-   5 1.33  19 1.39
  13  0.365  0.604  0.941-  19 1.39  17 1.43   3 1.46
  14  0.781  0.010  0.816-   9 1.37   4 1.48   1 1.49
  15  0.894  0.867  0.213-   7 1.43  11 1.47   9 1.53
  16  0.240  0.989  0.402-  11 1.43   2 1.44  20 1.48
  17  0.498  0.379  0.877-   4 1.35  13 1.43  18 1.55   3 2.03
  18  0.301  0.360  0.699-   6 1.46   5 1.50   3 1.54  17 1.55
  19  0.344  0.661  0.162-  12 1.39  13 1.39  11 1.48
  20  0.462  0.072  0.396-  16 1.48   5 1.49   7 1.52

  LATTYP: Found a triclinic cell.
 ALAT       =     5.9877466467
 B/A-ratio  =     1.4072158776
 C/A-ratio  =     3.1025439193
 COS(alpha) =     0.0011863853
 COS(beta)  =     0.6476078176
 COS(gamma) =     0.7341174849
  Lattice vectors:
 A1 = (   0.1078547181,  -0.2419282343,  -5.9818849867)
 A2 = (   5.7795907161,   0.5260576732,  -6.1088418992)
 A3 = ( -11.8727920696,  -7.8489940449, -11.9391877934)
Analysis of symmetry for initial positions (statically):
====================================================================
=

 Subroutine PRICEL returns:
 Original cell was already a primitive cell.
 Routine SETGRP: Setting up the symmetry group for a
 triclinic supercell.
 Subroutine GETGRP returns: Found  1 space group operations
 (whereof  1 operations were pure point group operations)
 out of a pool of  2 trial point group operations.

The static configuration has the point symmetry C_1
```

Figure B.2. 20-atom set atom positions before and after with VASP script file (cont.)

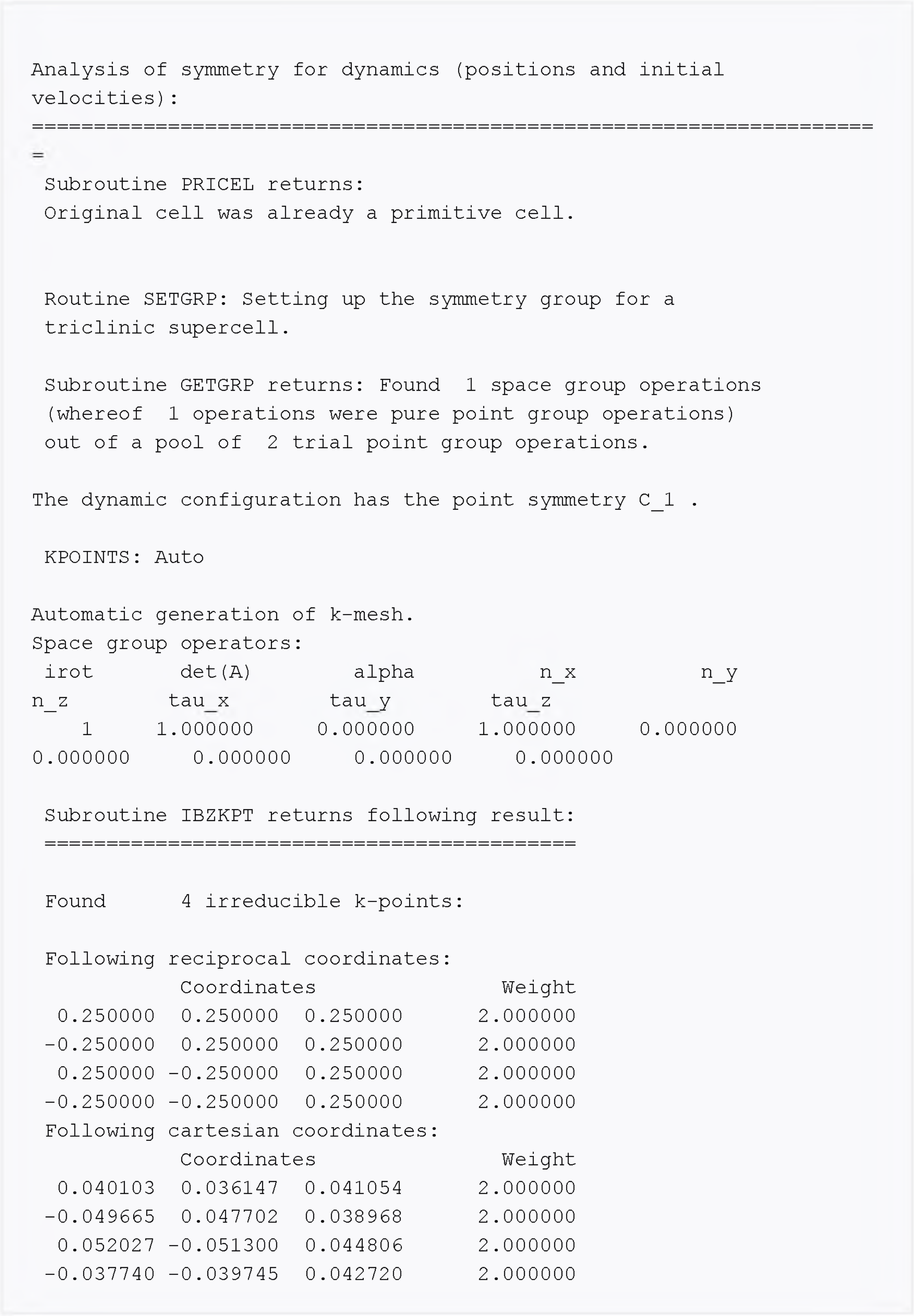

```
Analysis of symmetry for dynamics (positions and initial
velocities):
=====================================================================
=
 Subroutine PRICEL returns:
 Original cell was already a primitive cell.


 Routine SETGRP: Setting up the symmetry group for a
 triclinic supercell.

 Subroutine GETGRP returns: Found  1 space group operations
 (whereof  1 operations were pure point group operations)
 out of a pool of  2 trial point group operations.

The dynamic configuration has the point symmetry C_1 .

 KPOINTS: Auto

Automatic generation of k-mesh.
Space group operators:
 irot       det(A)        alpha          n_x          n_y
n_z        tau_x        tau_y        tau_z
    1     1.000000     0.000000     1.000000     0.000000
0.000000     0.000000     0.000000     0.000000

 Subroutine IBZKPT returns following result:
 ===========================================

 Found      4 irreducible k-points:

 Following reciprocal coordinates:
            Coordinates               Weight
  0.250000  0.250000  0.250000      2.000000
 -0.250000  0.250000  0.250000      2.000000
  0.250000 -0.250000  0.250000      2.000000
 -0.250000 -0.250000  0.250000      2.000000
 Following cartesian coordinates:
            Coordinates               Weight
  0.040103  0.036147  0.041054      2.000000
 -0.049665  0.047702  0.038968      2.000000
  0.052027 -0.051300  0.044806      2.000000
 -0.037740 -0.039745  0.042720      2.000000
```

Figure B.2. 20-atom set atom positions before and after with VASP script file (cont.)

```
k-points           NKPTS =      4   k-points in BZ     NKDIM =
4   number of bands    NBANDS=     52
   number of dos      NEDOS =    301   number of ions     NIONS =
20
   non local maximal  LDIM  =      4   non local SUM 2l+1 LMDIM =
8
   total plane-waves  NPLWV =  46656
   max r-space proj   IRMAX =      1   max aug-charges    IRDMAX=
3039
   dimension x,y,z NGX =    36 NGY =   36 NGZ =   36
   dimension x,y,z NGXF=    72 NGYF=   72 NGZF=   72
   support grid    NGXF=    72 NGYF=   72 NGZF=   72
   ions per type =              20
 NGX,Y,Z   is equivalent  to a cutoff of  10.45, 10.18, 10.00 a.u.
 NGXF,Y,Z  is equivalent  to a cutoff of  20.91, 20.35, 19.99 a.u.
 I would recommend the setting:
   dimension x,y,z NGX =    34 NGY =   35 NGZ =   36
 SYSTEM =  Auto generated by VASP_setup, v 2.1.3
 POSCAR =  z: 6

 Startparameter for this run:
   NWRITE =      2    write-flag & timer
   PREC   = normal    normal or accurate (medium, high low for
compatibility)
   ISTART =      0    job   : 0-new  1-cont  2-samecut
   ICHARG =      2    charge: 1-file 2-atom 10-const
   ISPIN  =      1    spin polarized calculation?
   LNONCOLLINEAR =      F non collinear calculations
   LSORBIT =      F    spin-orbit coupling
   INIWAV =      1    electr: 0-lowe 1-rand  2-diag
   LASPH  =      F    aspherical Exc in radial PAW
   METAGGA=      F    non-selfconsistent MetaGGA calc.
 Electronic Relaxation 1
   ENCUT  =  600.0 eV  44.10 Ry    6.64 a.u.  11.43 11.75
11.96*2*pi/ulx,y,z
   ENINI  =  600.0     initial cutoff
   ENAUG  =  644.9 eV  augmentation charge cutoff
   NELM   =     60;   NELMIN=  2; NELMDL=  0     # of ELM steps
   EDIFF  = 0.1E-05   stopping-criterion for ELM
   LREAL  =      F    real-space projection
   NLSPLINE    = F    spline interpolate recip. space projectors
   LCOMPAT=      F    compatible to vasp.4.4
   GGA_COMPAT  = T    GGA compatible to vasp.4.4-vasp.4.6
```

Figure B.2. 20-atom set atom positions before and after with VASP script file (cont.)

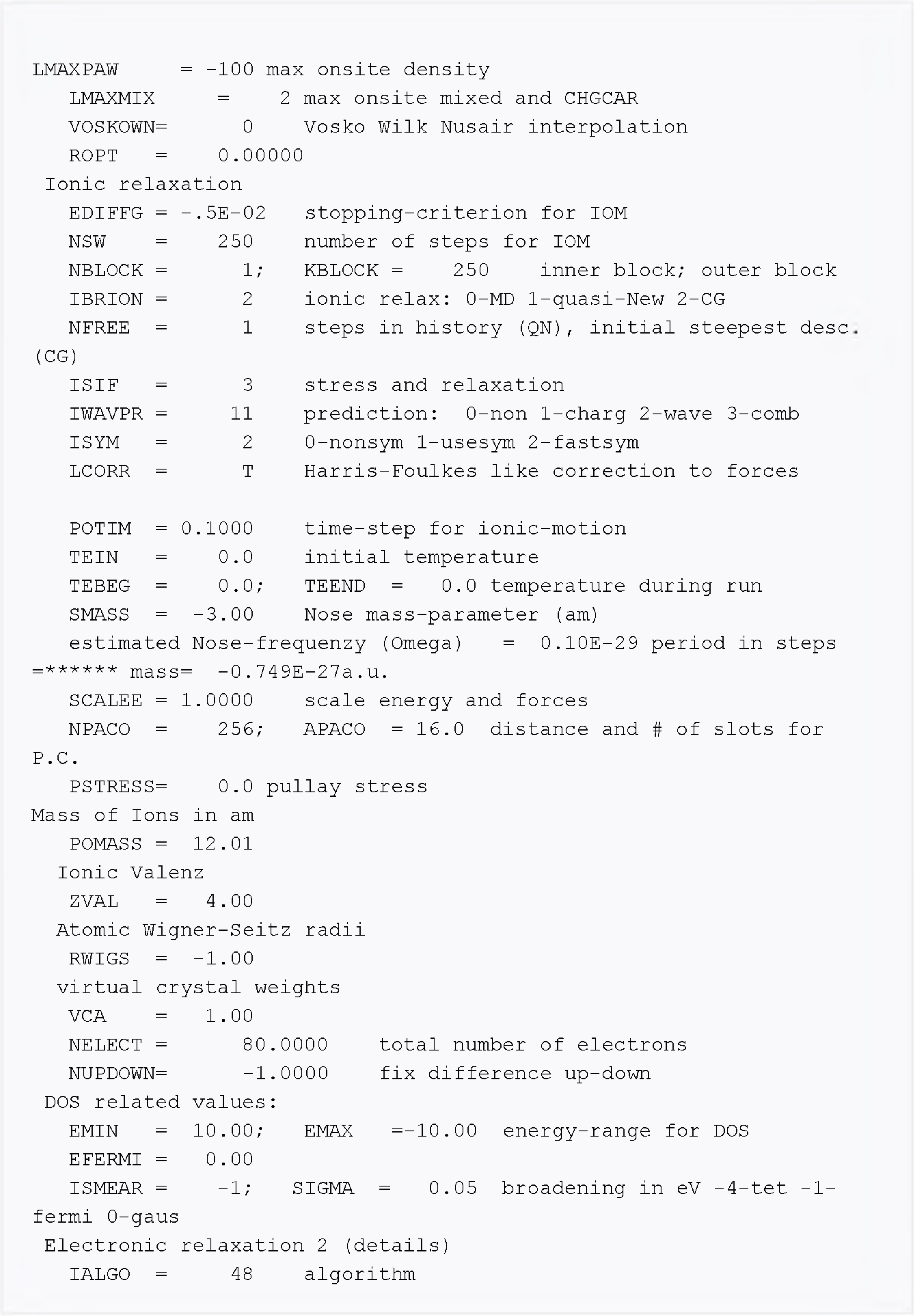

```
LMAXPAW     = -100 max onsite density
   LMAXMIX     =    2 max onsite mixed and CHGCAR
   VOSKOWN=      0    Vosko Wilk Nusair interpolation
   ROPT   =    0.00000
 Ionic relaxation
   EDIFFG = -.5E-02   stopping-criterion for IOM
   NSW    =    250    number of steps for IOM
   NBLOCK =      1;   KBLOCK =    250    inner block; outer block
   IBRION =      2    ionic relax: 0-MD 1-quasi-New 2-CG
   NFREE  =      1    steps in history (QN), initial steepest desc.
(CG)
   ISIF   =      3    stress and relaxation
   IWAVPR =     11    prediction:  0-non 1-charg 2-wave 3-comb
   ISYM   =      2    0-nonsym 1-usesym 2-fastsym
   LCORR  =      T    Harris-Foulkes like correction to forces

   POTIM  = 0.1000    time-step for ionic-motion
   TEIN   =    0.0    initial temperature
   TEBEG  =    0.0;   TEEND  =   0.0 temperature during run
   SMASS  =  -3.00    Nose mass-parameter (am)
   estimated Nose-frequenzy (Omega)   =  0.10E-29 period in steps
=****** mass=  -0.749E-27a.u.
   SCALEE = 1.0000    scale energy and forces
   NPACO  =    256;   APACO  = 16.0  distance and # of slots for
P.C.
   PSTRESS=    0.0 pullay stress
Mass of Ions in am
   POMASS =  12.01
  Ionic Valenz
   ZVAL   =   4.00
  Atomic Wigner-Seitz radii
   RWIGS  =  -1.00
  virtual crystal weights
   VCA    =   1.00
   NELECT =      80.0000    total number of electrons
   NUPDOWN=      -1.0000    fix difference up-down
 DOS related values:
   EMIN   =  10.00;   EMAX   =-10.00  energy-range for DOS
   EFERMI =   0.00
   ISMEAR =    -1;   SIGMA  =   0.05  broadening in eV -4-tet -1-
fermi 0-gaus
 Electronic relaxation 2 (details)
   IALGO  =     48    algorithm
```

Figure B.2. 20-atom set atom positions before and after with VASP script file (cont.)

```
LDIAG  =      T    sub-space diagonalisation (order eigenvalues)
   LSUBROT=      F    optimize rotation matrix (better conditioning)
   TURBO    =      0    0=normal 1=particle mesh
   IRESTART =      0    0=no restart 2=restart with 2 vectors
   NREBOOT  =      0    no. of reboots
   NMIN     =      0    reboot dimension
   EREF     =   0.00    reference energy to select bands
   IMIX   =      4    mixing-type and parameters
     AMIX     =   0.40;   BMIX     =  1.00
     AMIX_MAG =   1.60;   BMIX_MAG =  1.00
     AMIN     =   0.10
     WC   =   100.;   INIMIX=   1;  MIXPRE=   1;  MAXMIX= -45
 Intra band minimization:
   WEIMIN = 0.0010     energy-eigenvalue tresh-hold
   EBREAK =  0.48E-08  absolut break condition
   DEPER  =   0.30     relativ break condition
   TIME   =   0.40     timestep for ELM

  volume/ion in A,a.u.               =       9.70        65.43
  Fermi-wavevector in a.u.,A,eV,Ry     =   1.218720  2.303047
20.208448  1.485279
  Thomas-Fermi vector in A             =   2.353997
 Write flags
   LWAVE  =      F    write WAVECAR
   LCHARG =      F    write CHGCAR
   LVTOT  =      F    write LOCPOT, total local potential
   LVHAR  =      F    write LOCPOT, Hartree potential only
   LELF   =      F    write electronic localiz. function (ELF)
   LORBIT =      0    0 simple, 1 ext, 2 COOP (PROOUT)
 Dipole corrections
   LMONO  =      F    monopole corrections only (constant potential
shift)
   LDIPOL =      F    correct potential (dipole corrections)
   IDIPOL =      0    1-x, 2-y, 3-z, 4-all directions
   EPSILON=  1.0000000 bulk dielectric constant

 Exchange correlation treatment:
   GGA     =    --    GGA type
   LEXCH   =     7    internal setting for exchange type
   VOSKOWN=      0    Vosko Wilk Nusair interpolation
   LHFCALC =     F    Hartree Fock is set to
   LHFONE  =     F    Hartree Fock one center treatment
   AEXX    =    0.0000 exact exchange contribution
```

Figure B.2. 20-atom set atom positions before and after with VASP script file (cont.)

```
Linear response parameters
   LEPSILON=     F    determine dielectric tensor
   LRPA    =     F    only Hartree local field effects (RPA)
   LNABLA  =     F    use nabla operator in PAW spheres
   LVEL    =     F    velocity operator in full k-point grid
   LINTERFAST=   F  fast interpolation
   KINTER  =     0    interpolate to denser k-point grid
   CSHIFT  =0.1000    complex shift for real part using Kramers
Kronig
   OMEGAMAX=  -1.0    maximum frequency
   DEG_THRESHOLD= 0.2000000E-02 threshold for treating states as
degnerate
   RTIME   =    0.100 relaxation time in fs
 Orbital magnetization related:
   ORBITALMAG=     F  switch on orbital magnetization
   LCHIMAG   =     F  perturbation theory with respect to B field
   DQ        =  0.001000  dq finite difference perturbation B field
--------------------------------------------------------------------
-----------------------------------
```

Figure B.2. 20-atom set atom positions before and after with VASP script file (cont.)

```
30-atom sets initial list 1:{{1.01913, 6.0403,1.89946},
{5.63274,2.39898,5.46109},{2.47674,2.8279, 4.20045},
{3.43364,3.59198,2.1506},{3.13875,6.67895,6.37144},{6.08006,5.79328,
0.652371},{6.07824,3.35565,6.72227},{2.95514,6.4397,4.62026},{4.8297
8, 2.99628,4.7041},{2.48223, 6.13207, 6.08146},{4.22451,
4.66939,3.57519},{6.78571, 6.90225, 5.3503},{1.87691,
3.03816,5.17147},{1.05144, 0.616569, 0.148764},
{0.789685,2.93854,4.13859},{1.92215, 3.12918, 6.6111},{1.33765,
1.5468,4.47976},{4.34794, 6.23941, 0.55703},
{3.57553,6.47643,3.72109},
{5.09783,4.60282,4.66873},{5.30942,0.494591,0.580739},{2.35913,3.100
73,6.14657},{6.2554, 3.4423,4.34783}, {1.48316, 6.17198, 4.47282},
{4.77946,3.7138,5.35311},{4.42487, 3.86555, 6.1044},
{6.46007, 3.30237,2.50201},{4.64939, 3.87171, 1.57142},
{3.50199, 5.81221,2.63157},{3.05216, 3.35073, 6.65465};

30-atom sets VASP-relaxed list 1: total energy = -247.19066455 eV &
output atom list,
```

Figure B.3. 30-atom set atom positions before and after with VASP script file.

```
{{0.85432452,0.44464104,
0.59314269},{5.29860745,1.84235437,5.94813533},
{2.39026260,2.48209011,4.09781762},{3.15828000,2.28724871,2.76674567
},{3.07753880,6.39805955,6.48630269},{6.57260248,1.03108510,0.776431
13},{5.76647115,2.96159082,6.76195555},{2.95517788,5.96953217,5.0176
5249},{5.00412917,2.07178995,4.60481928},{1.72225924,5.15566353,4.55
163901},{4.93731991,5.11007560,3.49517591},{0.71797332,0.44106048,4.
07641058},{1.57058370,3.77763485,4.36632881},{1.96114492,6.84545222,
0.20411655},{0.41350423,2.94512378,4.15108072},{6.16052381,2.5013596
0,1.14933273},{1.07307487,1.74724529,4.08801019},{4.51948254,6.49081
764,0.10114679},{3.42029222,0.25231728,4.16186805},{5.37613394,4.320
82020,4.58287180},{5.32948570,0.65326961,6.84207864},{3.66962138,1.6
9089705,4.05762663},{5.91584537,3.10750165,3.88936041},{0.79367740,6
.13933560,4.24961016},{5.40702489,4.27240861,6.35619488},{5.09802069
,5.14787793,0.58620154},{5.82876938,3.32489911,2.27869028},{5.281778
85,4.63706830,2.03361938},{4.04565323,6.06215771,3.98271741},{3.0912
9136,2.64769215,1.53920108}};

VASP OUTCAR SCRIPT:
INCAR:
 POTCAR:   PAW_GGA C 05Jan2001
 POTCAR:   PAW_GGA C 05Jan2001
   VRHFIN =C: s2p2
   LEXCH  = 91
   EATOM  =   147.4688 eV,   10.8386 R
 TITEL  = PAW_GGA C 05Jan2001
   LULTRA =        F    use ultrasoft PP ?
   IUNSCR =        0    unscreen: 0-lin 1-nonlin 2-no
   RPACOR =     .000    partial core radius
   POMASS =   12.011; ZVAL   =    4.000    mass and valenz
   RCORE  =    1.500    outmost cutoff radius
   RWIGS  =    1.630; RWIGS  =     .863    wigner-seitz radius (au
A)
   ENMAX  =  400.000; ENMIN  =  300.000 eV
   ICORE  =        2    local potential
   LCOR   =        T    correct aug charges
   LPAW   =        T    paw PP
   EAUG   =  644.873
   DEXC   =     .000
   RMAX   =    2.266    core radius for proj-oper
   RAUG   =    1.300    factor for augmentation sphere
   RDEP   =    1.501    radius for radial grids
   RDEPT  =    1.300    core radius for aug-charg
```

Figure B.3. 30-atom set atom positions before and after with VASP script file (cont.)

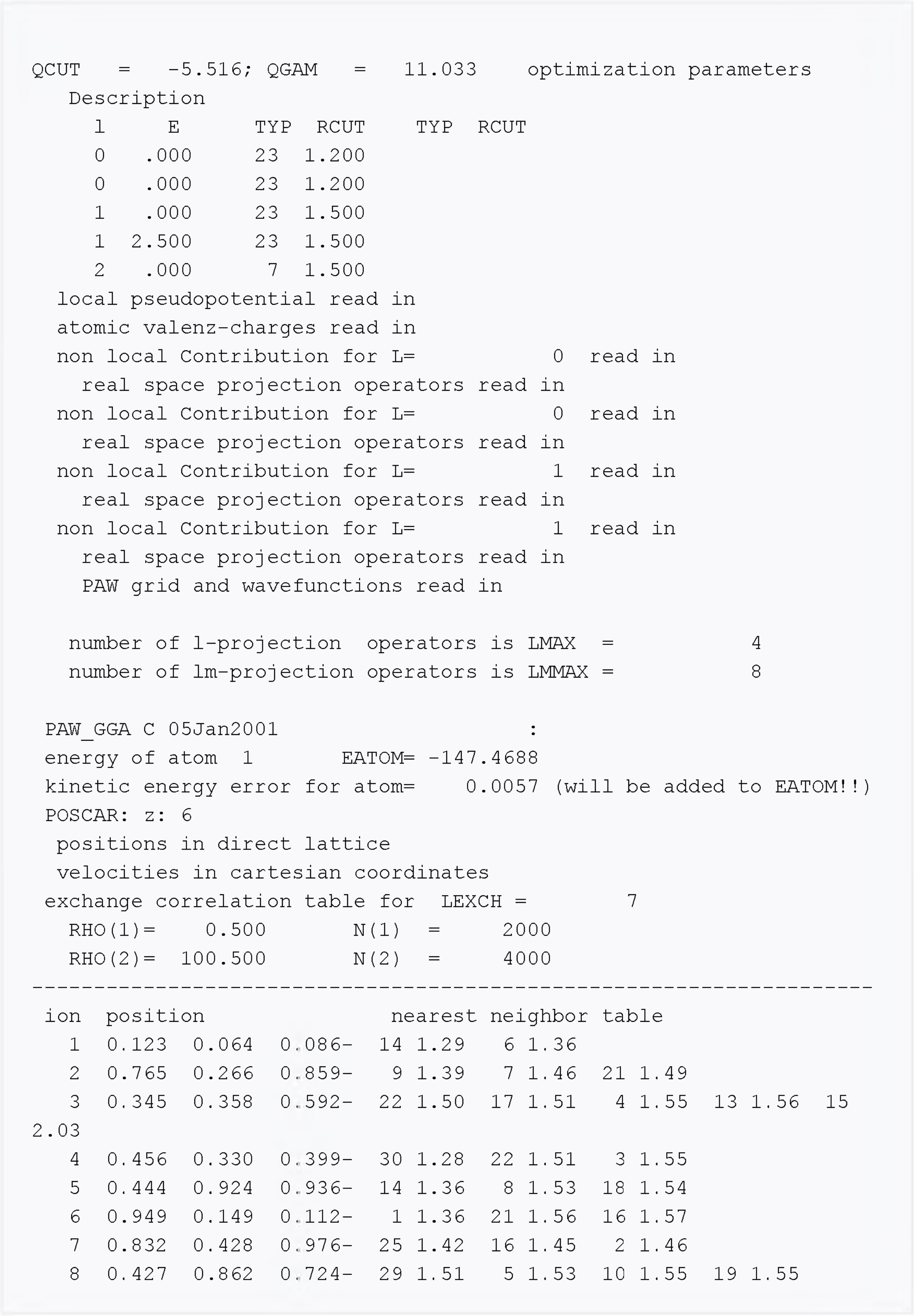

```
QCUT   =   -5.516; QGAM   =   11.033    optimization parameters
   Description
     l     E      TYP  RCUT    TYP  RCUT
     0   .000     23  1.200
     0   .000     23  1.200
     1   .000     23  1.500
     1  2.500     23  1.500
     2   .000      7  1.500
  local pseudopotential read in
  atomic valenz-charges read in
  non local Contribution for L=           0  read in
    real space projection operators read in
  non local Contribution for L=           0  read in
    real space projection operators read in
  non local Contribution for L=           1  read in
    real space projection operators read in
  non local Contribution for L=           1  read in
    real space projection operators read in
    PAW grid and wavefunctions read in

   number of l-projection  operators is LMAX  =           4
   number of lm-projection operators is LMMAX =           8

 PAW_GGA C 05Jan2001                    :
 energy of atom  1       EATOM= -147.4688
 kinetic energy error for atom=    0.0057 (will be added to EATOM!!)
 POSCAR: z: 6
  positions in direct lattice
  velocities in cartesian coordinates
 exchange correlation table for  LEXCH =        7
   RHO(1)=    0.500       N(1)  =     2000
   RHO(2)=  100.500       N(2)  =     4000
--------------------------------------------------------------------
 ion  position               nearest neighbor table
   1  0.123  0.064  0.086-  14 1.29   6 1.36
   2  0.765  0.266  0.859-   9 1.39   7 1.46  21 1.49
   3  0.345  0.358  0.592-  22 1.50  17 1.51   4 1.55  13 1.56  15
2.03
   4  0.456  0.330  0.399-  30 1.28  22 1.51   3 1.55
   5  0.444  0.924  0.936-  14 1.36   8 1.53  18 1.54
   6  0.949  0.149  0.112-   1 1.36  21 1.56  16 1.57
   7  0.832  0.428  0.976-  25 1.42  16 1.45   2 1.46
   8  0.427  0.862  0.724-  29 1.51   5 1.53  10 1.55  19 1.55
```

Figure B.3. 30-atom set atom positions before and after with VASP script file (cont.)

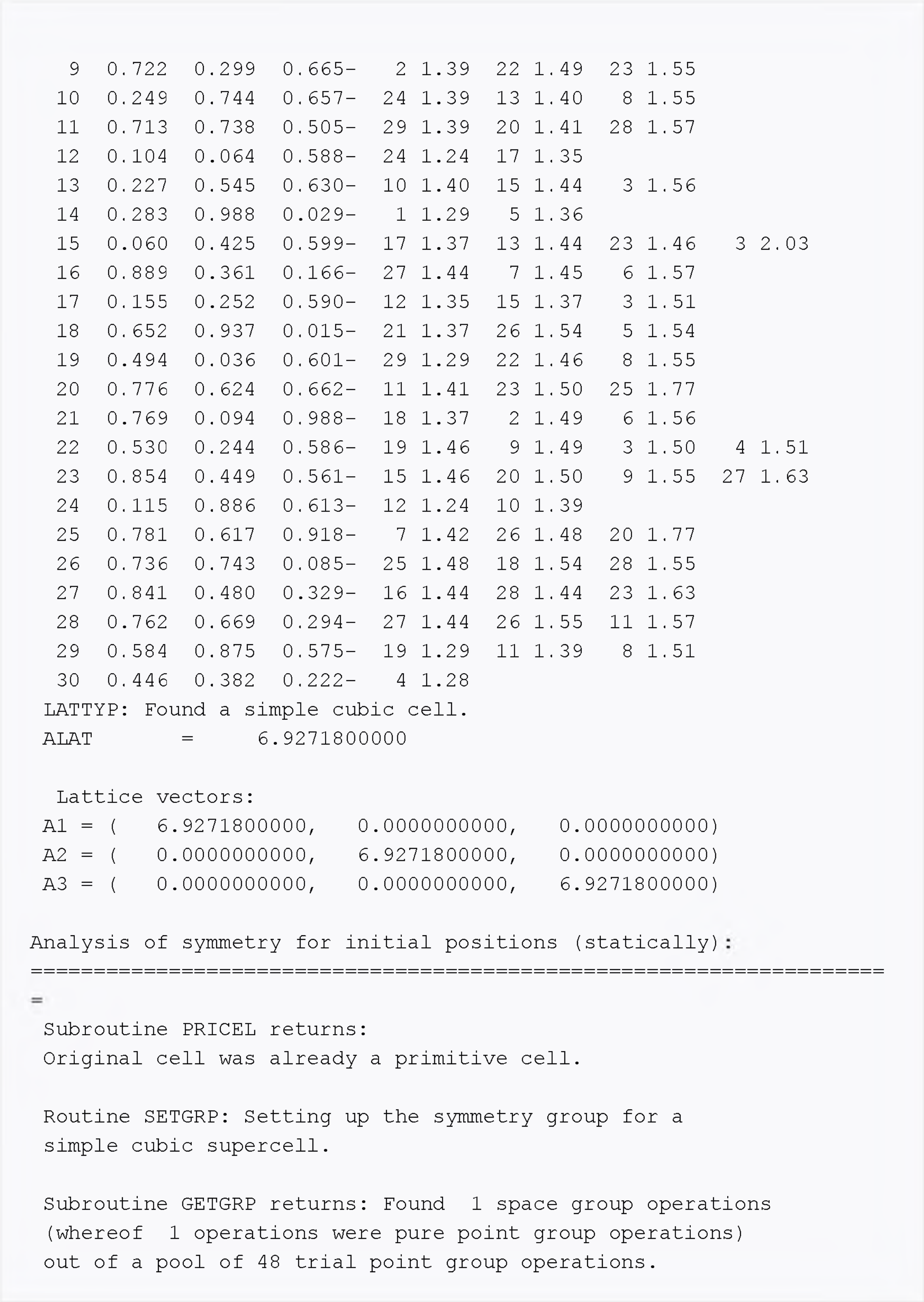

```
   9  0.722  0.299  0.665-   2 1.39  22 1.49  23 1.55
  10  0.249  0.744  0.657-  24 1.39  13 1.40   8 1.55
  11  0.713  0.738  0.505-  29 1.39  20 1.41  28 1.57
  12  0.104  0.064  0.588-  24 1.24  17 1.35
  13  0.227  0.545  0.630-  10 1.40  15 1.44   3 1.56
  14  0.283  0.988  0.029-   1 1.29   5 1.36
  15  0.060  0.425  0.599-  17 1.37  13 1.44  23 1.46   3 2.03
  16  0.889  0.361  0.166-  27 1.44   7 1.45   6 1.57
  17  0.155  0.252  0.590-  12 1.35  15 1.37   3 1.51
  18  0.652  0.937  0.015-  21 1.37  26 1.54   5 1.54
  19  0.494  0.036  0.601-  29 1.29  22 1.46   8 1.55
  20  0.776  0.624  0.662-  11 1.41  23 1.50  25 1.77
  21  0.769  0.094  0.988-  18 1.37   2 1.49   6 1.56
  22  0.530  0.244  0.586-  19 1.46   9 1.49   3 1.50   4 1.51
  23  0.854  0.449  0.561-  15 1.46  20 1.50   9 1.55  27 1.63
  24  0.115  0.886  0.613-  12 1.24  10 1.39
  25  0.781  0.617  0.918-   7 1.42  26 1.48  20 1.77
  26  0.736  0.743  0.085-  25 1.48  18 1.54  28 1.55
  27  0.841  0.480  0.329-  16 1.44  28 1.44  23 1.63
  28  0.762  0.669  0.294-  27 1.44  26 1.55  11 1.57
  29  0.584  0.875  0.575-  19 1.29  11 1.39   8 1.51
  30  0.446  0.382  0.222-   4 1.28
 LATTYP: Found a simple cubic cell.
 ALAT       =     6.9271800000

  Lattice vectors:
 A1 = (   6.9271800000,   0.0000000000,   0.0000000000)
 A2 = (   0.0000000000,   6.9271800000,   0.0000000000)
 A3 = (   0.0000000000,   0.0000000000,   6.9271800000)

Analysis of symmetry for initial positions (statically):
=====================================================================
=

 Subroutine PRICEL returns:
 Original cell was already a primitive cell.

 Routine SETGRP: Setting up the symmetry group for a
 simple cubic supercell.

 Subroutine GETGRP returns: Found  1 space group operations
 (whereof  1 operations were pure point group operations)
 out of a pool of 48 trial point group operations.
```

Figure B.3. 30-atom set atom positions before and after with VASP script file (cont.)

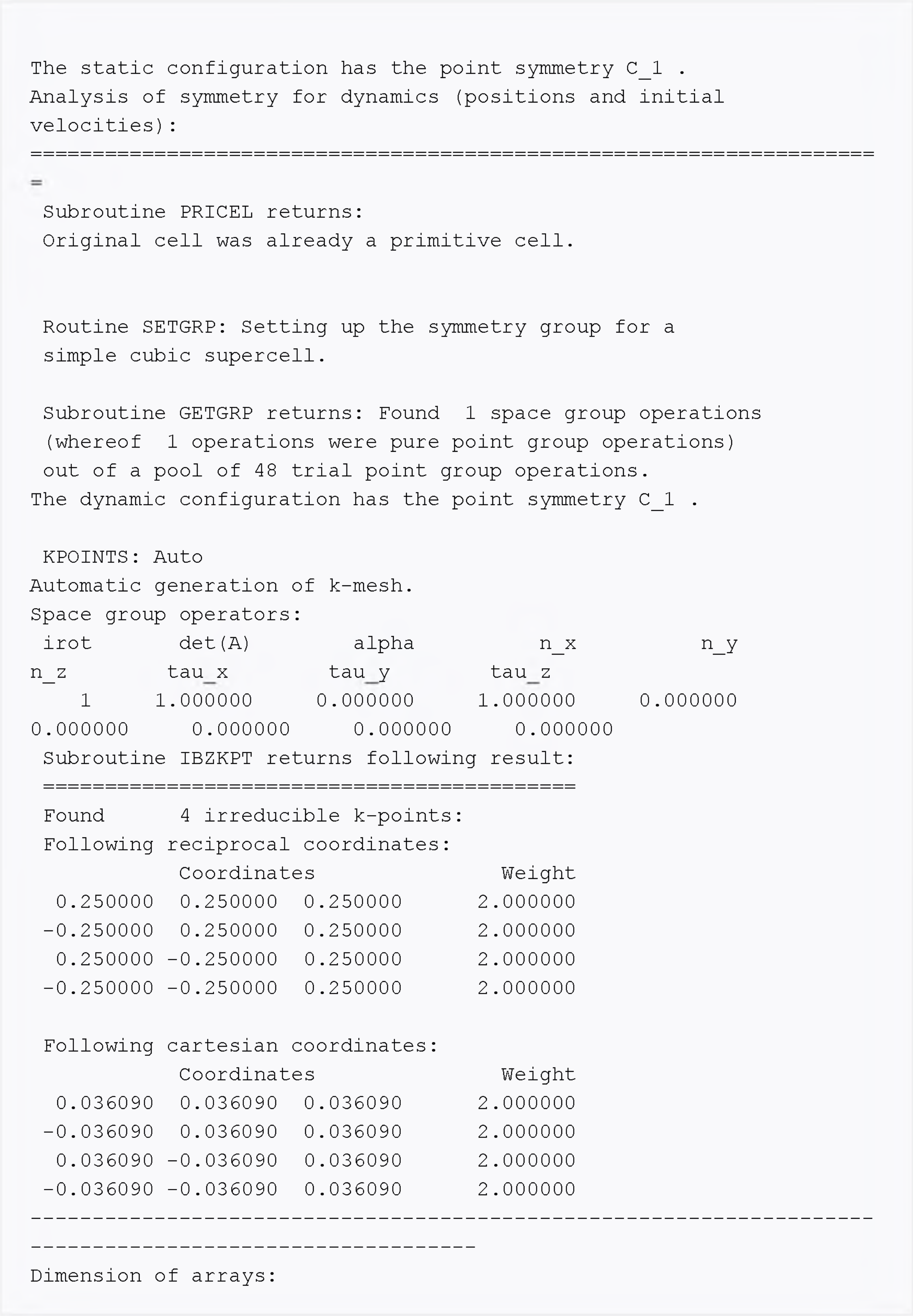

```
The static configuration has the point symmetry C_1 .
Analysis of symmetry for dynamics (positions and initial
velocities):
=====================================================================
=
 Subroutine PRICEL returns:
 Original cell was already a primitive cell.


 Routine SETGRP: Setting up the symmetry group for a
 simple cubic supercell.

 Subroutine GETGRP returns: Found  1 space group operations
 (whereof  1 operations were pure point group operations)
 out of a pool of 48 trial point group operations.
The dynamic configuration has the point symmetry C_1 .

 KPOINTS: Auto
Automatic generation of k-mesh.
Space group operators:
 irot       det(A)        alpha          n_x          n_y
n_z        tau_x        tau_y        tau_z
    1     1.000000     0.000000     1.000000     0.000000
0.000000     0.000000     0.000000     0.000000
 Subroutine IBZKPT returns following result:
 ===========================================
 Found      4 irreducible k-points:
 Following reciprocal coordinates:
            Coordinates               Weight
  0.250000  0.250000  0.250000      2.000000
 -0.250000  0.250000  0.250000      2.000000
  0.250000 -0.250000  0.250000      2.000000
 -0.250000 -0.250000  0.250000      2.000000

 Following cartesian coordinates:
            Coordinates               Weight
  0.036090  0.036090  0.036090      2.000000
 -0.036090  0.036090  0.036090      2.000000
  0.036090 -0.036090  0.036090      2.000000
 -0.036090 -0.036090  0.036090      2.000000
---------------------------------------------------------------------
------------------------------------
Dimension of arrays:
```

Figure B.3. 30-atom set atom positions before and after with VASP script file (cont.)

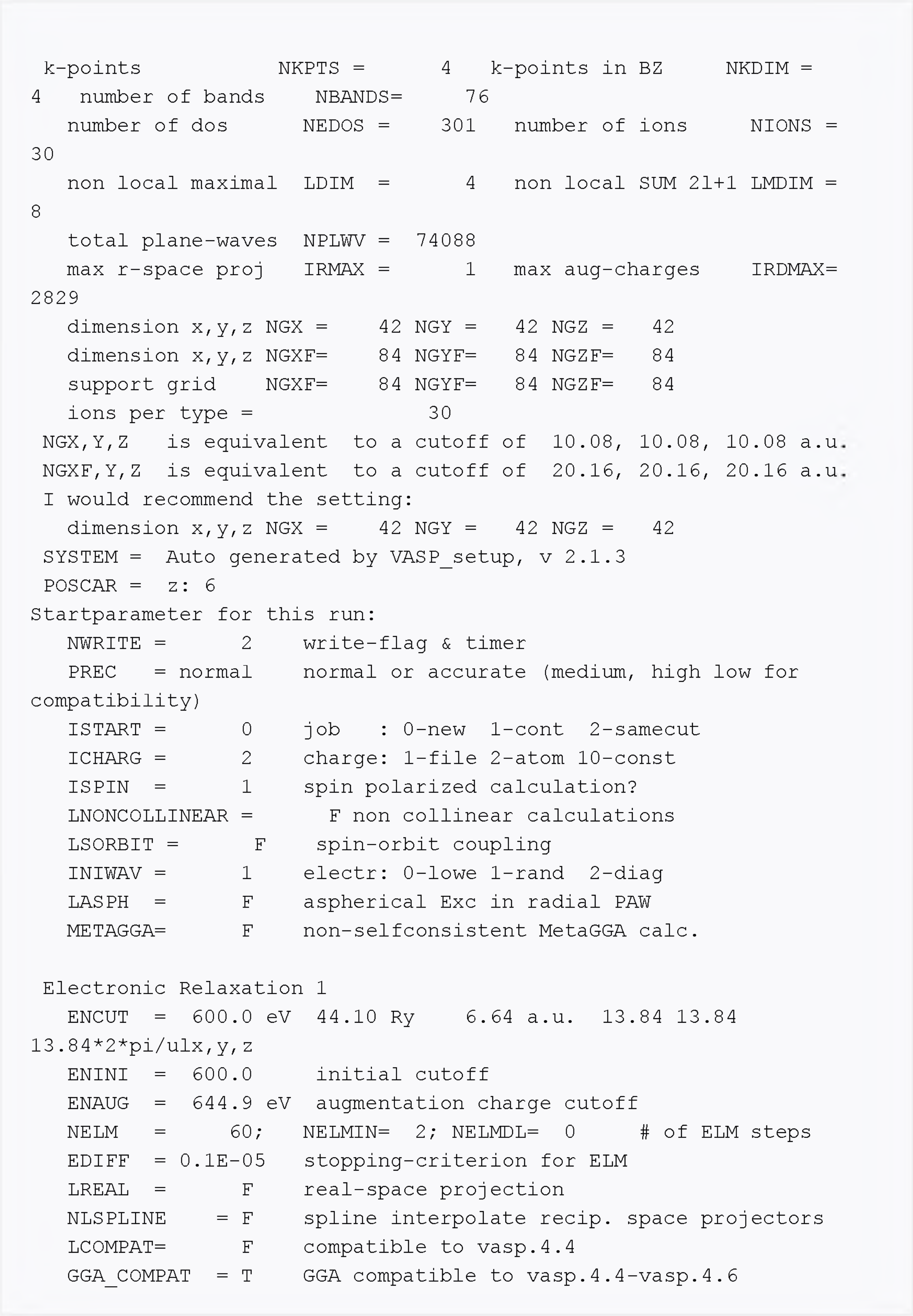

```
 k-points           NKPTS =      4   k-points in BZ     NKDIM =
4   number of bands    NBANDS=     76
   number of dos      NEDOS =    301   number of ions     NIONS =
30
   non local maximal  LDIM  =      4   non local SUM 2l+1 LMDIM =
8
   total plane-waves  NPLWV =  74088
   max r-space proj   IRMAX =      1   max aug-charges    IRDMAX=
2829
   dimension x,y,z NGX =    42 NGY =   42 NGZ =   42
   dimension x,y,z NGXF=    84 NGYF=   84 NGZF=   84
   support grid    NGXF=    84 NGYF=   84 NGZF=   84
   ions per type =              30
 NGX,Y,Z   is equivalent  to a cutoff of  10.08, 10.08, 10.08 a.u.
 NGXF,Y,Z  is equivalent  to a cutoff of  20.16, 20.16, 20.16 a.u.
 I would recommend the setting:
   dimension x,y,z NGX =    42 NGY =   42 NGZ =   42
 SYSTEM =  Auto generated by VASP_setup, v 2.1.3
 POSCAR =  z: 6
Startparameter for this run:
   NWRITE =      2    write-flag & timer
   PREC   = normal    normal or accurate (medium, high low for
compatibility)
   ISTART =      0    job   : 0-new  1-cont  2-samecut
   ICHARG =      2    charge: 1-file 2-atom 10-const
   ISPIN  =      1    spin polarized calculation?
   LNONCOLLINEAR =      F non collinear calculations
   LSORBIT =      F    spin-orbit coupling
   INIWAV =      1    electr: 0-lowe 1-rand  2-diag
   LASPH  =      F    aspherical Exc in radial PAW
   METAGGA=      F    non-selfconsistent MetaGGA calc.

 Electronic Relaxation 1
   ENCUT  =  600.0 eV  44.10 Ry    6.64 a.u.  13.84 13.84
13.84*2*pi/ulx,y,z
   ENINI  =  600.0     initial cutoff
   ENAUG  =  644.9 eV  augmentation charge cutoff
   NELM   =     60;   NELMIN=  2; NELMDL=  0     # of ELM steps
   EDIFF  = 0.1E-05   stopping-criterion for ELM
   LREAL  =      F    real-space projection
   NLSPLINE    = F    spline interpolate recip. space projectors
   LCOMPAT=      F    compatible to vasp.4.4
   GGA_COMPAT  = T    GGA compatible to vasp.4.4-vasp.4.6
```

Figure B.3. 30-atom set atom positions before and after with VASP script file (cont.)

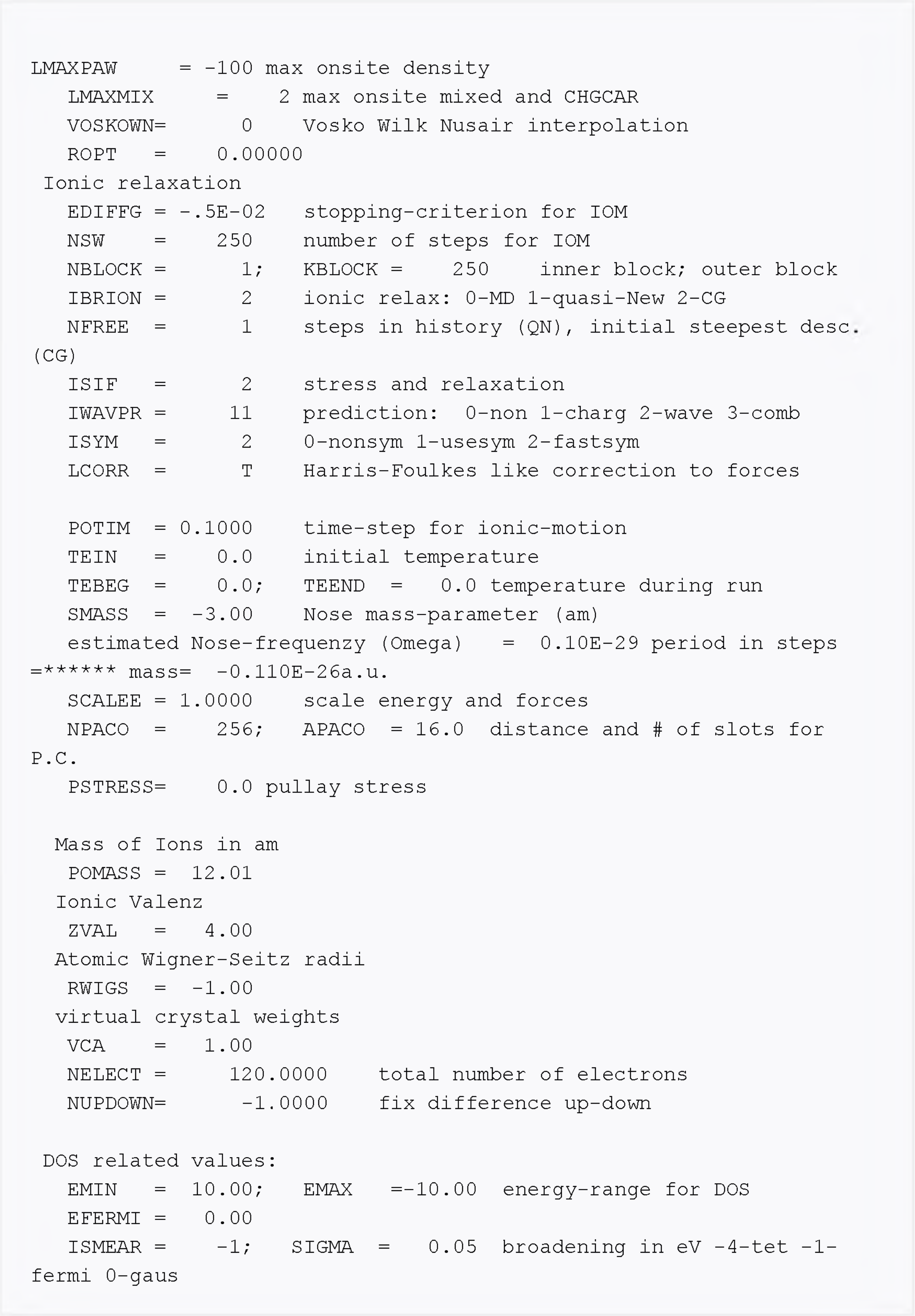

```
LMAXPAW     = -100 max onsite density
   LMAXMIX     =    2 max onsite mixed and CHGCAR
   VOSKOWN=      0    Vosko Wilk Nusair interpolation
   ROPT   =    0.00000
 Ionic relaxation
   EDIFFG = -.5E-02   stopping-criterion for IOM
   NSW    =    250    number of steps for IOM
   NBLOCK =      1;   KBLOCK =    250    inner block; outer block
   IBRION =      2    ionic relax: 0-MD 1-quasi-New 2-CG
   NFREE  =      1    steps in history (QN), initial steepest desc.
(CG)
   ISIF   =      2    stress and relaxation
   IWAVPR =     11    prediction:  0-non 1-charg 2-wave 3-comb
   ISYM   =      2    0-nonsym 1-usesym 2-fastsym
   LCORR  =      T    Harris-Foulkes like correction to forces

   POTIM  = 0.1000    time-step for ionic-motion
   TEIN   =    0.0    initial temperature
   TEBEG  =    0.0;   TEEND  =   0.0 temperature during run
   SMASS  =  -3.00    Nose mass-parameter (am)
   estimated Nose-frequenzy (Omega)   =  0.10E-29 period in steps
=****** mass=  -0.110E-26a.u.
   SCALEE = 1.0000    scale energy and forces
   NPACO  =    256;   APACO  = 16.0  distance and # of slots for
P.C.
   PSTRESS=    0.0 pullay stress

  Mass of Ions in am
   POMASS =  12.01
  Ionic Valenz
   ZVAL   =   4.00
  Atomic Wigner-Seitz radii
   RWIGS  =  -1.00
  virtual crystal weights
   VCA    =   1.00
   NELECT =     120.0000    total number of electrons
   NUPDOWN=      -1.0000    fix difference up-down

 DOS related values:
   EMIN   =  10.00;   EMAX   =-10.00  energy-range for DOS
   EFERMI =   0.00
   ISMEAR =    -1;   SIGMA  =   0.05  broadening in eV -4-tet -1-
fermi 0-gaus
```

Figure B.3. 30-atom set atom positions before and after with VASP script file (cont.)

```
Electronic relaxation 2 (details)
   IALGO  =     48    algorithm
   LDIAG  =      T    sub-space diagonalisation (order eigenvalues)
   LSUBROT=      F    optimize rotation matrix (better conditioning)
   TURBO    =      0    0=normal 1=particle mesh
   IRESTART =      0    0=no restart 2=restart with 2 vectors
   NREBOOT  =      0    no. of reboots
   NMIN     =      0    reboot dimension
   EREF     =   0.00    reference energy to select bands
   IMIX   =      4    mixing-type and parameters
     AMIX     =   0.40;   BMIX     =  1.00
     AMIX_MAG =   1.60;   BMIX_MAG =  1.00
     AMIN     =   0.10
     WC   =   100.;   INIMIX=   1;  MIXPRE=   1;  MAXMIX= -45

 Intra band minimization:
   WEIMIN = 0.0010     energy-eigenvalue tresh-hold
   EBREAK =  0.33E-08  absolut break condition
   DEPER  =   0.30     relativ break condition
   TIME   =   0.40     timestep for ELM
  volume/ion in A,a.u.               =      11.08        74.77
  Fermi-wavevector in a.u.,A,eV,Ry     =   1.165678  2.202813
18.487682  1.358806
  Thomas-Fermi vector in A             =   2.302201
 Write flags
   LWAVE  =      F    write WAVECAR
   LCHARG =      F    write CHGCAR
   LVTOT  =      F    write LOCPOT, total local potential
   LVHAR  =      F    write LOCPOT, Hartree potential only
   LELF   =      F    write electronic localiz. function (ELF)
   LORBIT =      0    0 simple, 1 ext, 2 COOP (PROOUT)


 Dipole corrections
   LMONO  =      F    monopole corrections only (constant potential
shift)
   LDIPOL =      F    correct potential (dipole corrections)
   IDIPOL =      0    1-x, 2-y, 3-z, 4-all directions
   EPSILON=  1.0000000 bulk dielectric constant
Exchange correlation treatment:
   GGA     =    --    GGA type
   LEXCH   =     7    internal setting for exchange type
   VOSKOWN=      0    Vosko Wilk Nusair interpolation
```

Figure B.3. 30-atom set atom positions before and after with VASP script file (cont.)

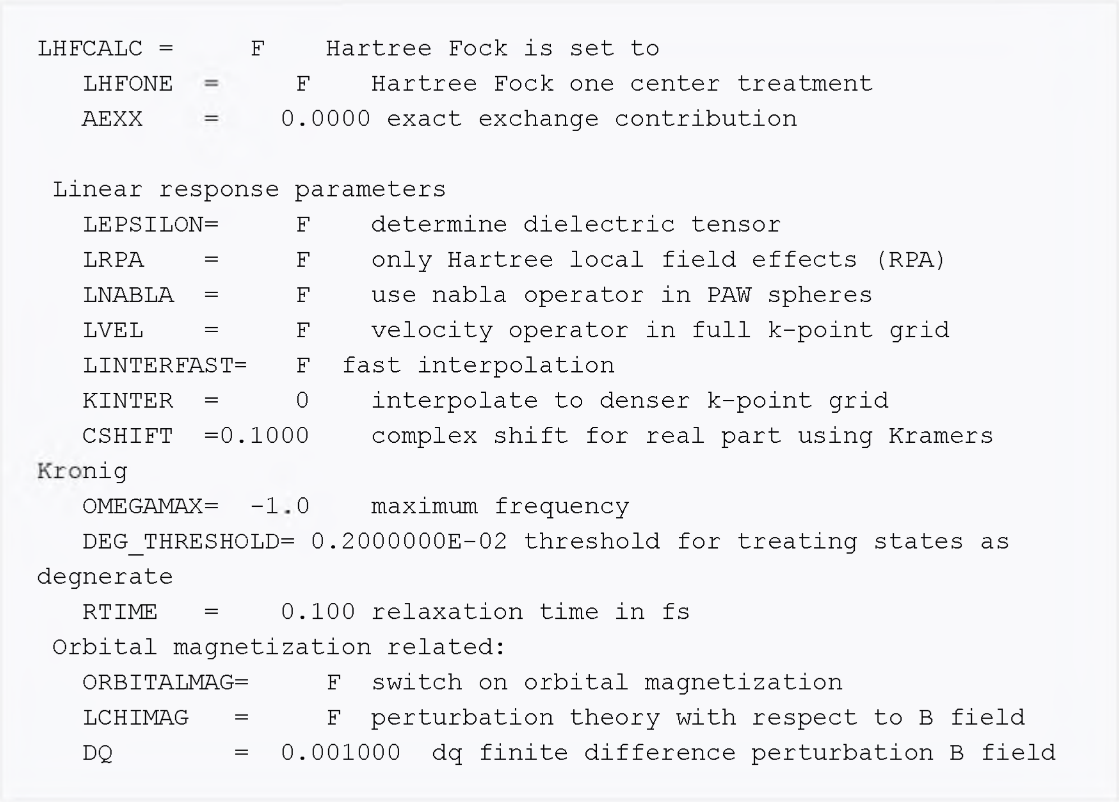

```
LHFCALC =     F    Hartree Fock is set to
   LHFONE  =     F    Hartree Fock one center treatment
   AEXX    =    0.0000 exact exchange contribution

 Linear response parameters
   LEPSILON=     F    determine dielectric tensor
   LRPA    =     F    only Hartree local field effects (RPA)
   LNABLA  =     F    use nabla operator in PAW spheres
   LVEL    =     F    velocity operator in full k-point grid
   LINTERFAST=   F  fast interpolation
   KINTER  =     0    interpolate to denser k-point grid
   CSHIFT  =0.1000    complex shift for real part using Kramers
Kronig
   OMEGAMAX=  -1.0    maximum frequency
   DEG_THRESHOLD= 0.2000000E-02 threshold for treating states as
degnerate
   RTIME   =    0.100 relaxation time in fs
 Orbital magnetization related:
   ORBITALMAG=     F  switch on orbital magnetization
   LCHIMAG   =     F  perturbation theory with respect to B field
   DQ        =  0.001000  dq finite difference perturbation B field
```

Figure B.3. 30-atom set atom positions before and after with VASP script file (cont.)

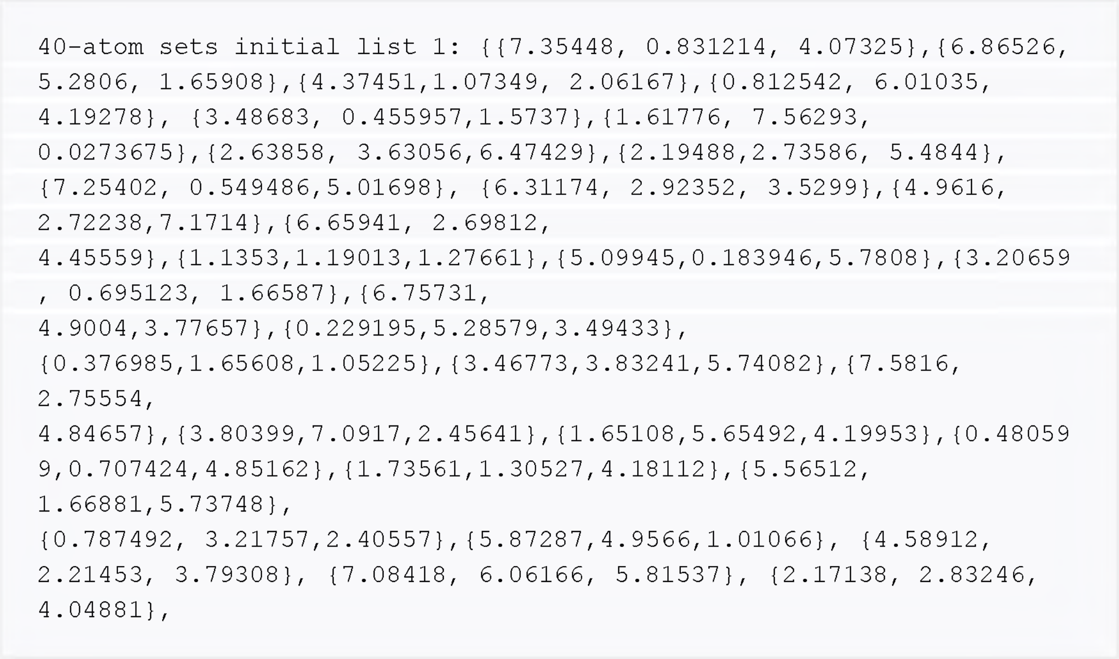

```
40-atom sets initial list 1: {{7.35448, 0.831214, 4.07325},{6.86526,
5.2806, 1.65908},{4.37451,1.07349, 2.06167},{0.812542, 6.01035,
4.19278}, {3.48683, 0.455957,1.5737},{1.61776, 7.56293,
0.0273675},{2.63858, 3.63056,6.47429},{2.19488,2.73586, 5.4844},
{7.25402, 0.549486,5.01698}, {6.31174, 2.92352, 3.5299},{4.9616,
2.72238,7.1714},{6.65941, 2.69812,
4.45559},{1.1353,1.19013,1.27661},{5.09945,0.183946,5.7808},{3.20659
, 0.695123, 1.66587},{6.75731,
4.9004,3.77657},{0.229195,5.28579,3.49433},
{0.376985,1.65608,1.05225},{3.46773,3.83241,5.74082},{7.5816,
2.75554,
4.84657},{3.80399,7.0917,2.45641},{1.65108,5.65492,4.19953},{0.48059
9,0.707424,4.85162},{1.73561,1.30527,4.18112},{5.56512,
1.66881,5.73748},
{0.787492, 3.21757,2.40557},{5.87287,4.9566,1.01066}, {4.58912,
2.21453, 3.79308}, {7.08418, 6.06166, 5.81537}, {2.17138, 2.83246,
4.04881},
```

Figure B.4. 40-atom set atom positions before and after with VASP script file.

```
{4.50387, 1.12211,5.61632}, {6.42532, 6.20206, 0.79182}, {0.91934,
5.21715,1.25672}, {0.420328, 2.07984, 5.7067}, {1.35013, 5.5876,
5.41213},
{5.80911, 3.2509, 1.22145}, {0.389835, 3.14735, 4.4324}, {5.42578,
2.69009, 2.61969}, {2.66483, 1.77949, 1.15587}, {2.06089, 4.19866,
2.11521}};

40-atom sets VASP-relaxed list 1: total energy = -324.94991187 eV &
output atom list,
{{7.41648671,0.72678419,5.37224473},{7.33790408,5.97804815,1.5463250
6},{3.11219479,1.13937511,3.00613400},{0.23227481,5.84056414,4.00324
472},
{2.02258449, 1.27816447, 6.10799249}, {1.60117389 , 7.01755184 ,
0.55092510},{2.95442923 , 2.47422562, 6.02051648},{1.96875678 ,
3.40216313 , 5.25070555},{6.76891247 , 7.23188441,
5.86814846},{5.76830937 , 2.97470706, 3.61570358},{5.06099259 ,
2.94092394 , 7.46775303}, {6.32801184 , 2.69788507 ,
4.67840054},{1.47865976 , 0.82570142,0.81604837},{6.18674363 ,
7.23514897, 7.24187610},{4.61000877 , 6.71693890
,3.47415380},{5.83521712 , 6.15809356 , 3.72859530},{6.98647508 ,
5.83092185, 2.84702183}, {1.18616707 , 2.10364181 , 1.16214168},
{3.96497096 , 2.82352168 , 6.75539224},{7.05610632,2.13161303
,5.85270068},{3.67240609 , 7.47218185, 3.20751495},{1.48096947 ,
5.28398448, 4.19017474}, {1.21102322 , 1.16454357 , 4.83921416},
{1.91376091, 1.70602303 , 3.59774211},
{6.18613294,2.05363620,7.09954327},{1.45749718 , 3.32737301 ,
1.05915999}, {5.49550501 , 4.97287400 , 0.81500555}, {3.99991247 ,
2.02356034 , 2.49126730},{6.74608253, 6.25576533 , 4.81784294},
{1.95765697 , 3.12208824 , 3.76826777},{6.04446113,0.87330798 ,
0.08515323},{6.24436146 , 6.04327418 ,
0.53228512},{1.11448713,5.83740273,1.13742996},{0.93206298 ,
2.37411431 , 5.76091274},{1.81154003, 4.85245127 , 5.49066283},
{5.16812378 , 3.71758579 , 1.13049612},{1.86093732 , 4.34477862 ,
3.07757156},{4.94095105, 2.96705606, 2.42114883},{1.95267107 ,
0.37120845 , 7.23791904},{1.65407349,4.54206223,1.68118155 }};

VASP OUTCAR SCRIPT:
INCAR:
 POTCAR:   PAW_GGA C 05Jan2001
 POTCAR:   PAW_GGA C 05Jan2001
   VRHFIN =C: s2p2
   LEXCH  = 91
   EATOM  =   147.4688 eV,   10.8386 Ry
```

Figure B.4. 40-atom set atom positions before and after with VASP script file (cont.)

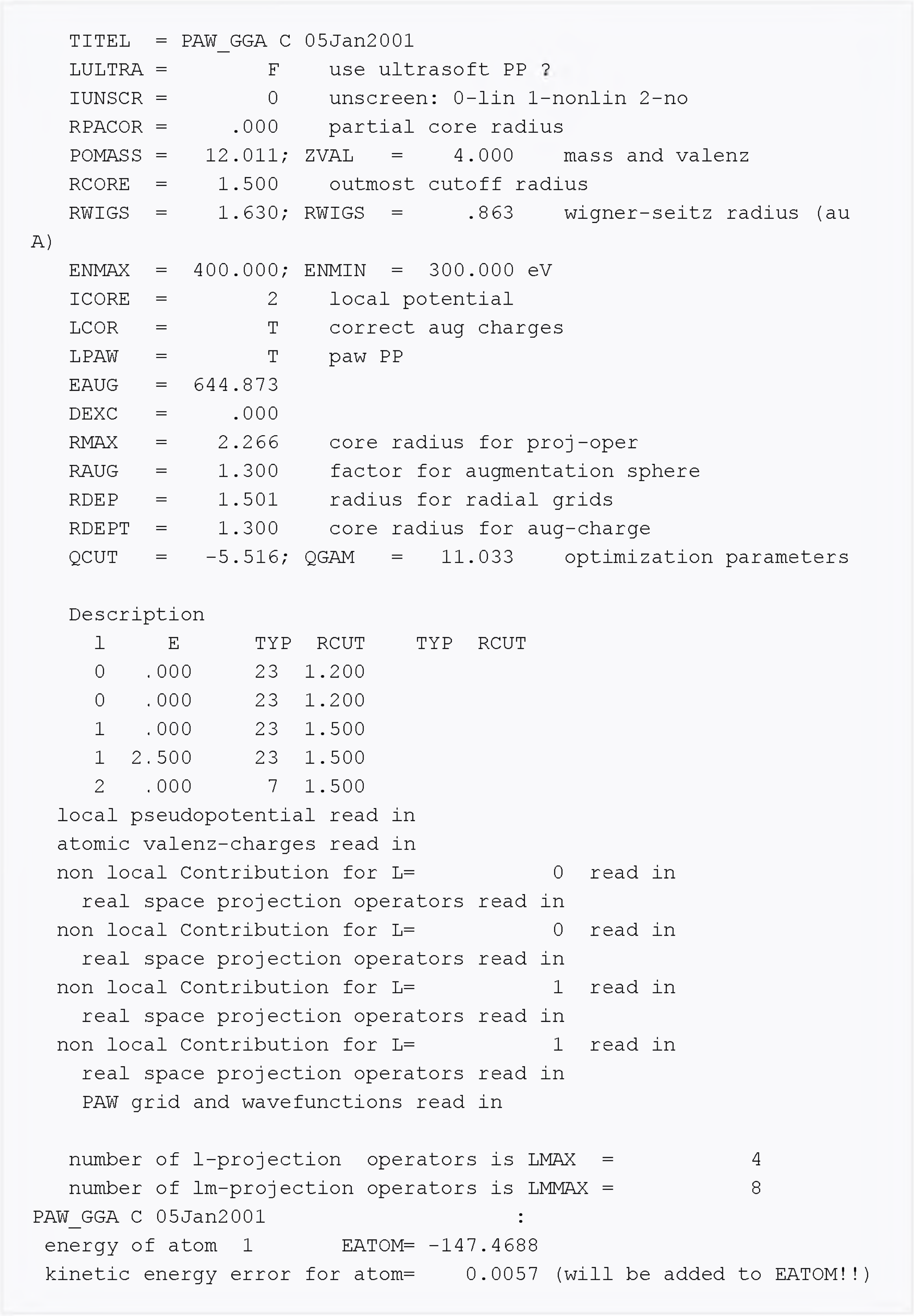

```
   TITEL  = PAW_GGA C 05Jan2001
   LULTRA =        F    use ultrasoft PP ?
   IUNSCR =        0    unscreen: 0-lin 1-nonlin 2-no
   RPACOR =     .000    partial core radius
   POMASS =   12.011; ZVAL   =    4.000    mass and valenz
   RCORE  =    1.500    outmost cutoff radius
   RWIGS  =    1.630; RWIGS  =     .863    wigner-seitz radius (au
A)
   ENMAX  =  400.000; ENMIN  =  300.000 eV
   ICORE  =        2    local potential
   LCOR   =        T    correct aug charges
   LPAW   =        T    paw PP
   EAUG   =  644.873
   DEXC   =     .000
   RMAX   =    2.266    core radius for proj-oper
   RAUG   =    1.300    factor for augmentation sphere
   RDEP   =    1.501    radius for radial grids
   RDEPT  =    1.300    core radius for aug-charge
   QCUT   =   -5.516; QGAM   =   11.033    optimization parameters

   Description
     l     E      TYP  RCUT    TYP  RCUT
     0   .000     23  1.200
     0   .000     23  1.200
     1   .000     23  1.500
     1  2.500     23  1.500
     2   .000      7  1.500
  local pseudopotential read in
  atomic valenz-charges read in
  non local Contribution for L=           0  read in
    real space projection operators read in
  non local Contribution for L=           0  read in
    real space projection operators read in
  non local Contribution for L=           1  read in
    real space projection operators read in
  non local Contribution for L=           1  read in
    real space projection operators read in
    PAW grid and wavefunctions read in

   number of l-projection  operators is LMAX  =           4
   number of lm-projection operators is LMMAX =           8
 PAW_GGA C 05Jan2001                    :
  energy of atom  1       EATOM= -147.4688
  kinetic energy error for atom=    0.0057 (will be added to EATOM!!)
```

Figure B.4. 40-atom set atom positions before and after with VASP script file (cont.)

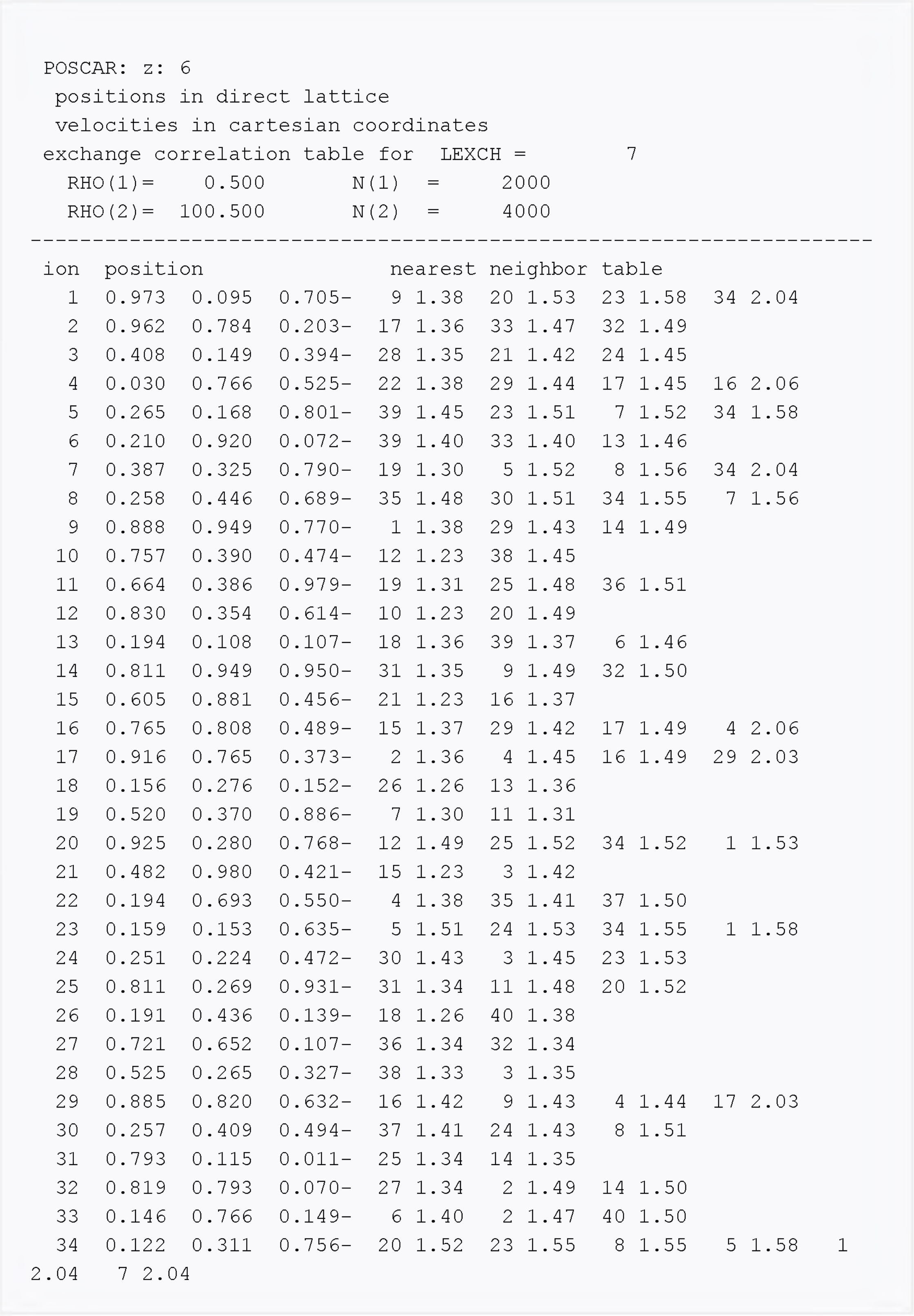

```
 POSCAR: z: 6
  positions in direct lattice
  velocities in cartesian coordinates
 exchange correlation table for  LEXCH =        7
   RHO(1)=    0.500       N(1)  =     2000
   RHO(2)=  100.500       N(2)  =     4000
--------------------------------------------------------------------
 ion  position               nearest neighbor table
   1  0.973  0.095  0.705-   9 1.38  20 1.53  23 1.58  34 2.04
   2  0.962  0.784  0.203-  17 1.36  33 1.47  32 1.49
   3  0.408  0.149  0.394-  28 1.35  21 1.42  24 1.45
   4  0.030  0.766  0.525-  22 1.38  29 1.44  17 1.45  16 2.06
   5  0.265  0.168  0.801-  39 1.45  23 1.51   7 1.52  34 1.58
   6  0.210  0.920  0.072-  39 1.40  33 1.40  13 1.46
   7  0.387  0.325  0.790-  19 1.30   5 1.52   8 1.56  34 2.04
   8  0.258  0.446  0.689-  35 1.48  30 1.51  34 1.55   7 1.56
   9  0.888  0.949  0.770-   1 1.38  29 1.43  14 1.49
  10  0.757  0.390  0.474-  12 1.23  38 1.45
  11  0.664  0.386  0.979-  19 1.31  25 1.48  36 1.51
  12  0.830  0.354  0.614-  10 1.23  20 1.49
  13  0.194  0.108  0.107-  18 1.36  39 1.37   6 1.46
  14  0.811  0.949  0.950-  31 1.35   9 1.49  32 1.50
  15  0.605  0.881  0.456-  21 1.23  16 1.37
  16  0.765  0.808  0.489-  15 1.37  29 1.42  17 1.49   4 2.06
  17  0.916  0.765  0.373-   2 1.36   4 1.45  16 1.49  29 2.03
  18  0.156  0.276  0.152-  26 1.26  13 1.36
  19  0.520  0.370  0.886-   7 1.30  11 1.31
  20  0.925  0.280  0.768-  12 1.49  25 1.52  34 1.52   1 1.53
  21  0.482  0.980  0.421-  15 1.23   3 1.42
  22  0.194  0.693  0.550-   4 1.38  35 1.41  37 1.50
  23  0.159  0.153  0.635-   5 1.51  24 1.53  34 1.55   1 1.58
  24  0.251  0.224  0.472-  30 1.43   3 1.45  23 1.53
  25  0.811  0.269  0.931-  31 1.34  11 1.48  20 1.52
  26  0.191  0.436  0.139-  18 1.26  40 1.38
  27  0.721  0.652  0.107-  36 1.34  32 1.34
  28  0.525  0.265  0.327-  38 1.33   3 1.35
  29  0.885  0.820  0.632-  16 1.42   9 1.43   4 1.44  17 2.03
  30  0.257  0.409  0.494-  37 1.41  24 1.43   8 1.51
  31  0.793  0.115  0.011-  25 1.34  14 1.35
  32  0.819  0.793  0.070-  27 1.34   2 1.49  14 1.50
  33  0.146  0.766  0.149-   6 1.40   2 1.47  40 1.50
  34  0.122  0.311  0.756-  20 1.52  23 1.55   8 1.55   5 1.58   1
2.04   7 2.04
```

Figure B.4. 40-atom set atom positions before and after with VASP script file (cont.)

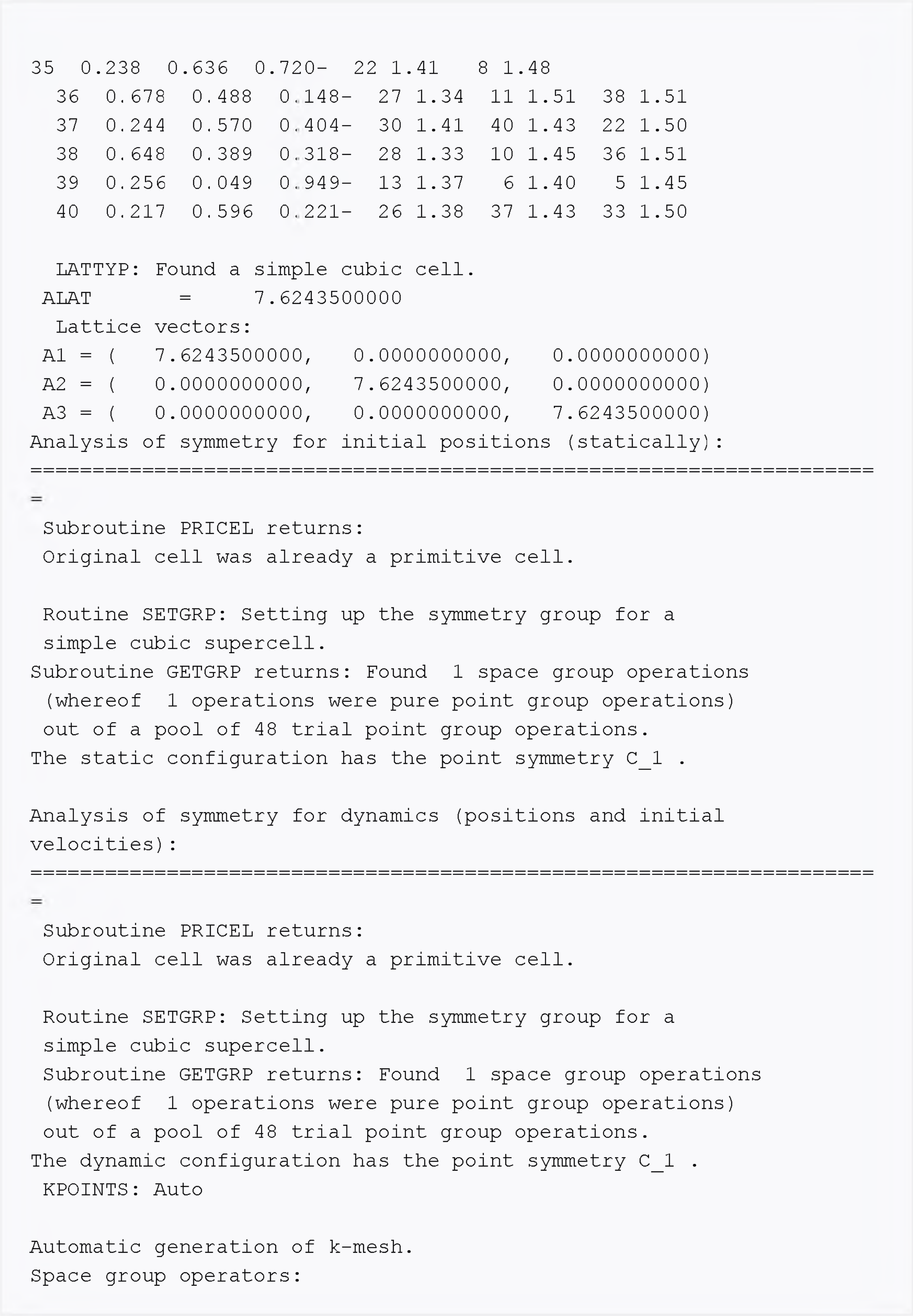

```
35  0.238  0.636  0.720-  22 1.41   8 1.48
  36  0.678  0.488  0.148-  27 1.34  11 1.51  38 1.51
  37  0.244  0.570  0.404-  30 1.41  40 1.43  22 1.50
  38  0.648  0.389  0.318-  28 1.33  10 1.45  36 1.51
  39  0.256  0.049  0.949-  13 1.37   6 1.40   5 1.45
  40  0.217  0.596  0.221-  26 1.38  37 1.43  33 1.50

  LATTYP: Found a simple cubic cell.
 ALAT       =     7.6243500000
  Lattice vectors:
 A1 = (   7.6243500000,   0.0000000000,   0.0000000000)
 A2 = (   0.0000000000,   7.6243500000,   0.0000000000)
 A3 = (   0.0000000000,   0.0000000000,   7.6243500000)
Analysis of symmetry for initial positions (statically):
====================================================================
=
 Subroutine PRICEL returns:
 Original cell was already a primitive cell.

 Routine SETGRP: Setting up the symmetry group for a
 simple cubic supercell.
Subroutine GETGRP returns: Found  1 space group operations
 (whereof  1 operations were pure point group operations)
 out of a pool of 48 trial point group operations.
The static configuration has the point symmetry C_1 .

Analysis of symmetry for dynamics (positions and initial
velocities):
====================================================================
=
 Subroutine PRICEL returns:
 Original cell was already a primitive cell.

 Routine SETGRP: Setting up the symmetry group for a
 simple cubic supercell.
 Subroutine GETGRP returns: Found  1 space group operations
 (whereof  1 operations were pure point group operations)
 out of a pool of 48 trial point group operations.
The dynamic configuration has the point symmetry C_1 .
 KPOINTS: Auto

Automatic generation of k-mesh.
Space group operators:
```

Figure B.4. 40-atom set atom positions before and after with VASP script file (cont.)

```
irot       det(A)        alpha          n_x          n_y
n_z        tau_x        tau_y        tau_z
    1     1.000000     0.000000     1.000000     0.000000
0.000000     0.000000     0.000000     0.000000

 Subroutine IBZKPT returns following result:
 ===========================================
 Found      4 irreducible k-points:
 Following reciprocal coordinates:
            Coordinates               Weight
  0.250000  0.250000  0.250000      2.000000
 -0.250000  0.250000  0.250000      2.000000
  0.250000 -0.250000  0.250000      2.000000
 -0.250000 -0.250000  0.250000      2.000000
 Following cartesian coordinates:
            Coordinates               Weight
  0.032790  0.032790  0.032790      2.000000
 -0.032790  0.032790  0.032790      2.000000
  0.032790 -0.032790  0.032790      2.000000
 -0.032790 -0.032790  0.032790      2.000000
--------------------------------------------------------------------
------------------------------------
 Dimension of arrays:
   k-points           NKPTS =      4   k-points in BZ     NKDIM =
4   number of bands    NBANDS=    102
   number of dos      NEDOS =    301   number of ions     NIONS =
40
   non local maximal  LDIM  =      4   non local SUM 2l+1 LMDIM =
8
   total plane-waves  NPLWV = 110592
   max r-space proj   IRMAX =      1   max aug-charges    IRDMAX=
3144
   dimension x,y,z NGX =    48 NGY =   48 NGZ =   48
   dimension x,y,z NGXF=    96 NGYF=   96 NGZF=   96
   support grid    NGXF=    96 NGYF=   96 NGZF=   96
   ions per type =               40
 NGX,Y,Z   is equivalent  to a cutoff of  10.47, 10.47, 10.47 a.u.
 NGXF,Y,Z  is equivalent  to a cutoff of  20.93, 20.93, 20.93 a.u.
 I would recommend the setting:
   dimension x,y,z NGX =    46 NGY =   46 NGZ =   46
 SYSTEM =  Auto generated by VASP_setup, v 2.1.3
 POSCAR =  z: 6
```

Figure B.4. 40-atom set atom positions before and after with VASP script file (cont.)

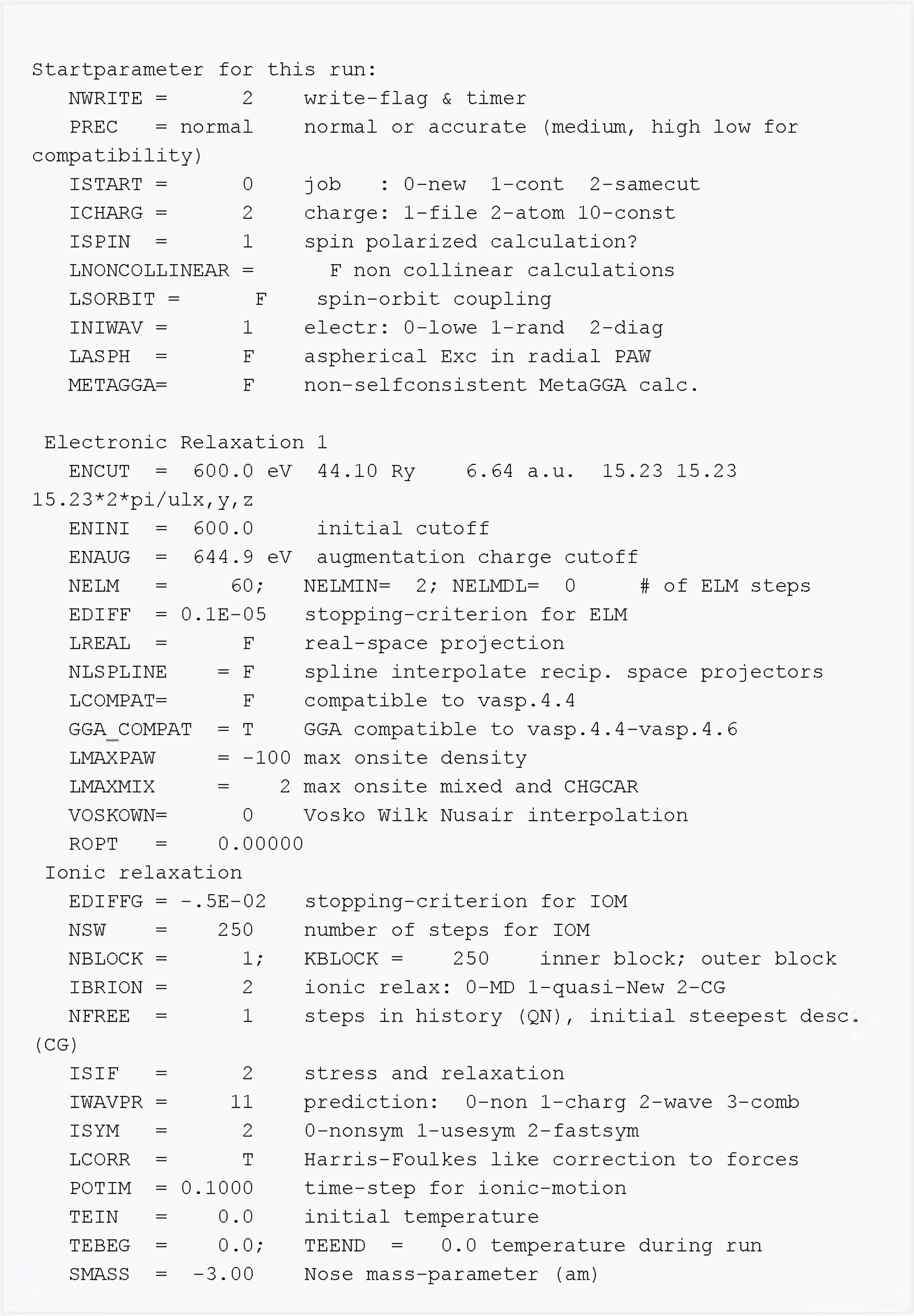

```
Startparameter for this run:
   NWRITE =      2    write-flag & timer
   PREC   = normal    normal or accurate (medium, high low for
compatibility)
   ISTART =      0    job   : 0-new  1-cont  2-samecut
   ICHARG =      2    charge: 1-file 2-atom 10-const
   ISPIN  =      1    spin polarized calculation?
   LNONCOLLINEAR =      F non collinear calculations
   LSORBIT =      F    spin-orbit coupling
   INIWAV =      1    electr: 0-lowe 1-rand  2-diag
   LASPH  =      F    aspherical Exc in radial PAW
   METAGGA=      F    non-selfconsistent MetaGGA calc.

 Electronic Relaxation 1
   ENCUT  =  600.0 eV  44.10 Ry    6.64 a.u.  15.23 15.23
15.23*2*pi/ulx,y,z
   ENINI  =  600.0     initial cutoff
   ENAUG  =  644.9 eV  augmentation charge cutoff
   NELM   =     60;   NELMIN=  2; NELMDL=  0     # of ELM steps
   EDIFF  = 0.1E-05   stopping-criterion for ELM
   LREAL  =      F    real-space projection
   NLSPLINE    = F    spline interpolate recip. space projectors
   LCOMPAT=      F    compatible to vasp.4.4
   GGA_COMPAT  = T    GGA compatible to vasp.4.4-vasp.4.6
   LMAXPAW     = -100 max onsite density
   LMAXMIX     =    2 max onsite mixed and CHGCAR
   VOSKOWN=      0    Vosko Wilk Nusair interpolation
   ROPT   =    0.00000
 Ionic relaxation
   EDIFFG = -.5E-02   stopping-criterion for IOM
   NSW    =    250    number of steps for IOM
   NBLOCK =      1;   KBLOCK =    250    inner block; outer block
   IBRION =      2    ionic relax: 0-MD 1-quasi-New 2-CG
   NFREE  =      1    steps in history (QN), initial steepest desc.
(CG)
   ISIF   =      2    stress and relaxation
   IWAVPR =     11    prediction:  0-non 1-charg 2-wave 3-comb
   ISYM   =      2    0-nonsym 1-usesym 2-fastsym
   LCORR  =      T    Harris-Foulkes like correction to forces
   POTIM  = 0.1000    time-step for ionic-motion
   TEIN   =    0.0    initial temperature
   TEBEG  =    0.0;   TEEND  =    0.0 temperature during run
   SMASS  =  -3.00    Nose mass-parameter (am)
```

Figure B.4. 40-atom set atom positions before and after with VASP script file (cont.)

```
estimated Nose-frequenzy (Omega)   =  0.10E-29 period in steps
=****** mass=  -0.133E-26a.u.
   SCALEE = 1.0000    scale energy and forces
   NPACO  =    256;   APACO  = 16.0  distance and # of slots for
P.C.
   PSTRESS=    0.0 pullay stress

  Mass of Ions in am
   POMASS =  12.01
  Ionic Valenz
   ZVAL   =   4.00
  Atomic Wigner-Seitz radii
   RWIGS  =  -1.00
  virtual crystal weights
   VCA    =   1.00
   NELECT =     160.0000    total number of electrons
   NUPDOWN=      -1.0000    fix difference up-down

 DOS related values:
   EMIN   =  10.00;   EMAX   =-10.00  energy-range for DOS
   EFERMI =   0.00
   ISMEAR =    -1;   SIGMA  =   0.05  broadening in eV -4-tet -1-
fermi 0-gaus

 Electronic relaxation 2 (details)
   IALGO  =     48    algorithm
   LDIAG  =      T    sub-space diagonalisation (order eigenvalues)
   LSUBROT=      F    optimize rotation matrix (better conditioning)
   TURBO    =      0    0=normal 1=particle mesh
   IRESTART =      0    0=no restart 2=restart with 2 vectors
   NREBOOT  =      0    no. of reboots
   NMIN     =      0    reboot dimension
   EREF     =   0.00    reference energy to select bands
   IMIX   =      4    mixing-type and parameters
     AMIX     =   0.40;   BMIX     =  1.00
     AMIX_MAG =   1.60;   BMIX_MAG =  1.00
     AMIN     =   0.10
     WC   =   100.;   INIMIX=   1;  MIXPRE=   1;  MAXMIX= -45

 Intra band minimization:
   WEIMIN = 0.0010     energy-eigenvalue tresh-hold
   EBREAK =  0.25E-08  absolut break condition
   DEPER  =   0.30     relativ break condition
```

Figure B.4. 40-atom set atom positions before and after with VASP script file (cont.)

```
TIME   =   0.40     timestep for ELM
  volume/ion in A,a.u.               =      11.08        74.77
  Fermi-wavevector in a.u.,A,eV,Ry     =   1.165678  2.202812
18.487673  1.358806
  Thomas-Fermi vector in A             =   2.302201
 Write flags
   LWAVE  =      F    write WAVECAR
   LCHARG =      F    write CHGCAR
   LVTOT  =      F    write LOCPOT, total local potential
   LVHAR  =      F    write LOCPOT, Hartree potential only
   LELF   =      F    write electronic localiz. function (ELF)
   LORBIT =      0    0 simple, 1 ext, 2 COOP (PROOUT)
 Dipole corrections
   LMONO  =      F    monopole corrections only (constant potential
shift)
   LDIPOL =      F    correct potential (dipole corrections)
   IDIPOL =      0    1-x, 2-y, 3-z, 4-all directions
   EPSILON=  1.0000000 bulk dielectric constant

 Exchange correlation treatment:
   GGA     =    --    GGA type
   LEXCH   =     7    internal setting for exchange type
   VOSKOWN=      0    Vosko Wilk Nusair interpolation
   LHFCALC =     F    Hartree Fock is set to
   LHFONE  =     F    Hartree Fock one center treatment
   AEXX    =    0.0000 exact exchange contribution

 Linear response parameters
   LEPSILON=     F    determine dielectric tensor
   LRPA    =     F    only Hartree local field effects (RPA)
   LNABLA  =     F    use nabla operator in PAW spheres
   LVEL    =     F    velocity operator in full k-point grid
   LINTERFAST=   F  fast interpolation
   KINTER  =     0    interpolate to denser k-point grid
   CSHIFT  =0.1000    complex shift for real part using Kramers
Kronig
   OMEGAMAX=  -1.0    maximum frequency
   DEG_THRESHOLD= 0.2000000E-02 threshold for treating states as
degnerate
   RTIME   =    0.100 relaxation time in fs

 Orbital magnetization related:
   ORBITALMAG=     F  switch on orbital magnetization
```

Figure B.4. 40-atom set atom positions before and after with VASP script file (cont.)

```
LCHIMAG    =      F  perturbation theory with respect to B field
   DQ        =  0.001000  dq finite difference perturbation B field
```

Figure B.4. 40-atom set atom positions before and after with VASP script file (cont.)

```
60-atom sets initial list 1: {{2.68703 6.33028 2.26156},{8.20933
3.16314 8.68335},{1.06176 0.936803 6.83376},{4.54773 6.88215
0.209531},
{6.76125 7.85195 3.22487},{6.85573 3.46256 1.6111},{7.65927 8.06596
5.22293},{0.414939 3.836 1.57013},{5.13281 5.81871 4.86813},{8.17233
6.84061 6.66908},{5.1045 0.806817 8.36273},{7.75093 3.40994
5.34469},
{1.10263 7.36519 8.04862},{1.68953 2.45685 5.41202},{0.894234
5.43162 3.14162},{5.97595 5.79184 6.81731},{3.67073 8.20922
4.26375},{3.29049 1.29831 6.1982},{0.202054 7.26247
3.97141},{2.32656 8.33883 2.43943},{7.22831 2.35545
3.75406},{2.01876 4.46444 6.65338},{1.79783 2.85767
0.192327},{4.29984 3.14729 2.69781},{7.35045 5.79355
2.50995},{1.51212 5.49817 0.419774},{8.69749 1.07102
1.85073},{7.81824 1.56701 5.8208},{5.01974 6.01936 2.53572},{4.94998
3.89774 0.675764},
{6.72603 1.7186 7.49285},{1.77642 1.60635 2.58768},{3.23361 4.66055
1.02183},{5.13513 8.05748 2.07021},{0.58237 3.61685
3.74991},{5.54278 8.65929 4.84759},{7.11035 8.40834
7.98801},{3.05746 4.91337 3.59288},{3.18659 7.34336
6.09988},{6.65655 5.89226 8.64504},{8.46688 7.40446
2.12553},{3.79731 3.63389 5.65873},{0.978991 5.94413
5.2513},{8.59667 5.09978 8.08289},{3.17686 6.0747 7.88489},{5.30155
1.98046 4.30759},{5.80204 3.67447 6.22561},{2.81229 0.997195
8.10759},{3.37694 1.83543 4.00277},{4.46572 2.40571 7.22575{1.34875
8.65573 4.86445},{5.17516 1.68332 1.47563},{6.88847 8.28168
1.27855},{6.70444 4.94635 4.09328},{0.597026 0.350959
0.0217009},{8.71787 0.930797 3.77527},{5.03375 8.08024
6.85953},{3.38011 0.691005 1.27451},{2.32003 6.84343
4.18673},{0.298564 3.57972 6.76683}};

60-atom sets VASP-relaxed list 1: total energy = -492.57777500 eV &
output atom list,
{1.80797028, 4.83502995, 3.51707220},{0.06948077, 4.90728747,
```

Figure B.5. 60-atom set atom positions before and after with VASP script file.

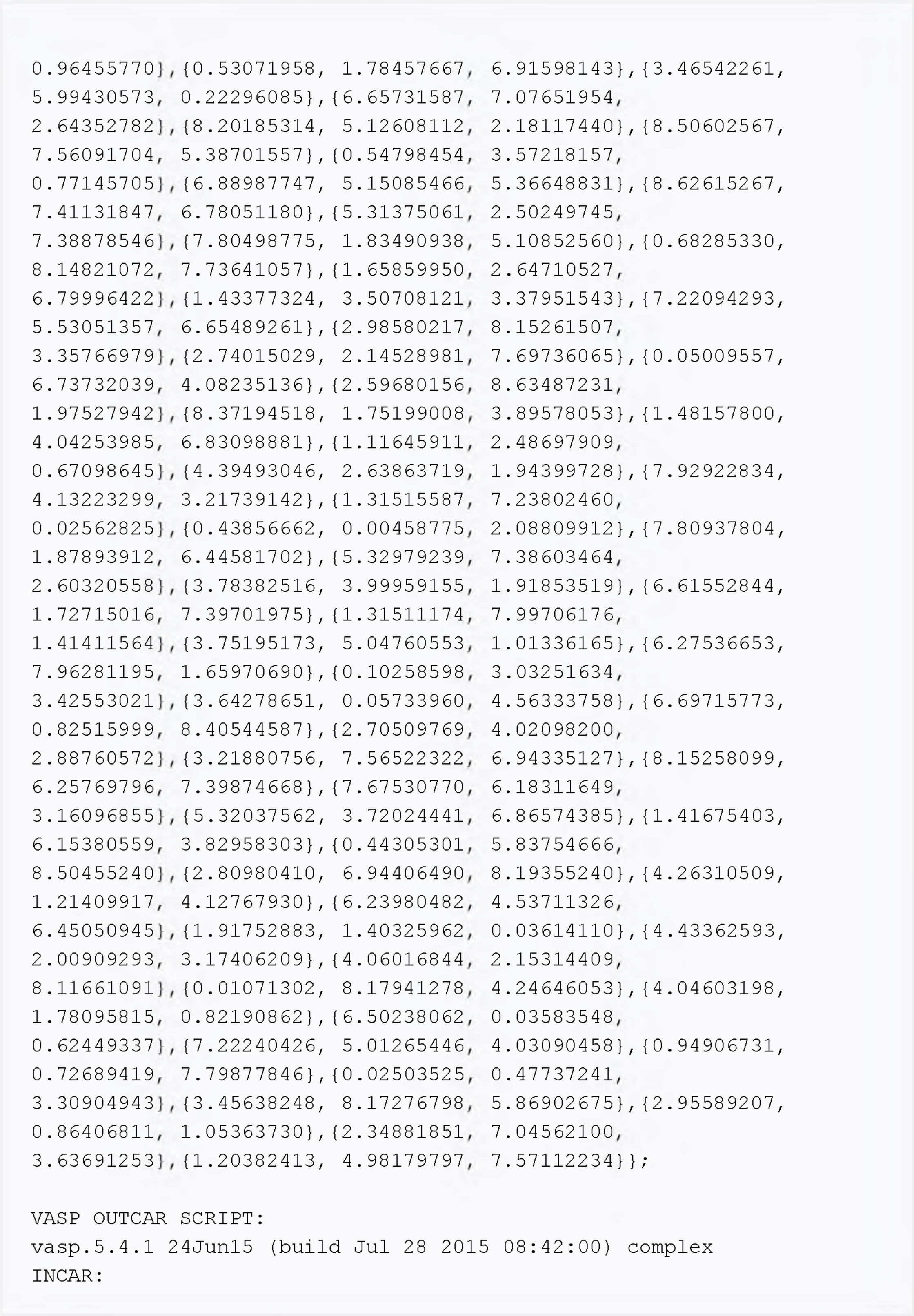

```
0.96455770},{0.53071958, 1.78457667, 6.91598143},{3.46542261,
5.99430573, 0.22296085},{6.65731587, 7.07651954,
2.64352782},{8.20185314, 5.12608112, 2.18117440},{8.50602567,
7.56091704, 5.38701557},{0.54798454, 3.57218157,
0.77145705},{6.88987747, 5.15085466, 5.36648831},{8.62615267,
7.41131847, 6.78051180},{5.31375061, 2.50249745,
7.38878546},{7.80498775, 1.83490938, 5.10852560},{0.68285330,
8.14821072, 7.73641057},{1.65859950, 2.64710527,
6.79996422},{1.43377324, 3.50708121, 3.37951543},{7.22094293,
5.53051357, 6.65489261},{2.98580217, 8.15261507,
3.35766979},{2.74015029, 2.14528981, 7.69736065},{0.05009557,
6.73732039, 4.08235136},{2.59680156, 8.63487231,
1.97527942},{8.37194518, 1.75199008, 3.89578053},{1.48157800,
4.04253985, 6.83098881},{1.11645911, 2.48697909,
0.67098645},{4.39493046, 2.63863719, 1.94399728},{7.92922834,
4.13223299, 3.21739142},{1.31515587, 7.23802460,
0.02562825},{0.43856662, 0.00458775, 2.08809912},{7.80937804,
1.87893912, 6.44581702},{5.32979239, 7.38603464,
2.60320558},{3.78382516, 3.99959155, 1.91853519},{6.61552844,
1.72715016, 7.39701975},{1.31511174, 7.99706176,
1.41411564},{3.75195173, 5.04760553, 1.01336165},{6.27536653,
7.96281195, 1.65970690},{0.10258598, 3.03251634,
3.42553021},{3.64278651, 0.05733960, 4.56333758},{6.69715773,
0.82515999, 8.40544587},{2.70509769, 4.02098200,
2.88760572},{3.21880756, 7.56522322, 6.94335127},{8.15258099,
6.25769796, 7.39874668},{7.67530770, 6.18311649,
3.16096855},{5.32037562, 3.72024441, 6.86574385},{1.41675403,
6.15380559, 3.82958303},{0.44305301, 5.83754666,
8.50455240},{2.80980410, 6.94406490, 8.19355240},{4.26310509,
1.21409917, 4.12767930},{6.23980482, 4.53711326,
6.45050945},{1.91752883, 1.40325962, 0.03614110},{4.43362593,
2.00909293, 3.17406209},{4.06016844, 2.15314409,
8.11661091},{0.01071302, 8.17941278, 4.24646053},{4.04603198,
1.78095815, 0.82190862},{6.50238062, 0.03583548,
0.62449337},{7.22240426, 5.01265446, 4.03090458},{0.94906731,
0.72689419, 7.79877846},{0.02503525, 0.47737241,
3.30904943},{3.45638248, 8.17276798, 5.86902675},{2.95589207,
0.86406811, 1.05363730},{2.34881851, 7.04562100,
3.63691253},{1.20382413, 4.98179797, 7.57112234}};

VASP OUTCAR SCRIPT:
vasp.5.4.1 24Jun15 (build Jul 28 2015 08:42:00) complex
INCAR:
```

Figure B.5. 60-atom set atom positions before and after with VASP script file (cont.)

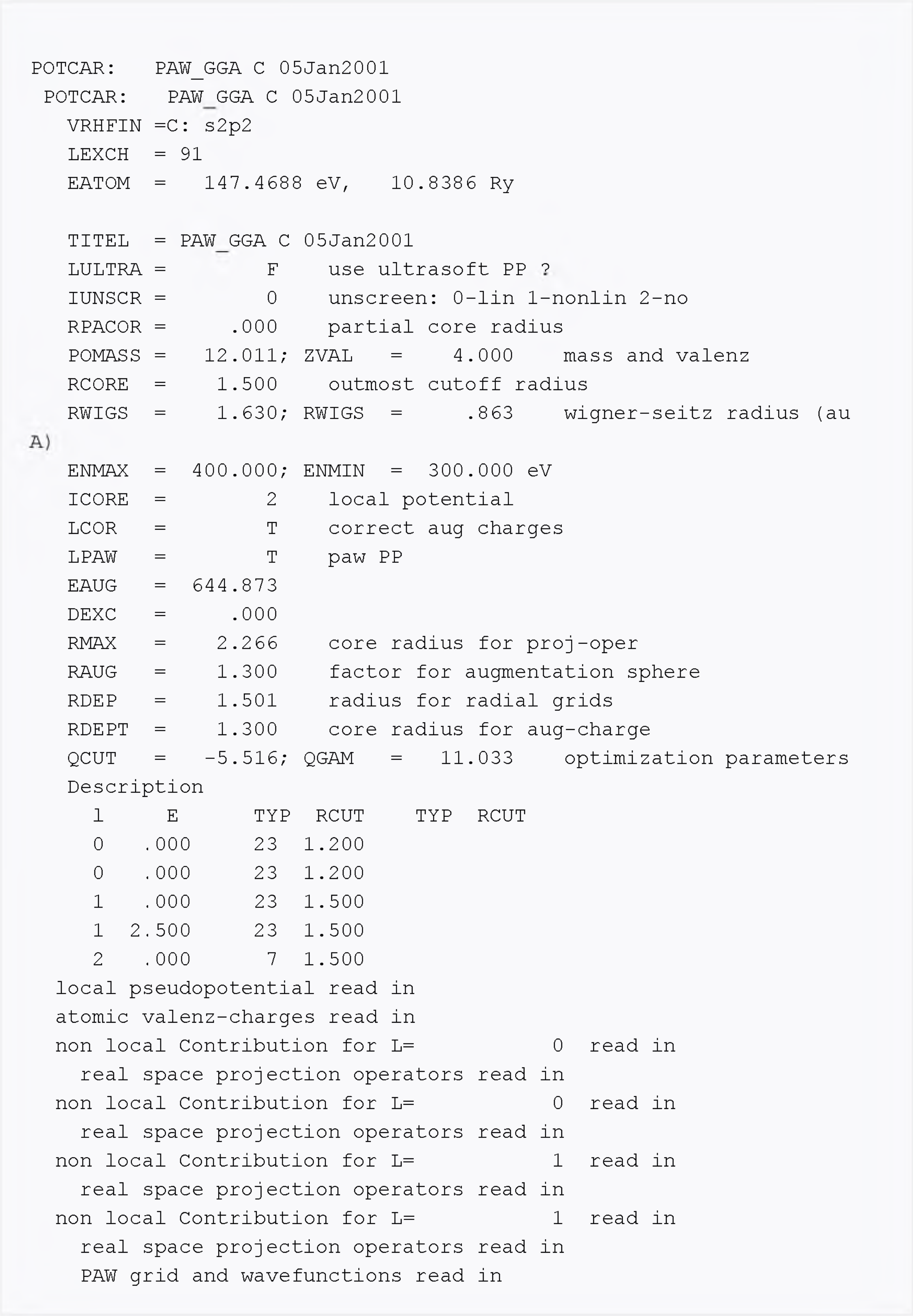

```
POTCAR:    PAW_GGA C 05Jan2001
 POTCAR:    PAW_GGA C 05Jan2001
   VRHFIN =C: s2p2
   LEXCH  = 91
   EATOM  =   147.4688 eV,   10.8386 Ry

   TITEL  = PAW_GGA C 05Jan2001
   LULTRA =        F    use ultrasoft PP ?
   IUNSCR =        0    unscreen: 0-lin 1-nonlin 2-no
   RPACOR =     .000    partial core radius
   POMASS =   12.011; ZVAL   =    4.000    mass and valenz
   RCORE  =    1.500    outmost cutoff radius
   RWIGS  =    1.630; RWIGS  =     .863    wigner-seitz radius (au
A)
   ENMAX  =  400.000; ENMIN  =  300.000 eV
   ICORE  =        2    local potential
   LCOR   =        T    correct aug charges
   LPAW   =        T    paw PP
   EAUG   =  644.873
   DEXC   =     .000
   RMAX   =    2.266    core radius for proj-oper
   RAUG   =    1.300    factor for augmentation sphere
   RDEP   =    1.501    radius for radial grids
   RDEPT  =    1.300    core radius for aug-charge
   QCUT   =   -5.516; QGAM   =   11.033    optimization parameters
   Description
     l     E      TYP  RCUT    TYP  RCUT
     0   .000     23  1.200
     0   .000     23  1.200
     1   .000     23  1.500
     1  2.500     23  1.500
     2   .000      7  1.500
  local pseudopotential read in
  atomic valenz-charges read in
  non local Contribution for L=           0  read in
    real space projection operators read in
  non local Contribution for L=           0  read in
    real space projection operators read in
  non local Contribution for L=           1  read in
    real space projection operators read in
  non local Contribution for L=           1  read in
    real space projection operators read in
    PAW grid and wavefunctions read in
```

Figure B.5. 60-atom set atom positions before and after with VASP script file (cont.)

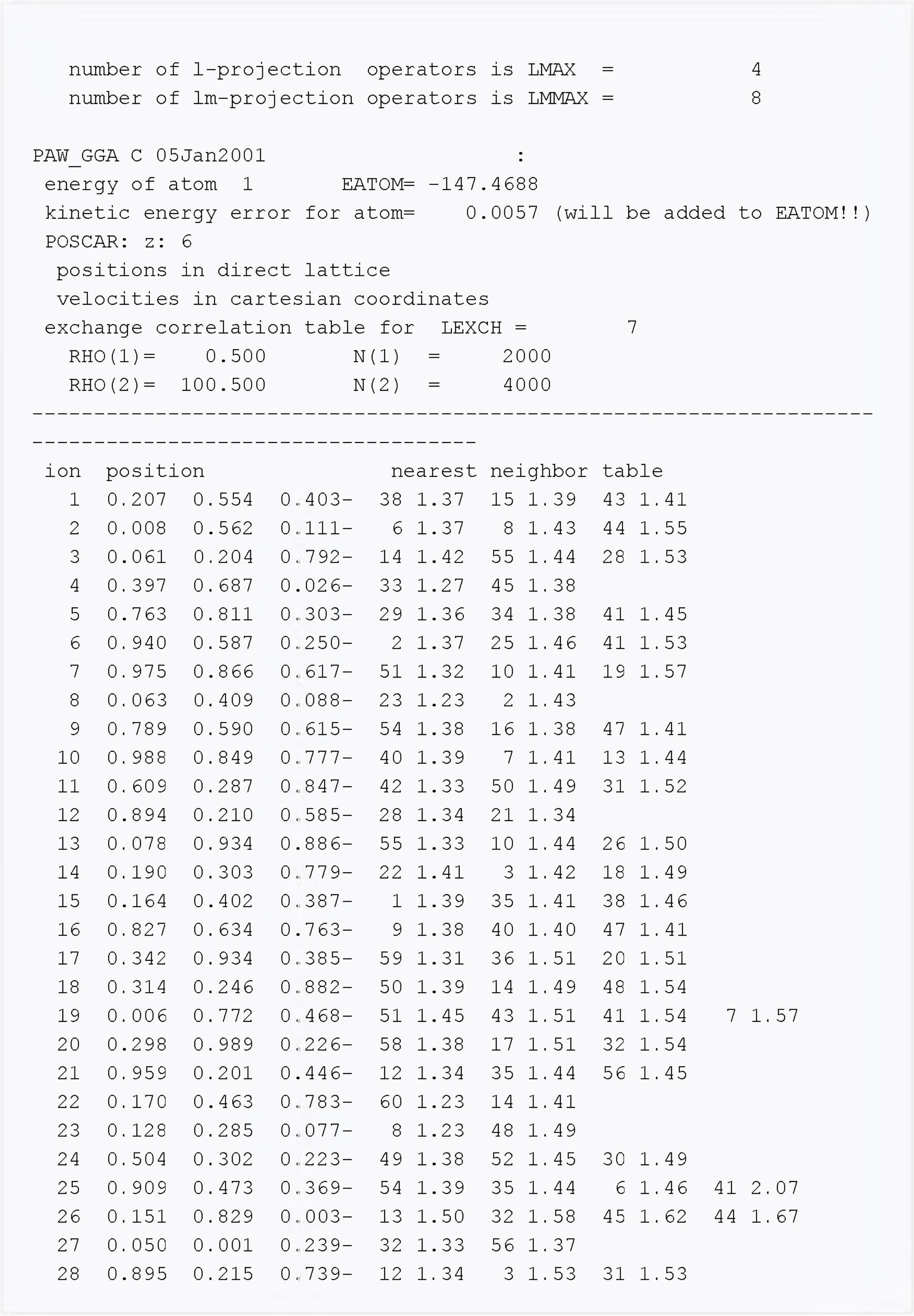

```
   number of l-projection  operators is LMAX  =           4
   number of lm-projection operators is LMMAX =           8

PAW_GGA C 05Jan2001                    :
 energy of atom  1       EATOM= -147.4688
 kinetic energy error for atom=    0.0057 (will be added to EATOM!!)
 POSCAR: z: 6
  positions in direct lattice
  velocities in cartesian coordinates
 exchange correlation table for  LEXCH =        7
   RHO(1)=    0.500       N(1)  =     2000
   RHO(2)=  100.500       N(2)  =     4000
--------------------------------------------------------------------
------------------------------------
 ion  position               nearest neighbor table
   1  0.207  0.554  0.403-  38 1.37  15 1.39  43 1.41
   2  0.008  0.562  0.111-   6 1.37   8 1.43  44 1.55
   3  0.061  0.204  0.792-  14 1.42  55 1.44  28 1.53
   4  0.397  0.687  0.026-  33 1.27  45 1.38
   5  0.763  0.811  0.303-  29 1.36  34 1.38  41 1.45
   6  0.940  0.587  0.250-   2 1.37  25 1.46  41 1.53
   7  0.975  0.866  0.617-  51 1.32  10 1.41  19 1.57
   8  0.063  0.409  0.088-  23 1.23   2 1.43
   9  0.789  0.590  0.615-  54 1.38  16 1.38  47 1.41
  10  0.988  0.849  0.777-  40 1.39   7 1.41  13 1.44
  11  0.609  0.287  0.847-  42 1.33  50 1.49  31 1.52
  12  0.894  0.210  0.585-  28 1.34  21 1.34
  13  0.078  0.934  0.886-  55 1.33  10 1.44  26 1.50
  14  0.190  0.303  0.779-  22 1.41   3 1.42  18 1.49
  15  0.164  0.402  0.387-   1 1.39  35 1.41  38 1.46
  16  0.827  0.634  0.763-   9 1.38  40 1.40  47 1.41
  17  0.342  0.934  0.385-  59 1.31  36 1.51  20 1.51
  18  0.314  0.246  0.882-  50 1.39  14 1.49  48 1.54
  19  0.006  0.772  0.468-  51 1.45  43 1.51  41 1.54   7 1.57
  20  0.298  0.989  0.226-  58 1.38  17 1.51  32 1.54
  21  0.959  0.201  0.446-  12 1.34  35 1.44  56 1.45
  22  0.170  0.463  0.783-  60 1.23  14 1.41
  23  0.128  0.285  0.077-   8 1.23  48 1.49
  24  0.504  0.302  0.223-  49 1.38  52 1.45  30 1.49
  25  0.909  0.473  0.369-  54 1.39  35 1.44   6 1.46  41 2.07
  26  0.151  0.829  0.003-  13 1.50  32 1.58  45 1.62  44 1.67
  27  0.050  0.001  0.239-  32 1.33  56 1.37
  28  0.895  0.215  0.739-  12 1.34   3 1.53  31 1.53
```

Figure B.5. 60-atom set atom positions before and after with VASP script file (cont.)

```
29  0.611  0.846  0.298-   5 1.36  34 1.45
  30  0.434  0.458  0.220-  33 1.39  38 1.45  24 1.49
  31  0.758  0.198  0.848-  37 1.36  11 1.52  28 1.53
  32  0.151  0.916  0.162-  27 1.33  20 1.54  26 1.58
  33  0.430  0.578  0.116-   4 1.27  30 1.39
  34  0.719  0.912  0.190-  53 1.33   5 1.38  29 1.45
  35  0.012  0.347  0.392-  15 1.41  25 1.44  21 1.44
  36  0.417  0.007  0.523-  46 1.38  57 1.45  17 1.51
  37  0.767  0.095  0.963-  53 1.25  31 1.36
  38  0.310  0.461  0.331-   1 1.37  30 1.45  15 1.46
  39  0.369  0.867  0.796-  57 1.26  45 1.45
  40  0.934  0.717  0.848-  10 1.39  16 1.40  44 1.56
  41  0.879  0.708  0.362-   5 1.45  54 1.53   6 1.53  19 1.54  25
2.07
  42  0.610  0.426  0.787-  47 1.30  11 1.33
  43  0.162  0.705  0.439-  59 1.30   1 1.41  19 1.51
  44  0.051  0.669  0.974-  60 1.48   2 1.55  40 1.56  26 1.67
  45  0.322  0.796  0.939-   4 1.38  39 1.45  26 1.62
  46  0.488  0.139  0.473-  49 1.25  36 1.38
  47  0.715  0.520  0.739-  42 1.30   9 1.41  16 1.41
  48  0.220  0.161  0.004-  23 1.49  55 1.53  18 1.54  58 1.55
  49  0.508  0.230  0.364-  46 1.25  24 1.38
  50  0.465  0.247  0.930-  18 1.39  52 1.48  11 1.49
  51  0.001  0.937  0.487-   7 1.32  56 1.39  19 1.45
  52  0.464  0.204  0.094-  58 1.44  24 1.45  50 1.48
  53  0.745  0.004  0.072-  37 1.25  34 1.33
  54  0.828  0.574  0.462-   9 1.38  25 1.39  41 1.53
  55  0.109  0.083  0.894-  13 1.33   3 1.44  48 1.53
  56  0.003  0.055  0.379-  27 1.37  51 1.39  21 1.45
  57  0.396  0.936  0.672-  39 1.26  36 1.45
  58  0.339  0.099  0.121-  20 1.38  52 1.44  48 1.55
  59  0.269  0.807  0.417-  43 1.30  17 1.31
  60  0.138  0.571  0.867-  22 1.23  44 1.48
  LATTYP: Found a simple cubic cell.
 ALAT       =     8.7276968000
  Lattice vectors:
 A1 = (   8.7276968000,   0.0000000000,   0.0000000000)
 A2 = (   0.0000000000,   8.7276968000,   0.0000000000)
 A3 = (   0.0000000000,   0.0000000000,   8.7276968000)

Analysis of symmetry for initial positions (statically):
====================================================================
 Subroutine PRICEL returns:
```

Figure B.5. 60-atom set atom positions before and after with VASP script file (cont.)

```
 Original cell was already a primitive cell.
 Routine SETGRP: Setting up the symmetry group for a
 simple cubic supercell.


 Subroutine GETGRP returns: Found  1 space group operations
 (whereof  1 operations were pure point group operations)
 out of a pool of 48 trial point group operations.

The static configuration has the point symmetry C_1 .
Analysis of symmetry for dynamics (positions and initial
velocities):
=====================================================================
=
 Subroutine PRICEL returns:
 Original cell was already a primitive cell.

 Routine SETGRP: Setting up the symmetry group for a
 simple cubic supercell.

 Subroutine GETGRP returns: Found  1 space group operations
 (whereof  1 operations were pure point group operations)
 out of a pool of 48 trial point group operations.
The dynamic configuration has the point symmetry C_1 .

 KPOINTS: Auto
Automatic generation of k-mesh.
Space group operators:
 irot       det(A)        alpha          n_x          n_y
n_z        tau_x        tau_y        tau_z
    1     1.000000     0.000000     1.000000     0.000000
0.000000     0.000000     0.000000     0.000000

 Subroutine IBZKPT returns following result:
 ===========================================
 Found      4 irreducible k-points:
 Following reciprocal coordinates:
            Coordinates               Weight
  0.250000  0.250000  0.250000      2.000000
 -0.250000  0.250000  0.250000      2.000000
  0.250000 -0.250000  0.250000      2.000000
 -0.250000 -0.250000  0.250000      2.000000
Following cartesian coordinates
```

Figure B.5. 60-atom set atom positions before and after with VASP script file (cont.)

```
  Coordinates               Weight
  0.028644  0.028644  0.028644      2.000000
 -0.028644  0.028644  0.028644      2.000000
  0.028644 -0.028644  0.028644      2.000000
 -0.028644 -0.028644  0.028644      2.000000
--------------------------------------------------------------------
------------------------------------
 Dimension of arrays:
   k-points           NKPTS =      4   k-points in BZ     NKDIM =
4   number of bands    NBANDS=    152
   number of dos      NEDOS =    301   number of ions     NIONS =
60
   non local maximal  LDIM  =      4   non local SUM 2l+1 LMDIM =
8
   total plane-waves  NPLWV = 157464
   max r-space proj   IRMAX =      1   max aug-charges    IRDMAX=
2994
   dimension x,y,z NGX =    54 NGY =   54 NGZ =   54
   dimension x,y,z NGXF=   108 NGYF=  108 NGZF=  108
   support grid    NGXF=   108 NGYF=  108 NGZF=  108
   ions per type =               60
 NGX,Y,Z   is equivalent  to a cutoff of  10.29, 10.29, 10.29 a.u.
 NGXF,Y,Z  is equivalent  to a cutoff of  20.57, 20.57, 20.57 a.u.
 I would recommend the setting:
   dimension x,y,z NGX =    52 NGY =   52 NGZ =   52
 SYSTEM =  Auto generated by VASP_setup, v 2.1.3
 POSCAR =  z: 6

 Startparameter for this run:
   NWRITE =      2    write-flag & timer
   PREC   = normal    normal or accurate (medium, high low for
compatibility)
   ISTART =      0    job   : 0-new  1-cont  2-samecut
   ICHARG =      2    charge: 1-file 2-atom 10-const
   ISPIN  =      1    spin polarized calculation?
   LNONCOLLINEAR =      F non collinear calculations
   LSORBIT =      F    spin-orbit coupling
   INIWAV =      1    electr: 0-lowe 1-rand  2-diag
   LASPH  =      F    aspherical Exc in radial PAW
   METAGGA=      F    non-selfconsistent MetaGGA calc
Electronic Relaxation 1
   ENCUT  =  600.0 eV  44.10 Ry    6.64 a.u.  17.43 17.43
17.43*2*pi/ulx,y,z
```

Figure B.5. 60-atom set atom positions before and after with VASP script file (cont.)

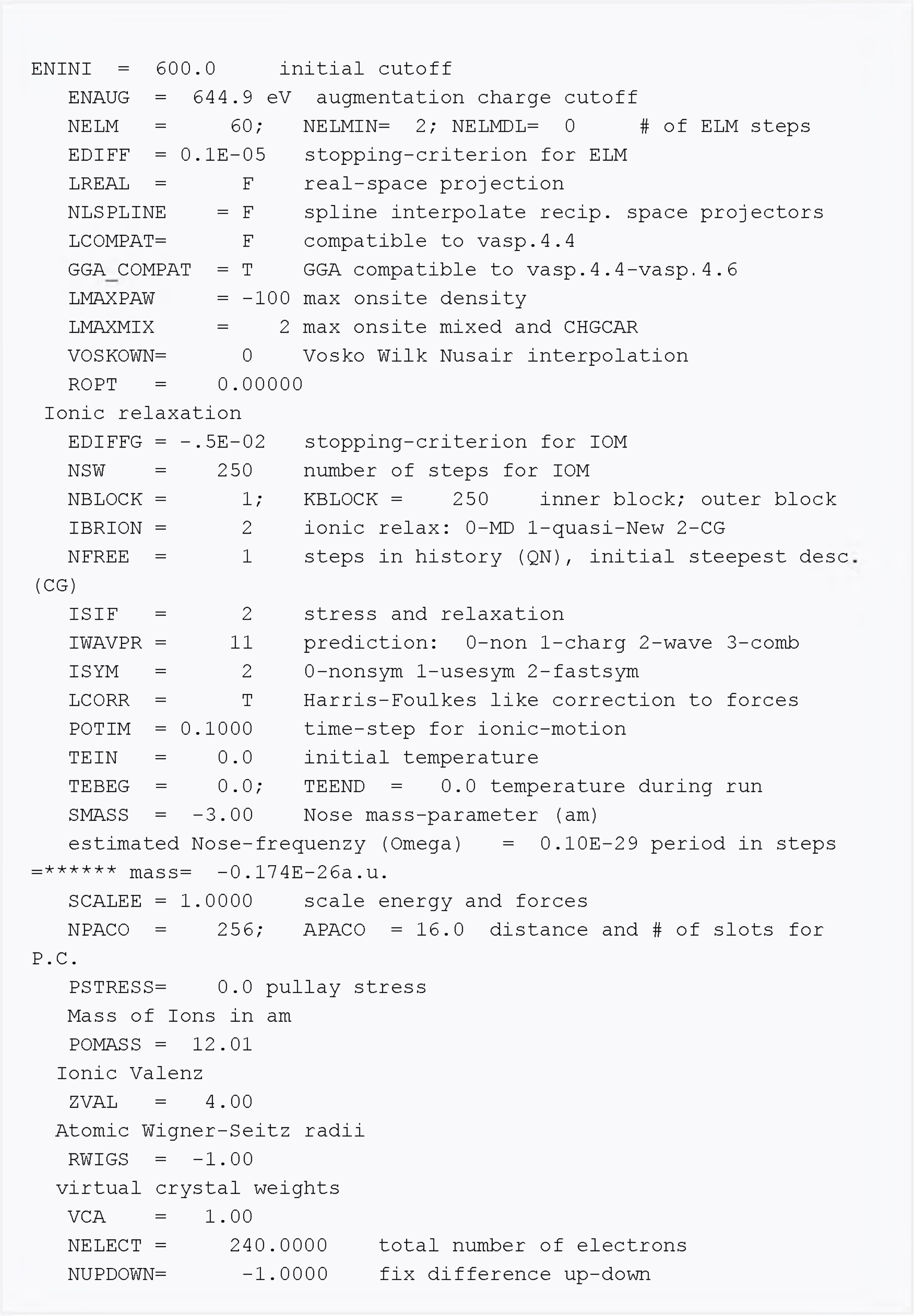

```
ENINI  =  600.0     initial cutoff
   ENAUG  =  644.9 eV  augmentation charge cutoff
   NELM   =     60;   NELMIN=  2; NELMDL=  0     # of ELM steps
   EDIFF  = 0.1E-05   stopping-criterion for ELM
   LREAL  =      F    real-space projection
   NLSPLINE    = F    spline interpolate recip. space projectors
   LCOMPAT=      F    compatible to vasp.4.4
   GGA_COMPAT  = T    GGA compatible to vasp.4.4-vasp.4.6
   LMAXPAW     = -100 max onsite density
   LMAXMIX     =    2 max onsite mixed and CHGCAR
   VOSKOWN=      0    Vosko Wilk Nusair interpolation
   ROPT   =    0.00000
 Ionic relaxation
   EDIFFG = -.5E-02   stopping-criterion for IOM
   NSW    =    250    number of steps for IOM
   NBLOCK =      1;   KBLOCK =    250    inner block; outer block
   IBRION =      2    ionic relax: 0-MD 1-quasi-New 2-CG
   NFREE  =      1    steps in history (QN), initial steepest desc.
(CG)
   ISIF   =      2    stress and relaxation
   IWAVPR =     11    prediction:  0-non 1-charg 2-wave 3-comb
   ISYM   =      2    0-nonsym 1-usesym 2-fastsym
   LCORR  =      T    Harris-Foulkes like correction to forces
   POTIM  = 0.1000    time-step for ionic-motion
   TEIN   =    0.0    initial temperature
   TEBEG  =    0.0;   TEEND  =   0.0 temperature during run
   SMASS  =  -3.00    Nose mass-parameter (am)
   estimated Nose-frequenzy (Omega)   =  0.10E-29 period in steps
=****** mass=  -0.174E-26a.u.
   SCALEE = 1.0000    scale energy and forces
   NPACO  =    256;   APACO  = 16.0  distance and # of slots for
P.C.
   PSTRESS=    0.0 pullay stress
   Mass of Ions in am
   POMASS =  12.01
  Ionic Valenz
   ZVAL   =   4.00
  Atomic Wigner-Seitz radii
   RWIGS  =  -1.00
  virtual crystal weights
   VCA    =   1.00
   NELECT =     240.0000    total number of electrons
   NUPDOWN=      -1.0000    fix difference up-down
```

Figure B.5. 60-atom set atom positions before and after with VASP script file (cont.)

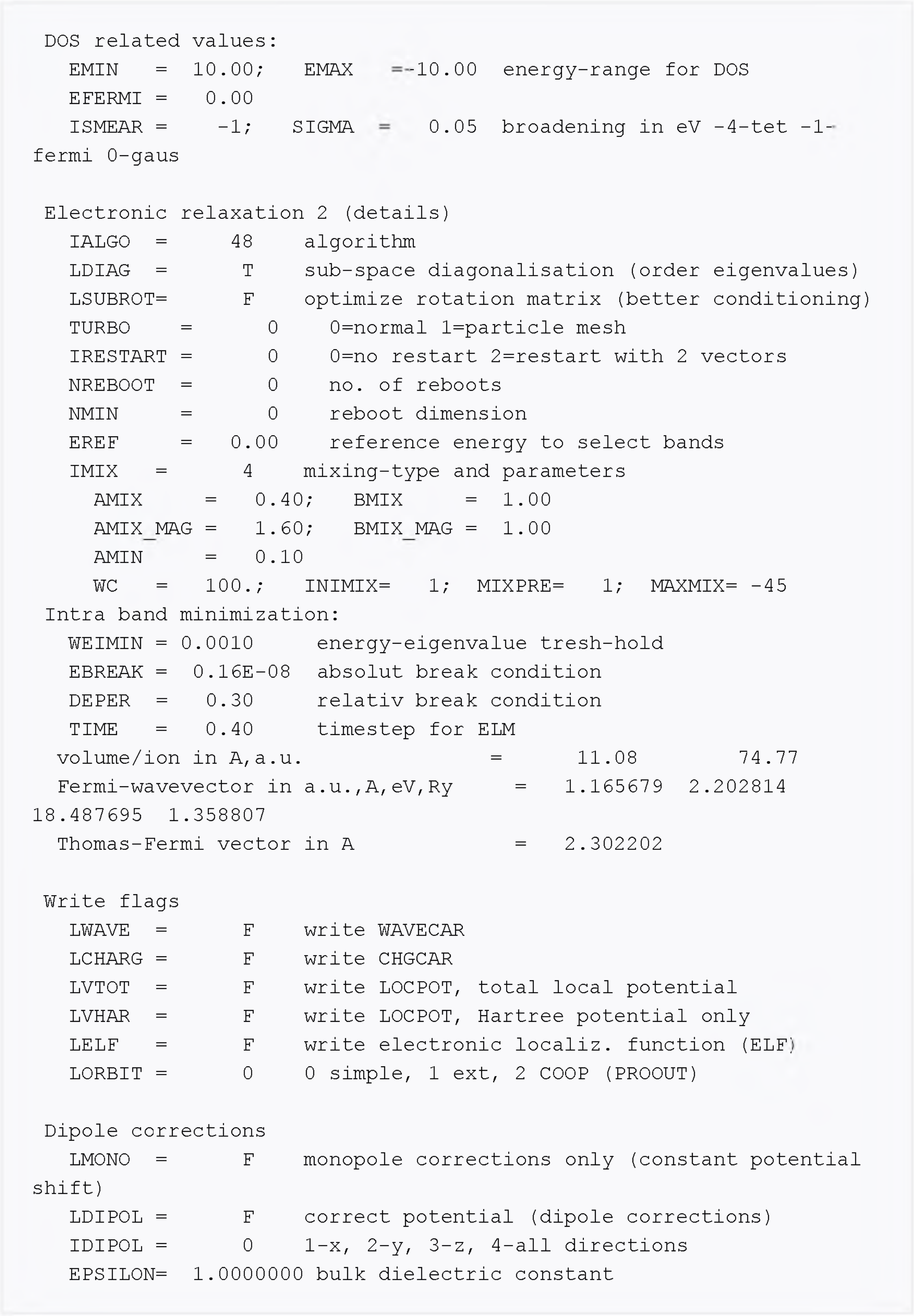

```
 DOS related values:
   EMIN   =  10.00;   EMAX   =-10.00  energy-range for DOS
   EFERMI =   0.00
   ISMEAR =    -1;   SIGMA  =   0.05  broadening in eV -4-tet -1-
fermi 0-gaus

 Electronic relaxation 2 (details)
   IALGO  =     48    algorithm
   LDIAG  =      T    sub-space diagonalisation (order eigenvalues)
   LSUBROT=      F    optimize rotation matrix (better conditioning)
   TURBO    =      0    0=normal 1=particle mesh
   IRESTART =      0    0=no restart 2=restart with 2 vectors
   NREBOOT  =      0    no. of reboots
   NMIN     =      0    reboot dimension
   EREF     =   0.00    reference energy to select bands
   IMIX   =      4    mixing-type and parameters
     AMIX     =   0.40;   BMIX     =  1.00
     AMIX_MAG =   1.60;   BMIX_MAG =  1.00
     AMIN     =   0.10
     WC   =   100.;   INIMIX=   1;  MIXPRE=   1;  MAXMIX= -45
 Intra band minimization:
   WEIMIN = 0.0010     energy-eigenvalue tresh-hold
   EBREAK =  0.16E-08  absolut break condition
   DEPER  =   0.30     relativ break condition
   TIME   =   0.40     timestep for ELM
  volume/ion in A,a.u.               =      11.08        74.77
  Fermi-wavevector in a.u.,A,eV,Ry     =   1.165679  2.202814
18.487695  1.358807
  Thomas-Fermi vector in A             =   2.302202

 Write flags
   LWAVE  =      F    write WAVECAR
   LCHARG =      F    write CHGCAR
   LVTOT  =      F    write LOCPOT, total local potential
   LVHAR  =      F    write LOCPOT, Hartree potential only
   LELF   =      F    write electronic localiz. function (ELF)
   LORBIT =      0    0 simple, 1 ext, 2 COOP (PROOUT)

 Dipole corrections
   LMONO  =      F    monopole corrections only (constant potential
shift)
   LDIPOL =      F    correct potential (dipole corrections)
   IDIPOL =      0    1-x, 2-y, 3-z, 4-all directions
   EPSILON=  1.0000000 bulk dielectric constant
```

Figure B.5. 60-atom set atom positions before and after with VASP script file (cont.)

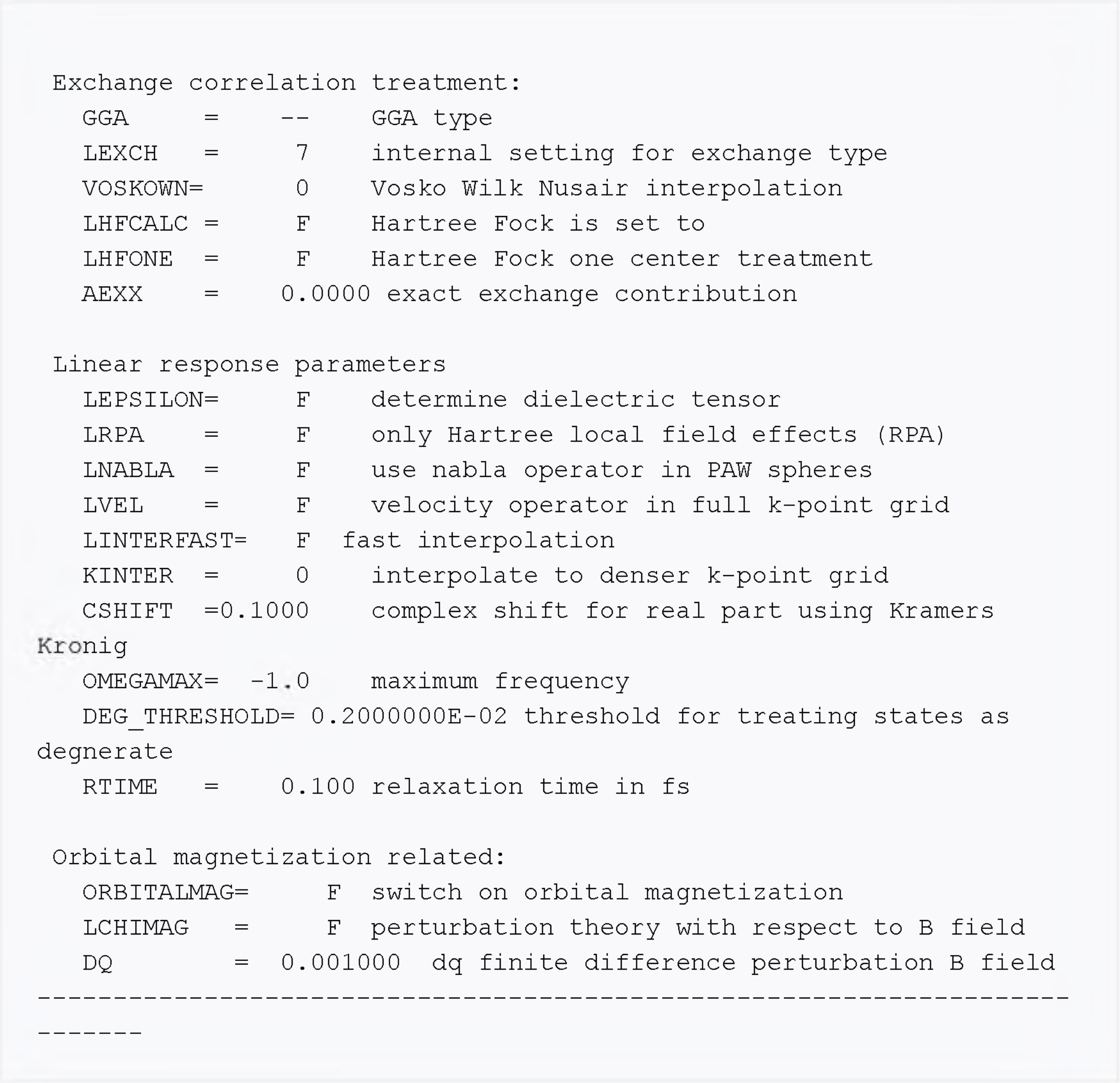

```
 Exchange correlation treatment:
   GGA     =    --    GGA type
   LEXCH   =     7    internal setting for exchange type
   VOSKOWN=      0    Vosko Wilk Nusair interpolation
   LHFCALC =     F    Hartree Fock is set to
   LHFONE  =     F    Hartree Fock one center treatment
   AEXX    =    0.0000 exact exchange contribution

 Linear response parameters
   LEPSILON=     F    determine dielectric tensor
   LRPA    =     F    only Hartree local field effects (RPA)
   LNABLA  =     F    use nabla operator in PAW spheres
   LVEL    =     F    velocity operator in full k-point grid
   LINTERFAST=   F  fast interpolation
   KINTER  =     0    interpolate to denser k-point grid
   CSHIFT  =0.1000    complex shift for real part using Kramers
Kronig
   OMEGAMAX=  -1.0    maximum frequency
   DEG_THRESHOLD= 0.2000000E-02 threshold for treating states as
degnerate
   RTIME   =    0.100 relaxation time in fs

 Orbital magnetization related:
   ORBITALMAG=     F  switch on orbital magnetization
   LCHIMAG   =     F  perturbation theory with respect to B field
   DQ        =  0.001000  dq finite difference perturbation B field
---------------------------------------------------------------------
-------
```

Figure B.5. 60-atom set atom positions before and after with VASP script file (cont.)

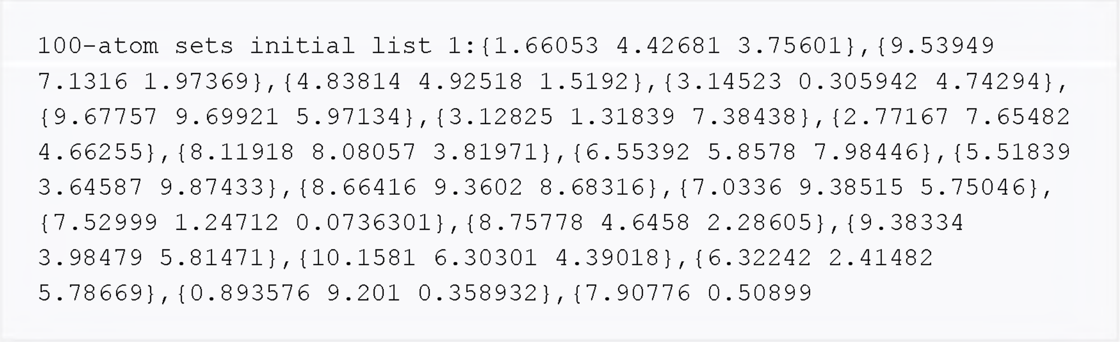

```
100-atom sets initial list 1:{1.66053 4.42681 3.75601},{9.53949
7.1316 1.97369},{4.83814 4.92518 1.5192},{3.14523 0.305942 4.74294},
{9.67757 9.69921 5.97134},{3.12825 1.31839 7.38438},{2.77167 7.65482
4.66255},{8.11918 8.08057 3.81971},{6.55392 5.8578 7.98446},{5.51839
3.64587 9.87433},{8.66416 9.3602 8.68316},{7.0336 9.38515 5.75046},
{7.52999 1.24712 0.0736301},{8.75778 4.6458 2.28605},{9.38334
3.98479 5.81471},{10.1581 6.30301 4.39018},{6.32242 2.41482
5.78669},{0.893576 9.201 0.358932},{7.90776 0.50899
```

Figure B.6. 100-atom set atom positions before and after with VASP script file.

```
6.79705},{5.57744 5.37312 3.53298},{0.925094 3.61663
8.51652},{3.85377 8.42548 0.066328},{4.67561 9.88145

6.62382},{2.17723 2.67657 1.27681},{3.86408 4.01218
6.18983},{3.59765 5.93641 3.12289},{2.73642 9.58062
2.00124},{0.483063 5.17559 6.2213},{7.01885 6.31966
1.12642},{4.16574 9.10085 3.42873},{1.6226 7.61344 1.65383},{3.65058
10.23 8.68793},{5.05388 6.74879 6.06189},{7.67622 5.66339
4.38742},{2.58169 1.09123 0.118191},{9.34729 10.1729
4.07829},{1.20854 9.71701 3.92132},{7.05199 2.61044 3.52454},4.9204
2.71789 2.12015},{5.38762 1.78139 8.52322},{6.31222 7.93625
0.412721},{9.01963 1.40547 8.6534},{0.509957 1.65123
2.74026},{6.5092 7.85922 6.95259},{8.93186 9.98932
1.42613},{0.350702 6.04635 0.819974},{5.02025 1.31789
0.0236393},{3.56558 6.81001 9.33497},{9.04341 2.99989
4.18641},{0.880595 1.72982 7.71227},{3.04304 4.18416
8.51422},{9.9063 1.47612 6.0887},{8.50776 6.10091 9.42134},{7.26331
0.444436,2.01907},{2.29782 8.37629 8.01978},{10.0407 7.03578
6.32999},{0.975669 5.45164 9.38611},{1.49183 2.75621
4.83209},{8.48799 5.26584 7.70978},{6.65685 7.70455
2.60566},{4.08431 2.08539 5.91243},{8.25527 3.15984
8.40906},{2.74331 6.04946 6.9078},{0.264456 7.71076
9.70512},{5.00589 7.16156 3.85627},{7.51178 3.11653
0.933599},{10.127 0.960987 0.686522},{6.54479 10.252
8.98597},{0.598903 10.1265 2.15079},{1.13759 10.2921
6.35031},{4.29081 2.93957 4.02964},{8.96533 7.51128
7.84678},{9.92251 3.83742 0.522512},{1.86802 4.6677 1.66506},{5.3883
6.24411 9.94171},{0.257195 8.78504 7.60777},{5.58718 4.19557
5.21272},{5.38078 3.61694 7.36366},{4.3042 8.19601 8.16105},{4.89353
0.592885 3.49251},{1.79972 3.35347 6.61613},{4.72251 9.86094
1.65193},{7.16846 4.62666 10.0449},{4.44203 7.86866 1.91247},{2.4760
1.6936 2.90854},{8.19991 1.34085 5.0451},{10.1539 8.40758
3.75161},{1.07004 0.0365735 8.81363},{8.4052 8.43842
0.0821403},{1.71209 5.99446 4.89442},{1.24137
8.53986,5.53387},{10.25063.49691 2.70491},{3.36182 2.6249
9.59105},{7.33992 4.03157 6.71294},{2.87231 4.66889
0.0234549},{6.42334 9.55233 3.90321},{9.01367 1.62715
2.23311},{8.1565 6.6896 6.08947},{3.49035 8.17894 6.3696},{6.28047
8.20662 8.88013}};
100-atom sets VASP-relaxed list 1: total energy = -824.47704229 eV &
output atom list,
{2.07198450,  4.66947600,  5.78141695},{0.07356387,
```

Figure B.6. 100-atom set atom positions before and after with VASP script file (cont.)

```
8.20690814,0.64559072},{4.41772277,  4.43707102,
1.48749803},{4.50532224,  1.13573838,  3.26089814},{10.07259985,
9.62245442,5.81171103},{3.56848815,  1.55129021,
7.23828036},{2.18950710,  7.12418662, 6.21966025},{7.97994387,
6.99594890,  4.16701636},{6.80154015,  6.99215113,
8.83765577},{6.01612674,  3.97005465,  8.93552038},{8.39782743,
9.51411199,  9.10434850},{6.07498378,  8.65510295,
5.68794641},{8.15243801,  2.95908403, 1.12916189},{0.81185062,
4.28436069,  2.51623927},{9.65751394,  3.24104668,
4.17542746},{0.12042272,  6.22648727,  5.70865957},{6.53448656,
2.49960604, 5.19696118},{1.18704934,  9.34483156,
0.95556206},{6.99260958,  9.87492746, 5.54070508},{5.50911485,
4.59221414,  3.73424421},{1.40447367,  3.17387894,
8.31440698},{3.70273581,  8.22093123,  0.63808673},{2.26166421,
9.80330313,  8.15253703},{2.82750239,  1.28158051,
1.39763736},{4.52459279,  2.92121714, 5.53348461},{5.01067679,
5.12720592,  2.52094660},{3.70752216,  0.46791682,
2.25951235},{9.79150610,  4.38775058,  5.06480219},{7.06844978,
7.27976554, 1.89809390},{3.68514982,  9.48621205,
2.95748338},{2.22967888,  8.21222201, 0.64506645},{2.77187053,
0.64616655,  7.81226761},{4.29572966,  6.92919218,
6.29790832},{7.87471150,  6.28149024,  5.44064193},{3.66914248,
2.33335067, 0.75834977},{9.78560036,  8.97513765,
4.52718408},{9.99361717,  8.61459717, 3.22841433},{7.69335458,
1.78953188,  4.89322908},{4.32801700,  3.01377262,
1.80443471},{4.86190205,  2.21668947,  7.66956292},{6.56260439,
7.34827269, 0.78539496},{8.90457971,  2.68417777,
7.30267021},{0.53378534,  1.88863665,  2.55483650},{5.67263047,
7.26906933,  6.09339629},{8.93417896,  0.51988415,
0.81833897},{1.27848796,  7.24814862,  0.53093337},{4.87430169,
3.05640513, 8.75755453},{4.64390371,  8.02207892,
9.81218534},{8.83736133,  2.12938633, 3.99059831},{9.91290055,
1.82246547, 6.87098094},{2.25185940,  3.69898112,
9.21864870},{9.41249014, 0.56235274,  6.21804674},{8.07235596,
7.18712895, 8.41240572},{8.70325447,  1.80670402,
1.44297422},{3.38057710,  8.83754243, 7.75298396},{9.15542558,
5.57714796,  5.51126443},{1.44360435,  5.79390374,
0.53078406},{2.09212932,  3.21889252,  6.15134329},{7.18255542,
5.99804834, 7.78250201},{7.05930582,  6.72212362,
3.16383728},{3.24269073,  2.49071855, 6.08891885},{8.08594785,
3.57451482,  7.64377827},{2.92680065,  5.92369735,
6.03940944},{0.31634167,  9.48420559, 10.09313505},{5.98980015,
5.79775440, 3.31320514},{7.40220577,  3.84309314,
```

Figure B.6. 100-atom set atom positions before and after with VASP script file (cont.)

```
0.62944948},{9.42392851,10.30571816,  1.96665686},{7.01725035,
9.79320271,  8.86150588},{10.31979965,
9.08713273,1.90685965},{0.20552334,  8.60160960,
6.57817571},{4.77836010,  2.44603702, 3.10323260},{8.97155715,
8.30188595,  8.46517526},{1.00584830,  5.10826270,
1.59213242},{3.66849259,  4.54653864,  0.22568160},{5.92255086,
7.40644692, 9.92588086},{0.01726996,  8.62891116,
8.00582502},{5.38279646,  3.21982301,  4.26845294},{5.55864624,
2.48882712,
6.31736275},{4.60518839,8.84056761,8.61233171},{4.95869370,
10.08764163, 3.67417820},{0.96677423,
2.68180991,7.13198988},{5.03575228, 9.84551081,
2.12130539},{6.50446580,  4.24098395,10.15018976},{4.23707452,
8.64352131, 1.81654065},{1.57669496,  1.46843590,
1.84270266},{7.99523025, 0.54707946,  5.67799374},{9.04971296,
7.90620186, 3.99351725},{0.92602883,  9.30541905,
8.75163340},{9.26888872, 10.15847494,9.96964815},{0.77705522,
5.01420504,  5.43754236},{0.79661664,  7.34716352,
6.10501602},{0.40471150,  3.20706293,  3.19093542},{3.66970881,
3.19893726, 9.81216703},{7.13415214,  4.47530568,
8.03059020},{2.42016751,  4.91767352,10.11776299},{5.80506333,
9.63885646,  4.78172114},{9.44638131,  1.34683203,
2.71720195},{6.85911001,  6.38704613,  6.33597379},{3.29689352,
7.90228317,6.75730604},{5.85560086, 9.51125518, 8.49846132}};

VASP OUTCAR SCRIPT:
INCAR:
 POTCAR:   PAW_GGA C 05Jan2001
 POTCAR:   PAW_GGA C 05Jan2001
   VRHFIN =C: s2p2
   LEXCH  = 91
   EATOM  =   147.4688 eV,   10.8386 Ry

   TITEL  = PAW_GGA C 05Jan2001
   LULTRA =        F    use ultrasoft PP ?
   IUNSCR =        0    unscreen: 0-lin 1-nonlin 2-no
   RPACOR =     .000    partial core radius
   POMASS =   12.011; ZVAL   =    4.000    mass and valenz
   RCORE  =    1.500    outmost cutoff radius
   RWIGS  =    1.630; RWIGS  =     .863    wigner-seitz radius (au
A)
   ENMAX  =  400.000; ENMIN  =  300.000 eV
   ICORE  =        2    local potential
```

Figure B.6. 100-atom set atom positions before and after with VASP script file (cont.)

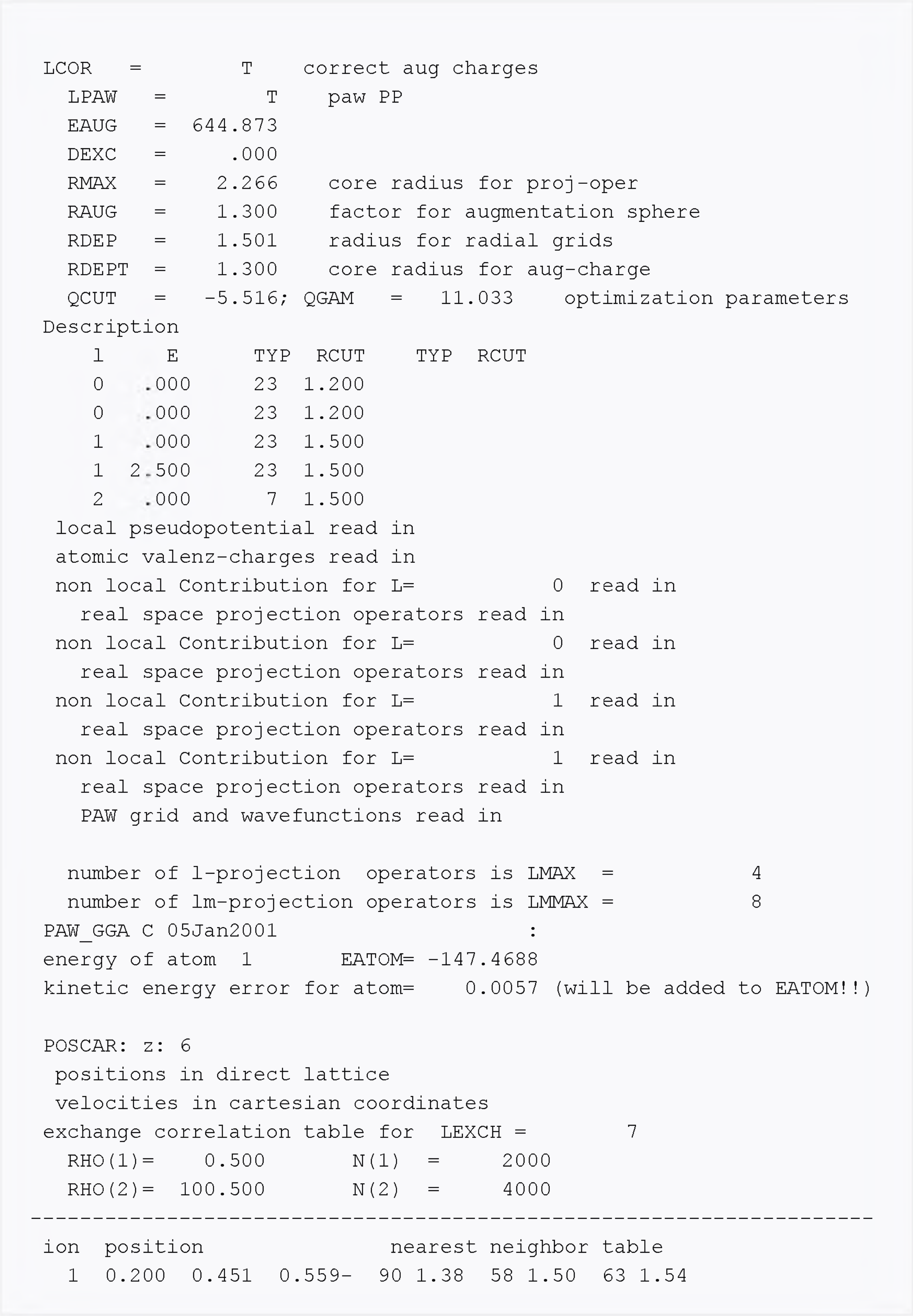

```
LCOR   =        T    correct aug charges
  LPAW   =        T    paw PP
  EAUG   =  644.873
  DEXC   =     .000
  RMAX   =    2.266    core radius for proj-oper
  RAUG   =    1.300    factor for augmentation sphere
  RDEP   =    1.501    radius for radial grids
  RDEPT  =    1.300    core radius for aug-charge
  QCUT   =   -5.516; QGAM   =   11.033    optimization parameters
Description
    l     E      TYP  RCUT    TYP  RCUT
    0    .000     23  1.200
    0    .000     23  1.200
    1    .000     23  1.500
    1   2.500     23  1.500
    2    .000      7  1.500
 local pseudopotential read in
 atomic valenz-charges read in
 non local Contribution for L=           0  read in
   real space projection operators read in
 non local Contribution for L=           0  read in
   real space projection operators read in
 non local Contribution for L=           1  read in
   real space projection operators read in
 non local Contribution for L=           1  read in
   real space projection operators read in
   PAW grid and wavefunctions read in

  number of l-projection  operators is LMAX  =           4
  number of lm-projection operators is LMMAX =           8
PAW_GGA C 05Jan2001                    :
energy of atom  1       EATOM= -147.4688
kinetic energy error for atom=    0.0057 (will be added to EATOM!!)

POSCAR: z: 6
 positions in direct lattice
 velocities in cartesian coordinates
exchange correlation table for  LEXCH =        7
  RHO(1)=    0.500       N(1)  =     2000
  RHO(2)=  100.500       N(2)  =     4000
--------------------------------------------------------------------
ion  position               nearest neighbor table
  1  0.200  0.451  0.559-  90 1.38  58 1.50  63 1.54
```

Figure B.6. 100-atom set atom positions before and after with VASP script file (cont.)

```
2  0.007  0.793  0.062-  69 1.54  46 1.54  64 1.58  18 1.62
    3  0.427  0.429  0.144-  26 1.38  39 1.46  74 1.47
    4  0.435  0.110  0.315-  71 1.35  27 1.44  80 1.52  82 2.06
    5  0.973  0.930  0.562-  70 1.36  36 1.47  52 1.50
    6  0.345  0.150  0.699-  32 1.34  40 1.52  61 1.52
    7  0.212  0.688  0.601-  91 1.42  63 1.42  99 1.46
    8  0.771  0.676  0.403-  60 1.39  87 1.42  34 1.46
    9  0.657  0.676  0.854-  53 1.35  75 1.46  59 1.50
   10  0.581  0.384  0.864-  83 1.34  47 1.47  94 1.52
   11  0.812  0.919  0.880-  89 1.39  68 1.43  72 1.49
   12  0.587  0.836  0.550-  96 1.36  44 1.50  19 1.53
   13  0.788  0.286  0.109-  66 1.26  54 1.32
   14  0.078  0.414  0.243-  73 1.25  92 1.33
   15  0.933  0.313  0.404-  49 1.39  28 1.46  92 1.47
   16  0.012  0.602  0.552-  91 1.37  90 1.41  56 1.48  28 2.06
   17  0.631  0.242  0.502-  38 1.39  78 1.49  77 1.65
   18  0.115  0.903  0.092-  64 1.50  69 1.56  31 1.57   2 1.62
   19  0.676  0.954  0.535-  96 1.43  86 1.44  12 1.53
   20  0.532  0.444  0.361-  65 1.36  26 1.42  77 1.48
   21  0.136  0.307  0.803-  51 1.35  81 1.35
   22  0.358  0.794  0.062-  84 1.36  31 1.47  48 1.52
   23  0.219  0.947  0.788-  32 1.34  55 1.53  88 1.55
   24  0.273  0.124  0.135-  85 1.34  27 1.48  35 1.49
   25  0.437  0.282  0.535-  78 1.37  61 1.46  77 1.56
   26  0.484  0.495  0.244-   3 1.38  20 1.42  65 1.43
   27  0.358  0.045  0.218-   4 1.44  24 1.48  30 1.50  82 1.65  80
2.02
   28  0.946  0.424  0.489-  56 1.42  15 1.46  90 1.52  16 2.06
   29  0.683  0.704  0.183-  41 1.22  60 1.38
   30  0.356  0.917  0.286-  27 1.50  84 1.52  80 1.58  82 1.63
   31  0.215  0.794  0.062-  46 1.36  22 1.47  18 1.57
   32  0.268  0.062  0.755-   6 1.34  23 1.34
   33  0.415  0.670  0.609-  44 1.43  99 1.47  63 1.72
   34  0.761  0.607  0.526-  98 1.36  56 1.46   8 1.46
   35  0.355  0.225  0.073-  39 1.41  24 1.49  93 1.56
   36  0.946  0.867  0.438-  37 1.36  87 1.40   5 1.47
   37  0.966  0.833  0.312-  36 1.36  87 1.41  69 1.44
   38  0.743  0.173  0.473-  17 1.39  49 1.50  86 1.50
   39  0.418  0.291  0.174-  35 1.41   3 1.46  71 1.49
   40  0.470  0.214  0.741-  47 1.37   6 1.52  78 1.55
   41  0.634  0.710  0.076-  29 1.22  75 1.37
   42  0.861  0.259  0.706-  62 1.26  50 1.39
   43  0.052  0.183  0.247-  85 1.33  92 1.47  97 1.54
```

Figure B.6. 100-atom set atom positions before and after with VASP script file (cont.)

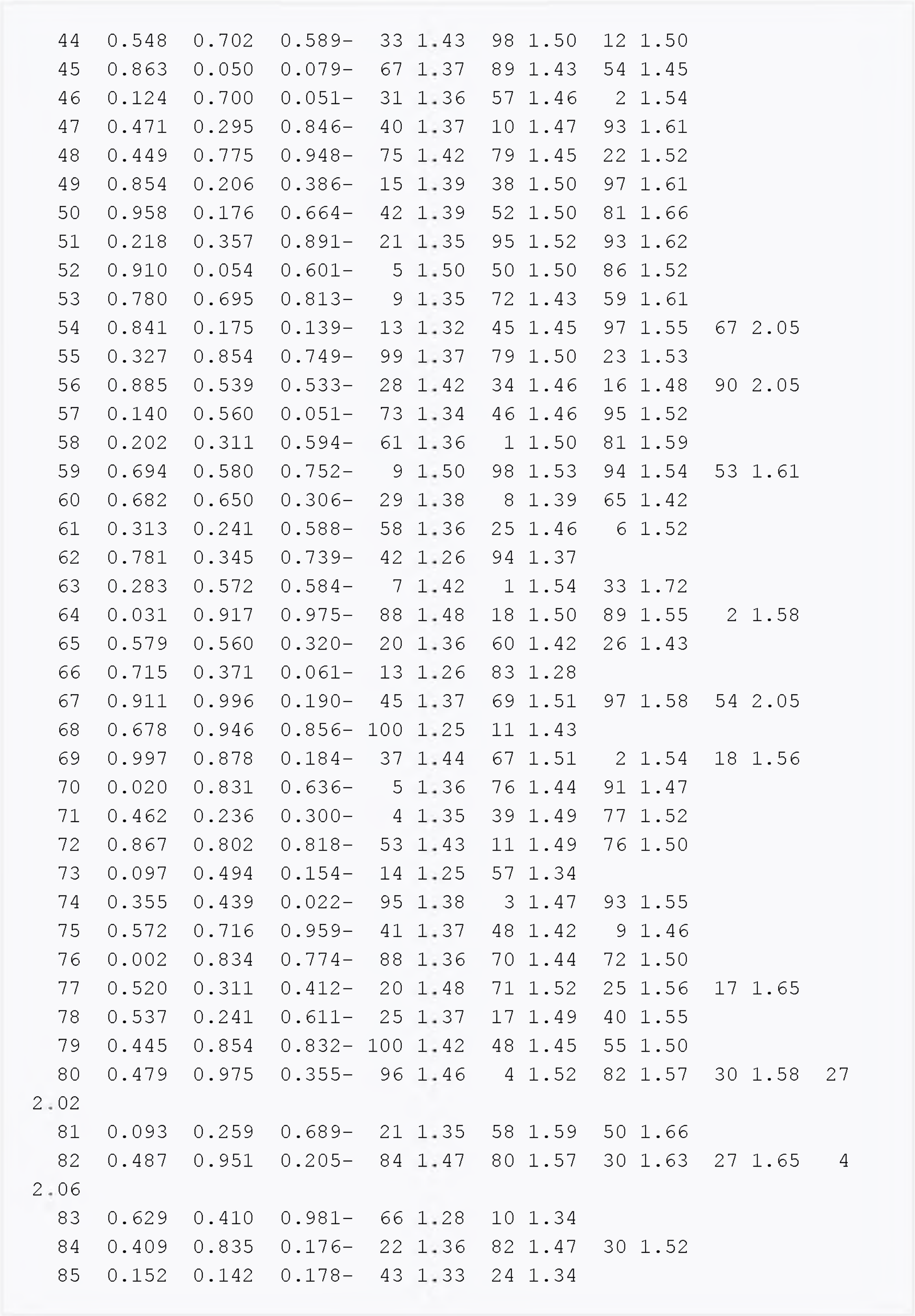

```
  44  0.548  0.702  0.589-  33 1.43  98 1.50  12 1.50
  45  0.863  0.050  0.079-  67 1.37  89 1.43  54 1.45
  46  0.124  0.700  0.051-  31 1.36  57 1.46   2 1.54
  47  0.471  0.295  0.846-  40 1.37  10 1.47  93 1.61
  48  0.449  0.775  0.948-  75 1.42  79 1.45  22 1.52
  49  0.854  0.206  0.386-  15 1.39  38 1.50  97 1.61
  50  0.958  0.176  0.664-  42 1.39  52 1.50  81 1.66
  51  0.218  0.357  0.891-  21 1.35  95 1.52  93 1.62
  52  0.910  0.054  0.601-   5 1.50  50 1.50  86 1.52
  53  0.780  0.695  0.813-   9 1.35  72 1.43  59 1.61
  54  0.841  0.175  0.139-  13 1.32  45 1.45  97 1.55  67 2.05
  55  0.327  0.854  0.749-  99 1.37  79 1.50  23 1.53
  56  0.885  0.539  0.533-  28 1.42  34 1.46  16 1.48  90 2.05
  57  0.140  0.560  0.051-  73 1.34  46 1.46  95 1.52
  58  0.202  0.311  0.594-  61 1.36   1 1.50  81 1.59
  59  0.694  0.580  0.752-   9 1.50  98 1.53  94 1.54  53 1.61
  60  0.682  0.650  0.306-  29 1.38   8 1.39  65 1.42
  61  0.313  0.241  0.588-  58 1.36  25 1.46   6 1.52
  62  0.781  0.345  0.739-  42 1.26  94 1.37
  63  0.283  0.572  0.584-   7 1.42   1 1.54  33 1.72
  64  0.031  0.917  0.975-  88 1.48  18 1.50  89 1.55   2 1.58
  65  0.579  0.560  0.320-  20 1.36  60 1.42  26 1.43
  66  0.715  0.371  0.061-  13 1.26  83 1.28
  67  0.911  0.996  0.190-  45 1.37  69 1.51  97 1.58  54 2.05
  68  0.678  0.946  0.856- 100 1.25  11 1.43
  69  0.997  0.878  0.184-  37 1.44  67 1.51   2 1.54  18 1.56
  70  0.020  0.831  0.636-   5 1.36  76 1.44  91 1.47
  71  0.462  0.236  0.300-   4 1.35  39 1.49  77 1.52
  72  0.867  0.802  0.818-  53 1.43  11 1.49  76 1.50
  73  0.097  0.494  0.154-  14 1.25  57 1.34
  74  0.355  0.439  0.022-  95 1.38   3 1.47  93 1.55
  75  0.572  0.716  0.959-  41 1.37  48 1.42   9 1.46
  76  0.002  0.834  0.774-  88 1.36  70 1.44  72 1.50
  77  0.520  0.311  0.412-  20 1.48  71 1.52  25 1.56  17 1.65
  78  0.537  0.241  0.611-  25 1.37  17 1.49  40 1.55
  79  0.445  0.854  0.832- 100 1.42  48 1.45  55 1.50
  80  0.479  0.975  0.355-  96 1.46   4 1.52  82 1.57  30 1.58  27
2.02
  81  0.093  0.259  0.689-  21 1.35  58 1.59  50 1.66
  82  0.487  0.951  0.205-  84 1.47  80 1.57  30 1.63  27 1.65   4
2.06
  83  0.629  0.410  0.981-  66 1.28  10 1.34
  84  0.409  0.835  0.176-  22 1.36  82 1.47  30 1.52
  85  0.152  0.142  0.178-  43 1.33  24 1.34
```

Figure B.6. 100-atom set atom positions before and after with VASP script file (cont.)

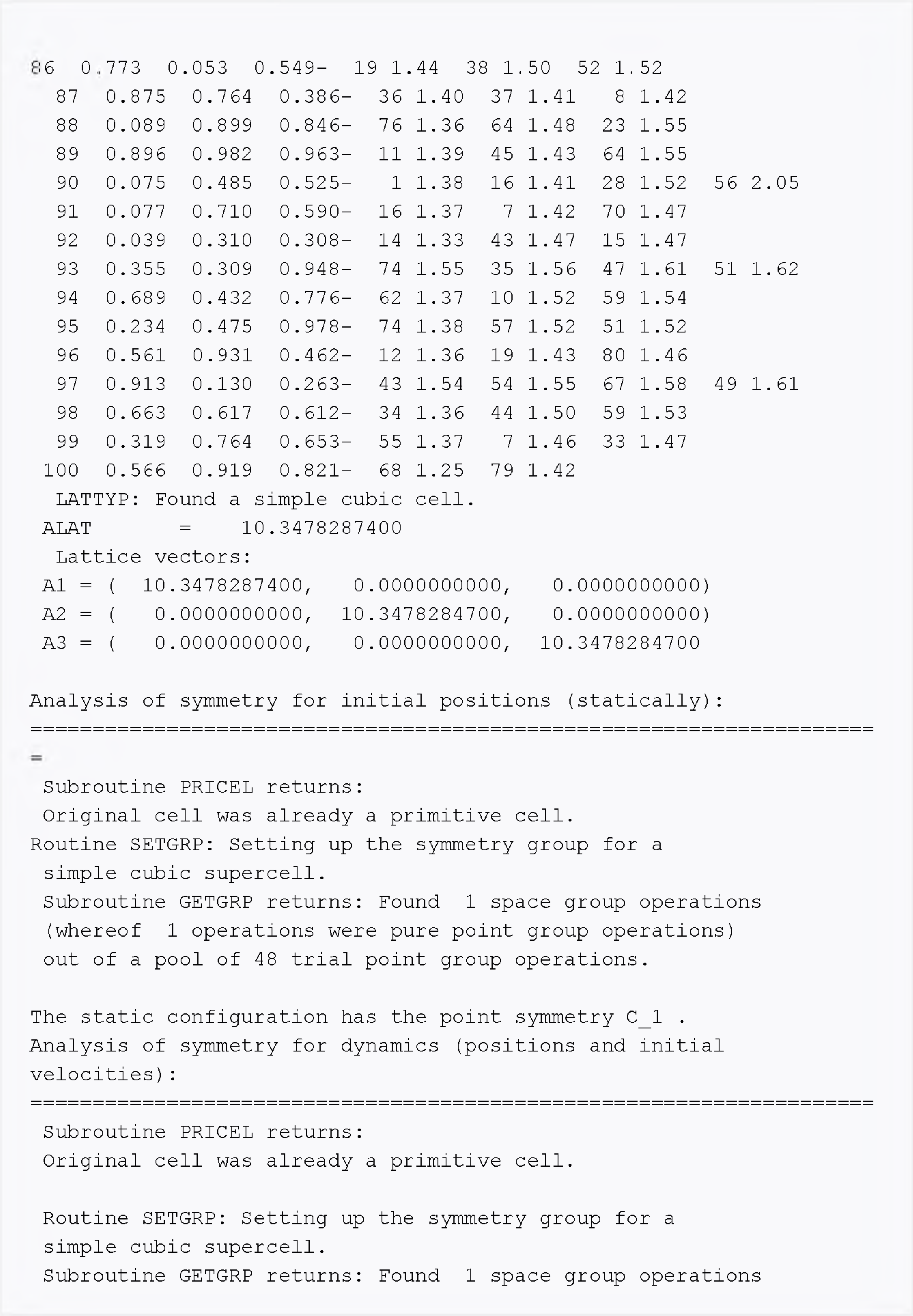

```
86  0.773  0.053  0.549-  19 1.44  38 1.50  52 1.52
  87  0.875  0.764  0.386-  36 1.40  37 1.41   8 1.42
  88  0.089  0.899  0.846-  76 1.36  64 1.48  23 1.55
  89  0.896  0.982  0.963-  11 1.39  45 1.43  64 1.55
  90  0.075  0.485  0.525-   1 1.38  16 1.41  28 1.52  56 2.05
  91  0.077  0.710  0.590-  16 1.37   7 1.42  70 1.47
  92  0.039  0.310  0.308-  14 1.33  43 1.47  15 1.47
  93  0.355  0.309  0.948-  74 1.55  35 1.56  47 1.61  51 1.62
  94  0.689  0.432  0.776-  62 1.37  10 1.52  59 1.54
  95  0.234  0.475  0.978-  74 1.38  57 1.52  51 1.52
  96  0.561  0.931  0.462-  12 1.36  19 1.43  80 1.46
  97  0.913  0.130  0.263-  43 1.54  54 1.55  67 1.58  49 1.61
  98  0.663  0.617  0.612-  34 1.36  44 1.50  59 1.53
  99  0.319  0.764  0.653-  55 1.37   7 1.46  33 1.47
 100  0.566  0.919  0.821-  68 1.25  79 1.42
  LATTYP: Found a simple cubic cell.
 ALAT       =    10.3478287400
  Lattice vectors:
 A1 = (  10.3478287400,   0.0000000000,   0.0000000000)
 A2 = (   0.0000000000,  10.3478284700,   0.0000000000)
 A3 = (   0.0000000000,   0.0000000000,  10.3478284700

Analysis of symmetry for initial positions (statically):
====================================================================
=
 Subroutine PRICEL returns:
 Original cell was already a primitive cell.
Routine SETGRP: Setting up the symmetry group for a
 simple cubic supercell.
 Subroutine GETGRP returns: Found  1 space group operations
 (whereof  1 operations were pure point group operations)
 out of a pool of 48 trial point group operations.

The static configuration has the point symmetry C_1 .
Analysis of symmetry for dynamics (positions and initial
velocities):
====================================================================
 Subroutine PRICEL returns:
 Original cell was already a primitive cell.

 Routine SETGRP: Setting up the symmetry group for a
 simple cubic supercell.
 Subroutine GETGRP returns: Found  1 space group operations
```

Figure B.6. 100-atom set atom positions before and after with VASP script file (cont.)

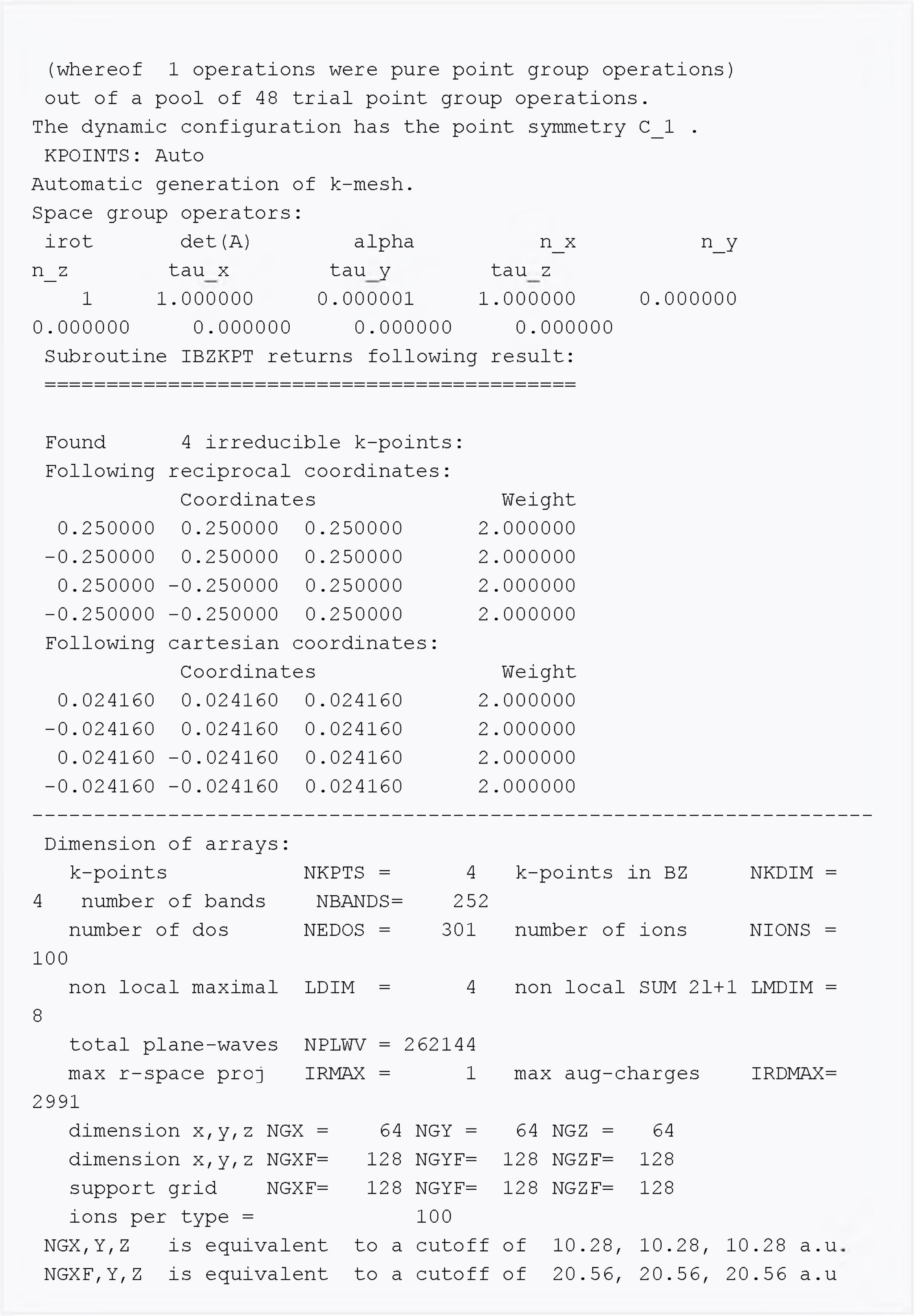

```
 (whereof  1 operations were pure point group operations)
 out of a pool of 48 trial point group operations.
The dynamic configuration has the point symmetry C_1 .
 KPOINTS: Auto
Automatic generation of k-mesh.
Space group operators:
 irot       det(A)        alpha          n_x          n_y
n_z        tau_x        tau_y        tau_z
    1     1.000000     0.000001     1.000000     0.000000
0.000000     0.000000     0.000000     0.000000
 Subroutine IBZKPT returns following result:
 ===========================================

 Found      4 irreducible k-points:
 Following reciprocal coordinates:
            Coordinates               Weight
  0.250000  0.250000  0.250000      2.000000
 -0.250000  0.250000  0.250000      2.000000
  0.250000 -0.250000  0.250000      2.000000
 -0.250000 -0.250000  0.250000      2.000000
 Following cartesian coordinates:
            Coordinates               Weight
  0.024160  0.024160  0.024160      2.000000
 -0.024160  0.024160  0.024160      2.000000
  0.024160 -0.024160  0.024160      2.000000
 -0.024160 -0.024160  0.024160      2.000000
---------------------------------------------------------------------
 Dimension of arrays:
   k-points           NKPTS =      4   k-points in BZ     NKDIM =
4   number of bands    NBANDS=    252
   number of dos      NEDOS =    301   number of ions     NIONS =
100
   non local maximal  LDIM  =      4   non local SUM 2l+1 LMDIM =
8
   total plane-waves  NPLWV = 262144
   max r-space proj   IRMAX =      1   max aug-charges    IRDMAX=
2991
   dimension x,y,z NGX =    64 NGY =   64 NGZ =   64
   dimension x,y,z NGXF=   128 NGYF=  128 NGZF=  128
   support grid    NGXF=   128 NGYF=  128 NGZF=  128
   ions per type =               100
 NGX,Y,Z   is equivalent  to a cutoff of  10.28, 10.28, 10.28 a.u.
 NGXF,Y,Z  is equivalent  to a cutoff of  20.56, 20.56, 20.56 a.u
```

Figure B.6. 100-atom set atom positions before and after with VASP script file (cont.)

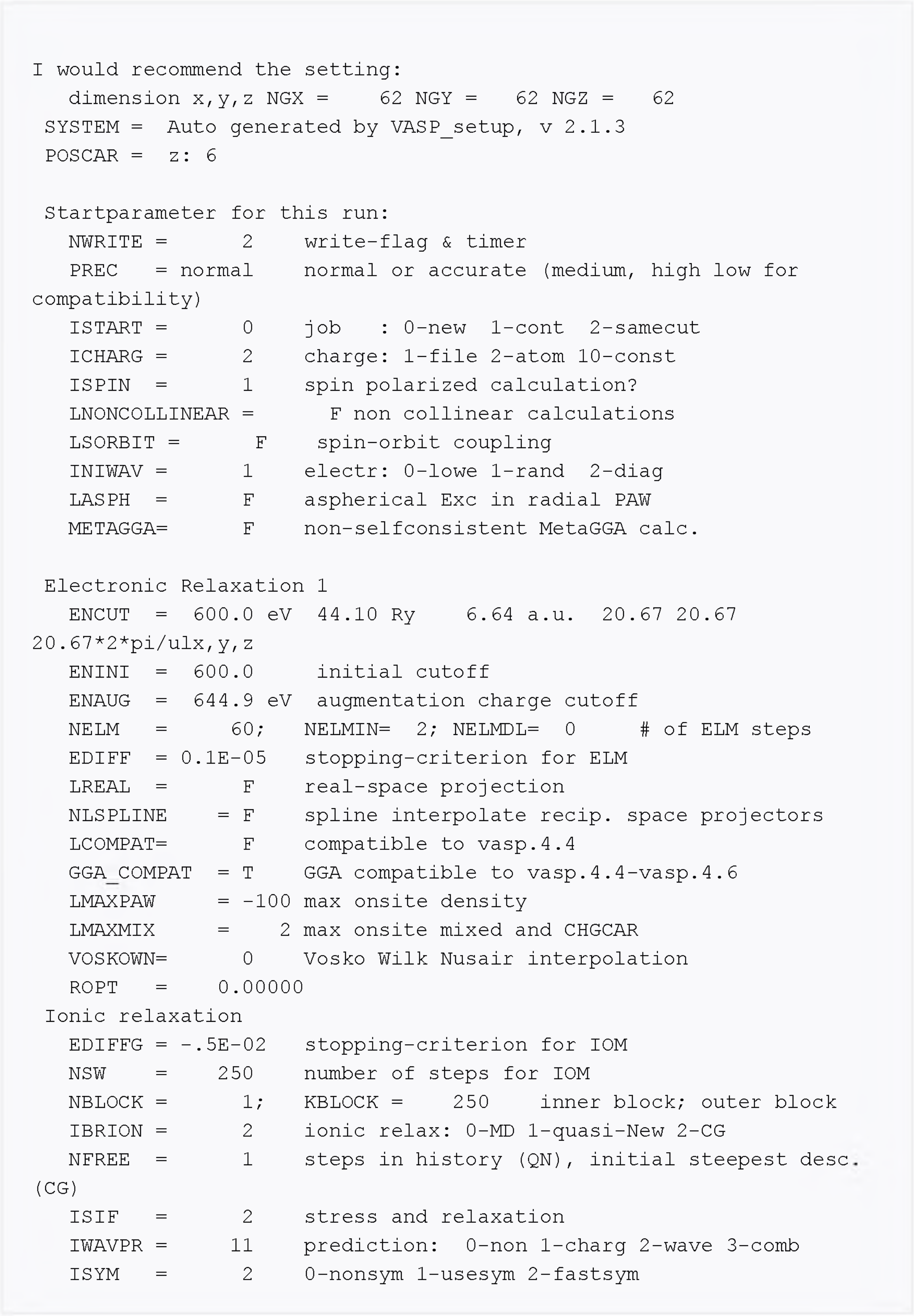

```
I would recommend the setting:
   dimension x,y,z NGX =    62 NGY =   62 NGZ =   62
 SYSTEM =  Auto generated by VASP_setup, v 2.1.3
 POSCAR =  z: 6

 Startparameter for this run:
   NWRITE =      2    write-flag & timer
   PREC   = normal    normal or accurate (medium, high low for
compatibility)
   ISTART =      0    job   : 0-new  1-cont  2-samecut
   ICHARG =      2    charge: 1-file 2-atom 10-const
   ISPIN  =      1    spin polarized calculation?
   LNONCOLLINEAR =      F non collinear calculations
   LSORBIT =      F    spin-orbit coupling
   INIWAV =      1    electr: 0-lowe 1-rand  2-diag
   LASPH  =      F    aspherical Exc in radial PAW
   METAGGA=      F    non-selfconsistent MetaGGA calc.

 Electronic Relaxation 1
   ENCUT  =  600.0 eV  44.10 Ry    6.64 a.u.  20.67 20.67
20.67*2*pi/ulx,y,z
   ENINI  =  600.0     initial cutoff
   ENAUG  =  644.9 eV  augmentation charge cutoff
   NELM   =     60;   NELMIN=  2; NELMDL=  0     # of ELM steps
   EDIFF  = 0.1E-05   stopping-criterion for ELM
   LREAL  =      F    real-space projection
   NLSPLINE    = F    spline interpolate recip. space projectors
   LCOMPAT=      F    compatible to vasp.4.4
   GGA_COMPAT  = T    GGA compatible to vasp.4.4-vasp.4.6
   LMAXPAW     = -100 max onsite density
   LMAXMIX     =    2 max onsite mixed and CHGCAR
   VOSKOWN=      0    Vosko Wilk Nusair interpolation
   ROPT   =    0.00000
 Ionic relaxation
   EDIFFG = -.5E-02   stopping-criterion for IOM
   NSW    =    250    number of steps for IOM
   NBLOCK =      1;   KBLOCK =    250    inner block; outer block
   IBRION =      2    ionic relax: 0-MD 1-quasi-New 2-CG
   NFREE  =      1    steps in history (QN), initial steepest desc.
(CG)
   ISIF   =      2    stress and relaxation
   IWAVPR =     11    prediction:  0-non 1-charg 2-wave 3-comb
   ISYM   =      2    0-nonsym 1-usesym 2-fastsym
```

Figure B.6. 100-atom set atom positions before and after with VASP script file (cont.)

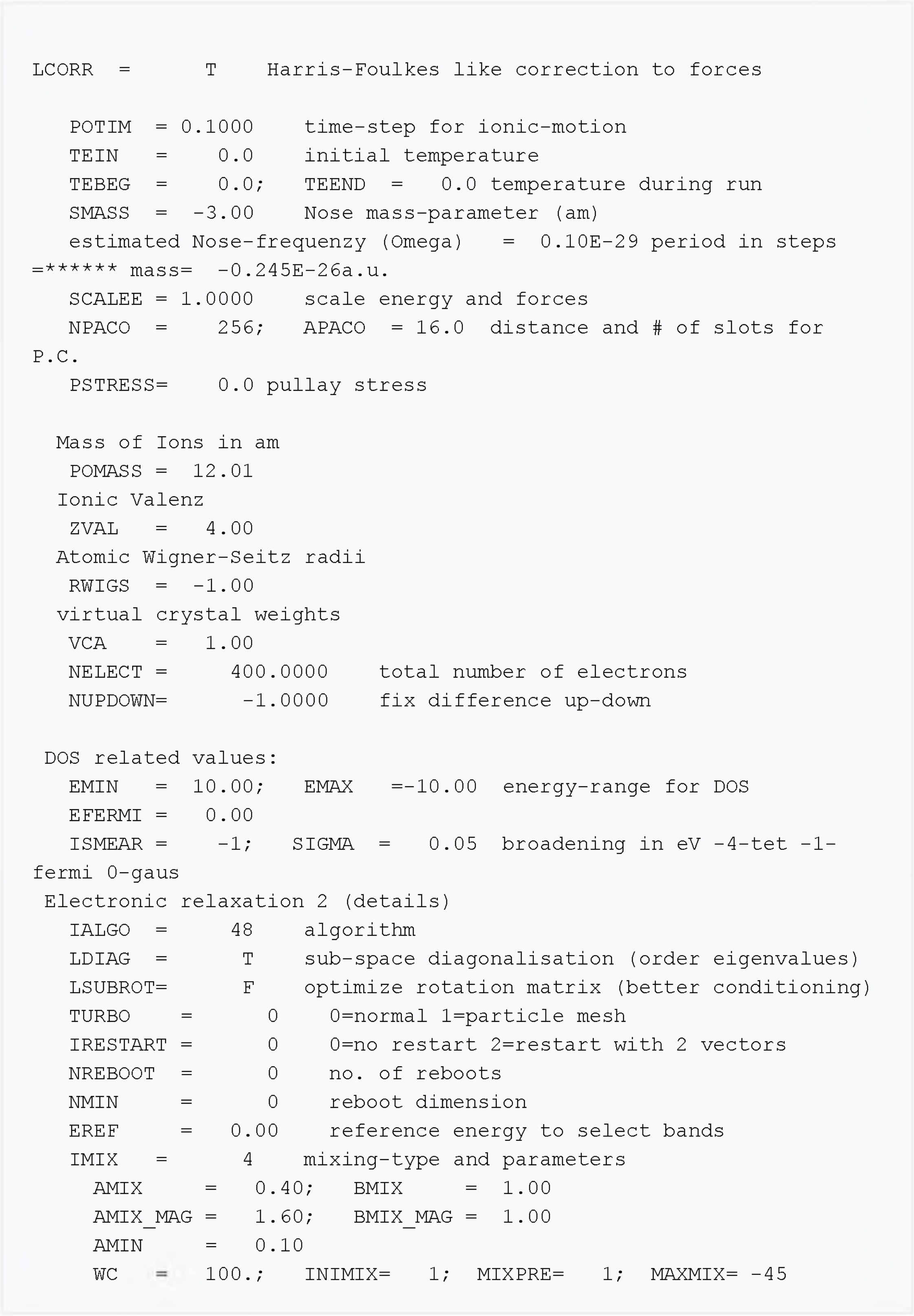

```
LCORR  =      T    Harris-Foulkes like correction to forces

   POTIM  = 0.1000    time-step for ionic-motion
   TEIN   =    0.0    initial temperature
   TEBEG  =    0.0;   TEEND  =   0.0 temperature during run
   SMASS  =  -3.00    Nose mass-parameter (am)
   estimated Nose-frequenzy (Omega)   =  0.10E-29 period in steps
=****** mass=  -0.245E-26a.u.
   SCALEE = 1.0000    scale energy and forces
   NPACO  =    256;   APACO  = 16.0  distance and # of slots for
P.C.
   PSTRESS=    0.0 pullay stress

  Mass of Ions in am
   POMASS =  12.01
  Ionic Valenz
   ZVAL   =   4.00
  Atomic Wigner-Seitz radii
   RWIGS  =  -1.00
  virtual crystal weights
   VCA    =   1.00
   NELECT =     400.0000    total number of electrons
   NUPDOWN=      -1.0000    fix difference up-down

 DOS related values:
   EMIN   =  10.00;   EMAX   =-10.00  energy-range for DOS
   EFERMI =   0.00
   ISMEAR =    -1;   SIGMA  =   0.05  broadening in eV -4-tet -1-
fermi 0-gaus
 Electronic relaxation 2 (details)
   IALGO  =     48    algorithm
   LDIAG  =      T    sub-space diagonalisation (order eigenvalues)
   LSUBROT=      F    optimize rotation matrix (better conditioning)
   TURBO    =      0    0=normal 1=particle mesh
   IRESTART =      0    0=no restart 2=restart with 2 vectors
   NREBOOT  =      0    no. of reboots
   NMIN     =      0    reboot dimension
   EREF     =   0.00    reference energy to select bands
   IMIX   =      4    mixing-type and parameters
     AMIX     =   0.40;   BMIX     =  1.00
     AMIX_MAG =   1.60;   BMIX_MAG =  1.00
     AMIN     =   0.10
     WC     =   100.;   INIMIX=   1;  MIXPRE=   1;  MAXMIX= -45
```

Figure B.6. 100-atom set atom positions before and after with VASP script file (cont.)

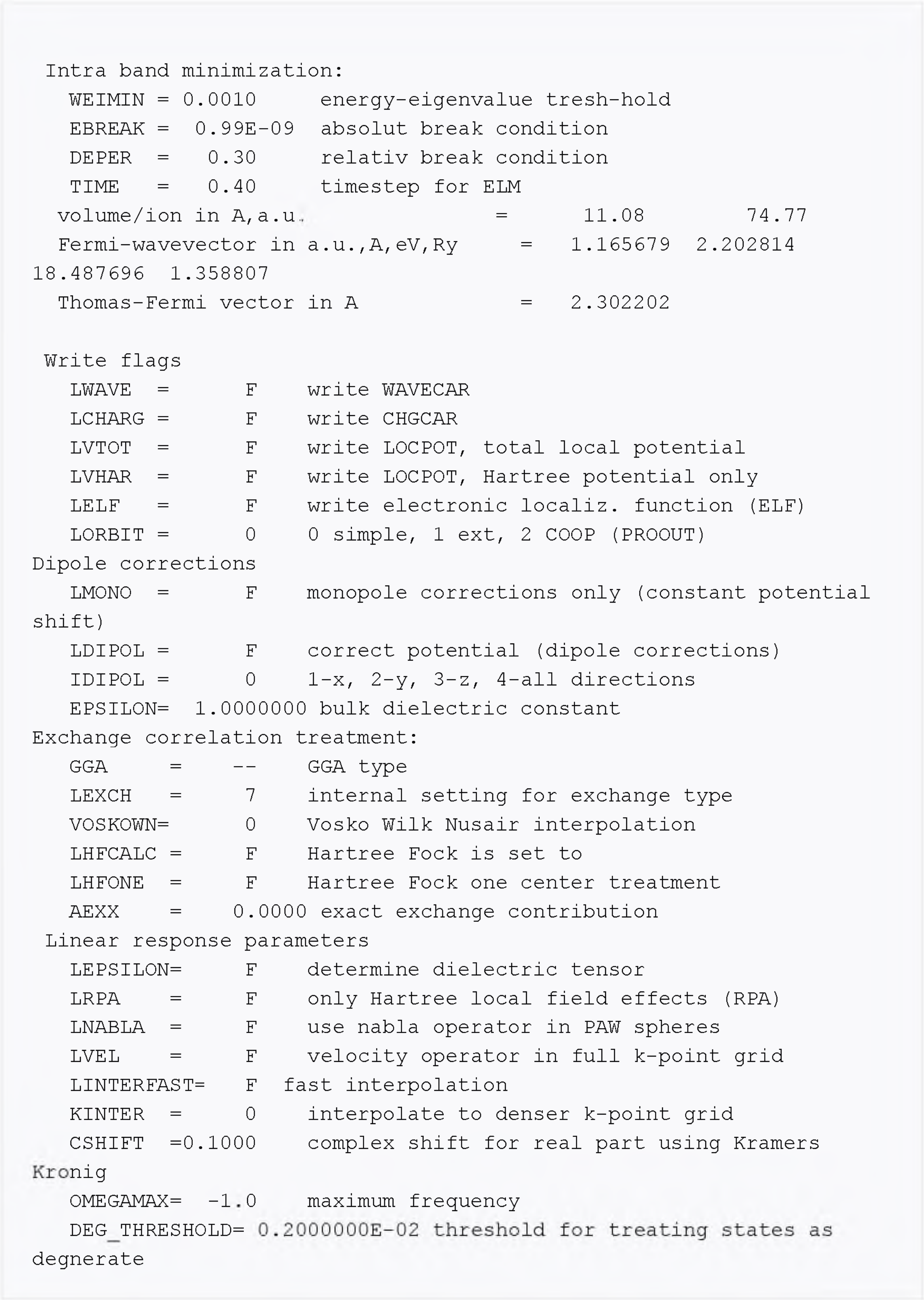

```
 Intra band minimization:
   WEIMIN = 0.0010     energy-eigenvalue tresh-hold
   EBREAK =  0.99E-09  absolut break condition
   DEPER  =   0.30     relativ break condition
   TIME   =   0.40     timestep for ELM
  volume/ion in A,a.u.               =      11.08        74.77
  Fermi-wavevector in a.u.,A,eV,Ry     =   1.165679  2.202814
18.487696  1.358807
  Thomas-Fermi vector in A             =   2.302202

 Write flags
   LWAVE  =      F    write WAVECAR
   LCHARG =      F    write CHGCAR
   LVTOT  =      F    write LOCPOT, total local potential
   LVHAR  =      F    write LOCPOT, Hartree potential only
   LELF   =      F    write electronic localiz. function (ELF)
   LORBIT =      0    0 simple, 1 ext, 2 COOP (PROOUT)
Dipole corrections
   LMONO  =      F    monopole corrections only (constant potential
shift)
   LDIPOL =      F    correct potential (dipole corrections)
   IDIPOL =      0    1-x, 2-y, 3-z, 4-all directions
   EPSILON=  1.0000000 bulk dielectric constant
Exchange correlation treatment:
   GGA     =    --    GGA type
   LEXCH   =     7    internal setting for exchange type
   VOSKOWN=      0    Vosko Wilk Nusair interpolation
   LHFCALC =     F    Hartree Fock is set to
   LHFONE  =     F    Hartree Fock one center treatment
   AEXX    =    0.0000 exact exchange contribution
 Linear response parameters
   LEPSILON=     F    determine dielectric tensor
   LRPA    =     F    only Hartree local field effects (RPA)
   LNABLA  =     F    use nabla operator in PAW spheres
   LVEL    =     F    velocity operator in full k-point grid
   LINTERFAST=   F  fast interpolation
   KINTER  =     0    interpolate to denser k-point grid
   CSHIFT  =0.1000    complex shift for real part using Kramers
Kronig
   OMEGAMAX=  -1.0    maximum frequency
   DEG_THRESHOLD= 0.2000000E-02 threshold for treating states as
degnerate
```

Figure B.6. 100-atom set atom positions before and after with VASP script file (cont.)

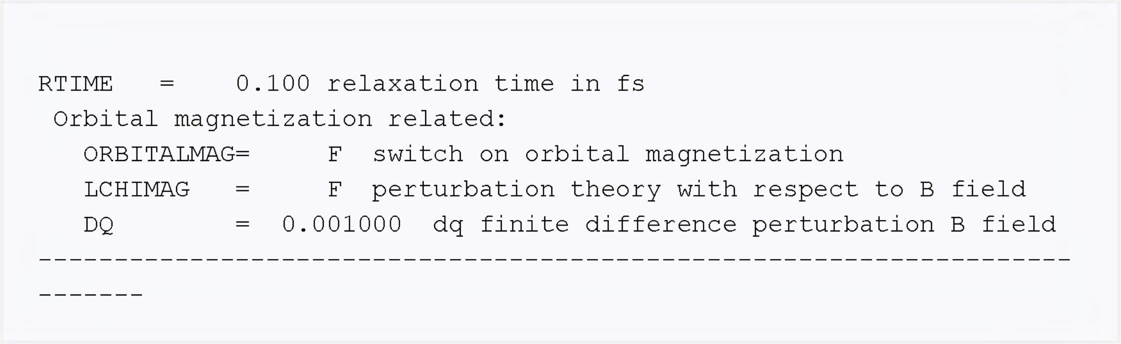

```
RTIME   =    0.100 relaxation time in fs
 Orbital magnetization related:
   ORBITALMAG=     F  switch on orbital magnetization
   LCHIMAG   =     F  perturbation theory with respect to B field
   DQ        =  0.001000  dq finite difference perturbation B field
--------------------------------------------------------------------
-------
```

Figure B.6. 100-atom set atom positions before and after with VASP script file (cont.)

REFERENCES

[1] Kasuya, D.; Yudasaka, M.; Takahashi, K.; Kokai, F.; Iijima, S. Selective Production of Single-Wall Carbon Nanohorn Aggregates and Their Formation Mechanism. *J. Phys. Chem.* **2002**, *B* 106, 4947.

[2] De Heer, W. A.; Poncharal, P.; Berger, C.; Gezo, J.; Song, Z. M.; Bettini, J.; Ugarte, D. Liquid Carbon, Carbon-glass Beads, and the Crystallization of Carbon Nanotubes. *Science* 307:5711. **2005**, pp. 907–910.

[3] Fraundorf, P.; Wackenhut, M. The Core structure of Pre-solar Graphite Onions. *Ap. J. Lett.* **2002,** 578(2): L153-156. (American Astronomical Society).

[4] Mandell E. S. Electron Beam Characterization of Carbon Nanostructures. Dissertation. **2007**, 565. https://irl.umsl.edu/dissertation/565.

[5] Fraundorf, P.; Hundley, T.; Lipp, M. Synthesis of Unlayered Graphene from Carbon Droplets: In Stars and in the Lab. *HAL-02238804*. **2019**.

[6] Frondel, C.; Marvin, U. B. Lonsdaleite, a Hexagonal Polymorph of Diamond. *Nature*. **1967**, 217, 587-589.

[7] Zicheng, P.; Hong, S.; Zhang, Y.; Chen, C. Harder than Diamond: Superior Indentation Strength of Wurtzite BN and Lonsdaleite. *Phys. Rev. Lett.* **2009**, 102, 055503.

[8] Whittaker, A. G.; Carbon: A New View of Its High-Temperature Behavior. *Science*. **1978**, 200, 763–764.

[9] Chalifoux, W.; Tykwinski, R. Synthesis of Polyynes to Model the sp-Carbon Allotrope Carbyne. *Nat. Chem.* **2010**, 2, 967–971.

[10] Konyashin, I.; Khvostov, V.; Babaev, V.; Guseva, M.; Mayer, J.; Sirenko, A. A New Hard Allotropic Form of Carbon: Dream or Reality? *International Journal of Refractory Metals & Hard Materials* 24, **2006**,17-23.

[11] Stephan, U.; Haase, M. A Molecular Dynamics Study and the Electronic Properties of Amorphous Carbon Using the Tersoff Potential. *J. Phys.: Condens. Matter* 5. **1993**, 9157-9168.

[12] Savvatimskiy, A. I. Liquid Carbon Density and Resistivity. *J. Phys. Condens. Matter* 20. **2008**, 114112

[13] Zazula, J. On Graphite Transformations at High Temperature and Pressure Induced by Absorption of the LHC Beam. LHC Project Note 78 / 97. **1997**, CERN, Geneva.

[14] Yang,C.C.; Li, S. Size-Dependent Temperature-Pressure Phase Diagram of Carbon. *J. Phys. Chem.* **2008**, 112(5), 1423– 1426.

[15] Gorrini, F.; Cazzanelli, M.; Bazzanella, N.; Edla, R.; Gemmi, M.; Cappello, V.; David, J.; Dorigoni, C.; Bifone, A.; Miotello, A. On the Thermodynamic Path Enabling a Room-Temperature, Laser-Assisted Graphite to Nanodiamond Transformation. *Sci. Rep. 6.* **2016**, 5244.

[16] Fraundorf, P.; Fraundorf, G.; Bernatowicz, T.; Lewis, R.; Ming, T. Stardust in the TEM. *Ultramicroscopy*. **1989**, 27:9.401-412

[17] Adroit Market Research**.** Global Advanced Carbon Materials market research report**.** April 23-**2019,** https://www.adroitmarketresearch.com/contacts/request-sample/749**.**

[18] Heck, P. R.; Greer, J.; Kööp, L.; Trappitsch, R.; Gyngard, F.; Busemann, H.; Maden, C.; Ávila, J. N.; Davis, A. M.; Wieler, R. Lifetimes of Interstellar Dust from Cosmic Ray Exposure Ages of Presolar Silicon Carbide. PNAS. **2020**, 117 (4): 1884 -1889. doi:10.1073/pnas.1904573117. PMC 6995017. PMID 31932423.

[19] Bernatowicz, T.; Fraundorf, G.; Ming, T.; Anders, E.; Wopenka, B.; Zinner, E.; Fraundorf, P. Evidence for Interstellar SiC in the Murray Carbonaceous Meteorite. *Nature 330*. **1987**, 728-730.

[20] Pillinger, C. Small minded - The Characterization of Interplanetary Dust by Electron Microscopy. *Nature 294*. **1981**, pages 517-518.

[21] Lugaro, M. Stardust from Meteorites: An Introduction to Presolar Grains. *World Scientific Publishing Company*. **2005**, 209 pp., ISBN 9812560998, 9789812560995.

[22] Burbidge, E. M.; Burbidge, G. R.; Fowler, W. A.; Hoyle, F. Synthesis of the Elements in Stars. *Rev. Mod. Phys. 29*. **1957**, 547-650.

[23] Bernatowicz, T. J.; Zinner, E. Astrophysical Implications of the Laboratory Study of Presolar Materials. *AIP*. **1996**, AIP Conference Proceedings 402.

[24] Croat, T.K.; Bernatowicz, T. J.; Amari, S.; Messenger, S.; Stadermann, F. J. Structural, Chemical, and Isotopic Microanalytical Investigations of Graphite from Supernovae. *Geochimica et Cosmochimica Acta*. **2003**, Vol 67, 24, 4705-4725.

[25] Croat, T. K.; Stadermann, F. J.; Bernatowicz, T. J. Presolar graphite from AGB Stars: Microstructure and s-process Enrichment. *Astrophysical Journal* 631. **2005**, 976-987.

[26] Bernatowicz, T. J.; Akande, O. W.; Croat, T. K.; Cowsik, R. Constraints on grain formation around carbon stars from laboratory studies of presolar graphite. *Astrophysical Journal* 631. **2005**, 988-1000.

[27] Wopenka, B.; Xu, Y. C.; Zinner, E.; Amari, S. Murchison Presolar Carbon Grains of Different Density Fractions: A Raman Spectroscopic Perspective. *Geochimica et Cosmochimica Acta.* **2013**, 106, 463–489. 10.1016/j.gca.2012.12.022.

[28] Johnson, S. L.; Heimann, P. A.; MacPhee, A. G.; Lindenberg, A. M.; Monteiro, O. R.; Chang, Z.; Lee, R. W.; Falcone, R. W. Bonding in Liquid Carbon Studied by Time-Resolved X-ray Absorption Spectroscopy. *Phys. Rev. Lett.* **2005**, 94, 057407.

[29] Born, M.; Oppenheimer, R. Zur Quantentheorie der Molekeln. *Ann. Phys.* **1927**, 389: 457-484. https://doi.org/10.1002/andp.19273892002.

[30] Hohenberg, P.; Kohn, W. Inhomogeneous Electron Gas. *Physical Review*. **1964**, 136 (3B), B864-B871.

[31] Kohn, W.; Sham, L. J. Self-Consistent Equations Including Exchange, and Correlation Effects. *Physical Review*. **1965**, 140 (4A), A1133–A1138.

[32] Hartee, D. R. The Wave Mechanics of an Atom with a Non-Coulomb Central Field. Part I.Theory and Methods. *Mathematical Proceedings of the Cambridge Philosophical Society.* **1928**, 24(1), 89-110. doi:10.1017/S0305004100011919

[33] Payne, M. C.; Teter, M. P.; Allan, D. C.; Arias, T. A.; Joannopoulos, J. D. Iterative Minimization Techniques for Ab initio Total-Energy Calculations: Molecular Dynamics and Conjugate Gradients. *Rev. Mod. Phys.* **1992**, 64(4), 1045-1097.

[34] Blöchl, P. E. Projector Augmented-Wave Method. *Phys. Rev.* **1994**, B50, 17953.

[35] Blochl, P. E.; Forst, C. J.; Schimpl, J. Projector Augmented Wave Method: ab initio Molecular Dynamics with Full Wave Functions. *Bulletin of Materials Science*. **2003**, 26(1), 33-41.

[36] Vanderbilt, D.Soft Self-Consistent Pseudopotentials in a Generalized Eigenvalue Formalism. *Phys. Rev. B*. **1990, 41,** 7892-7895.

[37] Kresse, G.; Joubert, D. From Ultrasoft Pseudopotentials to the Projector Augmented-Wave Method. *Phys. Rev. B*. **1999**, 59:1758.

[38] Kresse, G.; Marsman, M.; Furthmüller, J. VASP the Guide. University of Vienna Austria. **2005**, http://cms.mpi.univie.ac.at/vasp/vasp.pdf

[39] Monkhorst, H. J.; Pack, J. D. Special Points for Brillouin-Zone Integrations. *Phys. Rev. B*. **1976**, 13, 5188.

[40] Tersoff, J. New Empirical Approach for the Structure and Energy of Covalent Systems. *Phys. Rev. B.* **1988**, 37:12, 6991-7000.

[41] Tersoff,J. Empirical Interatomic Potential for Carbon, with Applications to Amorphous Carbon. *Phys. Rev. Lett.* **1988**, 61:25, 2879-2882.

[42] Stephan, U.; Haase, M. A Molecular Dynamics Study and the Electronic Properties of Amorphous Carbon Using the Tersoff Potential. *J. Phys.: Condens. Matter 5.* **1993**, 9157-9168

[43] Lonsdale, K.; Milledge H. J.; Nave, E. X-ray Studies of Synthetic Diamond. *Mineral Mag.* **1959**;32:158–201

[44] Tapia, A.; Canto, G.; Murrieta, G.; de Coss, R. Electronic Structure of FCC Carbon. *Journal of Experimental and Theoretical Physics Letters.* **2005**, 82:3, pp.120-123

[45] Murrieta,G.; Tapia, A.; de Coss, R. Structural Stability of Carbon in the Face-Centered-Cubic ($Fm\bar{3}m$) Phase. *Carbon.* **2004**, vol:42, Issue 4, pp 771-774

[46] Kelton, K.F.; Lee, G.W.;Gangopadhyay, A.K.; Hyers, R.W.; Rathz, T.J.; Rogers, J.R.; Robinson, M.B.; Robinson, D.S. First X-ray Scattering Studies on Electrostatically Levitated Metallic Fluids: Demonstrated Influence of Local Icosahedral Order on the Nucleation Barrier. *Phys. Rev. Lett.* **2003**, 90,195504.

[47] Barnard, A. S.; Russo, S. P.; Snookc, I. K. Ab *initio* Modeling of B and N in C_{29} and $C_{29}H_{24}$ Nano diamond. *J. Chem. Phys.* **2003**, 118 10725

[48] Kroto, H. W. The Stability of the Fullerenes C_n, with n = 24, 28, 32, 36, 50, 60 and 70. *Nature.* **1987**, 329, 529-531

[49] Dunk, P.W.; Kaiser, N. K.; Mulet-Gas, M.; Rodríguez-Fortea, A.; Poblet, J. M.; Shinohara, H.; Hendrickson, C. L.; Marshall, A. G.; Kroto, H. W. The Smallest Stable Fullerene, M@C28 (M = Ti, Zr, U): Stabilization and Growth from Carbon Vapor. *J. Am. Chem. Soc.* **2012**, 134:22, 9380-9389

[50] Dresselhaus, M.S.; Dresselhaus, G.; Eklund, P.C. Science of Fullerenes and Carbon Nanotubes. *Academic Press.* **1996**, San Diego, CA)

[51] Martin, J. M. L. C28: The Smallest Stable Fullerene?. *Chemical Physics Letters*, **1996**, 255:1–3,1-6, https://doi.org/10.1016/0009-2614(96)00354-5.

[52] McSkimin, H. J.; Andreatch, P. Elastic Moduli of Diamond as a Function of Pressure and Temperature. *J. Appl. Phys.* **1972**, 43, 2944

[53] Bernatowicz, T.; Cowsik, R.; Gibbons, P. C.;Lodders, K.; Fegley, Jr B.; Amari, S.; Lewis, R. S. Constraints on Stellar Grain Formation from Presolar Graphite in the Murchison Meteorite. *Astrophys. J.* **1996**, 472,760

[54] Fraundorf, P.; Pisane, K.; Mandell, E.; Collins, R. Zero-Loss/Deflection Map Analysis. *Microsc.Microanal.* **2010**, 16 (Supplement 2), 1534-1535

[55] Perdew, J. P.; Burke, K.; Ernzerhof, M. Generalized Gradient Approximation Made Simple. *Phys. Rev. Lett.* **1996**, 77, 3865

[56] Franzblau, D. S. Computation of Ring Statistics for Network Models of Solids. *Phys. Rev. B.* **1991**, 44, 10

[57] Cannella, C.; Goldman, N. Carbyne Fiber Synthesis within Evaporating Metallic Liquid Carbon. *J.Phys.Chem.* **2015**, 119, 29-31

[58] Morris, J. R.; Wang, C. Z.; Ho, K. M. Relationship Between Structure and Conductivity in Liquid Carbon. *Phys. Rev. B.* **1995**, 52

[59] Wu, C. J.; Glosli, J. N.; Galli, G.; Ree, F. H. Phys. Liquid-Liquid Phase Transition in Elemental Carbon: A First-Principles Investigation. *Rev. Lett.* **2002**, 89, 135701

[60] Marks, N. A.; Cooper, N. C.; McKenzie, D. R. Comparison of Density Functional, Tight-Binding, and Empirical Methods for the simulation of amorphous carbon *Phys. Rev. B.* **2002**, 65, 075411

[61] Deringer, V. L.; Csányi, G. Machine Learning Based Interatomic Potential for Amorphous Carbon. *Phys. Rev. B.* **2017**, 95, 094203

[62] Fraundorf, P.; Lipp, M.; Hundley, T.; Silva, C.; Chrostoski, P. Fraction Crystalline from Electron Powder Patterns of Unlayered Graphene in Solidified Carbon Rain. *Microscopy and Microanalysis*. **2020**, 26: S2 pp. 2838-2840

[63] Toh, C.; Zhang, H.; Lin, J.; Mayorov, A. S.; Wang, Y.; Orofeo, C. M. et al., Synthesis and Properties of Free-standing Monolayer Amorphous Carbon. *Nature*. **2020**, 577, 199-203

[64] Page, A. J.; Ding, F.; Irle, S.; Morokuma, K. Insights into Carbon Nanotube and Graphene Formation Mechanisms from Molecular Simulations: A Review. *Reports on Progress in Physics*. **2015**, 78, 036501

[65] Ohta,Y.; Okamoto, Y.; Page, A. J.; Irle, S. Morokuma,K. Quantum Chemical Molecular Dynamics Simulation of Single-Walled Carbon Nanotube Cap Nucleation on an Iron Particle. *American Chemical Society Nano*. **2009**, 3:11, 3413-3420.

[66] Los, J. H.; Fasolino, A. Intrinsic Long-Range Bond-Order Potential for Carbon: Performance in Monte Carlo Simulations of Graphitization. *Phys. Rev. B.* **2003**, 68.024107

[67] Rulis, P.; Chen, J.; Ouyang, L.; Ching, W. Y.; Su, X.; Garofalini, S. H. Electronic Structure and Bonding of Intergranular Glassy Films in Polycrystalline Si_3N_4: Ab initio Studies and Classical Molecular Dynamics Simulations. *Phys. Rev. B.* **2005**,71, 235317

VITA

Chathuri Chandani Silva was born in Panadura, Sri Lanka. In 2011, she earned her Bachelor of Science in Applied Sciences from University of Colombo, Sri Lanka. As part of her graduate studies, she enrolled at Pittsburg State University, Pittsburg Kansas, in 2013 and received a Master of Science in Physics in May 2015, with honors. During her time at Pittsburg State University, she received the awards for Excellence in Research (2015), Excellence in Teaching in Physics (2014), and the award for Excellence in Professional Services in the Department of Physics in 2015.

She earned her second Master of Science in Physics at University of Missouri - St. Louis in 2017. Following her studies, she received her Ph.D. in Physics jointly from the Missouri University of Science and Technology and the University of Missouri St. Louis in July 2021. She was awarded the Outstanding Teaching Assistant Award during the year 2020. Her accomplishments included presenting her research at conferences and publishing articles in scholarly journals. In addition, since 2000, she has been a member of the American Physical Society, Material Research Society, and American Association of Physics Teachers.